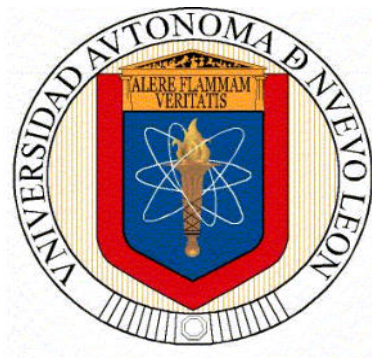# UNIVERSIDAD AUTÓNOMA DE NUEVO LEÓN
FACULTAD DE CIENCIAS QUÍMICAS

"METABOLOMIC AND BIODIRECTED PHYTOCHEMICAL STUDY OF *Hechtia glomerata*, EVALUATION OF ITS ANTIBACTERIAL AND CYTOTOXIC ACTIVITY, AND DETERMINATION OF THE MECHANISM OF ACTION OF ONE ACTIVE COMPOUND"

Presentada por:

TOMMASO STEFANI

Como requisito parcial para obtener el grado de

DOCTOR EN CIENCIAS CON ORIENTACIÓN EN FARMACIA

ENERO 2020

UNIVERSIDAD AUTÓNOMA DE NUEVO LEÓN

FACULTY OF CHEMICAL SCIENCES

METABOLOMIC AND BIODIRECTED PHYTOCHEMICAL STUDY OF *Hechtia glomerata,* EVALUATION OF ITS ANTIBACTERIAL AND CYTOTOXIC ACTIVITY, AND DETERMINATION OF THE MECHANISM OF ACTION OF ONE ACTIVE COMPOUND

By

TOMMASO STEFANI, MSc

**As a partial requirement to obtain the Degree of
DOCTOR IN SCIENCES with Orientation in Pharmacy**

January 2020

The experimental design and development of the present work was performed in the Laboratory of Natural and Synthetic Products, Faculty of Chemical Sciences at the Universidad Autónoma de Nuevo León.

METABOLOMIC AND BIODIRECTED PHYTOCHEMICAL STUDY OF *Hechtia glomerata*, EVALUATION OF ITS ANTIBACTERIAL AND CYTOTOXIC ACTIVITY, AND DETERMINATION OF THE MECHANISM OF ACTION OF ONE ACTIVE COMPOUND

Thesis Revision:

_____
Dr. María del Rayo Camacho Corona
Director

_____
Dr. Edgar Abraham García Zepeda
Co-director

_____
Dr. Francisco G. Avalos Alanís
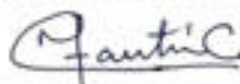Tutorial Committee

_____
Dr. Verónica M. Rivas Galindo
Tutorial Committee

_____
Dr. Elvira Garza González
Tutorial Committee

_____
Dr. María Julia Verde Star
Tutorial Commetteei

_____
Dr. María Elena Cantú Cardenas
Sub-Director of the Graduate School

METABOLOMIC AND BIODIRECTED PHYTOCHEMICAL STUDY OF *Hechtla glomerata*, EVALUATION OF ITS ANTIBACTERIAL AND CYTOTOXIC ACTIVITY, AND DETERMINATION OF THE MECHANISM OF ACTION OF ONE ACTIVE COMPOUND
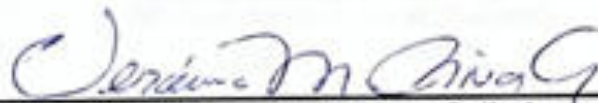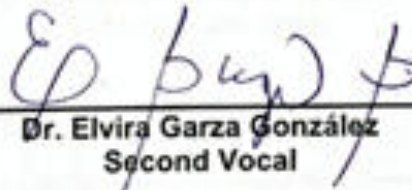
Thesis Approval:

_____
Dr. María del Rayo Camacho Corona
President

_____
Dr. Francisco G. Avalos Alanís
Secretary

_____
Dr. Verónica M. Rivas Galindo
First Vocal

_____
Dr. Elvira Garza González
Second Vocal

_____
Dr. María Julia Verde Star
Third vocal

_____
Dr. María Elena Cantú Cardenas
Sub-Director of the Graduate School

DEDICATION

To my husband Mabiel

To my parents

To my brother

To my grandparents

AKNOLEDGMENTS

To Dr. **José Rodríguez Rodríguez**, School of engineering and technology of information, Tecnológico de Monterrey. For the methylation of fraction 1 of the CHCl$_3$/MeOH extract.

To the professors, Dr. Lucía Guadalupe Cantú Cárdenas, Dr. María Elena Cantú Cárdenas, Dr. Verónica M. Rivas Galindo, Dr. María Araceli Hernández Ramírez. For all the help, the advice and support you gave me during my carrier. It means very much to me, thank you.

To the professors, Dr. Mónica A. Ramírez Cabrera, and Dr. Isaías Balderas Rentería for taking part in my doctoral formation.

To MSc Juan J. J. Carrizales Castillo and MSc Rodrigo Vázquez Briones for the help provided in the realization of the cytotoxicity assays and RNA extraction in the laboratory of INGGEN. To Kenya Guadalupe Flores Sandoval for the preparation of root extracts and the isolation of one compound.

To my friends of the QPNS laboratory: Deyaní Nocedo Mena, Luis Fernando Méndez Lopéz, Reyna Martha Gallegos Alvarado and Bryan Alejandro Espinosa Rodríguez.

To my friends Erikita, Mabiel and Magy. With you I have laughed and shared a lot, thank you so much for everything.

To my friends of the laboratory of drug design assisted by computer and synthesis of the UAQ, Dr. Romo, Giovanni, Cesar, Ivonne, Fernanda, Alex, Ray, Sam, Jonny and Amelia. For accepting me as I am and being so nice and kind and making me part of your group.

ABSTRACT

MSc. Tommaso Stefani   **Graduation date: March 2020**

Universidad Autónoma de Nuevo León   Faculty of Chemical Sciences

Title of the Study: METABOLOMIC AND BIODIRECTED PHYTOCHEMICAL STUDY OF *Hechtia glomerata*, EVALUATION OF ITS ANTIBACTERIAL AND CYTOTOXIC ACTIVITY, AND DETERMINATION OF THE MECHANISM OF ACTION OF ONE ACTIVE COMPOUND.

Number of pages: 326   **Candidate for the grade of Doctor in Science with Orientation in Pharmacy**

Purpose of the study: The pharmaceutical industry has left the active research and development of new antibiotics, and the lack of new molecules caused the antibacterial resistance to become an even more threatening issue. At the same time cancer resistance is also thriving, making old chemotherapeutic drugs useless. Therefore, there is the absolute need of new bioactive molecules to contrast these pathologies. Plants' natural products have always been a source for bioactive and structurally complex compounds and could represent a solution to these emerging health problems. The majority of the world still relies on the use of ethnomedicine for the treatment and prevention of diseases. This is why in this work a Mexican medicinal plant: *Hechtia glomerata* Zucc. known as Guapilla was investigated for its curative properties. The goal of this study was to find out the actual antibacterial and cytotoxic activity of this plant's extracts and its adequacy as source for biologically active compounds. Also, to isolate its major compounds and deeply investigate its secondary metabolites production. Finally, the mechanism of action of one of its bioactive constituents was investigated by microarray assay.

Results and conclusions: The major constituents of *H. glomerata*'s leaf organic extracts (Hex and C/M) were isolated and characterized. Also, a metabolomic study on all *H. glomerata*'s leaf extracts was performed by UPLC-QTOF-MS analysis. This allowed the identification of the chemical profile of the plant accounting for a total of 226 compounds comprising a 38% of flavonoids and stilbenes, 31% of terpenes and steroids, a 15% of phenolic acids and derivatives, 10% of fatty acids and hydrocarbons, 6% of nitrogen containing compounds. The statistical analysis of the date permitted the visualization of the main differences among the extracts. It was also performed a pathway analysis showing which ones are the most predominant biosynthetic routes of *H. glomerata*. The antibacterial and cytotoxic activity of both leaf and root extracts was investigated. The MIC values for the extracts against resistant bacteria were $\geq$ 500 µg/mL and were considered weak. Meanwhile of the isolated compounds only β-sitosteryl acetate had a MIC value of 100 µg/mL against carbapenem resistant *Acinetobacter baumannii*. The CHCl$_3$/MeOH leaf extract had instead activity against two sensitive bacterial strains: *Staphylococcus aureus* and *Enterobacter faecium* with MIC values of 125 and 62.5 µg/mL respectively. Therefore, a bioassay-guided directed study was performed, testing against these two bacteria the fractions of CHCl$_3$/MeOH extract. Fractions 1, 3 and 8 resulted to be the active ones, the most active being the fraction 8 with a MIC of 100 and 50 µg/mL against *S. aureus* and *E. faecium* respectively. The three active fractions were analyzed in order to identify their active components with GC-MS and/or HPLC-QTOF-MS. The extracts were also tested against cancer cells and only the organic leaf extracts resulted active (IC$_{50}$: 24-32 µg/mL). The most active

was the Hex extract which accounted for the higher number in cell lines inhibited. These results highlighted the lack in specificity of this extract and also its major constituent (β-sitosterol) was already widely studied in the literature. For these reasons it was decided to focus on the CHCl$_3$/MeOH extract, which presented activity against PC3 and was slightly active against MCF7 cell lines. A bioassay-guided directed study was also conducted on this extract showing fractions 3 and 4 as the most active ones. Hence their constituents were investigated giving a high similarity in their composition, especially they shared many hydroxycinnamic acid derivatives like *p*-coumaric and caffeic acid. Since these two compounds were found so abundant and were already isolated and characterized in the same extract, it was decided to test them against the two cancer cell lines. For the stability in culture medium of *p*-coumaric acid was selected for the microarray assay on PC3 cells. The results gave the up- and down-regulation of many genes involved in cancer, some of them specific for prostate cancer (PI3K/AKT, AMPK, MAPK, p53, RAS, and TNF among others). Some proteins of the pathways affected by *p*-coumaric acid treatment were modeled *in silico* and their probable binding sites identified by molecular docking. Finally, the complex ligand-proteins were submitted to molecular dynamic simulation and their binding energy calculated. The interactions leading to a negative binding energy confirm the spontaneous binding of the *p*-coumaric acid to its targets: MAPK8, MDM2, CCNB2, NTRK3, SLC2A4, MDM4 and the protein complex STK11-STRAD-CAB39.

The results obtained in this research confirmed *H. glomerata* as a source of antibacterial and cytotoxic compounds and its use in the Mexican

traditional medicine. In fact, many of the identified and isolated compounds are reported in the literature as bioactive. The deep study of its metabolome helped the higher characterization of this plant's metabolism and phytochemical composition. This study represents the first study of *H. glomerata* and hence it is an important piece of information regarding Mexican medicinal plants. Also, the microarray assay and *in silico* analysis helped the better understanding of the mechanism of action of *p*-coumaric acid. In fact, since this molecule interact with targets involved in many pathways its cytotoxicity results from the deregulation of various cellular processes comprising survival, growth, migration, and metabolism. Because of its tendency to bind with targets possessing a similar secondary structure, *p*-coumaric acid could also represent a good candidate for target fishing and the development of new anticancer drugs.

Dr. María del Rayo Camacho Corona
Thesis director

Dr. Edgar Abraham García Zepeda
Thesis Co-director

TABLE OF CONTENTS

LIST OF TABLES

LIST OF FIGURES

LIST OF SCHEMES AND EQUATIONS

LIST OF ABBREVIATIONS

Å	Angstrom
Ala	Alanine
ANOVA	Analysis of variance
Aq	Aqueous
Arg	Arginine
Asn	Asparagine
Asp	Aspartic acid
ATCC	American type culture collection
ATP	Adenosine triphosphate
C/M	CHCl3/MeOH
CA	Caffeic acid
Cal	Calories
CAM	Crassulacean acid metabolism
CAPE	Caffeic acid phenethyl ester
CC	Column chromatography
$Ce(SO_4)_2$	Cerium sulfate
CFU	Colony forming unit
$CHCl_3$	Chloroform
CO_2	Carbon dioxide
CRAB	Carbapenem resistant *A. baumannii*
CRPA	Carbapenem resistant *P. aeruginosa*
Cys	Cysteine
Da	Dalton
DCM	Dichloromethane
df	Degrees of freedom
DNA	Deoxyribonucleic acid
DR	Drug-resistant
E_{bound}	Binding energy
E_{lp}^{el}	Ligand-bound coulombic energy
E_{ls}^{el}	Ligand-free coulombic energy
E_{lp}^{vdW}	Ligand-bound van der Waals
E_{ls}^{vdW}	Ligand-free van der Waals
ECPE	*E. coli* producer of ESBL
EI	Electron ionization
EMEM	Eagle's minimal essential medium
ESBL	Extended spectrum β-lactamase

ETC	Electron transport chain
EtOAc	Ethyl Acetate
EtOH	Ethanol
F	F ratio
FA	Fatty acid
FC	Flash chromatography
F_{crit}	F critical
g	Grams
GC	Gas chromatography
Gln	Glutamine
GLOBOCAN	Global cancer observatory
Glu	Glutamic acid
Gly	Glycine
GT	Glucose transferase
h	Hour
H_2O	Water
H_2SO_4	Sulfuric acid
HCA	Hydroxy cinnamic acid
HCl	Hydrochloric acid
Hex	Hexane
HGT	Horizontal gene transfer
HMDB	Human metabolome database
HPLC	High-performance liquid chromatography
Hz	Hertz
IC_{50}	Half maximal inhibitory concentration
IR	Infra-red
IS	Internal standard
K	Kelvin
KCl	Potassium chloride
KPPE	*K. pneumoniae* producer of ESBL
KPPN	*K. pneumoniae* producer of NDM-1+
L	Liters
LCFA	Long chain fatty acid
Leu	Leucine
LIE	Linear interaction energy
LRSE	Linezolid resistant *S. epidermidis*
Lys	Lysine
m	Meters
M	Molarity
MD	Molecular dynamics
MDR	Multidrug-resistant

Me	Methyl
MeOH	Methanol
Met	Methionine
MIC	Minimum inhibitory concentration
mol	Moles
mp	Melting point
MRSA	Methicillin resistant *S. aureus*
MS	Mass spectrometry
Ms	Mean squares
MSA	Microtubule stabilizing agent
Na_2SO_4	Sodium sulfate
NaCl	Sodium chloride
$NaHCO_3$	Sodium bicarbonate
NCCLS	National committee for clinical laboratory standards
NDM	New Delhi metallo-β-lactamase
NIST	National institute of standards and technology
NMR	Nuclear magnetic resonance
ORKP	Oxacillin resistant *K. pneumoniae*
PBP	Penicillin binding protein
*p*CA	*p*-Coumaric acid
PCA	Principal component analysis
PDR	Pandrug-resistant
Phe	Phenylanaline
PMN	Plant metabolomic network
ppm	Parts per million
PTFE	Polytetrafluorethylene
QTOF	Quadrupole/time of flight
RMSD	Root-mean-square deviation
RMSF	Root-mean-square fluctuation
RNA	Ribonucleic acid
rpm	Rounds per minute
RPMI	Roswell park memorial institute
SAFA	Saturated fatty acid
Ser	Serine
SiO_2	Silica
SS	Sum of squares
Thr	Threonine
TLC	Thin layer chromatography
TMS	Tetramethylsilane
Trp	Triptophan

Tyr	Tyrosine
U	Units
UFA	Unsaturated fatty acid
UPLC	Ultra-high-performance liquid chromatography
UV	Ultraviolet
vdW	Van der Waals
VLCFA	Very long chain fatty acid
VRE	Vancomycin resistant enterococci
VREF	Vancomycin resistant *E. faecium*
WHO	World health organization
XDR	Extremely drug-resistant
XRD	X-ray diffraction

CHAPTER 1

1. INTRODUCTION

1.1 Bacterial resistance

Since the discovering of penicillin by Alexander Fleming, the use of antibiotics has allowed humanity to overcome many bacterial infections. The mechanism of action of these drugs it's usually focused on the disruption of the cell wall, fundamental for the bacteria's life. For example, β-lactams based agents, inhibit the synthesis of the peptidoglycan throughout the inactivation of DD-transpeptidase, and other penicillin binding proteins (PBPs) responsible of the cell wall production (1). These and other antibacterial molecules can exert their bactericidal activity also by hydroxyl radical formation, like norfloxacin and ampicillin. Some antibiotics are instead ribosome inhibitors, such as chloramphenicol, and tetracycline, and inhibitor of RNA polymerase like rifampicin (2). Other drugs of these kind are the macrolides, a group of molecules such as erythromycin, which bind ribosomal subunit 70S blocking the protein synthesis (3).

In the course of the decades a new phenomenon has become seriously problematic: the antibacterial resistance; which can lead to longer hospitalization periods and in some case in untreatable or difficult-to-treat infections (4).

There are different mechanisms of resistance that the bacteria can rely on to defend themselves from antibiotics (Figure 1.1). Four are the principals:

1. Degradation of the drug by the use of hydrolytic enzymes such as β-lactamase, which are specific for β-lactams

2. Modification of the active site of the target or the entire target macromolecule

3. Alteration of the metabolic pathway where the activity of the drug is exerted, so that it is removed

4. Use of efflux pumps to eliminate de drug from the cytoplasm of the bacteria.
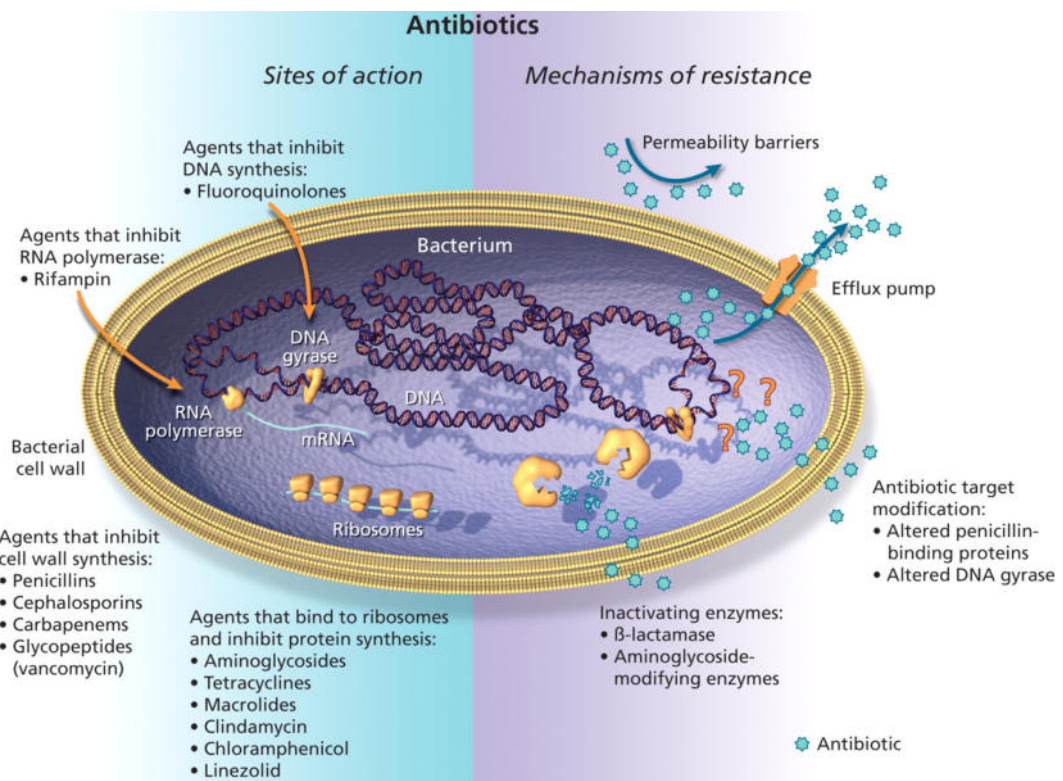
Figure 1.1 Some antibiotics site of actions and resistance mechanisms (*5*)

Other possible mechanisms of antibiotic resistance reported in the literature are the production of physical barriers, like biofilms with the objective of blocking the passage of the drug, which cannot reach the target. Also the bacteria can start a overproduction of the target so that a higher concentration of the drug is needed to exert its effect (*6*).

The resistant bacteria are classified internationally in base of their level of resistance (number of core antibiotic drugs) as drug-resistant (DR), multidrug-resistant (MDR), extensively or extremely drug-resistant (XDR) and pandrug-resistant (PDR) (*7*). To support the research and development of new antibiotics the world health organization (WHO) published a list of bacterial strains divided in to priority subgroups in base of their critical resistance level, from the now-days available antibiotics (*8*). The strains with a higher need of new antibiotics are listed in the Table 1.1.

Table 1.1 WHO priority list of pathogens for the research and development of new antibiotics

Priority	Bacteria	Resistance
CRITICAL	*Acinetobacter baumannii*	Carbapenems
	Pseudomonas aeruginosa	Carbapenems
	Enterobacteraceae	Carbapenems, 3rd gen. cephalosporins
HIGH	*Enterococcus faecium*	Vancomycin
	Staphylococcus aureus	Methicillin, Vancomycin
	Helicobacter pilori	Clarithromycin
	Campylobacter	Fluoroquinolones
	Salmonella spp.	Fluoroquinolones
	Neisseria gonorrhoeae	3rd gen. cephalosporins, Fluoroquinolones
MEDIUM	*Streptococcus pneumoniae*	Penicillin
	Haemopilus influenzae	Ampicillin
	Shigella spp.	Fluoroquinolones

The resistance to antibiotics can be generated by mutations which occurs every 10^7-10^8 cellular replications and, if favorable, they can be transmitted vertically through the successive generations of bacteria. Even if the hypothesis of a favorable mutation is statistically improbable, the resistance can also be transmitted from horizontal gene transfer (HGT), through mobile genetic elements such as plasmids, between different bacteria strains. These events are the result of the selective pressure that can derive from the use of antibiotics itself. This might take place in hospitals or can derive from the abuse of these drugs. In general, there are more than one cause, but it's appropriate to say that an improper use of antibiotics has given its contribution to the resistance development (*9*). In fact, despite the warnings in the matter, these drugs are overprescribed worldwide.

In some countries there is not a useful regulation and antibiotics are even sold over the counter, resulting into a cheap and easily accessible source of drugs and thus promoting overuse. Even if proper regulations about the use of antibiotics are present, in many cases they are wrongly prescribed. For example, studies in the U.S. have shown that the choice of agent, treatment indication and duration are incorrect from 30% to 50% of cases. These errors have questionable health benefits and increase genetic alteration, through antibiotic-induced gene expression. That enhances the virulence and mutagenesis spread thanks to HGT, and thus supporting the appearance of resistance.

Another cause of bacterial resistance is the extensive use of antibiotics in agriculture, to promote livestock growth and to prevent infections. The transfer of resistant bacteria strains from the animals to the farmers is known

since more than 35 years and more recently it was also demonstrated that resistant bacteria can be passed to consumers through meat products (*10*). Also, antibiotic agents sold for hygienic and cleaning purposes can play a contribution role in increasing the problem, blocking proper formation of the immune system in children.

Since the appearance of the first mechanisms of bacterial response to penicillin: the production of a modified version of its target DD-transpeptidase (as mention before), the so called β-lactamase which deactivates the penicillin molecule, new anti-bacterial molecules have been researched and synthesized in order to overcome the problem, but it seems to be a never ending loop (*11*). Therefore, the research of new drugs is of extreme importance, due to the menace that multidrug resistant bacterial strains represent. This fact implies a continuous need of new molecules in order to maintain the ability to fight bacterial infections, even the most common ones. There are just few available new antibiotics, and this is due to the lack research in this field by the majority of the big pharmaceutical companies. The massive neglect toward the production of new antibacterial agents, is the result of the low income that they produce in comparison with other drugs used in chronic-conditions (*12*). For all these reasons, the growth of bacterial resistance it's a health problem of outmost concern, but it's not the only one, in fact another significant problem is represented by cancer.

1.2 Cancer: drugs toxicity and resistance

One of the leading causes of death globally is cancer. Although since 1991 cancer mortality has dropped by 26% and the incidence in women and men at the beginning of 2018 was stable and declining respectively, the disease is still a big threat to human health. Especially in low- and middle-income countries, in which cancer mortality represents more than the 70% (*13*, *14*).

Cancer is the product of a deregulated cellular behavior, which allows a cell to escape the normal function and architecture that is characteristic of a given tissue. Tumor cells are therefore capable of unlimited proliferation (immortality), and thanks to the lack of recognition proteins they can spread to distant sites and thus invade different tissues through the metastasis process. A healthy cell can become cancerous from accumulation of deoxyribonucleic acid (DNA) defects and/or mutations, which can be enhanced or provoked by pollution and poor lifestyle choices or they can be inherited genetic tracts.

The global cancer observatory (GLOBCAN) 2018, estimated that 185 countries of the world had 18.1 million new cancer cases, 9.6 million cancer deaths in 2018, and 32.6 million people living with cancer (within 5 years of diagnosis) in 2012 worldwide (*14*, *15*). It is also expected to have 29.5 million new cancer cases and 9 to 15 million cancer deaths every year by 2040 (*16*). Also in 2015, the WHO estimated that in 91 of 172 countries cancer is the first or second cause of death before age 70 years, and it was third of fourth in other 22 countries (*14*).

The cancer treatments used today are surgery, radiations and drugs (chemotherapy). Of these, the last one represents a useful but rarely effective weapon arsenal and, it also comes with a lot of backfire. In fact, they can give temporary relief from symptoms and prolong the patient's life but the side effects of the majority of the drugs employed, such as platinum derivatives that today represent the 75% of anticancer drugs in use, are many and most of the times severe. Those effects can be so severe that the success of the cure itself depends on the ability of the patient's body to handle the drug's toxicity. In general, the patients suffer general cellular damaging which causes nausea, vomiting, myelo-suppression and immune-suppression, as well as more specific damage which results in ototoxicity, nephrotoxicity and hair loss, therefore side effects, are the main cause of failure of cancer treatments. The toxicity of these drugs is due to lack of specificity action, they are too reactive and affect all sorts of tissues. In fact, this may produces allergic reactions making it even more difficult for the patient to outstand the treatment (*17*).

The mechanism of action of these drugs is generally not completely understood, even though for some of them there is some evidence of more specifically targeted structures. For example, drugs like taxanes are said to be microtubule-stabilizing agents (MSAs), which means that they are able to block the cellular mitosis through the inhibition of the formation of the mitotic spindle. In a more chemical level, taxanes can block the polymerization of microtubules that are fundamental for cell reproduction (*18*). Platinum based drugs instead are known to cause apoptosis in cells throughout the distortion of the secondary structure of the DNA, displaying specific enzymes to activate in order to repair the damage, which is usually unrepairable. This causes the

subsequent activation of many proteins (like caspase) and hence the apoptotic signaling which leads to the programmed cell death. But not everything is known of their activity, and cellular targets, it is believed that they may take part into alternative apoptotic signaling (*19*). Another common cause of failure of the anticancer treatments is resistance, acquired or intrinsic. Acquired resistance can appear when chemotherapy goes on for long periods of time, instead intrinsic resistance is a resistance already proper of the type of neoplasia. The acquired resistance of a tumor can negatively affect a treatment that seemed to be having good results; that usually happens in patients with recurring tumors. The appearance of resistance is usually associated to three molecular mechanisms: increased DNA repair, altered cellular accumulation and increased drugs inactivation, which are currently under study (Figure 1.2) (*20*). Since drug resistance has developed rapidly new medicines are always required in order to find more efficient and less toxic new treatments. Hence is necessary to explore the available sources of new molecules and natural products, due to their structural variability and biological activities are likely to be useful.
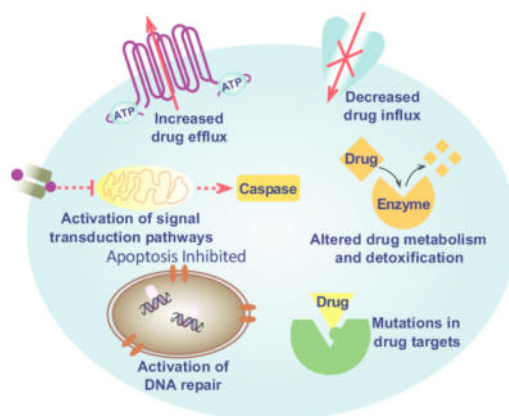
Figure 1.2 Resistance mechanisms in tumor cells (*21*)

1.3 Plants natural products as a potential drugs source

Nature is a vast pool of biologically active molecules. From all the natural sources available, one of the most significant and most used since ancient times is represented by the vegetal kingdom (*22*). Metabolites and biomolecules are of outmost interest in pharmaceutical chemistry, due to their variable forms and activities. Medicinal plants and other natural products have been the first source of drugs, and many of the pharmaceutical products we use today come from isolated natural products from plants (*23*). There are many reports that state the biological activities of the natural products of plants such as antifungal, antibacterial, anticancer, antiviral, anti-inflammatory, anti-infective, antimutagenic, antidiabetic, anti-nociceptive, hypolipidemic, antioxidant, and antimalarial activities (*24*, *25*).

Treatment of diseases like bacterial infection and cancer, need a continuous provision of new drugs, and plants can be a useful source of lead molecules. Many are already in use, for example in cancer therapy there are various useful phytochemicals such as vinka alkaloids, epipodophyllotoxins, taxanes, camptothecins, cephalotaxines and flavones (Figure 1.3). There are also many herbs that if consumed contribute to fight cancer like garlic, ginger, turmeric, green tea, cilantro, and basil.

The WHO has estimated that approximately 80% of people worldwide relay on ethnic medicine for their primary health care. Some of the medicinal plants used around the world have resulted to contain active principles such as taxol and camptothecin. Among other anticancer plants are marijuana

(*Cannabis sativa*), yew (*Taxus baccata*), sunflower (*Helianthus annus*), licorice (*Glycyrrhiza glabra*), etc (*16*).

Phytochemicals with antibiotic activity are divided into several categories. The first category comprehends phenolics and polyphenols, some of which are simple bioactive phytochemicals composed by a single substituted phenolic ring; for example, caffeic and cinnamic acid. Others instead are more complex such as quinones, flavonoids, tannins and coumarins. The molecules in this group are also known for their antioxidant activity, which makes them also protective toward the infected tissue (*26*). In the second category there are terpenoids and essential oils, which represent mostly fragrant unsaponificable lipids. Some essential oils that showed antibacterial activity can be extracted from various plants, such as oregano (*Origanum syriacum* L.), thyme (*Thymus syriacus* L.), and cinnamon (*Cinnamomum zeylanicum* L.). The essential oils of these plants contain terpenoids like thymol which have a good activity against gram-negative bacteria (*27*).

Another category is represented by the alkaloids, which are the most abundant phytochemicals produced by plants and sometimes the reason why they are present is not entirely clear. They have many and different structures and origins, and thus they cannot be classified with a single taxonomic principle. The alkaloids are classified by chemical structure, biochemical origin and/or natural origin. From the chemical structure they are divided in two main groups: the heterocyclic or typical alkaloids and the non-heterocyclic or atypical alkaloids. Some examples of typical alkaloids with antibacterial activity

are quinolines, indoles and phenanthridines (*28*). Other molecules that showed antibiotic capabilities are lectins and polypeptides (*29*).

Plant products and metabolites are numerous and have displayed plenty of useful activities, so this work will focus into the isolation and structural characterization of compounds with antibacterial and cytotoxic activities from *Hechtia glomerata* as well as the determination of mode of action of the most active compound.

Vincristine

Paclitaxel

Epipodophyllotoxin

Camptothecin

Cephalotaxine
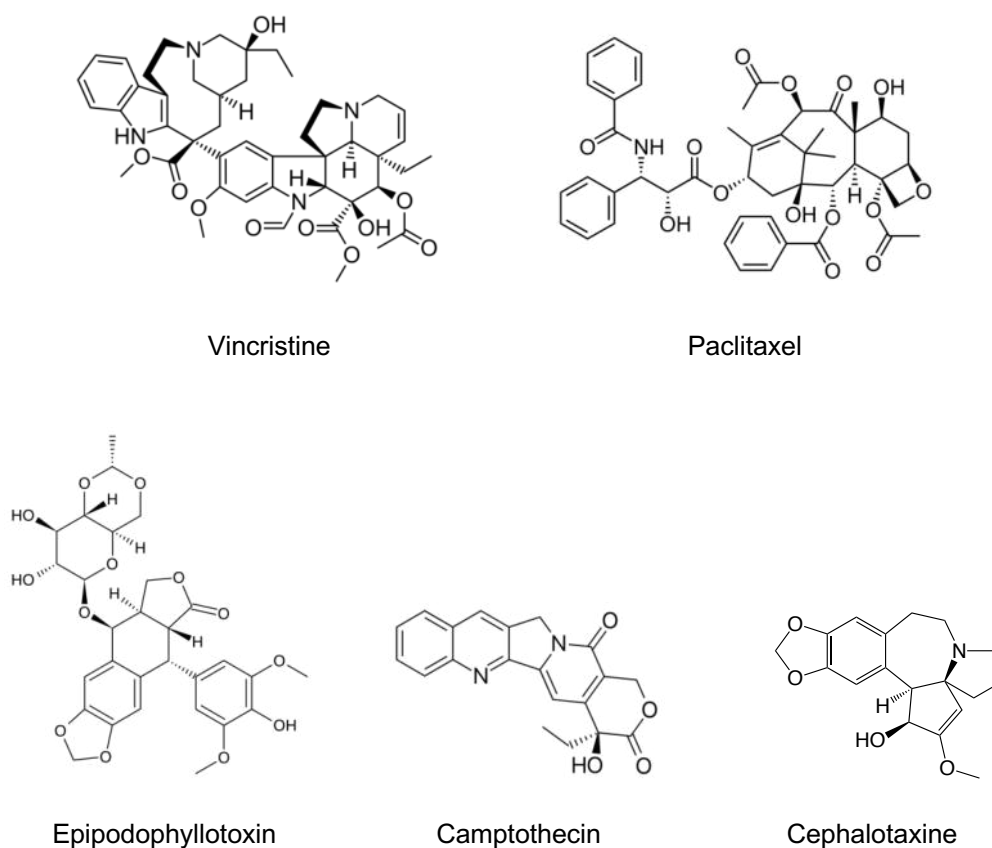
Figure 1.3 Some antitumor natural products derived from plants already in use

CHAPTER 2

2. BACKGROUND

2.1 Bromeliaceae family

The Bromeliaceae family is a large group of angiosperms, monocots, commelinids plants. It comprehends 58 genera and about 3140 species and its divided in eight subfamilies (Figure 2.1): Brocchinioideae, Lindmanioideae, Tillandsioideae, Hechtioideae, Navioideae, Pitcairnioideae, Puyoideae and Bromelioideae (*30*). Almost all the family plants are mainly found in the American continent, except for one species *Pitcairnia felicina* which is from Africa. Some of these plants have been studied and their phytochemicals isolated and characterized (Table 2.1) however their biological activities are yet to be investigated. In Mexico there are 426 species of Bromeliads (*31*) some are widely known, such as pineapple (*Ananas comosus*) and some other have already been studied for pharmacological purposes (*32–37*) and part of their composition has already been elucidated (*38*, *39*). Bromeliaceae are mostly known from their edible fruits, such as *A. comosus* which is the most known and studied among them (*40*).

A molecular common mark of this family are betaines which are always found, even in small concentration (*41*). These kinds of molecules are able to protect proteins and membranes from the osmotic stress effects of high salt and low water concentrations. For example, trimethylglycine and trigonelline (Figure 2.2), which are always found in the family of Bromeliaceae, are two of

a group of compounds known as osmoprotectants. Cells undergoing osmotic stress produce and accumulate additional levels of osmoprotectants such as betaine.

Figure 2.1 Representative species of bromeliads subfamilies (*30*); Brocchinioideae: (a) *Brocchinia prismatica*, Venezuela; (b) *B. reducta*, Venezuela and Guyana; (c) tree-like *B. micrantha*, Venezuela and Guyana. Lindmanioideae: (d) *Lindmania guianensis*, Venezuela and Guyana; (e) *Connellia augustae*, Venezuela and Guyana. Tillandsioideae: (f) *Catopsis berteroniana*, Florida to Brazil; (g) *Guzmania lingulata*, Central and South America; (h) *Tillandsia dyeriana*, Ecuador; (i) *T. setacea* (above branch) and *T. usneoides* (spanish moss, below branch), widespread; (j) *Vriesea heliconioides*, Mexico to Bolivia; (k) *T. ionantha*, flowers, Central America. Hechtiodeae: (l) *Hechtia mooreana*, Mexico; (m) partial inflorescence, *H. rosea*, Mexico. Navioideae: (n) *Navia aff. lactea*, Venezuela; (o) *Sequencia serrata*, Colombia. Pitcairnioideae: (p) *Pitcairnia holstii*, Venezuela; (q) bird-pollinated flowers, *P. undulata*, Mexico; (r) *Deuterocohnia lotteae*, Bolivia; (s) *Encholirium spectabile*, Brazil; (t) *Dyckia lindevaldae*, Brazil. Puyoideae: (u) *Puya chilensis*, Chile. Bromelioideae: (v) *Bromelia macedoi*, Brazil; (w) *Fernseea bocainensis*, Brazil; (x) *Cryptanthus fosterianus*, Brazil; (y) *Neoregelia eleutheropetala* var. Bicolor, tropical America; and (z) *Canistrum alagoanum*, Brazil.

The likely physical basis of the protective effect is the ability of betaine solutions to associate with protein surfaces to help maintain the native protein structure. By maintaining proteins in their hydrated form, they are more likely to function normally, even when in the presence of inhibitory concentrations of salt (*42*). There are also various reports of metabolomic studies of the constituents of *A. comosus*, where many components are reported from the fruit peel, pulp, juice and crown leaves (*39, 43*). The reported metabolites were identified by ultra-high-performance liquid chromatography coupled with mass spectrometry detector equipped with quadrupole and time of flight tandem mass analyzers (UPLC-QTOF-MS). Also, in the plant metabolic network (PMN) are reported 2,162 molecules supposedly identified from *A. comosus* and reported throughout the years (*44*). Other composition of bromeliads reported are *Encholirium spectabile*, *Neoglaziovia variegata* and Macambira (*Bromelia laciniosa*) (*38*). Their volatile compounds were identified by gas chromatography coupled with mass spectrometry (GC-MS).

A. comosus contains, like the most of species of Bromeliaceae, a mixture of enzymes (mostly cysteine proteases) named bromelain (Table 2.1) with promising anticancer activities (*45, 46*). Also water extracts from the crown leaves of pineapple showed high antibacterial activity and wound healing properties (*47*). Even from the solid state fermentation of the pineapple residues, using *Kluyveromyces marxianus* were produced secondary products that could lead to interesting anticancer and antioxidant agents (*48*). With the same activity as the pineapple extracts are the ones from the Flaming Torch (*Billbergia pyramidalis*), which contain an enzyme mixture (cysteine protease)

similar to the bromelain, and that showed antiproliferative effects on malignant cell lines (*49*).
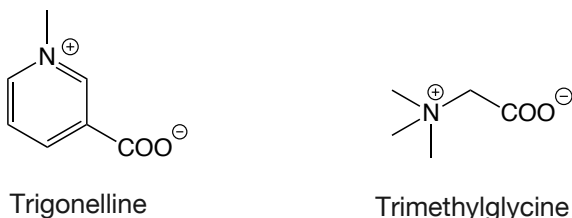
Figure 2.2 Structures of two betaines found in some studied plants of the Bromeliaceae family

Between other plants that have demonstrated some biological activity there is *E. spectabile*, which contains various active phytochemicals such as alkaloids, coumarins, flavonoids and terpenes. The leaves extracts of this plant have shown a good antibacterial and antioxidant activity, especially the ethanol and hexane extracts which contained primarily flavonoids and tannins, lignans, terpenes and steroids (*32*). The chloroform extract of the Jamaican Ball Moss (*Tillandsia recurvata* L.) had interesting anticancer activity against melanoma, breast and prostate cancer; the phytochemicals responsible for antitumor activity were two dicinnamates (*50*). The extracts of *N. variegata* and *B. laciniosa* showed antibacterial activity (*51*) and some metabolites of *Bromelia balansae* has shown antimycobacterial activity (*52*).

Concerning antibacterial and antitumor activity of the phytochemicals from the Bromeliaceae family, some extracts are known to have activity (Table 2.2), evidencing the lack of knowledge about their constituents and biological properties. Since the known plants have already shown antibacterial and anticancer activities, it is more than worth to study and explore the vast possibilities that this family of plants has to offer.

15

Table 2.1 Some species of Bromeliaceae family and their isolated compounds (*41*).
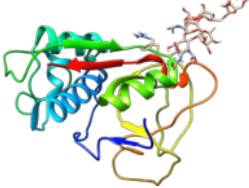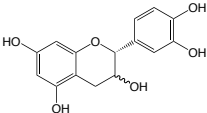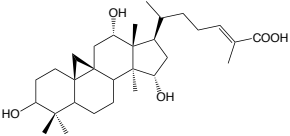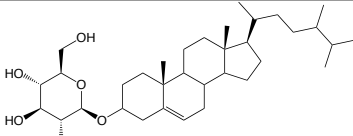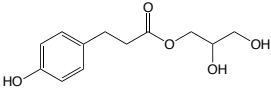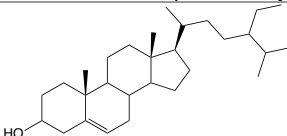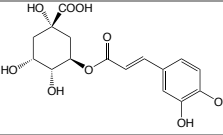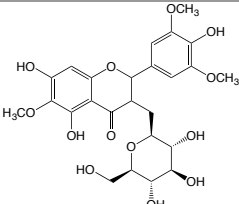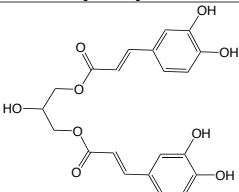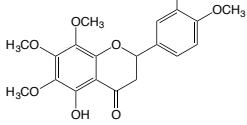
Subfamily	Plant	Constituents
Bromelioideae	*Ananas comosus*	Bromelain Catechin (*S*)/Epicatechin (*R*)
	Ananas comosus var. Cayenne	Ananasic acid
	Ananas erectofolius	Campesteryl 3 -*O*-β-*D*-glucopyranoside
	Greigia sphacelata	1,3-*O*-di-trans-*p*-coumaroylglycerol
Pitcairnioideae	*Hechtia rosea*	β-Sitosterol
	Hechtia scariosa	
Tillandsioideae	*Tillandsia brachycaulos*	Chlorogenic acid
	Tillandsia fasciculata	3-*O*-glicopyranosil-6,3',5'-trimethoxy- 3,5,7,4'-tetrahydroxyflavone
	Tillandsia streptocarpa	1,3-*O*-dicaffeoylglycerides
	Tillandsia recurvata	5-hydroxy-2-(3-hydroxy-4-methoxyphenyl)-6,7,8-trimethoxychroman-4-one

Table 2.2 Extracts of Bromeliaceae species and their biological activities

Plant/part	Extract	Constituents	Biological activity	Reference
A. comosus / fruits, stems, leaves	H_2O, fermented wastes, juice	bromelain	Anticancer, antibacterial	(*46–48, 53*)
B. arenaria / fruits	juice	-	Anticancer	(*54*)
B. antiacantha / leaves, fruits	EtOH	-	Antibacterial, cytotoxic	(*55*)
B. balansae / fruits	MeOH	-	Antioxidant, antimycobacterial	(*52*)
B. laciniosa /whole plant	EtOH	-	Antibacterial	(*51*)
B. pinguin / twigs, leaves	Petroleum ether, EtOAc, EtOH, MeOH, H_2O	-	Anticancer	(*41, 56*)
B. pyramidalis / leaves	Homogenization medium[*] / Cys enzyme	Cys-enzyme	Anticancer	(*49*)
E. spectabile / leaves	EtOH	-	Antioxidant, antibacterial	(*32, 33*)
N. variegata / flowers	EtOH	-	Antibacterial, photoprotective	(*35, 51*)
T. recurvata / whole plant	$CHCl_3$ / Dicinnamates	dicinnamates	Anticancer, antibacterial	(*50*)
T. imperialis / leaves, flowers	Hexane, CH_2Cl_2, MeOH	-	Antibacterial	(*57*)
T. aeranthos / leaves	H_2O	-	Antibacterial	(*58*)
T. usneoides / leaves	H_2O	-	Antibacterial	(*58*)

17

2.2 Chemistry of the Genus *Hechtia*

Figure 2.3 *Hechtia glomerata* Zucc.

The plant under study is known in Mexico as *Guapilla* or *Lechugilla* (*Hechtia glomerata* Zucc.), shown in Figure 2.3. The plant can be easily found in Texas, Mexico (especially the northern states) and Guatemala. It also belongs to the previously cited family of *Bromeliaceae* and like the other plants of its family, is native of Latino America, and because of its vast distribution is considered today the Bromeliad with the larger habitat (*59*). The people from Coahuila, (Mexico) use this plant for the treatment of tumors (personal communication of Biologist M.C. Mauricio González Ferrara). The 19th century medical gazette of Mexico and other two articles reported the use of this plant as food, prepared as flavored waters or as a source of starch. Also it is reported its use, in various preparations, as medicine for treatment of respiratory and urogenital tracts diseases (colds, bronchitis, laryngitis,

whooping cough, nephritis, urethritis and cystitis) (*40*, *60*, *61*). Also, *H. glomerata* is taxonomically related to another phylum of the Bromeliads, the genus *Tillandsia* (*30*) which has already shown anticancer activity (*50*, *62–64*).

H. glomerata is also classified as a crassulacean acid metabolism (CAM) plant, which is common for plants that live in arid environments (*65*). Very little or nothing is known about the chemistry of this plant and the genus *Hechtia*, in which the plant is included. Even if the activity of their phytochemicals is acknowledged indirectly through ethnical medicine there are just few proofs that these plants actually contain bioactive molecules, like and for example compounds with hypoglycemic effects (*66*). In more recent works it has been reported the activities of the infusion of the leaves of the Tlasolmic (*H. podantha*) against dysentery, and the false agave (*H. scariosa* or *H. texensis*; Figure 2.4) as lice shampoo (*67*, *68*).

Figure 2.4 *Hechtia scariosa* (right) and *Hechtia rosea* (left)

From *H. scariosa* and *H. rosea* were isolated two interesting steroids: β-sitosterol and hecogenin (Figure 2.5), both molecules were derivatized.
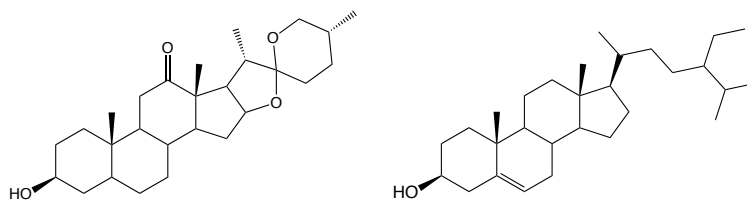
Figure 2.5 Chemical structures of hecogenin (right) and β-sitosterol (left)

Thus, the natural products and semi-synthetic derivatives, showed effects on various carcinomic tissues, with good results in the reduction of cell proliferation (*41, 69, 70*). On our knowledge, the cited activities represent the only pharmacological and phytochemical-related information available in the literature about the genus *Hechtia* (Table 2.3)*. Therefore, it was conducted a review of Bromeliaceae family, with emphasis on the antibacterial and anticancer activities in which this work was centered.

Table 2.3 Ethnical use of *Hechtia* species and isolated compounds

Plant/part	Extraction	Constituents	Ethnical use	Reference
H. glomerata / leaves	Infusion	-	Colds, bronchitis, laryngitis, whooping cough, nephritis, urethritis and cystitis	(*40, 60, 61*)
H. melanocarpa / whole plant	Steam raw	-	Diabetes, hyperglycemia	(*66*)
H. rosea / leaves	Infusion	β-sitosterol hecogenin	Cancer	
H. podantha / leaves	Infusion	-	Dysentery	(*41, 67, 68*)
H. scariosa / leaves	Infusion	β-sitosterol hecogenin	Pests, cancer	

CHAPTER 3

3. SCIENTIFIC CONTRIBUTION, HYPOTHESIS AND AIMS

3.1 Scientific Contribution

The main contributions of this work are in the field of phytochemistry, with the first isolation procedures and characterization of the natural products obtained from *Hechtia glomerata* Zucc. The composition of the organic and aqueous extracts of the plant was also explored by UPLC-QTOF-MS and GC-MS, allowing the performance of the first metabolomic study over this species. It was also investigated if the extracts and the isolated molecules have antibacterial and cytotoxic activities and how they are able to exert these activities.

3.2 Hypothesis

Hechtia glomerata Zucc. has phytochemicals with antibacterial and/or cytotoxic activities, of which one active compound will have a different mechanism of action from those previously reported in the literature.

3.3 Aims

3.3.1 General aim

To perform the phytochemical, bioassay guided isolation and metabolomic study of *Hechtia glomerata*, determine its antibacterial, cytotoxic activity and mechanism of action of one active compound.

3.3.2 Specific aims

1. To investigate the bibliographic information concerning the vegetal specie under study.

2. To dry and ground plant material

3. To prepare organic and aqueous extracts and fractionate them

4. To isolate, purify and structurally characterize the major components of the organic extracts

5. To evaluate the antibacterial and cytotoxic activity of raw extracts and isolated compounds

6. To perform the cytotoxic activity screening of the chloroform/methanol extract fractions

7. To determine the chemical composition of the most active fractions

8. To carry out a metabolomic study of *Hechtia glomerata* Zucc.

9. To identify the mechanism or possible mechanism of action of one active compound

CHAPTER 4

4. MATERIALS AND METHODS

4.1 Material and equipment

Performance of column chromatographies (CCs) was carried out using silica gel (SiO_2) branded EMD chemicals Inc. with a particle size of 0.040-0.063 mm as stationary phase. The mobile phases were solvents as: petroleum ether, hexane (Hex), chloroform ($CHCl_3$), dichloromethane (DCM), Ethyl acetate (EtOAc), acetone, methanol (MeOH) and distilled water (H_2O). All solvents were reactive grade and branded Baker, USA.

Thin layer chromatographies (TLCs) were carried out using silica gel films over aluminum 60 F_{254} of 20x20 cm and 0.2 mm of thickness, and silica gel plates over glass 60 F_{254} of 20x20 cm and 2.0 mm of thickness, branded Merck KGA.

The compounds were revealed using a UV lamp (λ: 254 nm and 365 nm) branded Spectroline, a solution of ceric sulfate stain, a vanillin reagent or Dragendorff's reagent. The determination of melting point was performed using a Fisher-Johns apparatus. The structural elucidation was realized by 1 and 2D NMR nuclear magnetic resonance of hydrogen and carbon (^{1}H and ^{13}C NMR) in a Brüker NMR400 equipment of 400 MHz and using tetramethylsilane as internal standard (TMS).

Other techniques used for characterization were high resolution MS, infrared spectroscopy in a Brüker ALPHA ATR-FTIR spectrometer, X-ray diffraction (XRD) in a Bruker SMART APEX and a Brüker-D2 Phaser and elemental analysis.

Metabolomic study was carried out using an ultra-high-performance liquid chromatography (UPLC) Agilent 1290 with a detector Q/TOF 6545, 2.2 µm hydrophilic polytetrafluorethylene (PTFE) syringe filters (Millipore Sigma & trade Millex^{TM}), the UPLC was equipped with a column ZOBRAX Eclipse Pluse C18 HD 2.1 x 50mm and 1.8 µ pores; all the solvents used in the process were high-performance liquid chromatography (HPLC) grade; the employed databases for the compound identification were METLIN Mass Spectral Database, PubChem, The Human Metabolomic Database (HMDB), Lipid Maps, PhytoHub, ReSpect for Phytochemicals, Knapsack and Plant Metabolomic Network (PMN); the statistical analysis was performed using the online platform MetaboAnalyst 4.0.

For the antibacterial activity assays were used bidistilled water, dimethylsulfoxyde (DMSO) (J.T.Baker, USA), Mueller-Hinton broth (Difco), blood agar base (HIMEDIA), defibrinated sheep blood (E&O Laboratories), normal laboratory glassware and plastic materials (testing tubes, petri dishes, 96-wells microplates, etc.), Incubator INC-80 (Prendo), Freezer -80°C (Panasonic). Microplates were read with a Bio Rad LightOne Illuminator.

Anticancer assays were performance used milli q water, DMSO (J.T.Baker, USA), RPMI 1640 or Dulbecco's modified essential medium (DMEM) (Corning), Freezer -80°C (Panasonic), Freezer -20°C (Panasonic), Refrigerator 4°C (Panasonic), Laminar flow hood (BIOBASE), vacuum pump

(Fisherbrand), Invertoscope (Carl Zeiss). Microplates were read with a BioTek ELx800 Absorbance Microplate Reader.

For the microarray assay, RNA was extracted using TRIzol™ Reagent (Invitrogen). The RNA quality was done on agarose gel (1%), and total RNA was quantified with an Eppendorf 6131 biophotometer (Eppendorf, Hauppauge, NY, USA). The cDNA was synthetized for both treated and untreated control. Then hybridization was carried out on a H35K chip (UNAM) in a hybridization chamber G2534A (Agilent, Santa Clara, CA, USA). The hybridized chip was read with a laser confocal read system ScanArray 4000 (Packard BioChips Technologies (Massachusetts 01821, USA). The obtained data was processed with Array-Pro analyzer 6.3.

In silico analysis were done in three UNIX based machines, with 8 and 32 cored processors. Programs used for the molecular docking were AutoDock 4.0 and Chimera v1.13.1 (Reagents of the University of California). Molecular dynamics simulations were carried out using the programs Schrödinger release 2019-3: Desmond Molecular Dynamics System, (D. E. Shaw Research, New York, NY, 2019) and Maestro-Desmond Interoperability Tools, (Schrödinger, New York, NY, 2019).

4.2 Phytochemistry of *Hechtia glomerata*

Phytochemical study was carried out in the Natural and Synthetic Products (PNS) Laboratory, Division of Postgraduate Studies, Faculty of Chemical Sciences (FCQ), Universidad Autónoma de Nuevo León (UANL).

4.2.1 Plant material preparation and maceration

Plant selected for this study was collected in Rayones, Nuevo León, Mexico, (25°01′00″N 100°05′00″O, 906 m a.s.l.), on February 15th, 2017 and identified by the biologist Mauricio González Ferrara. The vegetal material was composed of aerial parts with their roots one of them was selected (in base of its integrity and size) and was sent to the herbarium of the faculty of biology of the UANL. The plant was there characterized and coded with the voucher number 028029.

The rest of plant material was cleaned and then the roots and pinecone were separated from the leaves. Leaves (10.5 Kg) and roots (1.5 Kg) were dried in darkness. Afterwards they were first ground in a coffee grinder and then in a blender. This process reduces the particles size and gains the largest contact surface, leading to the optimization of the extractions. Subsequently, the ground leaves were weighted (1.985 kg) and transferred into a 15 L carboy, which was labelled with the plant's name. Then approximatively 10 L of hexane were added, and it was left at room temperature (r.t.) for 48 hours. At the end of the extraction time, the vegetable material was separated from the organic extract by filtration, first by gravity and then under vacuum. The hexane extract was distilled under reduced pressure into a rotary-evaporator. The dried extract was weighted (9.5 g) and kept in a flask away from the light at 4°C until its use. Then, recovered vegetable material was extracted by maceration with a 10 L chloroform/methanol (1:1) mixture six consecutive times (until the extract resulted clear), the extracts were filtrated, distilled under vacuum, combined, weighted (85 g) and kept in a flask at -20°C. At last 20g of the vegetable material was also macerated for 24 hours in distilled water (250 mL)

at 4°C to prevent fermentation. Then the extract was filtrated, lyophilized, weighted (2.1010 g) and kept in a flask at -20°C in the dark. On the other hand, 300 g of fresh vegetable material was blended with distilled water, filtered and the aqueous extract was lyophilized, weighted (8.3799 g) and kept at -20ºC until its use. For the roots the same procedure of extraction was used, the only difference was in the quantity of processed vegetal material (100 g) and the absence of fresh aqueous extract. The hexane extract resulted in 164.2 mg (0.16 % yield), the $CHCl_3/MeOH$ extract gave 3.4230 g (3.42 % yield) and the aqueous extract 153.9 mg (0.15 % yield). The whole procedure of the preparation and maceration of the vegetal material, as explained in this paragraph, are schematized in the following flux diagrams (Scheme 4.1 and Scheme 4.2).

Ground fresh leaves
10.5Kg

Dried vegetal
material 2.29Kg

Extraction of fresh
leaves

Hexane
maceration

Lyophilization

Fresh leaves aquous
extract 8.3799g

Recovered vegetal
material

Hexane extract

CHCl$_3$/MeOH 1:1
maceration (x6)

Distillation

Dryed hexane
extract 9.5g

Recovered vegetal
material

CHCl$_3$/MeOH
extract

H$_2$O   maceration

Distillation

Dryed
CHCl$_3$/MeOH
extract 85g

Aquous extract

Lyophilization

Dryed Aquous
extract 2.1010g

Scheme 4.1 Flux diagram of the leaves' extraction process

Dried ground roots
100 g

Hexane maceration

Recovered vegetal material

Hexane extract

CHCl₃/MeOH 1:1 maceration (x5)

Distillation

Dryed hexane extract 164.2mg

Recovered vegetal material

CHCl₃/MeOH extract

H₂O maceration

Distillation

Dryed CHCl₃/MeOH extract 3.423g

Aquous extract

Lyophilization

Dryed Aquous extract 153.9mg
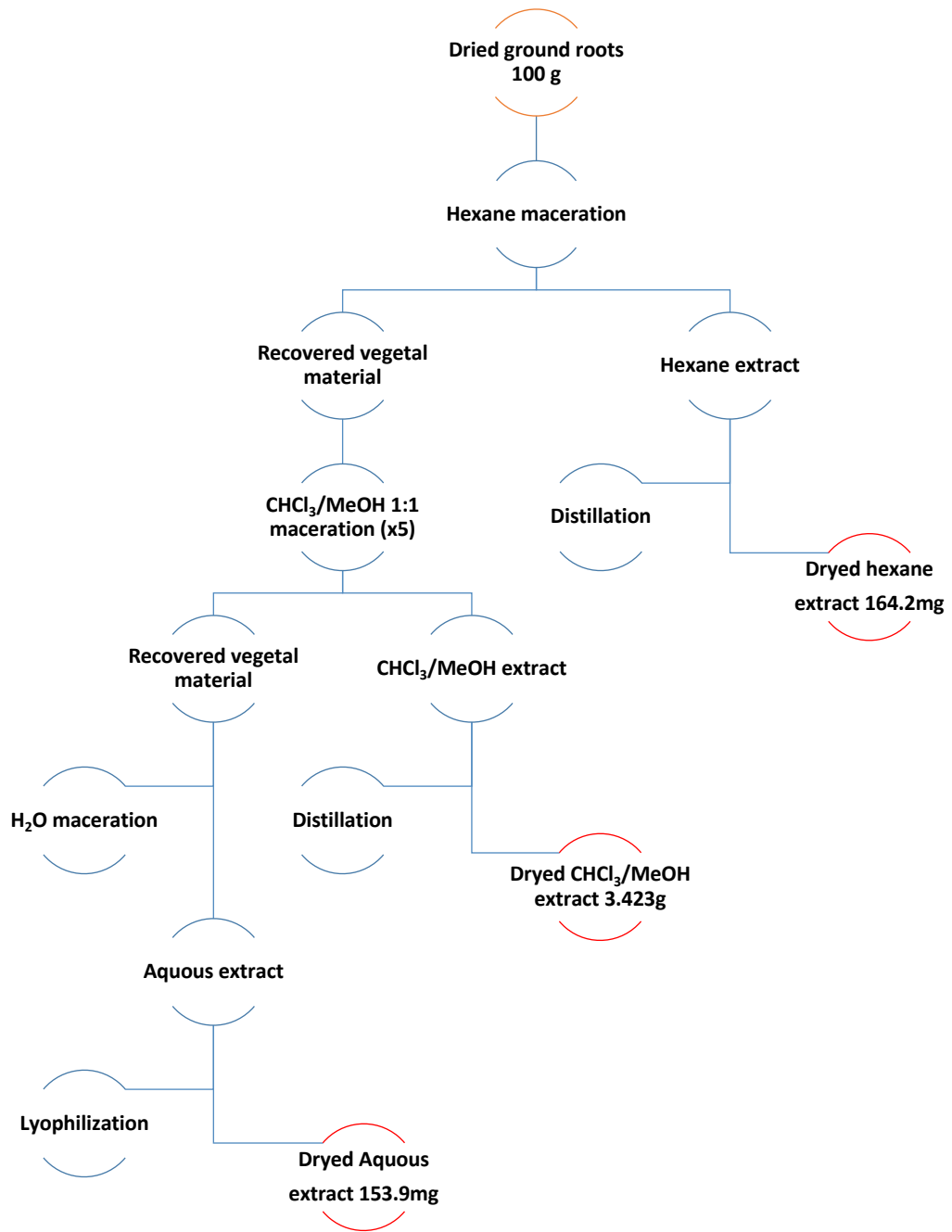
Scheme 4.2 Flux diagram of the roots' extraction process

4.2.2 Fractionation of the leaf hexane extract

Hexane extract (9.5 g) was first analyzed by thin layer chromatography (TLC) observing the TLC plates under UV light and sprayed with ceric sulfate. It was then decided to fractionate it by column chromatography using silica gel (190 g) as stationary phase and a gradient of hexane/ethyl acetate as mobile phase. A total of two-hundred and twenty-six fractions were obtained and observed under UV lights and with the developing reagents. They were pooled into sixteen fractions according to their chromatographic similitude and were treated with different chromatographic techniques (Table 4.1).

Table 4.1 Fractions of hexane extract

Fractions		Polarity	Isolated compound
1-5	A	100% Hexane	1
6-28	B	100% Hexane	-
29-44	C	98:2 Hex/EtOAc	2
45-65	D	96:4 - 94:6 Hex/EtOAc	-
66-84	E	94:6 - 92:8 Hex/EtOAc	-
85-88	F	92:8 Hex/EtOAc	-
89-124	G	90:10 Hex/EtOAc	3-4
125-137	H	90:10 - 85:15 Hex/EtOAc	5
138-151	I	85:15 - 80:20 Hex/EtOAc	-
152-161	J	70:30 Hex/EtOAc	-
162-170	K	60:40 Hex/EtOAc	-
171-179	L	50:50 Hex/EtOAc	-
180-192	M	50:50 Hex/EtOAc	-
193-212	N	40:60 Hex/EtOAc	-
213-219	O	100% EtOAc	-
220-226	P	100% MeOH	-

4.2.3 Isolation and purification of phytochemicals

4.2.3.1 Isolation and purification of nonacosane (1)

Compound 1 precipitated from the fraction A as a white amorphous wax-like solid (178.2 mg, 0.00008977%). Then it was analyzed by TLC with three different systems (Hex/EtOAc, Hex/CHCl$_3$, Petroleum ether/EtOAc) to determine the purity. The compound does not reveal under UV light and it was found pure with ceric sulfate, revealing as a brown spot.

4.2.3.2 Isolation and purification of hexatriacontanyl stearate (2)

The compound was cleaned and separated from the other components of the fractions C, D, E and F by washing it consecutively with cold hexane, until it was white. It appeared as a white wax-like solid (266.8 mg, 0.00011426%), it was also observed by TLC with three different systems (Hex/EtOAc, Hex/acetone, Hex/CHCl$_3$) to determine purity. It did not reveal under the UV light, but it was found pure with ceric sulfate as well, developed as a dark brown spot.

4.2.3.3 Isolation and purification of hexacosanol (3)

This compound crystalized as a white translucent solid from the fraction G, and it was cleaned deeply by sucesivelly crystallizations in CHCl$_3$ as well as isocratic column chromatography (CC) with 2.34 g of silica gel and eluted with a gradient of Hex/DCM. From this column was obtained 29.3 mg (0.00001476%) of hexacosanol. The purity compound was determined by bi-dimensional (2D) TLC: 7x7 cm eluted first with a 7:3 DCM/Hex mixture and

then perpendicularly with an 85:15 Hex/EtOAc mixture. The alcohol barely developed with the UV light as a light-blue stain and with ceric sulfate as a black stain.

4.2.3.4 Isolation and purification of oleic acid (4)

It was separated and purified by a preparative TLC, from the fraction G. TLC was done on silica gel glass plate 20 x 20 cm. Once the sample (max 100 mg) was deposited on the plate it was eluted with 85:7.5:7.5 Hex/Acetone/acetic acid, then the plate was observed under the UV light in order to localize the desired compound (reveals as light-blue flame in the 365 nm UV light). The silica containing the compound was then scratched from the plate and macerated four times in 90:10 $CHCl_3$/MeOH for 30 minutes. The recovered palmitoleic acid (17.7 mg, 0.00000892%) was a colorless oil and its purity was determined by TLC with three different systems (DCM/Hex, Hex/EtOAc, Hex/Acetone/Acetic acid) and 2D TLC: 7x7 cm eluted first with 70:30 DCM/Hex and then perpendicularly with 85:7.5:7.5 Hex/Acetone/acetic acid. Also, the compound revealed as a black flame with ceric sulfate.

4.2.3.5 Isolation and purification of β-sitosterol (5)

It was separated with good purity from fraction H by a gradient CC with 11 g of silica gel as SP and a gradient of Hex/EtOAc. The compound presented itself as a whitish-yellow amorphous solid (271.3 mg, 0.00013668%) that crystalized in $CHCl_3$. The compound purity was also determined by 2D TLC: 7x7 cm and eluted first with a 7:3 Hex/EtOAc and then perpendicularly with a

9:1 CHCl$_3$/EtOAc. β-Sitosterol did not revealed at 254 and 365nm UV light, but it revealed as a purple flame with ceric sulfate.

4.2.4 GC-MS analysis of leaf hexane extract and isolated compounds

Hexane extract and compounds 1-7 were analyzed by GC-MS using an HP-5MS GC capillary column (30 m x 0.25 mm x 0.25 μm film thickness). Helium was used as carrier gas at a flow rate of 1.0 mL/min; the ion source and splitless injector were at a temperature of 230°C and 250°C, respectively and the volume of injection was 1-2 μL of a solution of 1 mg/mL of extract or isolated compounds in CHCl$_3$. Oven temperature was programmed from 50°C to 285°C at a ramping rate of 2°C/min. Electron ionization energy was set at 70 eV, and fragments from 1 to 3000 Da were collected. The instrumental conditions of the analysis are reported in the Table 4.2.

Table 4.2 GC-MS experiment conditions

Parameter	Condition
GC column	HP-5MS pf 30m x 0.250mm x 0.25μM
Carrier gas	Helium, 1mL/min, constant flux
Hoven	50°C-0min, 2°C/min-285°C-35min
Injector	250°C, splitless
Detector	MSD
Ionic source	230°C

The reported results are referenced on the base of the NIST library version 1.7[a].

Were also calculated the relative retention indices (Equation 4.1) of the compounds.

$$I = \left[\frac{t'_{r(unknown)} - t'_{r(n)}}{t'_{r(N)} - t'_{r(n)}} \right] \times (100 \times z) + (100 \times n)$$

Equation 4.1 Retention index for gradient limits in GC experiments

4.2.5 Fractionation of the leaf CHCl$_3$/MeOH (1:1) extract

Chloroform/methanol extract (87 g) was first analyzed by TLC under UV light and revealed with ceric sulphate. It was then decided to fractionate it by column chromatography using silica gel (2 Kg) as stationary phase and a gradient of hexane/ethyl acetate/MeOH/H$_2$O. A total of 241 fractions were obtained and observed under UV light and with developing reagents. They were pooled for chromatographic similitude into 19 final fractions (Table 4.3). For biological assays the fractions were reunited into 8 macro-fractions in order to simplify their evaluation (Table 4.4).

Table 4.3 Fractions of CHCl$_3$/MeOH (1:1) extract

Fractions		Polarity	Isolated compound
1-12	A	100% Hexane	6
13-24	B	100% Hex - 90:10 Hex/EtOAc	-
25-26	C	90:10 - 80:20 Hex/EtOAc	-
27-39	D	80.20 - 70:30 Hex/EtOAc	7-8
40-66	E	70:30 - 50:50 Hex/EtOAc	-
67-72	F	50:50 - 30:70 Hex/EtOAc	
73-78	G	20:80 Hex/EtOAc	9-10
79-102	H	20:80 Hex/EtOAc	
103-110	I	20:80 - 100% EtOAc	-
111-121	J	90:10 - 70:30 EtOAc/MeOH	11
122-132			
133-138	K	70:30 - 60:40 EtOAc/MeOH	-
139-150	L	60:40 - 50:50 EtOAc/MeOH	-
151-162	M	50:50 - 40:60 EtOAc/MeOH	-
163-174	N	40:60 - 30:70 EtOAc/MeOH	-
175-186	O	30:70 - 20:80 EtOAc/MeOH	-
187-210	P	20:80 - 10:90 EtOAc/MeOH	-
211-222	Q	100% MeOH - 95:5 MeOH/H$_2$O	-
223-240	R	90:10 - 50:50 MeOH/H$_2$O	12
241	S	50:50 MeOH/H$_2$O	

Table 4.4 Pooled fractions of CHCl$_3$/MeOH (1:1) extract

Pooled fraction		Solubility	Polarity
1-24	1	Hexane/hot CHCl$_3$	Lowest
25-66	2	CHCl$_3$	Low
67-102	3	Acetone	Medium
103-121	4	Acetone	Medium
122-138	5	Acetone/MeOH	Medium-high
139-162	6	MeOH	high
163-240	7	MeOH	high
241	8	MeOH/H$_2$O	highest

4.2.6 Methylation of pooled fraction 1

Fraction 1 (27.3 mg) was added to a 20 mL vial and were dissolved in 1 mL of toluene. Then it was added to the stirring solution 1 mL glyceryl triundecanoate as internal standard (0.1005 g in 25 mL toluene) and 2 mL of sulfuric acid 7% solution in MeOH. The vial was heated in a water bath at 80 °C for 1.5 h then let cool at room temperature. To reaction was added 4 mL hexane and the mixture was stirred 1 minute in a vortex. The vial was keep until the separation of phases occurred. The organic phase was dried with Na$_2$SO$_4$ anhydrous and transferred into a 10 mL volumetric flask. To the aqueous phase was added other 4 mL of hexane and the extraction was repeated. The second organic phase was also dried with Na$_2$SO$_4$ anhydrous and added to the first one. The pooled organic phase was then brought to a final volume of 10 mL with hexane.

4.2.7 Isolation and purification of phytochemicals

4.2.7.1 Isolation and purification of heneicosane (6)

It was recovered from fraction A, a white wax-like precipitate (206.2 g, 0.00010388%). The compound does not reveal under UV light and it was found pure with ceric sulfate, revealing as a brown spot.

4.2.7.2 Isolation and purification of triacontanol (7)

From fraction D, it was recovered a white crystalline solid. The solid was washed several times with hexane and cold chloroform in order to eliminate the other less polar components of the fraction. The white crystals were filtrated and air dried giving a white sticky solid which was not visible under UV light but revealed with ceric sulfate. It was obtained in high purity (55.0 mg, 0.00002771%).

4.2.7.3 Isolation and purification of *p*-coumaric acid (8)

From fractions F-H, it was recovered a white-yellowish amorph solid. The solid was washed several times with hexane and cold chloroform in order to eliminate the other less polar components of the fraction. The white-yellowish solid was filtrated and air dried giving a whitish solid which was visible under UV light as a dark spot (254 nm) and revealed with ceric sulfate. It was obtained in high purity (6.6 mg, 0.0003%).

4.2.7.4 Isolation and purification of margaric acid (9)

From fractions F-H, it was recovered a pinkish amorph solid. The solid was washed several times with methanol in order to eliminate the other more polar components of the fraction. After the solid was washed it was air dried giving a whitish solid which was not visible under UV light but revealed with ceric sulfate. It was recovered in low purity (12.4 mg, 0.0006%).

4.2.7.5 Isolation and purification of caffeic acid (10)

From fraction I it was recovered a greenish amorph solid precipitate. The solid was then separated from the other components of the fraction by preparative TLC. Then it was purified with CC, still retaining some decomposition byproducts. Once the greenish solid was dried *in vacuo* it gave a green solid which was visible under UV light as a dark spot (254 nm) and revealed with ceric sulfate. It was obtained in high purity (3.0 mg, 0.0002%).

4.2.7.6 Isolation and purification of daucosterol (11)

The compound precipitated from fraction J as a white solid and it was washed with methanol several times, submerging the methanol suspension of the dirty compound in an ultrasounds bath for 15 minutes. The procedure was repeated until the solid resulted completely white and the methanol colorless. It was recovered with high purity (272.0 mg, 0.00013703%).

4.2.7.7 Isolation and purification of KCl (12)

Potassium chloride precipitated during the drying of the whole extract, and it was washed first first with CHCl$_3$ and then with MeOH until it was white. The process was repeated every time that a new volume of the (10 L) extract was concentrated by rotatory evaporation. Then the solid was recovered from the flask using methanol and an ultrasounds bath. The solid was then filtrated *in vacuo* resulting in 2.2787 g (0.00114796%). The compound does not reveal under the UV light or with ceric sulfate.

4.2.7.8 X-ray analysis of KCl (12)
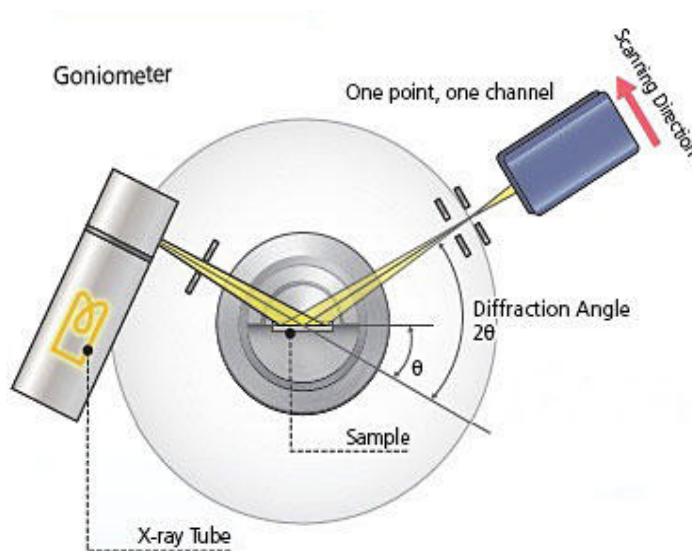
Figure 4.1 Example of XRD analysis

For the characterization of KCl isolated from the CHCl$_3$/MeOH extract an X-ray diffraction was necessary. The analysis was conducted first with the pure dusted crystalline compound confronting with the in-house database the obtained diffractogram (exploring XRD analysis).

Table 4.5 Exploring XRD analysis conditions

Experimental Condition of Exploring XDR Analysis	
2θ Range	5°- 90°
Step	0.050°
Step time	1.1 seconds
Temperature	25°C

The conditions for the IS-XRD analysis are reported in table 4.5. Once a matching compound was found its identity was confirmed by the addiction of an internal standard to the pure compound 12 (IS-XRD analysis). The conditions for this experiment are reported in table 4.6.

Table 4.6 IS-XRD analysis conditions

Experimental Condition of IS-XDR Analysis	
2θ Range	5°- 90°
Step	0.050°
Step time	2.0 seconds
Radiation of X-ray Tube (CuKα)	$\lambda = 1.5418$ (average α_1 and α_2)
Compound 12 crystalline solid	93.23%
KCl (IS)	6.76%

4.2.8 Fractionation of the leaf dry aqueous extract

The dry aqueous extract (972.3mg) was first analyzed by TLC (normal and reverse phase) observing the chromatographic plates under UV light and revealed with ceric sulfate. It was then decided to fractionate it by flash chromatography using a C18 reverse phase cartridge as stationary phase and a gradient of MeOH/H_2O as mobile phase. A total of 6 soluble fractions plus a part of the extract that resulted non-soluble in the hydro-alcoholic eluent were obtained and observed under UV light and with the developing reagents. They were pooled for chromatographic similitude into 5 final fractions (Table 4.7).

Table 4.7 Fractions of the dry aqueous extract (1:1)

Pooled	fraction	Polarity
1	A	50:50 H_2O/MeOH
2	B	60:40 H_2O/MeOH
3	C	70:30 H_2O/MeOH
4-6	D	80:20-100% H_2O/MeOH
7	E	H_2O soluble

4.3 Derivatization of the isolated compounds

4.3.1 Acetylation of β-sitosterol (5)
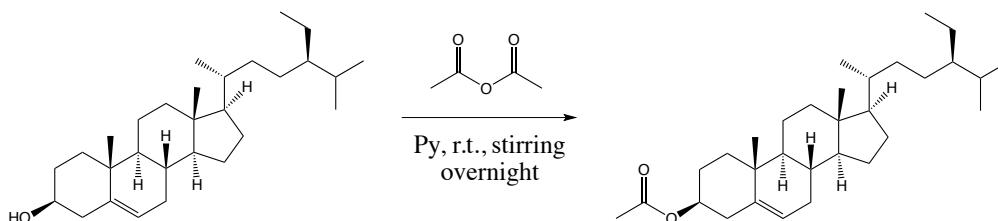
Figure 4.2 Acetylation of β-sitosterol

β-sitosterol (25.3 mg, 0.06 mmol) was added in a 7 mL vial, then 0.5 mL of pyridine was poured into the vial and the mixture was maintained in constant agitation. At this point 0.5 mL of acetic anhydride were added drop wise to the stirring solution (final concentration: 0.06 M), then the reaction was left stirring overnight at room temperature (r.t.). The reaction mixture was then diluted in 10 mL CHCl$_3$ and washed four times with a 10 mL HCl 10% solution to eliminate the pyridine. The organic fraction was then dried with anhydrous sodium sulfate and concentrated under reduced pressure to give 27.3 mg (0.06 mmol) of acetylated product. The yield of the reaction was > 99%. A schematic representation of the reaction is shown in figure 4.2.

4.3.2 Acetylation of daucosterol (11)
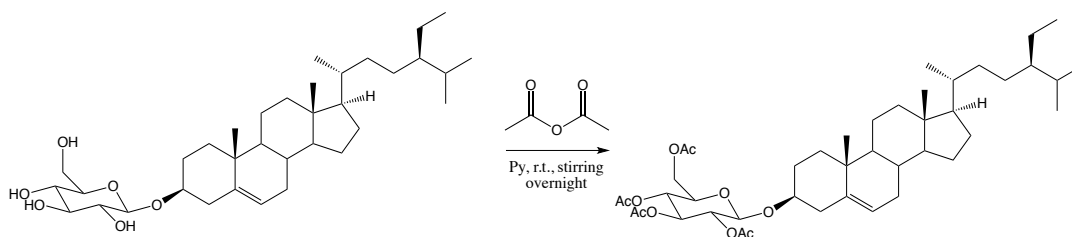
Figure 4.3 Acetylation of β-sitosteryl β-*D*-glucopyranoside (daucosterol)

Daucosterol (29.7 mg, 0.05 mmol) was added in a 7 mL vial. Then 0.3 mL of pyridine was poured into the vial and the mixture was maintained in constant agitation, until the solid was completely solubilized. At this point 0.7 mL of acetic anhydride were added drop wise to the stirring solution (final concentration 0.05 M), then the reaction mixture was left stirring overnight at room temperature (r.t.). The reaction mixture was then diluted in 10 mL CHCl$_3$ and washed four times with a 10 mL HCl 10% solution to eliminate the pyridine. The organic fraction was then dried with anhydrous sodium sulfate and concentrated under reduced pressure to give 33.8 mg (0.05 mmol) of acetylated product. The yield of the reaction was of 91%. A schematic representation of the reaction is shown in figure 4.3.

4.3.3 Methylation of oleic acid (4)
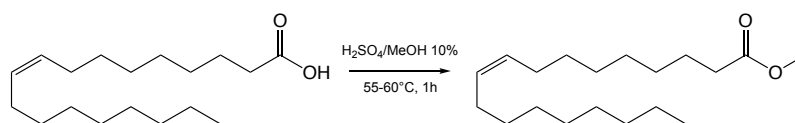
Figure 4.4 Methylation of oleic acid (C18:1, Δ^9)

Oleic acid (3.3 mg, 0.01 mmol) was added in a 7 mL vial. Then 0.1 mL of toluene was poured into the vial and the mixture was maintained in constant agitation, until the solid was completely solubilized. At this point 0.1 mL of a solution of H_2SO_4 in MeOH at 10% were added drop wise to the stirring solution (final concentration 0.06 M), then the reaction mixture was left stirring overnight at room temperature (r.t.). The reaction mixture was then diluted in 10 mL EtOAc and washed four times with a 10 mL NaCl 5% solution, then it was washed once with $NaHCO_3$ to neutralize the pH. The organic fraction was then dried with anhydrous sodium sulfate and concentrated under reduced pressure to give 3.8 mg (0.01 mmol) of acetylated product. The yield of the reaction was of >99%. A schematic representation of the reaction is shown in figure 4.4.

4.4 Metabolomics

4.4.1 UPLC-QTOF-MS analysis

Hexane, $CHCl_3$/MeOH (1:1), dry and fresh aqueous extracts were solubilized in a mixture of MeOH and H_2O (1:1) HPLC grade by sonicating. Samples were then centrifuged twice for 5 minutes at 10,000 revolutions per minute (rpm) and then the solutions were filtered through 2.2 µm syringe filters.

Once the solutions were ready, they were injected by an automatic sampler into the column of UPLC equipment. The extracts were eluted with a gradient of H_2O and methanol, for 11 minutes with constant flow and pressure (Table 4.8).

Table 4.8 UPLC elution parameters.

Time	H_2O	MeOH	Flow	Pressure
6.00	0.00 %	100.00 %	0.250 mL/min	900.00 bar
10.00	0.00 %	100.00 %	0.250 mL/min	900.00 bar
11.00	70.00 %	30.00 %	0.200 mL/min	900.00 bar

The retrieved data was first analyzed by the equipment library METLIN. Then all the compounds that were not possible to identify were then investigated throughout various plant natural products databases. They were finally identified by comparison of their molecular weights with the reported ones.

4.4.2 Statistical analysis

Data obtained from UPLC-Q/TOF-MS analysis was submitted in the platform MetaboAnalyst 4.0. The modules employed were the Statistical

Analysis, which comprises various statistical and machine learning methods and the Integrating Enrichment Analysis and Pathway Topology Analysis for the metabolic pathway visualization. Each compound of the four extracts was reported on a table with their abundances in triplicate, in a dummy variable file fashion. The latter contains an abundance value or a zero, indicating the presence or the absence of a compound from a certain extract. In base of their abundance the program generates a series of scores which are then used to obtain a graphical comparison of the extracts. Once the table of the compounds was submitted the data was normalized using the default normalization parameters of the program. Different set of normalization parameters were tried in order to give the best result. At the end a logarithmic normalization was selected, together with the mean centering of the data. Also, a second table containing the compound classes was created and submitted to the program.

After normalization the data finally underwent various statistical analysis: principal component analysis (PCA), analysis of variance (ANOVA) and metabolic pathways analysis. The latter was also used in the validation of cytotoxicity results.

4.4.2.1 Analysis of variance (ANOVA)

The analysis of variance or ANOVA (*71*) is a statistical test with the objective of determining the difference between two or more groups of variables. ANOVA checks the impact of one or more factors by comparing the means of different samples. It consists first in the calculation of the comparing factors: number of groups, sum of variables, average of variables and variance

among each group variables. Then these values are used "between group variability" and "within group variability" (Figure 4.5), which are the main indicators of the presence or absence of a difference among the samples.
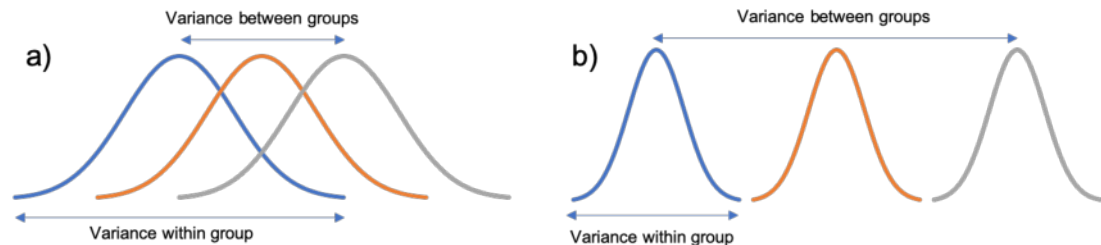
Figure 4.5 Variance between groups and within group for a null hypothesis (a) and a non-null hypothesis (b)

To calculate these values the means (μ_n) and grand mean (μ, mean of sample means) of each sample were calculated and used to obtain their squared standard deviations (SS). The SS were also multiplied by each sample size in order to give more weight to the larger samples. This was done for both variabilities obtaining the sum-of-squares for between-groups and within-group (SS_b and SS_w). Then the degrees of freedom are calculated for between (df_b) and within (df_w) group variabilities which are the number of samples means and the sum of the sample sizes minus the number of samples respectively. Then each SS is divided by its own df to obtain the mean square for within (MS_w) and between (MS_b) groups variabilities. All these calculated variables are a statistical estimation of the difference among the considered samples. This difference is also represented, in more general way, by two variables which are F-ratio (F) also called F-statistic and F-critical (F_{crit}). F is the ratio of between groups and within group variabilities, instead F_{crit} is considered as the cut-off value of the significance level (α). To represent F_{crit} the F values of multiple experiments must be plotted into a diagram called F-

distribution (Figure 4.6). The F_{crit} value represent the beginning of an area of the plot called critical region which represent the probability of a null hypothesis based on α (0.05). Therefore, for a hypothesis to be null the value of F must be lower than the value of F-critical and fall in the critical region, while a non-null hypothesis must have and F with a higher value. Another way to evaluate the ANOVA result is by checking the p-value, if it is lower than the selected α value the null hypothesis is rejected.
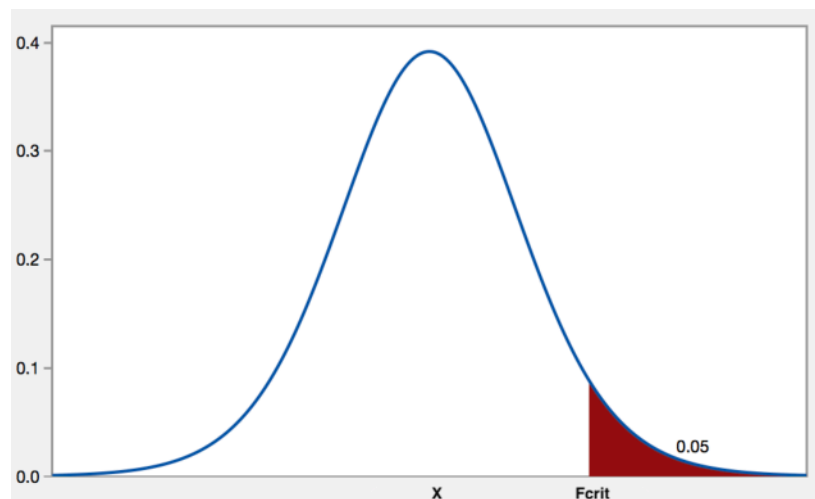
Figure 4.6 F-distribution with F-critical and critical area

A One-Way, Two-Way and Three-Way ANOVA were used in the statistical manipulation of the cytotoxicity data since the experiments were conducted with the same conditions and on the same population. For the interpretation of the One-Way ANOVA results a t-test was employed, because the statistical analysis only gives as a result that at least two groups of samples are different from one another. The t-test allows a much specific comparation of two selected samples, giving their difference with one another. The term used to determine this aspect is the p-value calculated for both edges of the distribution or "tails". If the p-value is lower than α level selected (0.05) than

the two compared samples are probable to belong to two entirely different populations. The magnitude of their difference depends on the extent of their numerical variance (*72*). In the metabolomic study the ANOVA was performed by the open access web platform MetaboAnalyst v4.0 (*73*). And the results were represented in various ways, the most intuitive being the hierarchical clustering (dendrogram and heatmap). The latter was obtained through the measure of the differences and similitudes among the extracts, which was given by the Euclidean measure and the Ward clustering algorithm. All results of the cytotoxicity assays were processed through ANOVA analysis performed with the software Prism v8.2.1.

4.4.2.2 Principal component analysis (PCA)

The principal component analysis (PCA) is a statistical method often employed in unsupervised metabolomic approaches. It consists in a multivariate analysis that allows the visualization of the relationships among large data sets. Data needs to be normalized and centered (often mean-centered) before the statistical analysis. Then the values are transformed into a set of linearly correlated variables called principal components. These components are defined so that each one of them contains the highest level possible of variance. This way the system is described by the lowest number of orthogonal coordinates it requires. The results of the analysis are showed in the form of two- or three-dimensional plot of the generated component scores (factor scores) against the orthogonal components. The simplicity of results allows a more direct and intuitive analysis of the system's differences. PCA can be used for supervised and reinforcement learning, such as

classification or regression, clustering and dimensionality reduction. It can also detect abnormalities in a large set of data and predict structured object, which is used in machine learning and data mining. Mostly PCA is employed in explorative data analysis, like in this work, and to make predictive models.

4.4.2.3 Pathway analysis

In the pathway analysis the identified compounds of a sample or extract, either by their names or IDs (KEGG, HMDB and PubChem), are confronted with the metabolites of another similar organism. In the database are also reported the biosynthetic and metabolic pathways of each metabolite for the selected organism. When an identified compound matches one in the database, its biosynthetic pathway is also shown. This generates a plot reporting the matched metabolites over their pathway impact. The latter reflects the number of compounds matched and the compound identity. The more identified compounds match the metabolites in the database and the more central is the role of the compound in the organism metabolism, the higher is the final score. The result of the analysis is a two-dimensional plot, reporting each identified metabolic pathway as a dot. The dots with higher score are bigger and shifted at higher pathway impact values and are considered the main pathways represented by the identified compounds.

4.5 Biological assays

The antibacterial activity assay of phytochemicals and raw extracts were done in the Department of Gastroenterology of the University Hospital of the UANL. Instead the cytotoxic activity of the raw extracts was done in the Faculty of Pharmacy, Universidad Autónoma del Estado de Morelos. At last the mechanism of action assay was done in the laboratory of Genetic Engineering of the Postgraduate School of the UANL.

4.5.1 Bacterial strains and inoculum preparation

The antibacterial essays were performed using nine drug-resistant clinically isolated strains. The Gram-negative resistant bacteria are carbapenem resistant *Acinetobacter baumannii* (12-666), *Escherichia coli* producer of ESBL (14-2081), carbapenems resistant *Pseudomonas aeruginosa* (13-1391), oxacillin resistant *Klebsiella pneumoniae* (OXA-48), *K. pneumoniae* NDM-1+ (14-3335) resistant to carbapenems, and wide spectrum cephalosporins, *K. pneumoniae* producer of ESBL (14-2081). Instead the Gram-positive resistant bacteria are methicillin resistant *Staphylococcus aureus* (14-2095), linezolid resistant *Staphylococcus epidermidis* (14-583), vancomycin resistant *Enterococcus faecium* (10-984). Also, five sensitive strains purchased from the American type culture collection (ATCC) were employed. The Gram-negative are *E. coli* (ATCC 25922), *P. aeruginosa* (ATCC 9027), *K. pneumoniae* (ATCC 13883). Meanwhile the Gram-positive sensitive bacteria are: *S. aureus* (ATCC 25923), and *E. faecium* (ATCC 29212).

The strains were inoculated into plates prepared with 5% blood agar and cultured for 24 hours, with the exception of the carbapenem resistant *P. aeruginosa* and *S. epidermidis* strains, which were left for 48 hours (Figure 4.7).

Figure 4.7 Example of inoculum of *E. faecium* in agar blood

For the preparation of the inoculum for the assay, three to five colonies from each culture were transferred to tubes with sterile saline solution, and the turbidity was adjusted to McFarland's 0.5 (1.5×10^8 CFU/ml). Then 10 µl were then transferred into 11 ml Mueller Hinton broth to reach a concentration of 5×10^5 CFU/ml (*74*), according to the National Committee for Clinical Laboratory Standard (NCCLS) guidelines (*75*).

4.5.2 Antibacterial activity assay

The antibacterial activity was determined by the microdilution method. The essay was performed in 96-well microplates, adding 100 µL of culture medium in each well of the plate. Then in first and second well of the row A, were added 100 µL of the work solution (in duplicate) containing raw extracts,

extract fractions, isolated compounds or positive control (levofloxacin) with a concentration of 4X (2000µg/mL or 800µg/mL). The content of the wells was then mixed with multichannel micropipette, and from this mixture 100 µL were transferred to row B to produce a dilution 1:2, and this was repeated until reaching the row G, discarding the last 100 µL. Later 100 µL were taken from the tube with bacterial suspension previously adjusted to 0.5 McFarland and added to the wells with or without sample, for the negative and positive controls.

← 500 or 200 µg/mL
← 250 or 100 µg/mL
← 125 or 50 µg/mL
← 62.5 or 25 µg/mL
← 31.25 or 12.5 µg/mL
← 15.63 or 6.25 µg/mL
← 7.81 or 3.13 µg/mL
← Medium sterility control
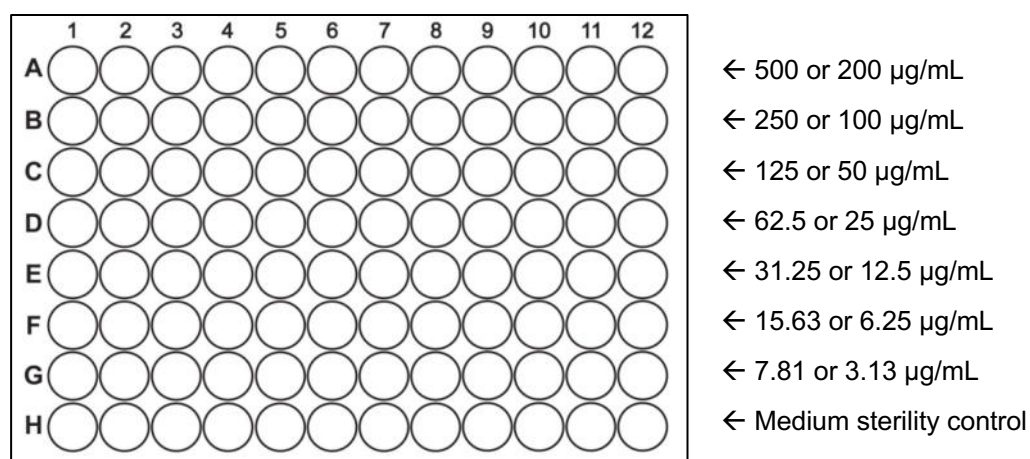
The microplate was then placed in the incubator at 37°C for 24 to 48 h. At the end of the incubation time the growth or inhibition of the bacteria was evaluated visually, taking as inhibition the wells where nor turbidity nor bacterial bottom deposition were observed. Each concentration was evaluated in duplicate. Levofloxacin was used as reference standard for the resistant strains while ampicillin (8 µg/mL) was used as positive control for the sensible strains. The minimum inhibitory concentrations (MICs) were determined (*76*).

4.5.3 Cell lines growth and harvest

For the cytotoxic assays were used the following cellular lines obtained from the American Type Culture Collection (ATCC): liver cancer cells Hep3B and HepG2, lung cancer cells A549, cervix cancer cells HeLa, breast cancer cells MCF7, prostate cancer cells PC3, and normal immortalized hepatocytes IHH. Cells were cultured in RPMI 1640 or EMEM medium, supplemented with 10% (v/v) inactivated fetal bovine serum, 100 U/mL penicillin and 100 µg/mL streptomycin sulfate, 2 µg/mL glutamine, 0.25 µg/mL amphotericin B and the needed growth factors. Cells were maintained in a humidified atmosphere (95% humidity) with 5% CO_2 at 37°C for 24 h prior to the addition of the extracts, fractions or compounds (*70*). Right before treatment cells were removed from the tissue culture flasks by treatment with trypsin and diluted with fresh media.

4.5.4 Cytotoxic activity assay

The cytotoxic activities were determined using the metabolism-dependent dye Owen's reagent (MTS) or WST1 in a microculture method. Cell suspensions, containing 5000 or 7500 cells per well, were added into 96-well microplates, and incubated at 37°C for 24h in a 5% CO_2 atmosphere to reach exponential growth. After 24h, 100 µL of tested compounds, raw extracts or positive control at various concentrations were added to each well starting from 100 µg/mL. The cultures were exposed to compounds for 48h. After incubation time, cells were stained by the addition of 40µL of MTS or WST1. After 2 hours of incubation at 37°C in a humidified atmosphere (95% humidity) with 5% CO_2 the absorbance at 490nm was read in a microplate reader. The

inhibitory concentration at 50% (IC_{50}) was determined (*77*). Paclitaxel was used as positive control. Extracts and fractions were considered active when their IC_{50} gave $\leq$ 30 µg/mL. This threshold was selected in accordance to the National Committee for Clinical Laboratory Standards (NCCLS) guidelines. The latter also stipulates that extracts shall be tested at a centration not exceeding 1 mg/mL (*78*).

4.5.5 Biodirected cytotoxicity screening

The biodirected cytotoxicity screening was done by WST1 cytotoxic assay. PC3 and MCF7 cells were treated for 48h with 100, 50 and 25 µg/mL of each fraction of $CHCl_3$/MeOH extract. The percentage of viable cells per well was then obtained.

4.5.6 Microarray assay

PC3 and MCF7 cells were treated for 24h with the selected compound at its IC_{50}. Untreated cells were used for the comparation of the gene expression after treatment. Total ribonucleic acid (RNA) isolation was pursued using TRIzol™ Reagent (Invitrogen), following manufacturer instructions. The quality control of RNA was determined by using agarose gel (1%) and total RNA was quantified in an Eppendorf 6131 biophotometer (Eppendorf, Hauppauge, NY, USA). RNA quantity was adjusted to 20 µg for both treated and untreated controls. The modified complementary DNA (cDNA possessing the nucleotide aminoallyl-uridine) was synthesized using the amino-allyl cDNA labeling kit. The fluorescent dyes Cy3 and Cy5 from the CyDye Post-Labeling Reactive Dye Packs were used for labeling the cDNA. Each vial of fluorescent

dye was dissolved in 3 µL of DMSO and mixed with one specific cDNA. A NucAway column were used to eliminate the excess of unbound fluorophore (*79–83*).

The microarray hybridization was performed on a 35K human genes chip using the procedure described in the protocol by MYcroarray Company (Ann Arbor, MI, USA). The procedure took place in a hybridization chamber G2534A (Agilent, Santa Clara, CA, USA), fluorophore incorporation efficiency was analyzed measuring absorbance at 555 nm for Cy3 and 647 nm for Cy5 using Gene Pix 4000B scanner. Data was then submitted to statistical analysis performed using the GenArise package in order to obtain Zscore values, which were negative or positive according to down- or up-regulated genes expression after treatment with the compound. Genes with Zscore ≥ +2 and Zscore ≤ -2 were selected to carry out the gene expression analysis. Both lists of genes were analyzed separately for the biological pathways identification, using bioinformatics tools such as Database for Annotation, Visualization and Integrated Discovery (DAVID) version 6.8. The database tools employed in the analysis were: Functional Annotation and Gene Functional Classification (*83, 84*).

4.6 *In silico* study

4.6.1 Explorative docking

The crystalline structure of the target protein was retrieved from the Protein Data Bank (*85*). Incomplete protein structures were fixed through the generation of theoretical models using online platforms such as I-TASSER, Galaxy WEB and SWISS-MODEL (*86–88*). The obtained models were completed with their cofactors (if possible) and submitted to a brief molecular dynamic of 2 ns, using the software Maestro release 2019-3 (Schrödinger) (*89*). The 3D model of the ligand was drawn using the molecular builder Avogadro 1.2.0 (*90*). These files were then opened with the opensource molecular modeling program UCSF Chimera (*91*), and were both prepared for the molecular docking. Using the Docking Preparation wizard (DockPrep) available in the program the functional groups of target and ligand were determined, and the polar and non-polar hydrogens were added. Small protein chain gaps or missing residues were replaces using the Dunbrack 2010 rotamers library (*92*). AutoDock Vina version 1.1.2 plug-in was used in Chimera for the docking experiments. The opal web service (server: http://nbcr-222.ucsd.edu/opal2/services/vina_1.1.2) was used as host for the docking simulations. The resulting docked structures of the ligand were then rewritten separately as .pdb files for a simpler handling and were processed in the Maestro suit (Figure 4.8).
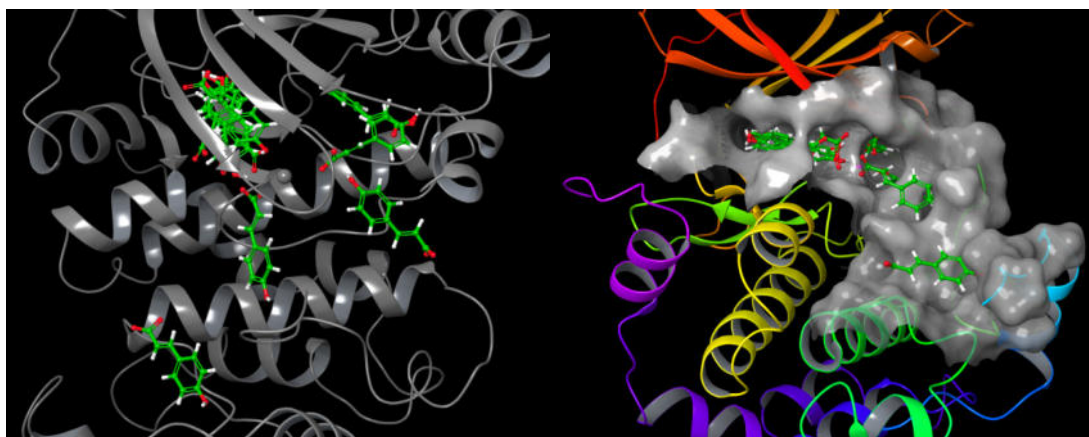
Figure 4.8 Example of Docking results viewed in Maestro: docked ligand structures in protein ribbons (left); docked ligand structures in the active site cavity represented as a molecular surface (right)

4.6.2 Molecular dynamics (MD)

The pdb files of protein and docked ligand structures were processed by the software Maestro. First the structures were preprocessed with the preprocess wizard and the protein structure fixed and its energy was minimized. One docked ligand structure was selected in base of its score, site of binding and protein interaction. The best docked ligand and protein structures were then merged, and the resulting file was processed with the molecular builder wizard of the Desmond suit of Maestro. The ligand-protein complex was enclosed into an orthorhombic boundary box and solvated adding water molecules in the SPC model. The model represents the hydrogens and the oxygen of the water molecules as charged sphere. Na^+ ions were used to neutralize eventual residual charges of the protein. Meanwhile both Na^+ and Cl^- ions were added to a concentration of 0.15 M in order to generate a physiological-like salinity. If the protein was of the transmembrane type, a membrane was generated before solvation using

phosphatidyl choline (POPC; 300 K) as phospholipids. The resulting file was saved into a cms format.

Using the Desmond's molecular dynamics wizard, the molecular dynamics conditions were set. The duration of the simulation was set to 10 ns, the recording interval for the trajectory was every 10 ps and the consequent approximate number of frames was 1000. The temperature was set to 310.15 K (corporeal temperature), while the system's pressure to 1.013225 bars.

To maintain these conditions Nose-Hoover chain algorithm and Martyna-Tobias chain algorithm were used as thermostat and barostat respectively. The Coulombic interaction was calculated by the short-range method and the cutoff was set to 9.0 Å. Finally the bonded RESPA integration was performed with time step of 2.0 fs (near: 2.00 and far: 6.00) (*93*). Table 4.9 reports all the settings employed in the MD simulations.

Table 4.9 MD's settings

System Builder	
Na^+ and Cl^- concentration	0.15 M
Membrane	POPC 300K
Molecular Dynamic	
Simulation time	10 ns
Trajectory recording interval	10 ps
Frames number	1000
Temperature	310.15 K
Pressure	1.01325 bar
Coulombic cutoff	9.0 Å
RESPA time step	2.0 fs

4.6.3 Cluster analysis and binding energy (ΔE_{bound}) determination

Results of molecular dynamics were processed with the Desmond trajectory clustering wizard. The output cms file was clustered to a maximum of 5 clusters for each target protein, which were selected and exported from the trajectory movie. The clusters with the higher number of members were considered as the representative for each ligand-protein complex. Also, using the simulation event analysis and simulation quality analysis wizards the goodness of the results was checked. The variation of volume ($Å^3$), temperature (K), pressure (bar), potential energy and total energy (kcal/mol) of the system were analyzed for their average, standard deviation and slope (ps^{-1}). The results were also plotted in order to check visually the quality of the analysis (Figure 4.10 A).
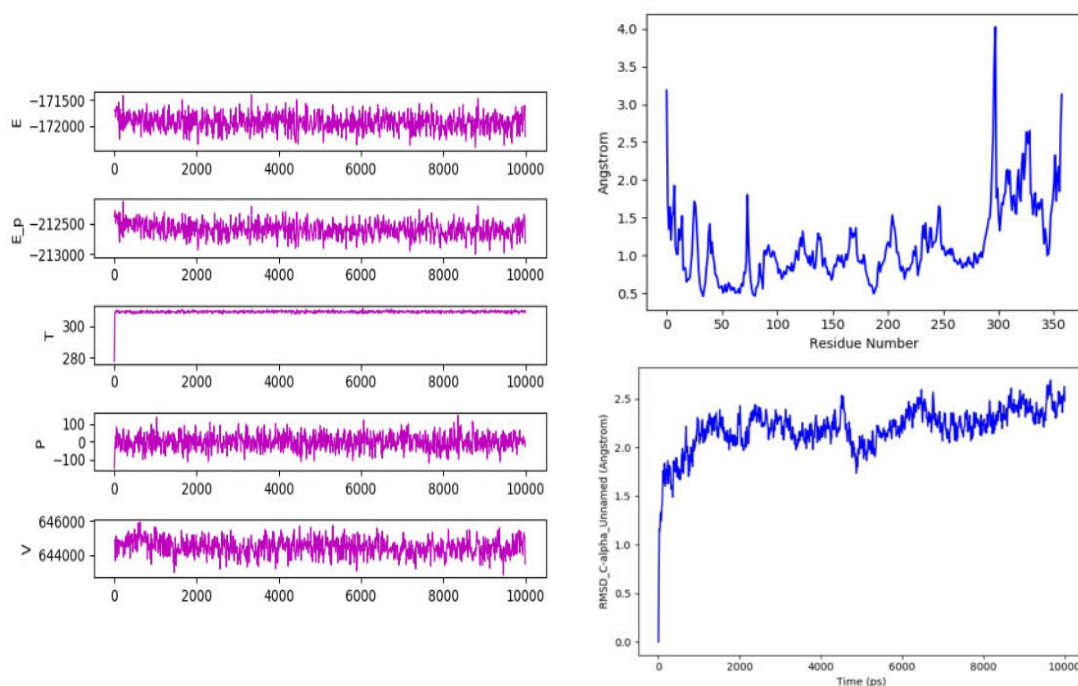
Table 4.10 Example of MDs parameters monitored during the simulation. A) From top to bottom: total energy, potential energy, temperature, pressure, volume (simulation time: 0-10,000 ps). B) Top: protein residues movement (Å), RMSF; bottom: protein backbone (C_α) movement (Å), RMSD.

Other properties of the system that were checked are the coulomb and van der Waals interaction energies, root-mean-square deviation (RMSD) of atomic positions and root-mean-square fluctuation (RMSF) of atomic positions. In this specific case it was decided to monitor with the RMSD the movement of the protein backbone (Cα) and with the RMSF the movement of the protein residues. The RMSD and RMSF were graphed in order to visualize the average movement of the system over the simulation time (Figure 6.10 B). After the more representative cluster was selected, the electrostatic and van der Waals (vdW) energy for the bound and free ligand were calculated using the Desmond simulation event analysis wizard. These parameters were considered as the ligand-protein (bound) and ligand-solvent (free) interaction energies for both coulombic (E_{lp}^{el} and E_{ls}^{el}), and vdW (E_{lp}^{vdW} and E_{ls}^{vdW}) parameters. Finally, the binding energy (ΔE_{bound}) was calculated with the linear interaction energy (LIE) equation (Equation 4.2).

$$\Delta E_{bound} = \alpha\left(E_{lp}^{vdW} - E_{ls}^{vdW}\right) + \beta\left(E_{lp}^{el} - E_{ls}^{el}\right) + \gamma$$

Equation 4.2 Linear interaction energy (LIE) equation

In the equation α, β and γ are scaling factors which have the default values of 0.16, 0.5 and 0. The LIE equation is used in cheminformatics to find a suitable compounds for disease-related targets or to predict the goodness of a ligand-protein interaction (*94*).

CHAPTER 5

5. RESULTS AND DISCUSSION

5.1 Phytochemistry

5.1.1 Preparation of the vegetal material

The first step in the preparation of the vegetal material was the drying of leaves and roots in the darkness. In particular the leaves were then cut into small pieces to allow a faster dehydration of the very juicy and water reach tissues. Instead the roots were left to dry almost intact to reduce the oxidation of its components. The drying process was fundamental in the prevention of the growth of microorganisms on the plant samples which would have modified the metabolites content of the plant, leading to a wrong identification of the plant's phytochemical composition. Also, the drying process eliminates the water from the material, fixes the phytochemicals and reduces the probability of molding of the vegetal material. The leaves were allowed to dry for 1 month at room temperature and away from the sun light. The low temperature and the dark conditions were of outmost importance, since the plant composition was unknown. In fact, heating or exposing to the light the vegetal material could have caused the degradation of sensible and important molecules.

Some plant's leaves were dried and were blended fresh in distilled water. This was done in the hypothesis that some of the compounds of the plant could have been decomposed during the drying process. This might have happened throughout oxidation by the oxygen present in the air or the

reaction of some components with each other. These reactions could be explained by the growing concentration of the compounds in the tissues while drying or simply by the exposure to the atmosphere, when the cellular structures were broken in the preparation of the vegetal material. So, by blending the leaves fresh and conserving the lyophilized extract at 4 °C, it was ensured the stabilization of the extracted molecules.

The double grounding of the dried leaves and roots, first grounded into a coffee grinder and then into a blender, was of outmost importance to reduce as much as possible the particles size. This will give a more intimate contact between the solvent and the vegetal material during the maceration and allow the solvent to penetrate the cellular structures to maximize the extraction.

5.1.2 The hexane maceration

The first volatile solvent extract was made in hexane with the purpose of defating the vegetal material. This solvent, being very non-polar, has the ability of extracting the majority of the non-polar metabolites, such as fatty acids, triglycerides, terpenoids, steroids, between others. So, this maceration had the objective of simplify the sequent and much more complex extract. The molecules that were isolated from the fractionation of the leaves extract were five, from compound 1 to 5 and their physical, chemical and spectroscopic properties are described in the next paragraphs. Instead for the roots, since no chromatographic separation was planned just a small quantity of material was macerated.

5.1.3 Leaves isolated and purified phytochemicals

5.1.3.1 Physic and spectroscopic data of nonacosane (1)
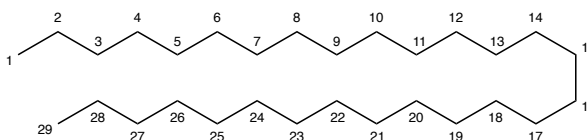
Figure 5.1 Structure of nonacosane (1)

Compound 1 (Figure 5.1) was found to be soluble in nonpolar solvents like hexane or $CHCl_3$ and its solubilization was facilitated by heating the solvent. It had a low melting point (mp) of 43-46°C and its molecular formula is $C_{29}H_{60}$.

IR (cm^{-1}): 2800-3000, 1485, 750. ^1H NMR (400 MHz, $CDCl_3$) δ (ppm): 0.88 (t, *J*=6.8 Hz, 6H, 2Me), 1.25 (s, 54H). ^{13}C NMR (100 MHz, $CDCl_3$) δ (ppm): 14.28 (2Me), 22.86 (C-2;C-22), 29.53 (C-4;C-20), 29.86 (21C), 32.09 (C-3;C-21). GC-MS R_t (min): 102.298; (EI) m/z: 408 ($M^{+\bullet}$), 57 (100%), 71 (80%), 85 (70%), 43 (50%), 99 (25%).

5.1.3.1.1 Structural elucidation of nonacosane (1)
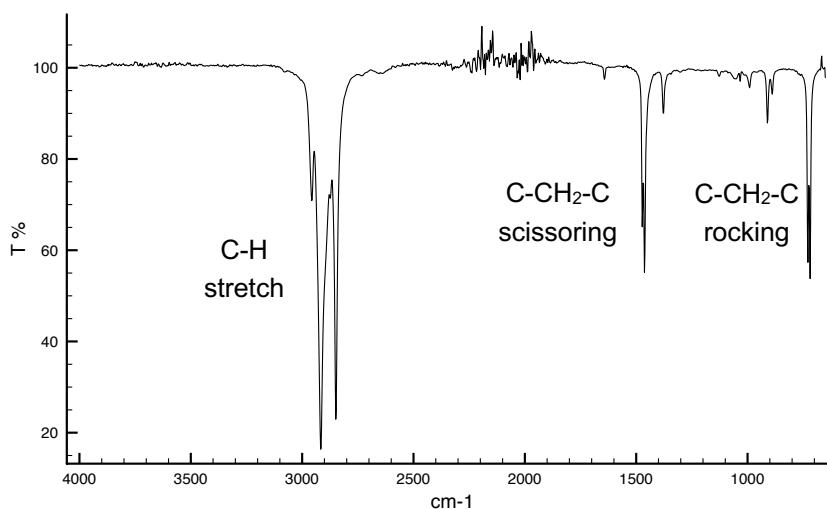
Figure 5.2 IR spectrum of nonacosane (1)

The IR spectrum (Figure 5.2) of this compound showed only hydrocarbon signals: the aliphatic C-H stretching from 2800 to 3000 cm^{-1}, and the CH_2 scissoring at 1485 cm^{-1} and rocking at 750 cm^{-1}, indicative of long carbon chain.
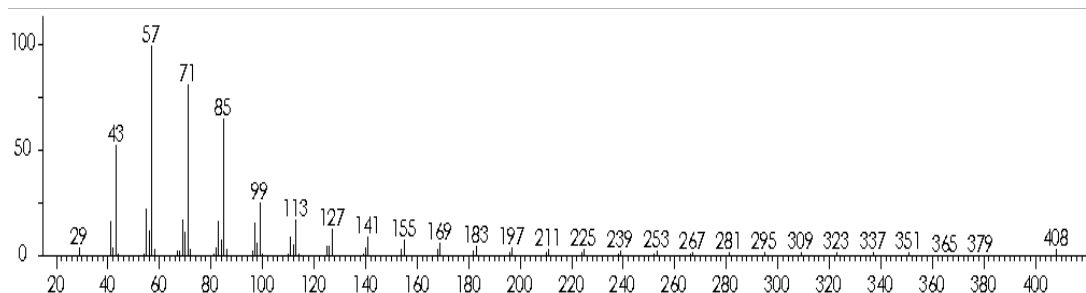
Figure 5.3 EI/MS spectrum of nonacosane (1)

The electron ionization mass spectrum (Figure 5.3) of nonacosane is typical of a long chain alkane. This is clear from the constant difference of 14 between the various ion peaks. This loss doesn't represent an actual weight but indicate instead the repetitive loss of a 28 Da fragment. This is characteristic of this class of molecules. Among the important peaks of the spectrum are the molecular ion (M$^{+\bullet}$), with a weight of 408 m/z and the base peak of 57 m/z also characteristic of alkanes. The identity of the molecule was also confirmed by comparation of the spectrum with the NIST library.

The ^{1}H NMR spectrum (Figure 5.4) showed signals typical of alkanes molecules, with an upfield triplet that integer for 6 hydrogens at 0.88 ppm (*J*=6.8 Hz, 2Me) and a less downfield singlet that integer for the other 54 protons. The absence of any other signal was indicative of the alkane nature of the molecule.

The ^{13}C NMR spectrum (Figure 5.5) also showed an alkane pattern with very few signals, which were related to a pair of carbons each: the terminal methyl groups at 14.28 ppm, and all the other carbons following them in chain, at 22.86 ppm (C-2 and C-22), 29.53 ppm (C-4, C-20) and 32.09 ppm (C-3, C-21). Then it was present a much more intense signal at 1.25 ppm related to all the other carbons of the molecule (21C).
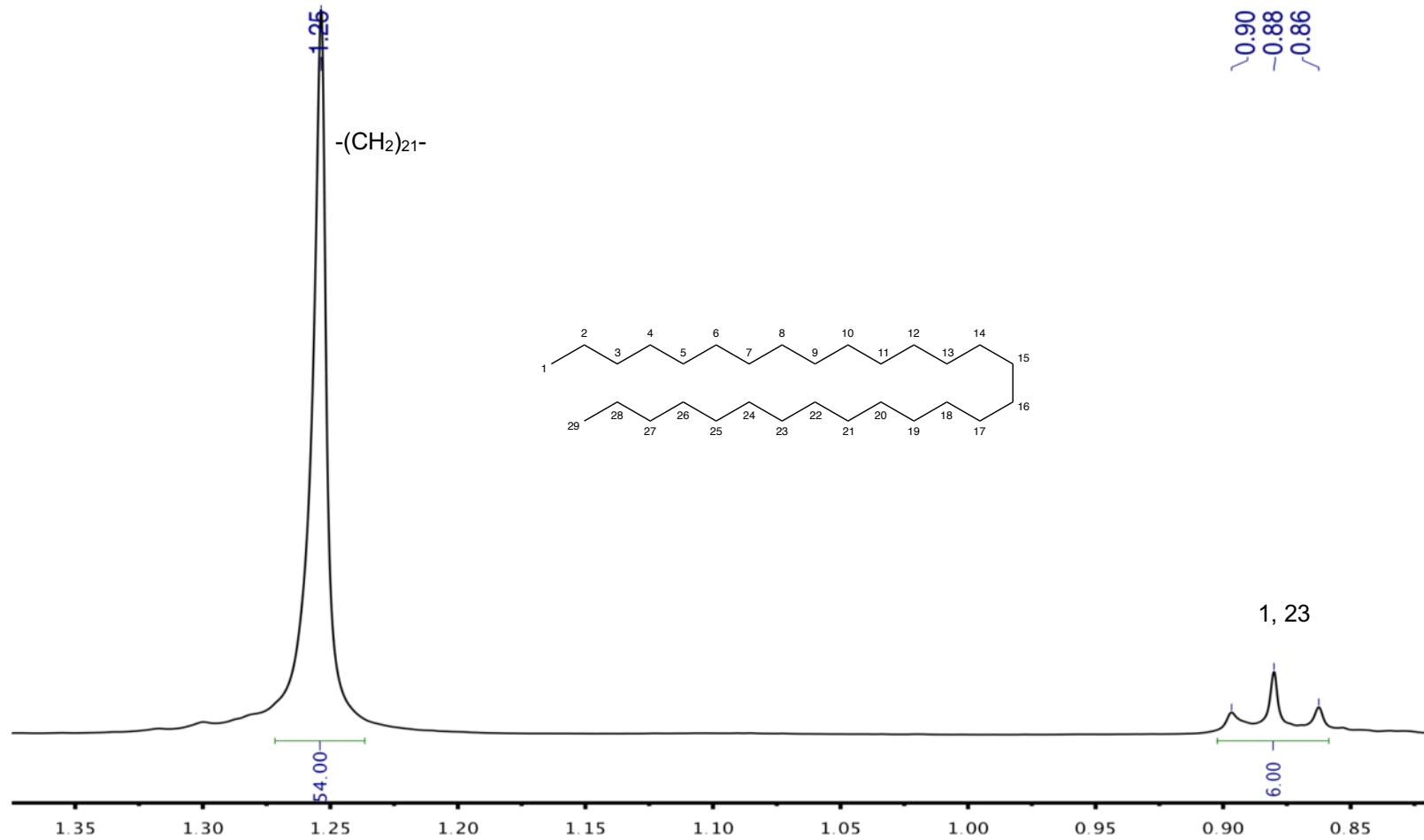
Figure 5.4 ^{1}H NMR spectrum (400MHz, CDCl$_3$) of nonacosane (1)
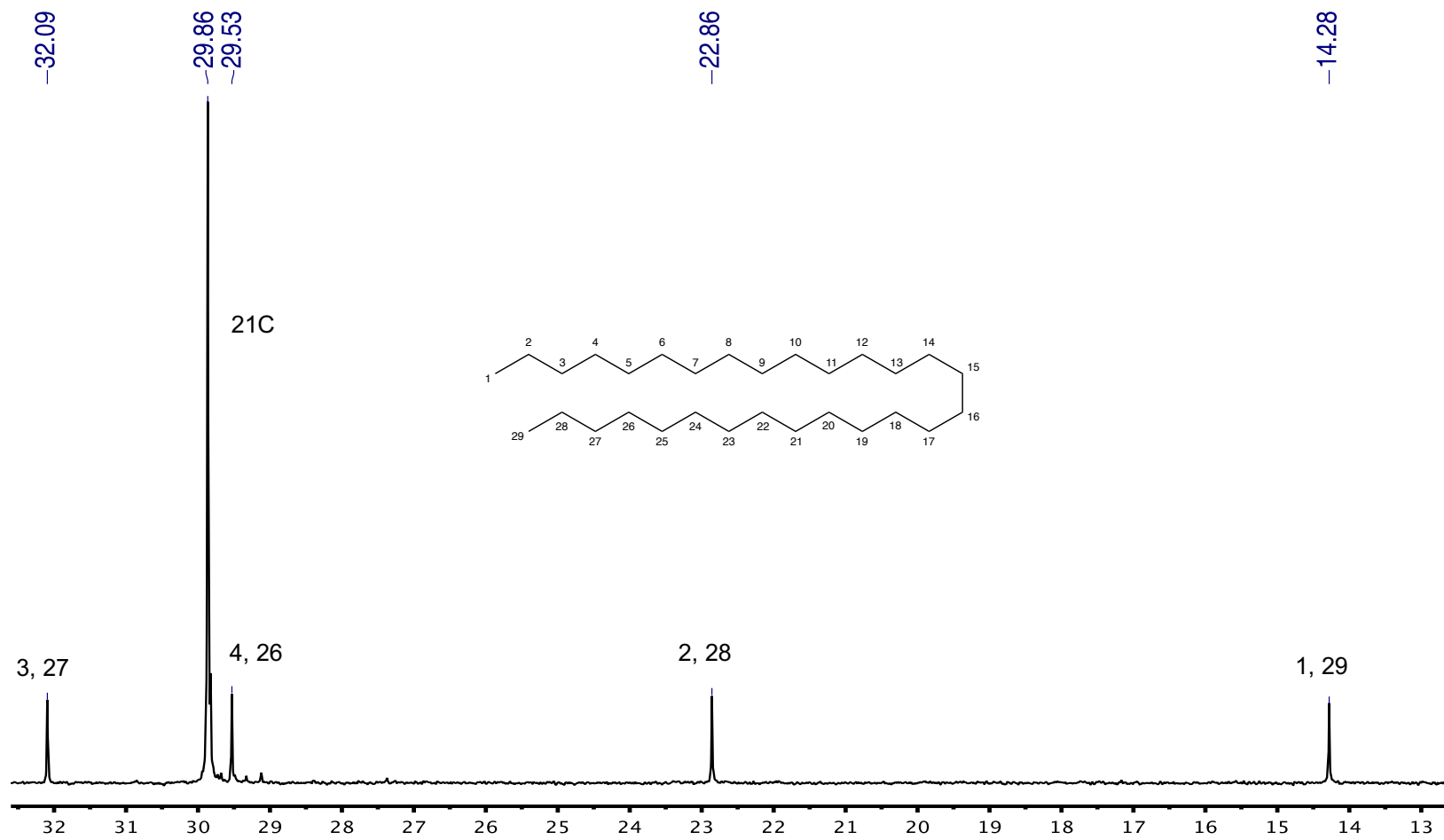
Figure 5.5 ^{13}C NMR spectrum (100MHz, CDCl$_3$) of nonacosane (1)

5.1.3.2 Physic and spectroscopic data of hexatriacontanyl stearate (2)
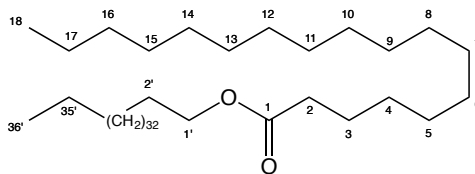
Figure 5.6 Structure of hexatriacontanyl stearate (2)

This long chain wax (Figure 5.6) was very soluble in $CHCl_3$ and partially soluble in hexane. It had mp of 73-75°C and its molecular formula is $C_{54}H_{108}O_2$.

IR (cm^{-1}): 2800-3000, 1750, 1485, 1185, 750. ^1H NMR (400 MHz, $CDCl_3$) δ (ppm): 0.87 (t, J=6.7 Hz, 6H, 2Me), 1.25 (s, 94H), 1.61 (p, J=6.9 Hz, 4H), 2.28 (t, J=7.5 Hz, 2H), 4.05 (t, J=6.7 Hz, 2H). ^{13}C NMR (100MHz, $CDCl_3$) δ (ppm): 14.12 (2Me), 22.70 (C-17;C-35'), 25.05 (C-34'), 25.95 (C-16), 28.67 (C-15), 29.37 (C-32';C-33'), 29.71 (40C), 31.94 (C-2';C-3), 34.44 (C-2), 64.40 (C-1'), 174.01 (C-1).

5.1.3.2.1 Structural elucidation of hexatriacontanyl stearate (2)

The IR spectrum (Figure 5.7) of the molecule showed aliphatic signals between 2800 and 3000 cm^{-1} and relative CH_2 scissoring and rocking respectively at 1485 and 750 cm^{-1}. Then it showed a carbonyl signal at 1750 cm^{-1} and a C-O stretching at 1185 cm^{-1}, indicating a long chain ester.

The ^1H NMR spectrum (Figure 5.8) showed signals typical of long chain esters, with a upfield triplet at 0.87 ppm (J= 6.7, 6H, 2Me) that integer for 6 hydrogens and a more downfield singlet that integer for the other 94 protons (1.25 ppm), typical of long chains of CH_2. Then a triplet at 2.28 ppm (J=7.5 Hz, 2H, H-2), is indicative of the presence of a carbonyl group attached to a long

chain of carbons and at last, the proton signal indicative of the presence of an oxygen directly attached to a CH_2 is the triplet at 4.05 ppm (J=6.7 Hz, 2H, H-1) and a pentaplet at 1.61 ppm (J=6.9 Hz, 4H, H-3; H2') relative the hydrogens 3 and 2'. The ^{13}C NMR spectrum (Figure 5.9) also showed a long chain ester molecule pattern with very few signals in the downfield region and a lot of signals in the upfield region of the spectrum. A very intense signal at 29.71 ppm corresponds to the majority of the CH_2 of the molecule. But the signals that were decisive to characterize the molecule are the one at 65.40 ppm relative to the carbon attached to the oxygen and the one at 174.01 ppm which is characteristic of esters' carbonyl groups.
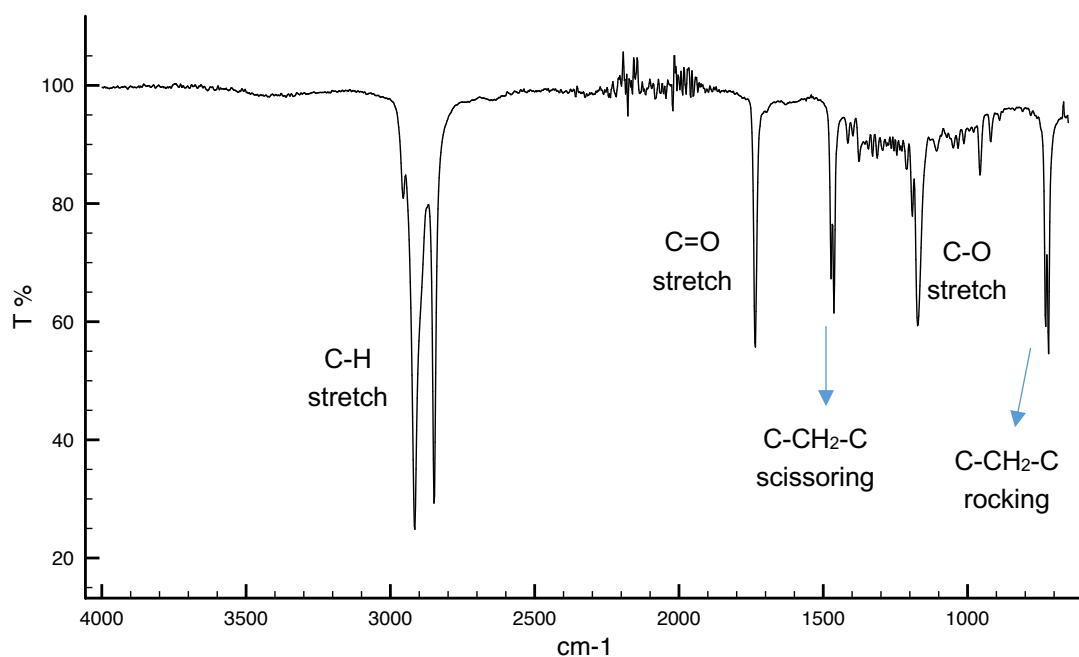
Figure 5.7 IR spectrum of hexatriacontanyl stearate (2)
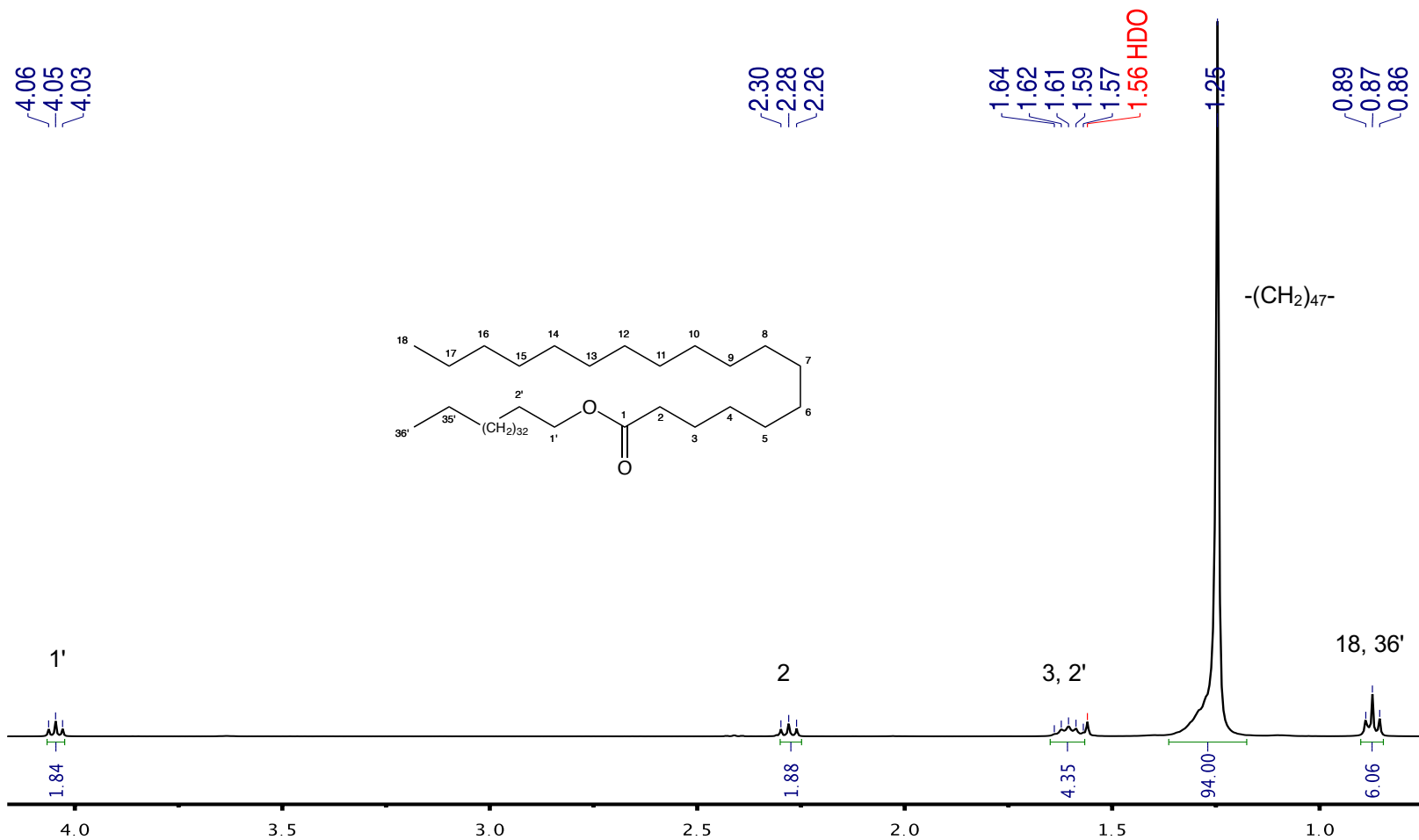
Figure 5.8 ^{1}H NMR spectrum (400MHz, CDCl$_3$) of hexatriacontanyl stearate (2)
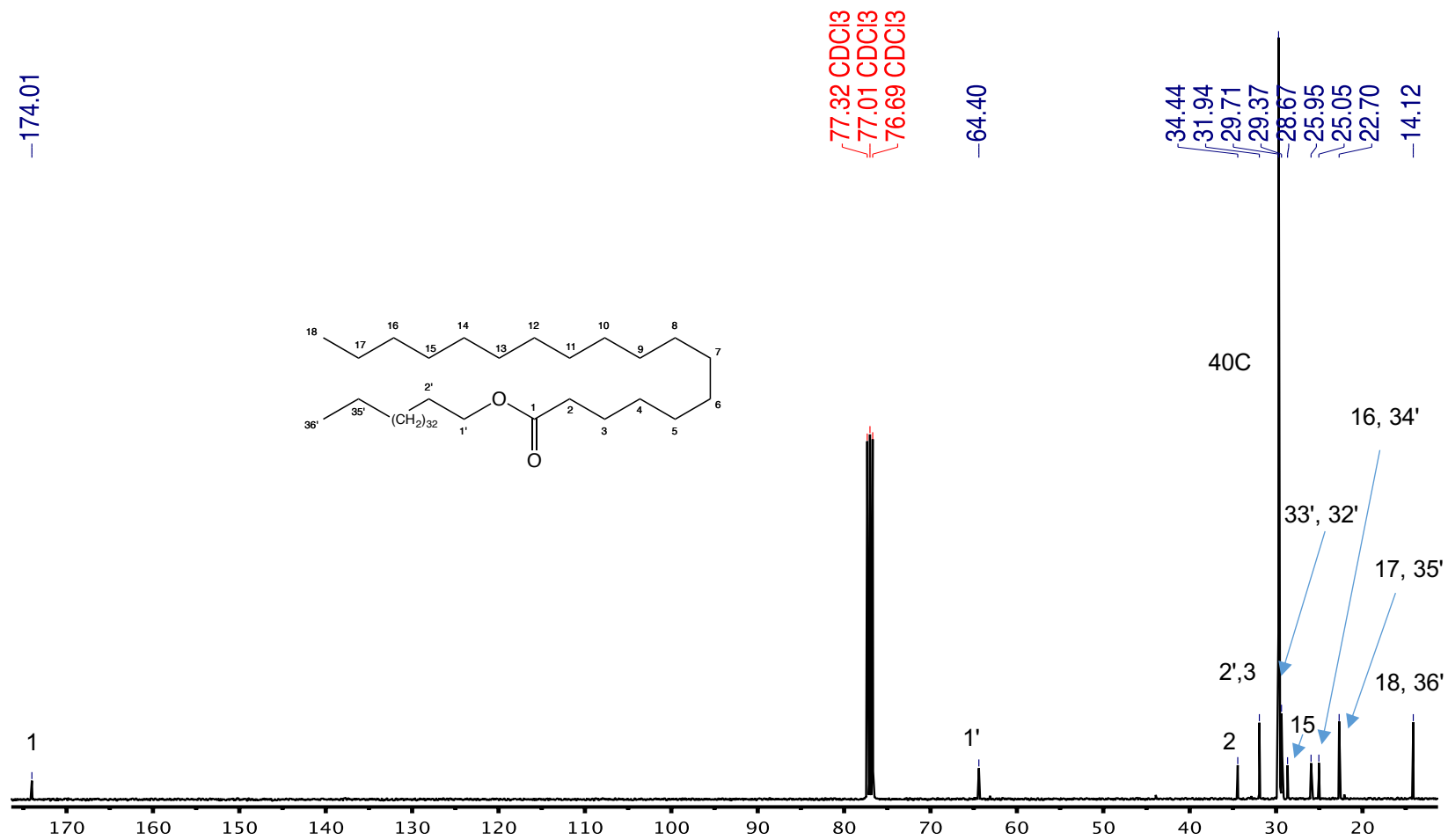
Figure 5.9 ^{13}C NMR spectrum (100MHz, CDCl$_3$) of hexatriacontanyl stearate (2)

5.1.3.3 Physic and spectroscopic data of hexacosanol (3)
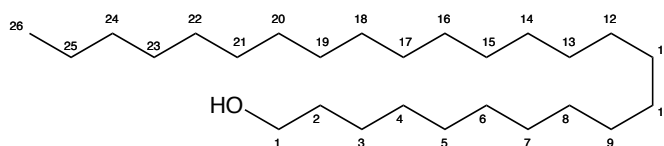
Figure 5.10 Structure of hexacosanol (3)

The alcohol (Figure 5.10) gave crystals in small flat crystals flakes with a chromium shade. It resulted to be very soluble in $CHCl_3$ but less soluble in other nonpolar solvents. The compound resulted to have mp of 76-77°C and its molecular formula is $C_{23}H_{48}O$.

IR (cm^{-1}): 3300, 2800-3000, 1485, 11050, 750. ^1H NMR (400 MHz, $CDCl_3$) δ (ppm): 0.88 (t, *J*=6.8 Hz, 3H), 1.25 (s, 46H), 1.57 (p, *J*=13.2, 6.7 Hz, 2H), 3.64 (t, *J*=6.6 Hz, 2H). ^{13}C NMR (100MHz, $CDCl_3$) δ (ppm): 14.12 (CH_3), 22.70 (C-25), 25.75 (C-24), 29.37 (C-23), 29.44 (C-2), 29.71 (18C), 31.93 (C-3), 32.83 (C-2), 63.12 (C-1).

5.1.3.3.1 Structural elucidation of hexacosanol (3)

The IR spectrum (Figure 5.11) of the compound showed an O-H stretching signal at 3300 cm^{-1} and also it was visible a C-O stretching at 1050cm^{-1}. The rest of the signals were all aliphatic C-H stretching (from 2800 to 3000 cm^{-1}) and bending (scissoring: 1485 cm^{-1} and rocking: 750 cm^{-1}). All the signals were indicative of a long carbon chain alcohol.

The ^1H NMR spectrum (Figure 5.12) showed signals typical of long chain alcohol, with an upfield triplet at 0.88 ppm (*J*=6.8 Hz, 3H, Me) that integer for the terminal methyl group and a more downfield singlet that integer for the

other 46 protons (1.25 ppm), typical of long chains of CH_2. Then a double pentaplet at 1.57 ppm (J=11.3, 6.8 Hz, 2H, H-2) followed by a triplet at 3.64 ppm (J=6.6 Hz, 2H, H-1), are indicative of the presence of an oxygen attached to a long chain of carbons. The absence of any other signal showed that oxygen doesn't have any substituent and that the molecule is an alcohol. The ^{13}C NMR spectrum (Figure 5.13) also showed a long chain alcohol molecule pattern with very few signals in the downfield region and a lot of signals in the upfield region of the spectrum. A very intense signal at 29.71 ppm is related to the majority of the CH_2 of the molecule. But the signal that was decisive to characterize the molecule was the one at 63.12 ppm relative to the carbon attached to the oxygen which is characteristic of alcohols.
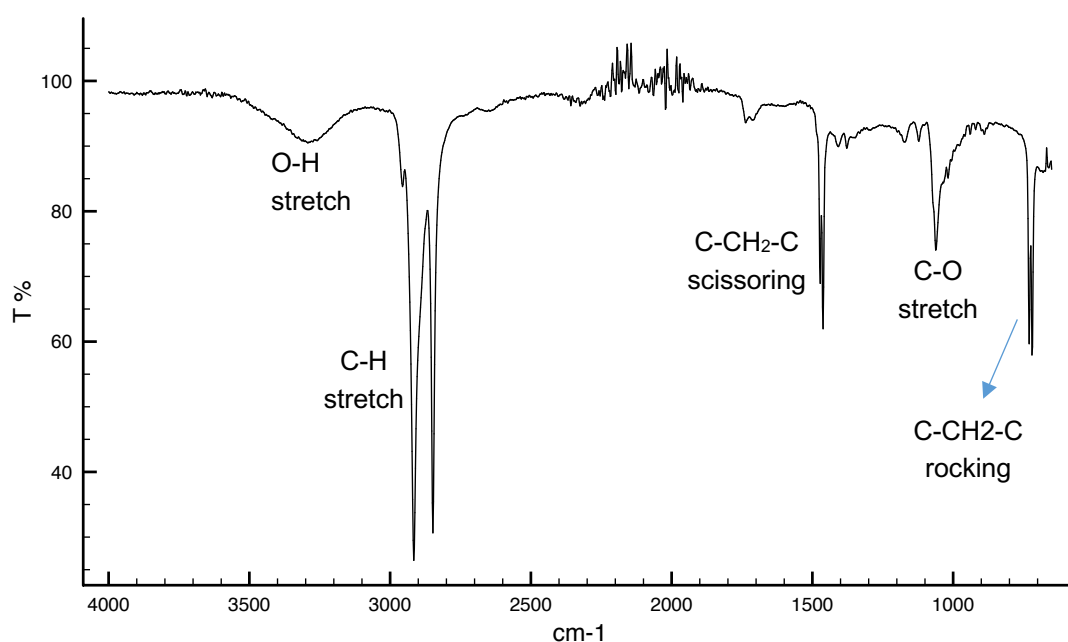
Figure 5.11 IR spectrum of hexacosanol (3)
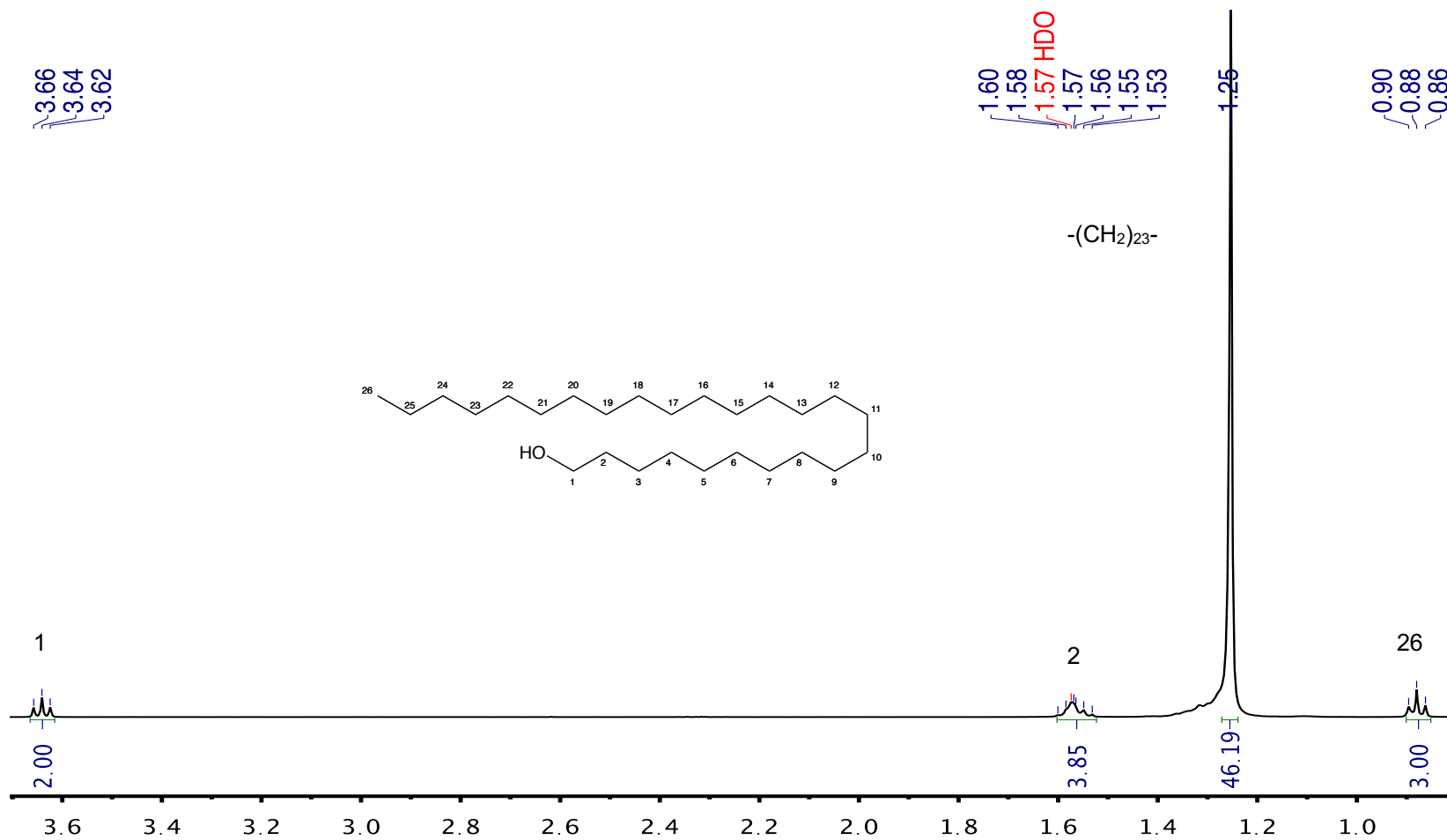
Figure 5.12 ^{1}H NMR spectrum (400MHz, CDCl$_3$) of hexacosanol (3)l
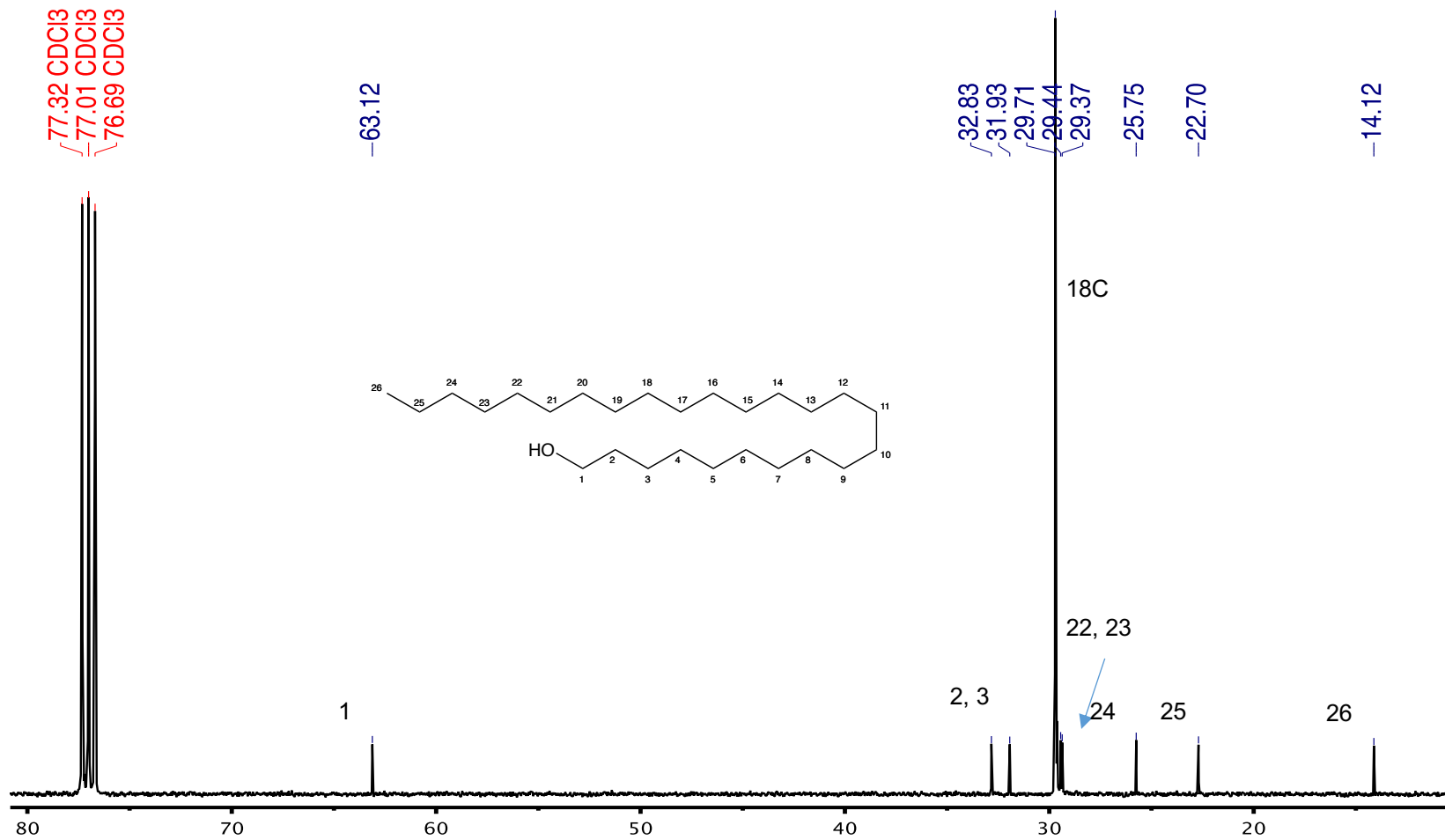
Figure 5.13 ^{13}C NMR spectrum (100MHz, CDCl$_3$) of hexacosanol (3)

5.1.3.4 Physic and spectroscopic data of oleic acid (4)
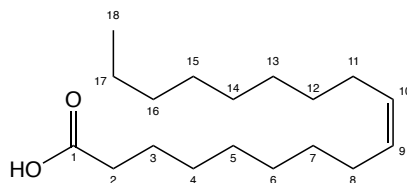
Figure 5.14 Structure of oleic acid (4)

This fatty acid (Figure 5.14) was very soluble in $CHCl_3$ and in the majority of the other nonpolar solvents. It had mp < 25°C, it is transparent, colorless oil and its molecular formula is $C_{18}H_{34}O_2$ (18:1Δ9). The spectroscopic data of compound 4 is shown in Table 5.1.

Table 5.1 Spectroscopic data of oleic acid (4)

n	^1H NMR (500 MHz, CDCl$_3$) δ (ppm), (*95*)	^1H NMR (400 MHz, CDCl$_3$) δ (ppm), 4	^{13}C NMR (125MHz, CDCl$_3$) δ (ppm), (*95*)	^{13}C NMR (100MHz, CDCl$_3$) δ (ppm), 4
1	-	-	180.2065	179.02
2	2.3495 t	2.35 (t, *J*=7.5 Hz, 2H)	34.0529	33.91
3	1.6326 p	1.63 (p, *J*=7.3 Hz, 2H)	31.7903	31.93
4	-	-	29.7376	31.91
5	-	-	29.6750	-
6	-	-	29.1471	-
7	-	-	29.0665	-
8	2.0125 q	2.01 (psq, *J*=6.4 Hz, 2H)	27.2225	27.22
9	5.3546 q	5.35 (m, 1H)	130.0219	130.02
10	5.3397 q	5.34 (m, 1H)	129.7343	129.72
11	2.0125 q	2.01 (psq, *J*=6.4 Hz, 2H)	27.1518	27.16
12	-	-	29.0299	-
13	-	-	29.0003	-
14	-	-	24.6533	24.70
15	-	-	22.6721	22.68
16	0.8834	0.88 (t, *J*=6.7 Hz, 3H)	14.1286	14.11

5.1.3.4.1 Structural elucidation of oleic acid (4)

The ^{1}H NMR spectrum (Figure 5.15) showed signals typical of unsaturated long chain molecule, with a upfield triplet at 0.88 ppm (J=6.7 Hz, 3H, Me) that integer for the terminal methyl group and a more downfield multiplet that integer for other 18 protons (1.28 ppm), typical of long chains of CH_2. Then a pentaplet at 1.63 ppm (J=7.3 Hz, 2H, H-3) followed by a pseudo quartet at 2.01 ppm (J=6.4 Hz, 4H, H-8 and H-11), which are relative to the CH_2 in β to the carboxyl group and the two allylic CH_2 positions of the molecule respectively. At 2.35 ppm there is a triplet (J=7.5 Hz, 2H, H-2), that is due to the protons in the α position with respect on the carboxyl group and was consequently indicative of a carboxylic acid. The last signals are two multiplets at 5.35 ppm (m, 1H, H-9) and 5.34 ppm (m, 1H, H-10) typical of monounsaturated fatty acids.

The ^{13}C NMR spectrum (Figure 5.16) also showed a long chain fatty acid pattern with very few characteristic signals in the downfield region: at 179.02 ppm (the Sp^2 carbon of the carboxylic group, C-1) and at 130.02 ppm and 129.72 ppm (the Sp^2 carbons of the double bond of the molecule, C-9 and C-10). There were instead a lot of signals in the upfield region of the spectrum (Figure 5.17): at 33.91 ppm (the carbon in α to the carboxyl group, C-2), at 31.93 ppm (the carbon in β to the carboxyl group, C-3). Then between 29.00 ppm and 29.80 ppm there is a region intensively populated of signals which correspond to the majority of the CH_2 of the molecule and its characteristic of monounsaturated fatty acids. Following at 27.22 ppm and 27.16 ppm are the signals relative to the allylic carbons (C-8 and C-11) and at 24.70 ppm, 22.68

ppm and 14.11 ppm there are the final carbons of the chain of the acid, respectively C-14, C-15 and the terminal methyl group C-16.

The molecule was also analyzed using 2D NMR experiments: ^{1}H-^{1}HCOSY, ^{1}H-^{13}C HSQC, ^{1}H-^{13}C HMBC and 1H-^{1}H NOESY. All the spectra confirmed the same molecule and in particular the HSQC experiment was important for the precise assignation of all the signals of the molecule (Figure 5.18).

All the assigned signals were also confirmed from the literature (*95*), although the inconsistence between the integration of some of the protons in the ^{1}H NMR spectrum (specifically the allylic and vinylic protons) still rise some doubts about the purity of the sample. This last one was confirmed by GC-MS analysis, but the current hypothesis is that the sample is probably a mixture of the *cis* and *trans* isomers of the monounsaturated fatty acid.
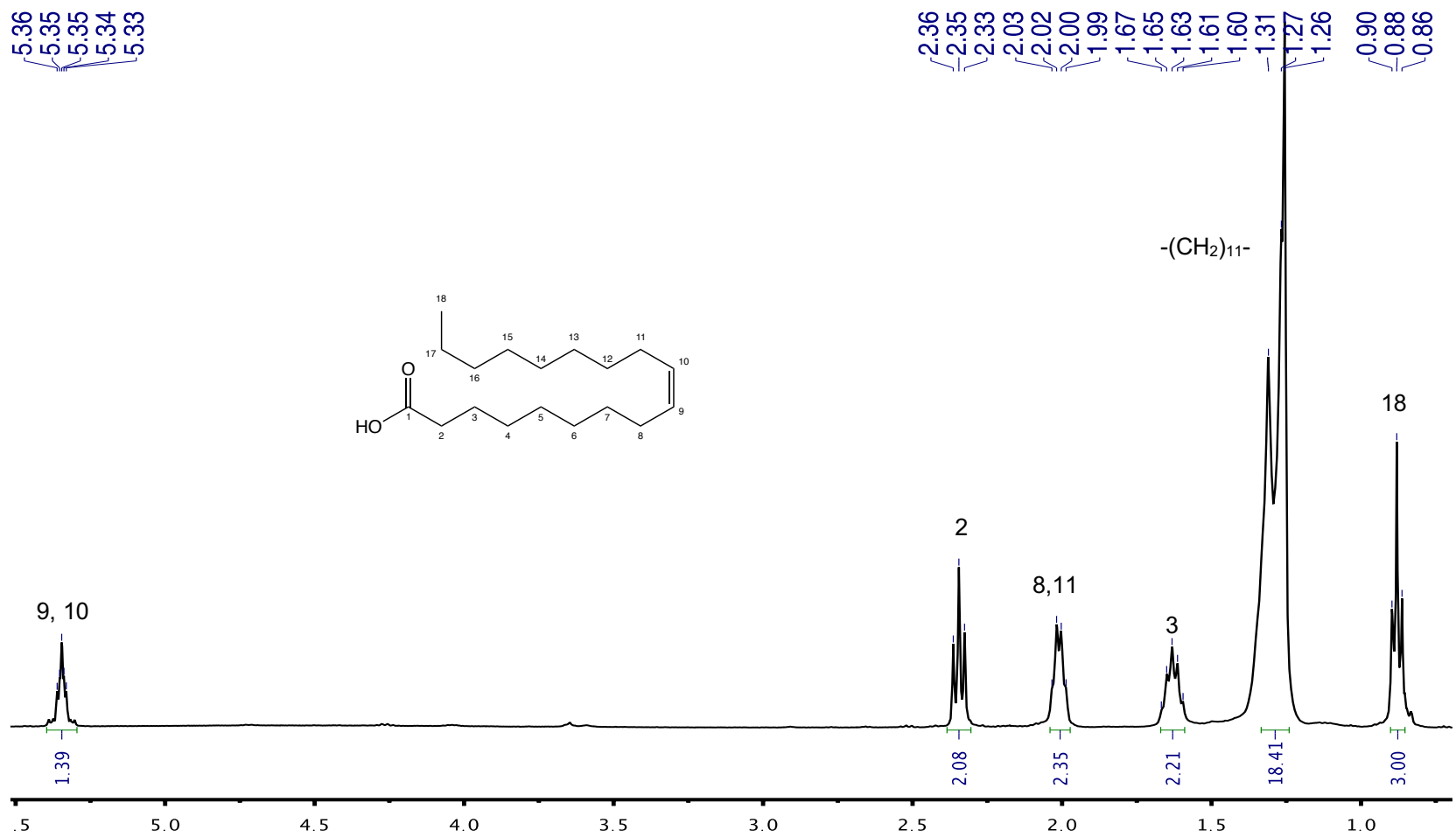
Figure 5.15 ^{1}H NMR spectrum (400MHz, CDCl$_3$) of oleic acid (4)
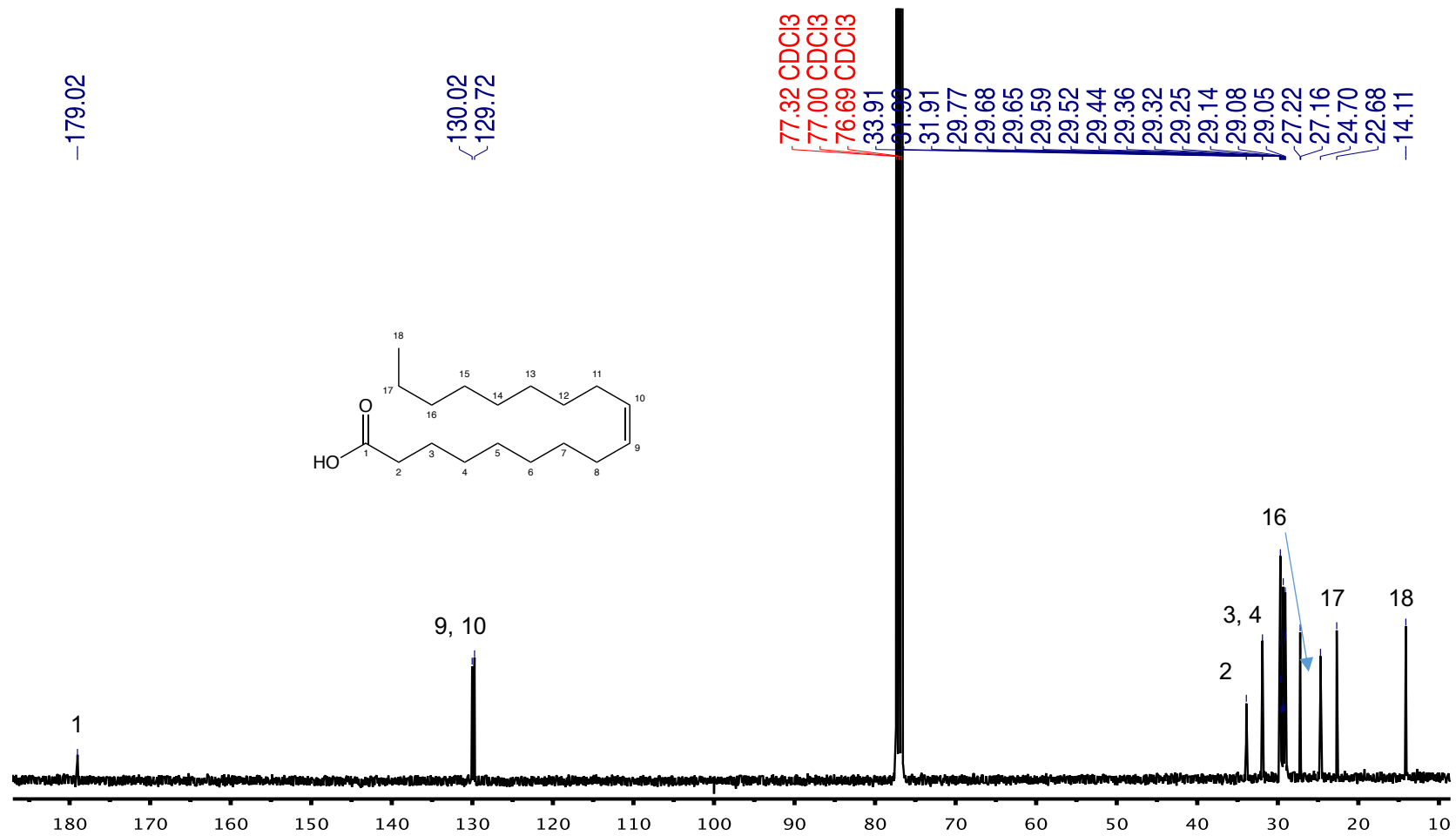
Figure 5.16 ^{13}C NMR spectrum (100MHz, CDCl$_3$) of oleic acid (4)
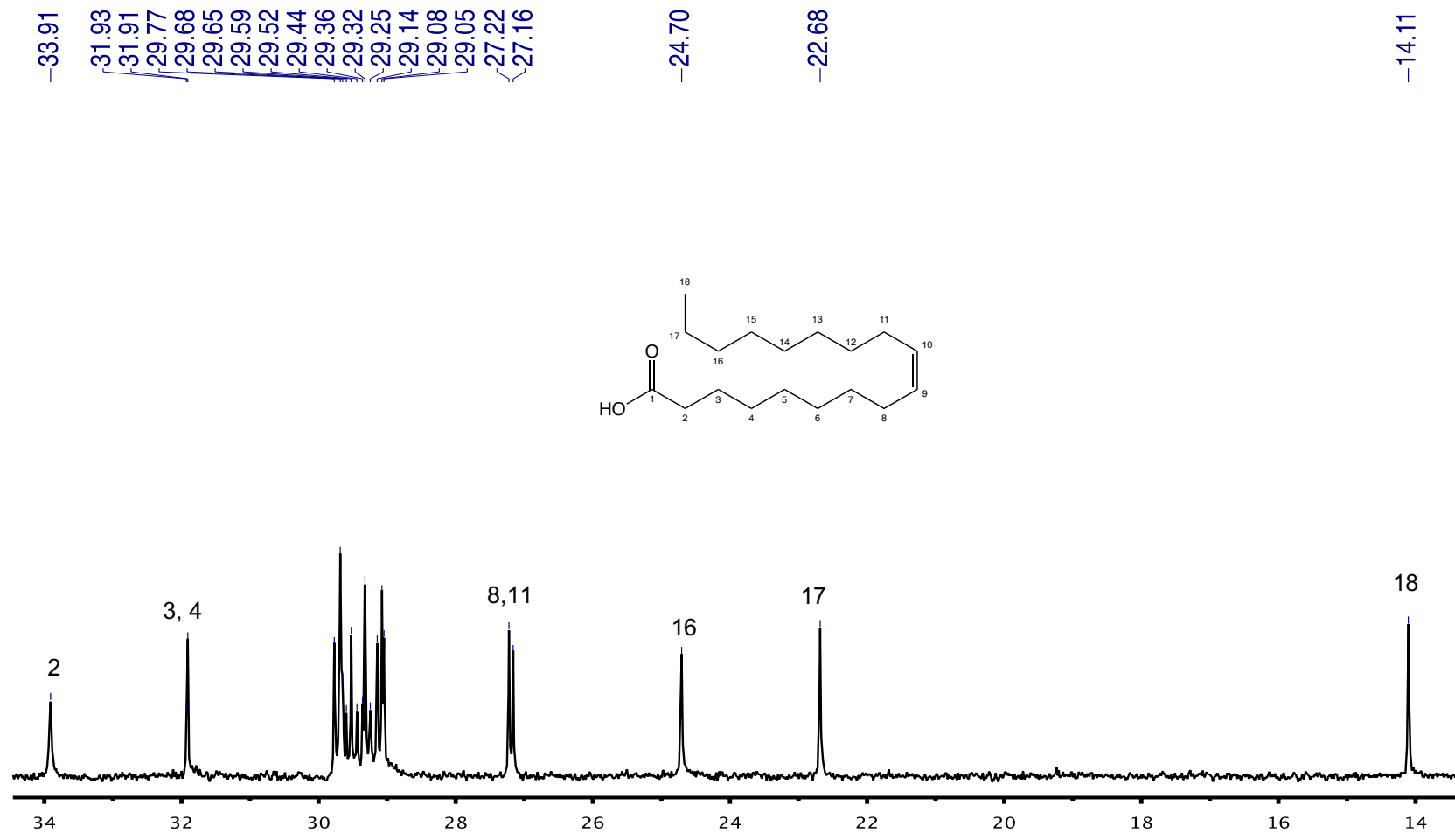
Figure 5.17 ^{13}C NMR spectrum (100MHz, CDCl$_3$) of oleic acid (4) - expansion
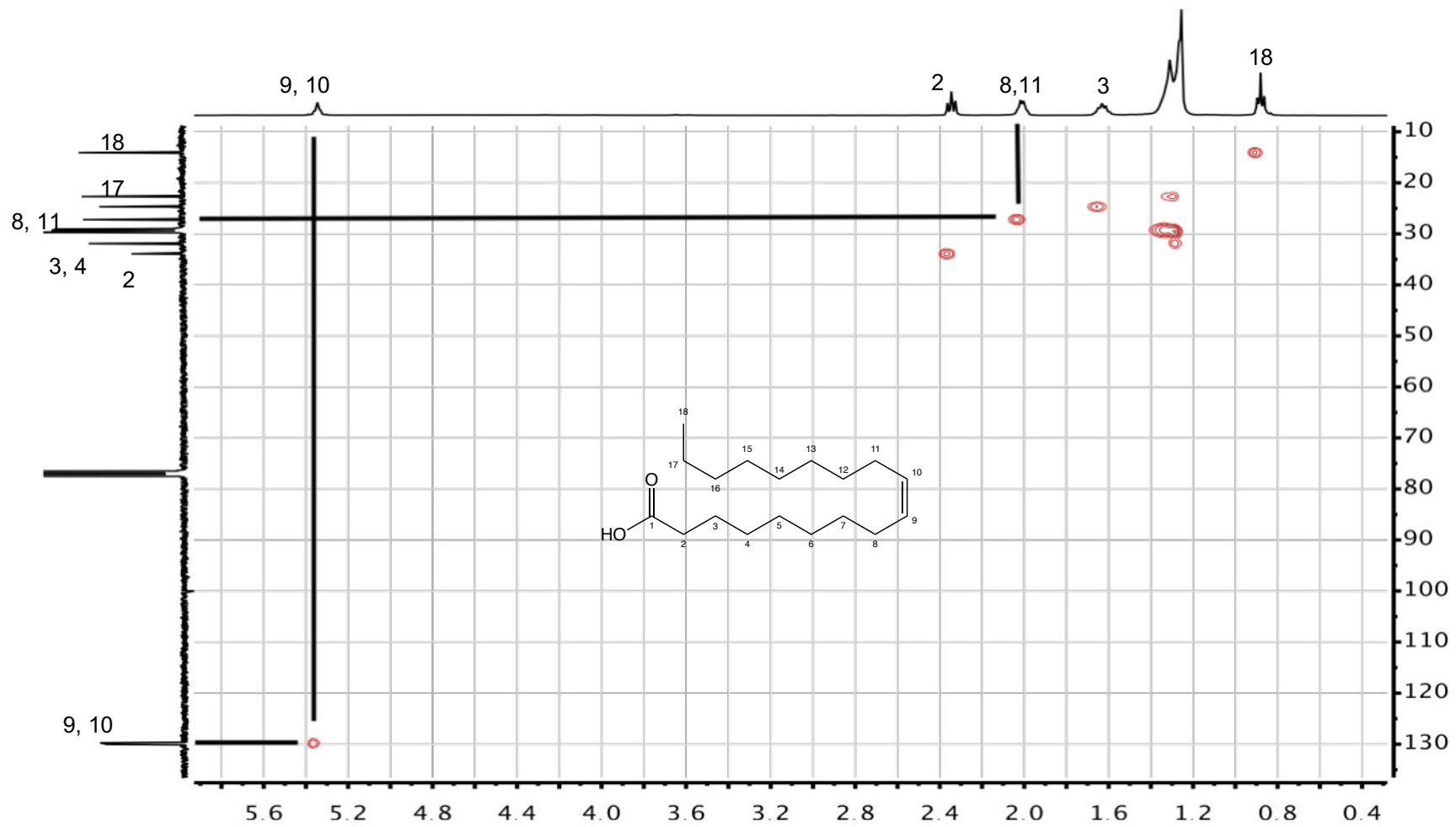
Figure 5.18 ^{1}H-^{13}C HSQC spectrum (400MHz, CDCl$_3$) of oleic acid (4)

5.1.3.5 Physic and spectroscopic data of β-sitosterol (5)
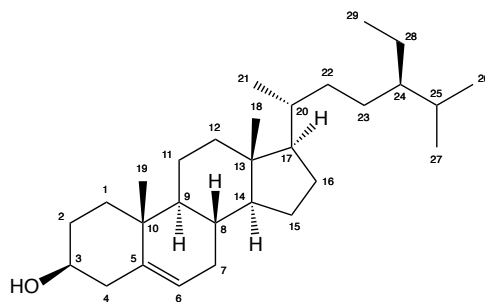
Figure 5.19 Structure of β-sitosterol (5)

Compound 5 (Figure 5.19) was separated in large amounts from its fraction and after purification by CC it was found to crystalize into colorless-yellowish needles. The pure steroid has a strong tea odor. It resulted to be very soluble in $CHCl_3$ but less soluble in other nonpolar solvents, unless other components of its native fraction were dissolved first. The compound resulted to have mp of 138-140°C and its molecular formula is $C_{29}H_{50}O$. The following spectral data for compound 5 were also confronted with the literature (Table 5.2).

^{1}H NMR (400 MHz, $CDCl_3$) δ (ppm): 0.68 (s, 3H), 0.81 (d, *J*=6.9 Hz, 3H), 0.83 (d, *J*=7.4 Hz, 3H), 0.84 (t, *J*=7.4 Hz, 3H), 0.92 (d *J*=6.6 Hz, 3H), 1.01 (s, 3H), 1.68 (de, *J*=7.4, 6.8 Hz, 1H), 1.84 (m, 3H), 1.99 (m, 2H), 2.29 (ddd, *J*=20.9, 13.3, 2.6 Hz, 2H), 3.52 (m, 1H), 5.35 (psd, *J*=5.5Hz, 1H). ^{13}C NMR (100MHz, $CDCl_3$) δ (ppm): 11.87 ppm (C-18), 11.99 ppm (C-29), 18.79 ppm (C-21), 19.04 ppm (C-27), 19.41 (C-19), 19.83 ppm (C-26), 21.10 (C-11), 23.08 (C-28), 24.31 (C-15), 26.09 (C-23), 28.26 (C-16), 29.17 (C-25), 31.68 (C-2), 31.91 (C-8), 31.93 (C-7), 33.96 (C-22), 36.16 (C-20), 36.52 (C-10), 37.26 (C-1), 39.79 (C-12), 42.32 (C-4), 42.33 (C-13), 45.84 (C-24), 50.14 (C-

9), 56.07 (C-17), 56.78 (C-14), 71.82 (C-3), 121.72 (C-6), 140.76 (C-5). GC-MS R$_t$ (min): 115.146; (EI) m/z: 414 (M$^{+\bullet}$), 396 (50%), 329 (50%), 273 (25%), 255 (25%).

5.1.3.5.1 Structural elucidation of β-sitosterol (5)
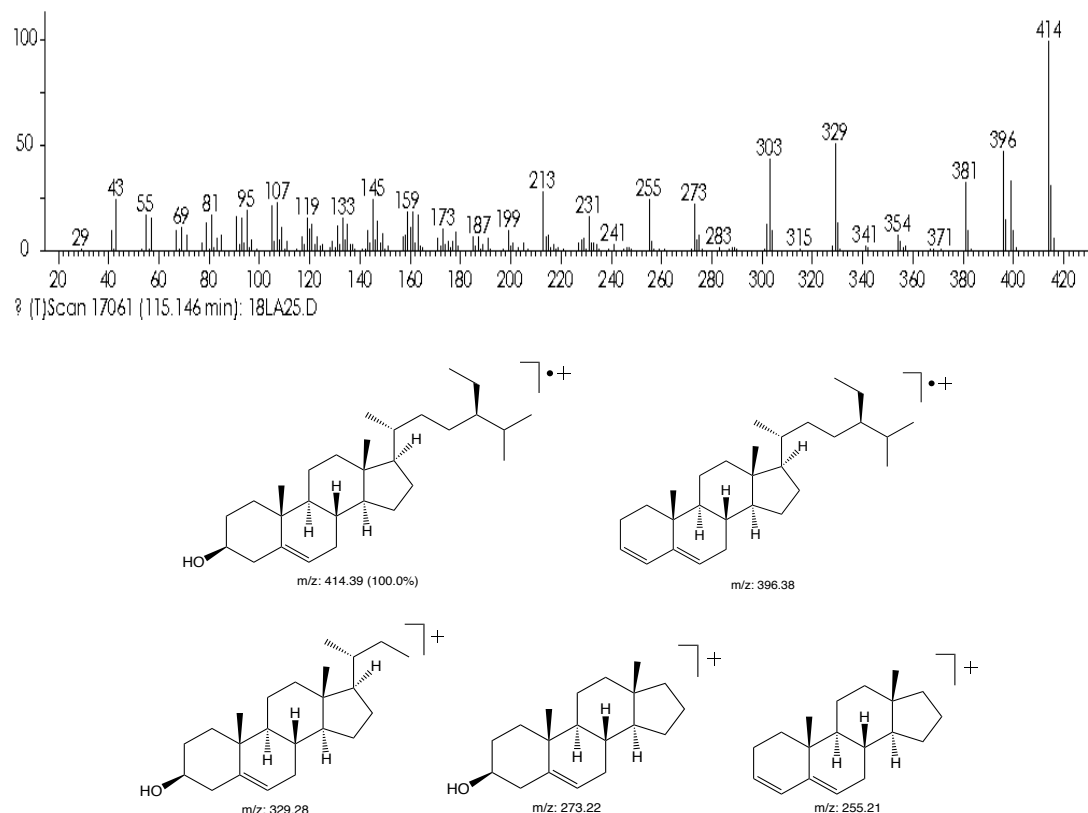
Figure 5.20 EI/MS of β-sitosterol (5) and characteristic fragmentations

The EI/MS spectrum of compound 5 showed loss of 18 units from the molecular ion (m/z: 414), which is characteristic of secondary alcohols. This fragmentation generates the radical cation with m/z 396 important for the structure elucidation. Other fragmentations of particular relevance are the partial loss of the side chain, as a radical of 85 Da, giving as result a cation with m/z 329. Also, the total loss of the side chain, as a radical of 141 Da giving the cation with m/z 273 is characteristic of sterols. The last cation of m/z 255

can be generated as well from the radical cation of 396 m/z, which gives as well important information over the molecule's structure. The mass spectrum and the most important fragments in the process of confirmation of the sterol are reported in figure 5.20. The NIST library was also used to counter check the obtained results.

The ^{1}H NMR spectrum (Figure 5.21) showed signals typical of a steroid, with a lot of signals in the upfield region. They are given from all the protons of the aliphatic hydrogens of the four rings and substituents of the molecule. The most important and simpler to recognize are the signals relative to all the CH$_3$ of the compound, which give very intense, of small multiplicity and upfield signals: the singlet at 0.68 ppm (3H, Me-18), the doublet at 0.81 ppm (J=6.9 Hz, 3H, Me-27), the doublet at 0.83 ppm (J=7.4 Hz, 3H, Me-26), the triplet at 0.84 (J=7.4 Hz, 3H, Me-29), the doublet of 0.92 ppm (J=6.6 Hz, 3H, Me-21) and the singlet at 1.01 ppm (3H, Me-19). Other signals that were assigned are some more downfield signals: the double heptaplet at 1.68 ppm (J=7.4, 6.8 Hz, 1H, H-25), a multiplet that integer for three protons at 1.84 ppm (H-1a, H-2b and H-16a), as visible from the HSQC spectrum. Then follow another multiplet that integer for other two protons at 1.99 ppm (H-2a and H-12a) also confirmed by the HSQC spectrum, the signal at 2.29 ppm (ddd, J=20.9, 13.3, 2.6 Hz, 2H, H-4). The multiplet relative to the proton germinal to the hydroxyl group at 3.52 ppm (m, 1H, H-3), the position of the latter was also confirmed by the HMBC experiment was the ^3J correlation between H-3 and C-5 was also observed. Then it is followed by the most shielded signal of the vinylic hydrogen at 5.35 ppm (psd, J=5.5 Hz, 1H, H-6) and the position of the double bond was also confirmed by ^3J correlation between H6 and C-10 and H-3 and

C-5; these last signals in particular were the decisive ones in the characterization of the type of sterol analyzed.

The ^{13}C NMR spectrum (Figure 5.22) also showed a steroid pattern with very few signals in the downfield region: a quaternary carbon at 140.76 ppm (C-5), the vinylic carbon at 121.72 ppm (C-6), these two signals were decisive for the characterization of the sterol, because confirmed the presence of the double bond and its position in the molecule (as shown by the HMBC correlations). Then there is the carbon directly attached to the hydroxyl group at 71.82 ppm (C-3), which also was important to confirm the presence of a hydroxyl group (as shown by the HMBC correlations). In contrast to the downfield region, there were a lot of signals in the upfield region of the spectrum (Figure 5.23) which were all relative to the protons of the steroid rings and lateral chain. Especially simple to recognize were the methyl carbons at 11.87 ppm (C-19), 11.99 ppm (C-29), 18.79 ppm (C-21), 19.04 ppm (C-27), 19.41 (C-18) and 19.83 ppm (C-26). These signals are the most shielded of the spectrum and are characteristic of steroid molecules. It was also taken a 1D DEPT135 spectrum (Figure 5.24) which was useful to individuate some overlapping signals like the ones at 31.93 and 31.91 ppm (C-7 and C-8). The assigned signals were also confirmed from the literature (*96*).

The molecule was also analyzed using 2D NMR experiments: ^{1}H-^{1}HCOSY, ^{1}H-^{13}C HSQC, ^{1}H-^{13}C HMBC (Figure 5.25) and 1H-^{1}H NOESY. All the spectra confirmed the same molecule and in particular the NOESY experiment was important for the determination of the stereocenters configuration (Figure 5.26). In fact, from the NOESY spectrum was possible to

observe the lack of correlation between the H_3 and any other methyl group of the molecule. The most important being Me-18 and Me-19 which are clearly pointing on the opposite diastereotopic face of the molecule. The configurations of these groups with respect to the one of the H_3, confirms the configuration for all the stereocenters of the steroid as the β stereoisomer of the sitosterol.

Table 5.2 Spectroscopic data of β-sitosterol (5)

n	^{1}H NMR (400 MHz, CDCl$_3$) δ (ppm), (*96*)	^{1}H NMR (400 MHz, CDCl$_3$) δ (ppm), 5	^{13}C NMR (100MHz, CDCl$_3$) δ (ppm), (*96*)	^{13}C NMR (100MHz, CDCl$_3$) δ (ppm), 5
1a	-	1.84 m	37.2	37.26
1b	-	-		
2a	-	1.99 m	31.6	31.68
2b	-	1.84 m		
3	3.52 m	3.52 m	71.8	71.82
4	-	2.29 (ddd, *J*=20.9, 13.3, 2.6 Hz, 2H)	42.3	42.32
5	-	-	140.7	140.76
6	5.35 dt	5.35 (psd, *J*=5.5 Hz, 1H)	121.7	121.72
7	-	-	31.9	31.93
8	-	-	31.9	31.91
9	-	-	50.1	50.14
10	-	-	36.5	36.52
11	-	-	21.1	21.10
12a	-	1.99 m	39.8	39.79
12b	-	-		
13	-	-	42.3	42.33
14	-	-	56.8	56.78
15	-	-	24.3	24.31
16a	-	1.84 m	28.2	28.26
16b	-	-		
17	-	-	56.0	56.07
18	0.68 s	0.68 s	11.9	11.87
19	1.01 s	1.01 s	19.4	19.41
20	-	-	36.1	36.16
21	0.92 d	0.92 (d *J*=6.6 Hz, 3H)	18.8	18.79
22	-	-	33.9	33.96
23	-	-	26.0	26.09
24	-	-	45.8	45.84
25	-	1.68 (dh, *J*=7.4, 6.8 Hz, 1H)	29.1	29.17
26	0.83 d	0.83 (d, *J*=7.4 Hz, 3H)	19.8	19.83
27	0.81 d	0.81 (d, *J*=6.9 Hz, 3H)	19.0	19.04
28	-	-	23.0	23.08
29	0.84 t	0.84 (t, *J*=7.4 Hz, 3H)	12.0	11.99
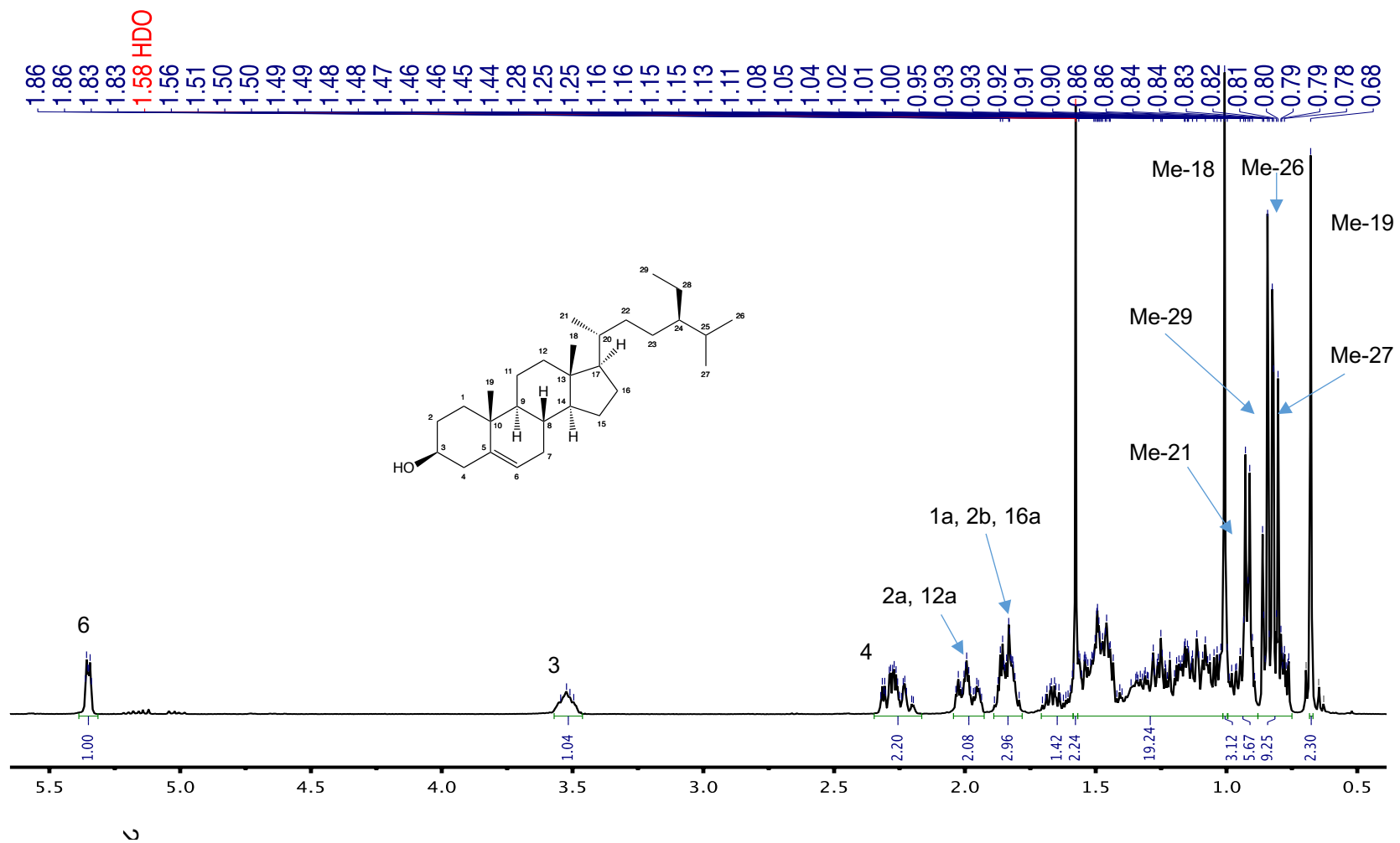
Figure 5.21 ^{1}H NMR spectrum (400MHz, CDCl$_3$) of β-sitosterol (5)
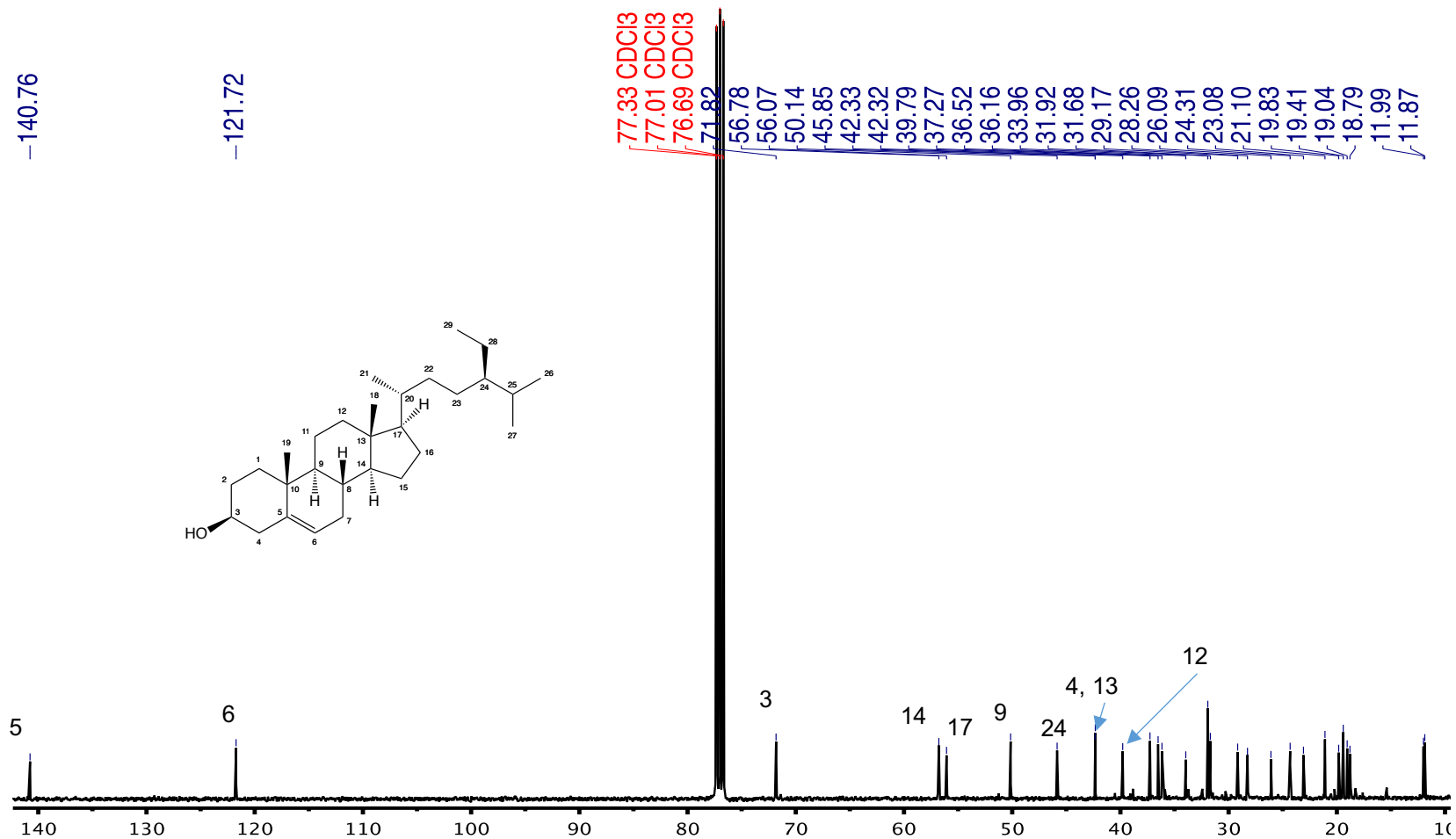
Figure 5.22 ^{13}C NMR spectrum (100MHz, CDCl$_3$) of β-sitosterol (5)
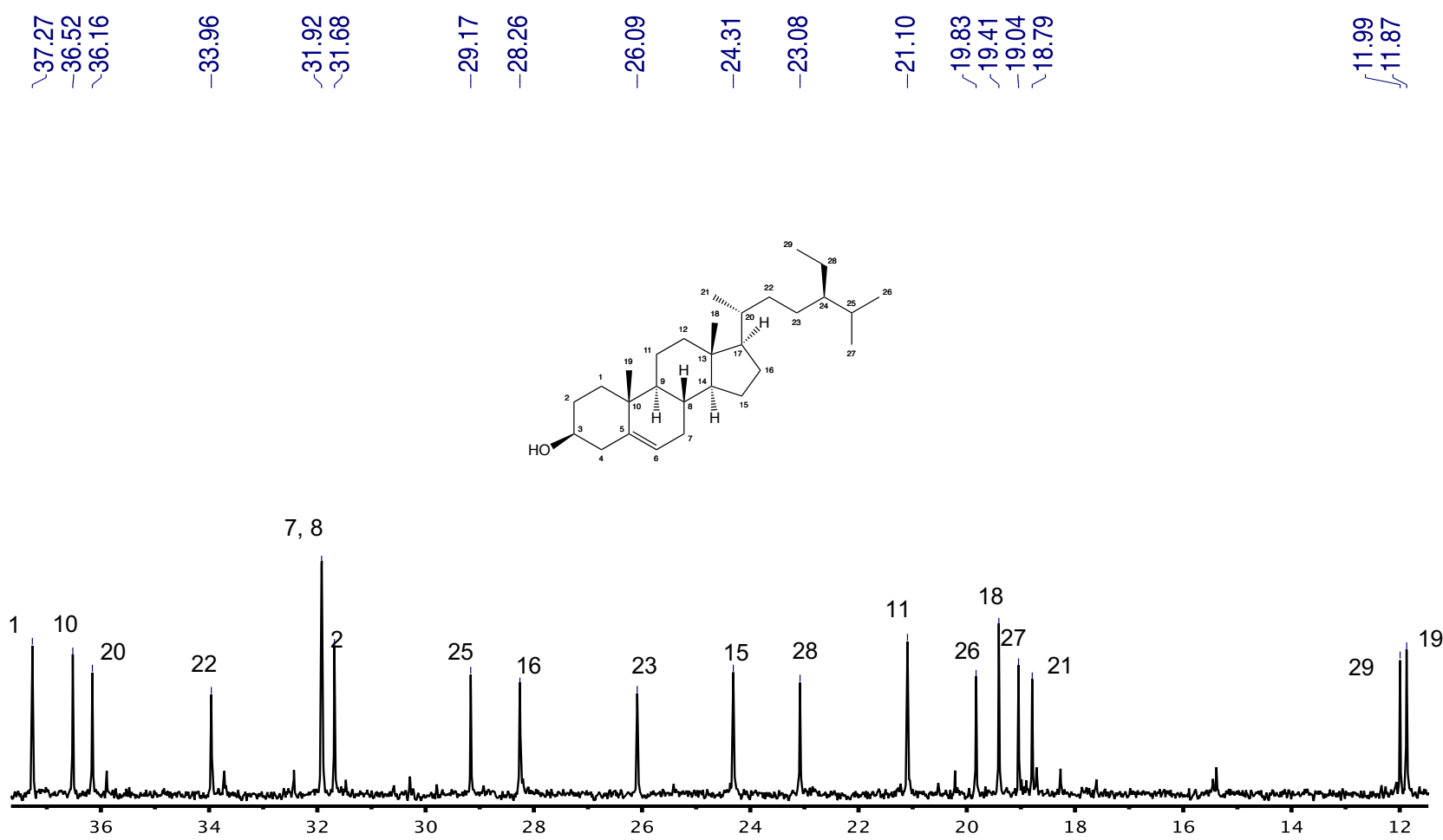
Figure 5.23 ^{13}C NMR spectrum (100MHz, CDCl$_3$) of β-sitosterol (5) – expansion
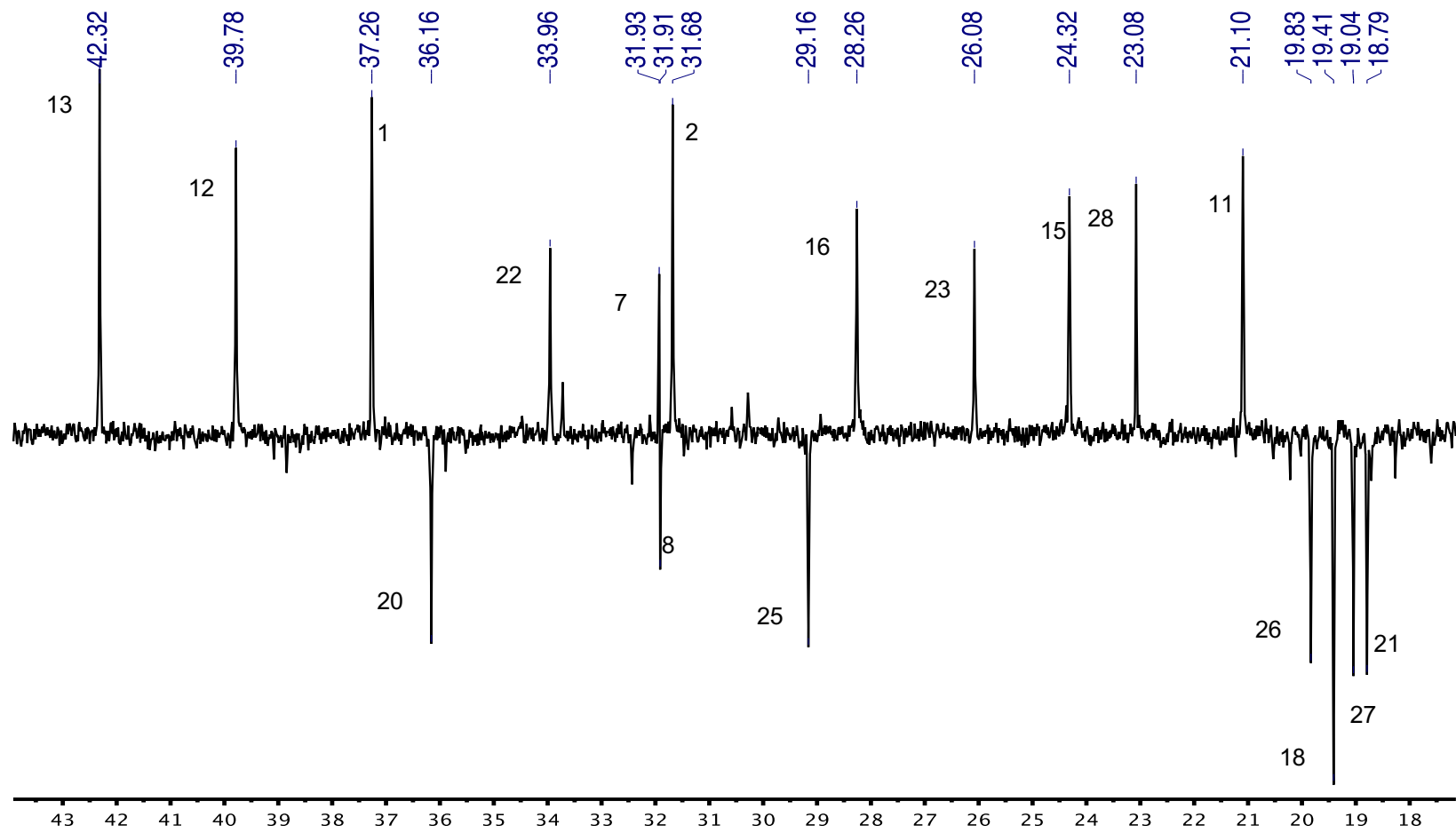
Figure 5.24 ^{1}D DEPT135 spectrum (100MHz, CDCl$_3$) of β-sitosterol (5) - expansion
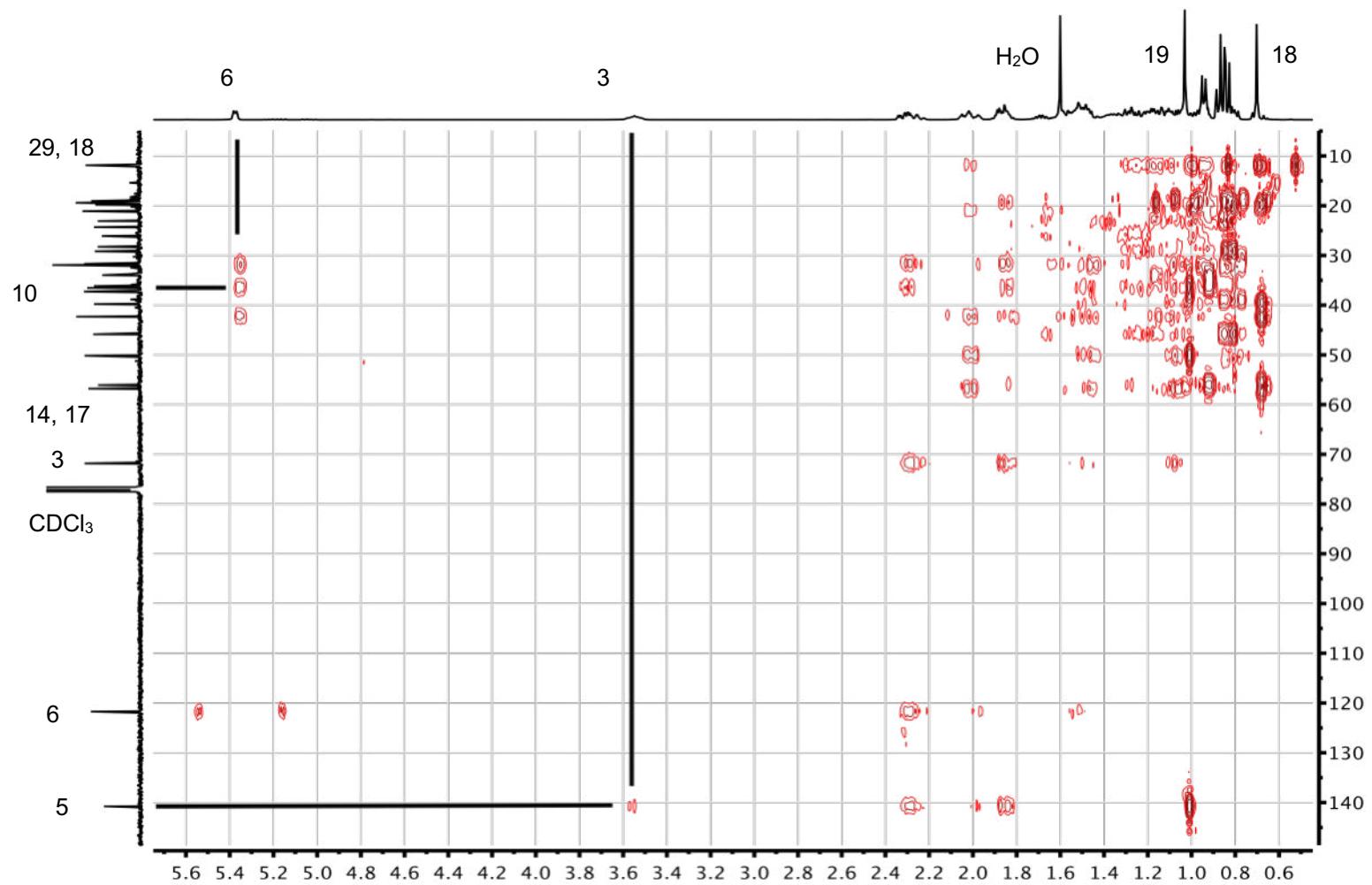
Figure 5.25 ^{1}H-^{13}C HMBC spectrum (400MHz, CDCl$_3$) of β-sitosterol (5)
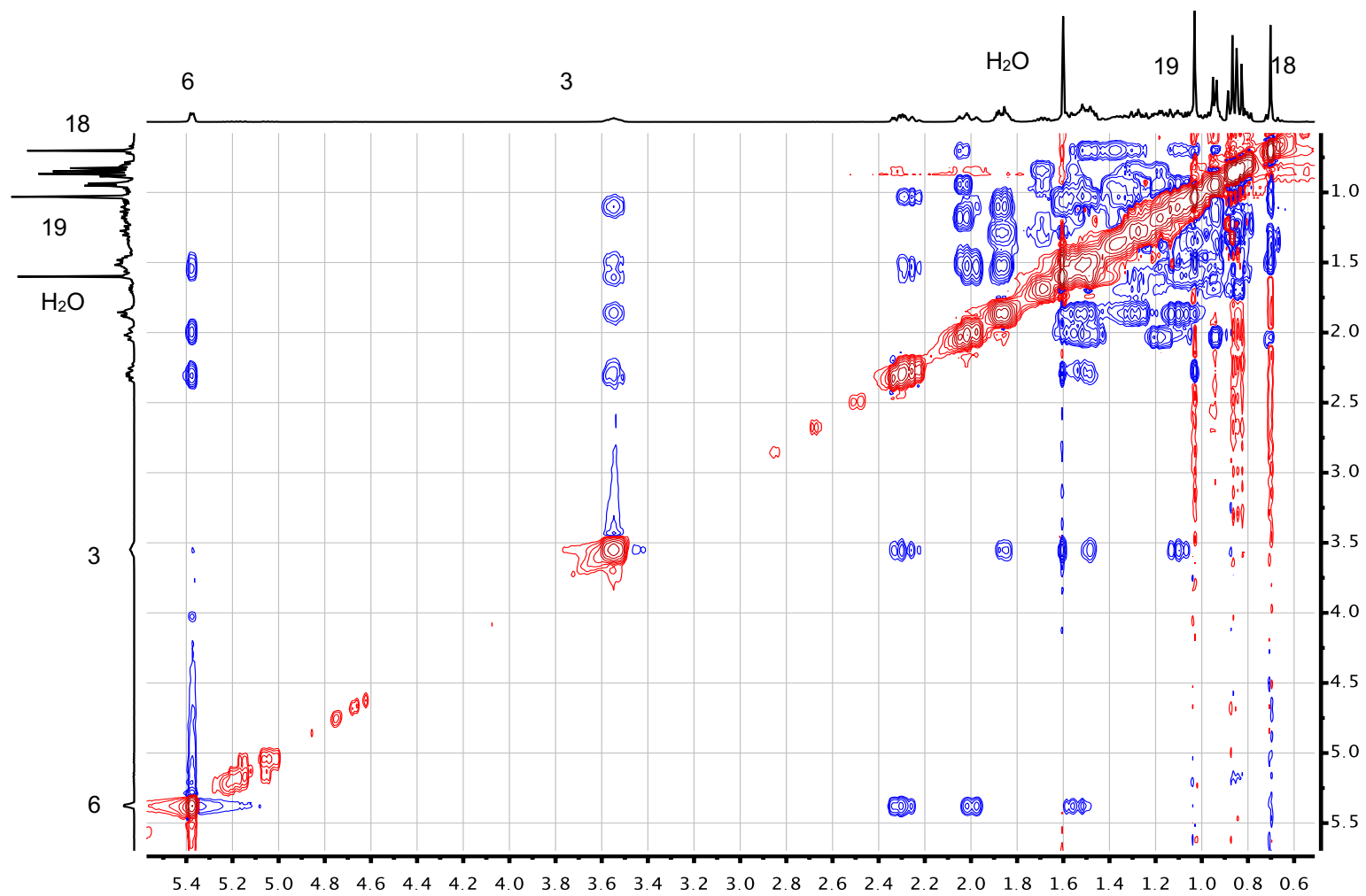
Figure 5.26 ^{1}H-^{1}H NOESY spectrum (400MHz, CDCl$_3$) of β-sitosterol (5)

5.1.3.6 Physic and spectroscopic data of β-sitosteryl acetate (5a)
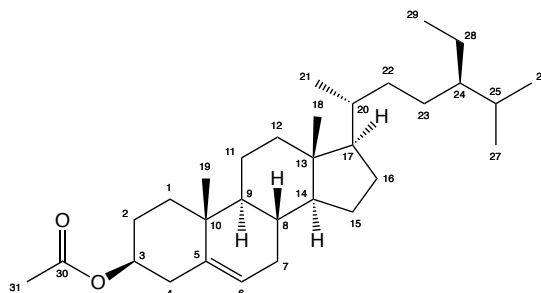
Figure 5.27 Structure of β-sitosteryl acetate (5a)

Compound 5a (Figure 5.27) present itself as a white solid which crystalize in $CHCl_3$. It was found to be perfectly soluble in $CHCl_3$, less in other non-polar solvents, like the natural product (5) from which it was derived it does not reveal under the UV light, it is just barely visible as a black shadow at 254 nm. It has mp of 126-128 °C and a molecular formula of $C_{31}H_{52}O_2$. The following spectral data for compound 5a were also confronted with the literature (Table 5.3).

^{1}H NMR (400 MHz, $CDCl_3$) δ (ppm): 0.70 (s, 3H), 0.84 (d, J=6.7 Hz, 3H), 0.85 (d, J=7.7 Hz, 3H), 0.86 (t, J=7.7 Hz, 3H), 0.94 (d, J=6.4 Hz, 3H), 1.04 (s, 3H), 2.05 (s, 3H), 2.34 (d, J=7.7 Hz, 2H), 4.62 (m, 1H), 5.40 (psd, J=5.0 Hz, 1H). ^{13}C NMR (100MHz, $CDCl_3$) δ (ppm): 11.86 ppm (C-18), 11.99 ppm (C-29), 18.79 ppm (C-21), 19.04 ppm (C-25), 19.32 (C-19), 19.82 ppm (C-26), 21.04 (C-11), 21.45 (C-31), 23.08 (C-28), 24.30 (C-15), 26.09 (C-23), 27.78 (C-16), 28.25 (C-2), 29.17 (C-27), 31.87 (C-8), 31.91 (C-7), 33.95 (C-22), 36.16 (C-20), 36.66 (C-10), 37.00 (C-1), 38.13 (C-4), 39.73 (C-12), 42.32 (C-13), 45.85 (C-24), 50.04 (C-9), 56.05 (C-17), 56.70 (C-14), 73.99 (C-3),

122.64 (C-6), 139.66 (C-5), 170.53 (C-31). GC-MS R_t (min): 118.70; (EI) m/z: 456 (M$^{+•}$), 413 (1%), 396 (100%), 329 (1%), 273 (15%), 255 (15%).

5.1.3.6.1 Structural elucidation of β-sitosteryl acetate (5a)
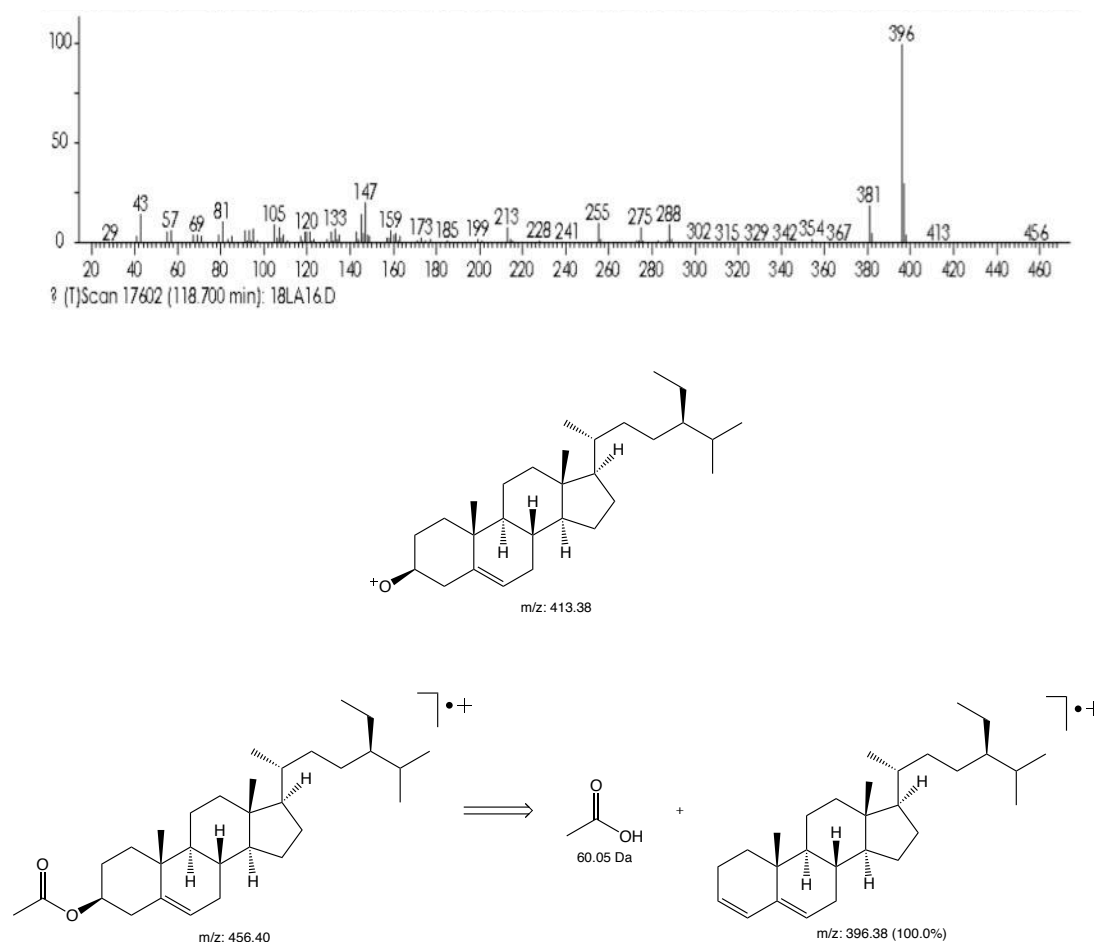
Figure 5.28 EI/MS of β-sitosteryl acetate (5a) and characteristic fragmentations

Fragmentation of the acetyl sitosterol gave rise to the same loss of its raw material the β-sitosterol. In fact, we can find the same peaks but with different intensities. This is due to the easier loss of the acetyl group in form of acylium cation or in for of neutral acetic acid. The fragmentations have very different probabilities of taking place and the cause of this is the different

stability of their products. The radical cation with m/z 396 (base peak) is the most probable product of the fragmentation, because the side product of the process is a neutral molecule of acetic acid. Instead the formation of the cation with m/z 413 is very improbable, because of the high electronegativity of the oxygen which cannot retain the positive charge. The rest of the important fragments are the result of the loss of the side chain of the sterol, much like in the β-sitosterol (329, 275 y 255). Fragments and mass spectrum are reported in the figure 5.28.

The ^{1}H NMR spectrum (Figure 5.29) showed signals typical of a steroid, with a lot of signals in the upfield region. These signals are given from all the protons of the aliphatic hydrogens of the four rings and substituents of the molecule, as it was also seen in the previous steroidal molecules. The most important and simpler to recognize are the signals relative to all the CH_3 of the compound, which give very intense, of small multiplicity and upfield signals: the singlet at 0.70 ppm (3H, Me-18), the doublet at 0.84 ppm (J=6.9 Hz, 3H, Me-27), the doublet at 0.86 ppm (J=7.4 Hz, 3H, Me-26), the triplet at 0.85 (J=7.4 Hz, 3H, Me-29), the doublet of 0.94 ppm (J=6.6 Hz, 3H, Me-21) and the singlet at 1.04 ppm (3H, Me-19). Other signals that were assigned are some more downfield signals: the singlet at 2.05 ppm (3H, Me-31), the latter is characteristic of an acetyl group and it confirmed the acetylation of the molecule. Then a multiplet at 4.62 ppm (m, 1H, H-3) relative to the proton germinal to the acetyl group and then the most shielded signal of the vinylic hydrogen at 5.40 ppm (psd, J=5.0 Hz, 1H, H-6); these last signals in particular were the decisive ones in the characterization of the type of sterol analyzed.

The ^{13}C NMR spectrum (Figure 5.30) also showed a steroid pattern with very few signals in the downfield region: two Sp^2 quaternary carbons at 170.53 ppm (C-30) and at 139.66 ppm (C-5), relative to the carbonyl of the acetyl group and the totally substituted vinylic carbon respectively. Then the tertiary vinylic carbon at 122.64 ppm (C-6), these three signals were decisive for the characterization of the acetylated sterol, because confirmed the presence of the double bond and that its position in the molecule did not change through the reaction. If the position of the double bond was different, the signals of the carbons C-5 and C-6 would have been also less shielded than they are as shown in the literature and was also confirmed the presence of the acetyl group bound to the molecule. Then there is the carbon directly attached to the acetyl group at 73.99 ppm (C-3), which also was important to confirm the presence of an esterified hydroxyl group. In contrast to the downfield region, there were a lot of signals in the upfield region of the spectrum which were all relative to the protons of the steroid rings and lateral chain. Especially fast to recognize were the methyl carbons at 11.86 ppm (C-18), 11.99 ppm (C-29), 18.82 ppm (C-21), 19.04 (C-19), 19.32 ppm (C-26) and 29.17 ppm (C-27). These signals are the most shielded of the spectrum and are characteristic of steroid molecules (Figure 7.31). It was also taken a 1D DEPT135 spectrum (Figure 5.32) which was useful to discriminate between carbons carrying an even or an odd number of hydrogens. The assigned signals were also confirmed from the literature (*78*).

Table 5.3 Spectroscopic data of β-sitosteryl acetate (5a)

n	^{1}H NMR (400 MHz, CDCl$_3$) δ (ppm), (*97*)	^{1}H NMR (400 MHz, CDCl$_3$) δ (ppm), 5a	^{13}C NMR (100MHz, CDCl$_3$) δ (ppm), (*97*)	^{13}C NMR (100MHz, CDCl$_3$) δ (ppm), 5a
1	-	-	36.9	37.00
2	-	-	29.0	
3	4.62 m	4.62 (m, 1H)	73.7	73.99
4	-	2.34 (m, 2H)	38.1	38.13
5	-	-	139.7	139.66
6	5.36 (t, *J*=5.4 Hz, 1H)	5.40 (psd, *J*=5.0 Hz, 1H)	122.5	122.64
7	-	-	31.9	31.91
8	-	-		31.87
9	-	-	50.0	50.04
10	-	-	36.5	36.66
11	-	-	21.0	21.04
12	-	-	39.7	39.73
13	-	-	42.3	42.32
14	-	-	56.7	56.70
15	-	-	24.9	24.30
16	-	-	28.2	27.78
17	-	-	56.0	56.05
18	0.77 s	0.70 s	11.8	11.86
19	0.99 s	1.04 s	19.0	19.04
20	-	-	36.1	36.16
21	0.87 d	0.94 (d, *J*=6.4 Hz, 3H)	19.8	19.82
22	-	-	34.4	33.95
23	-	-	27.1	26.09
24	-	-	45.8	45.85
25	-	-	23.0	18.79
26	-	0.85 (d, *J*=7.7 Hz, 3H)	19.3	19.32
27	-	0.84 (d, *J*=6.7 Hz, 3H)	29.6	29.17
28	-	-	18.7	23.08
29	0.84 (t, *J*=6.6 Hz, 3H)	0.86 (t, *J*=7.7 Hz, 3H)	11.9	11.99
30	-	-	170.9	170.53
31	2.04 s	2.05s	-	21.45
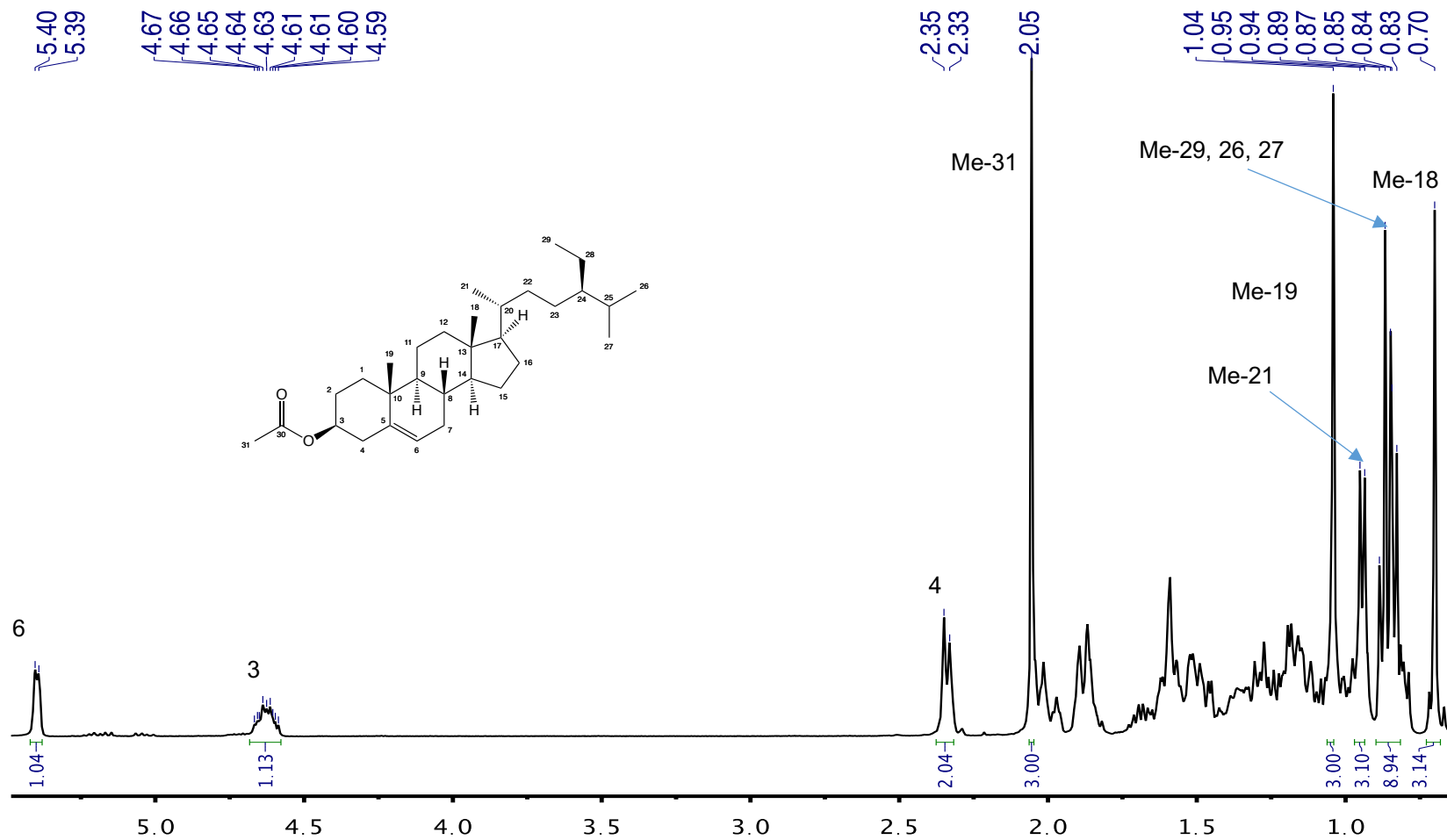
Figure 5.29 ^{1}H NMR spectrum (400MHz, CDCl$_3$) of β-sitosteryl acetate (5a)
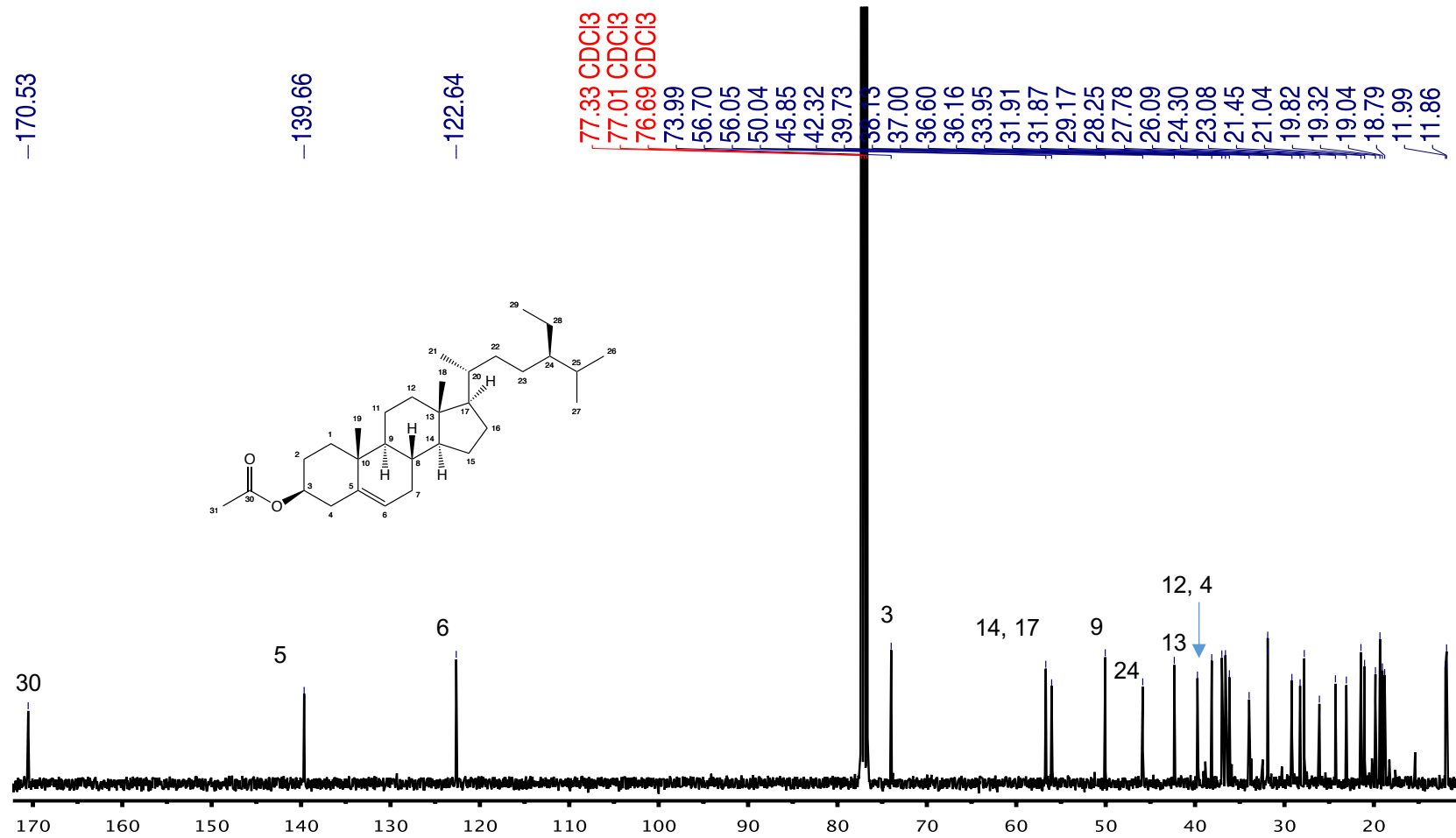
Figure 5.30 ^{13}C NMR spectrum (100MHz, CDCl$_3$) of β-sitosteryl acetate (5a)
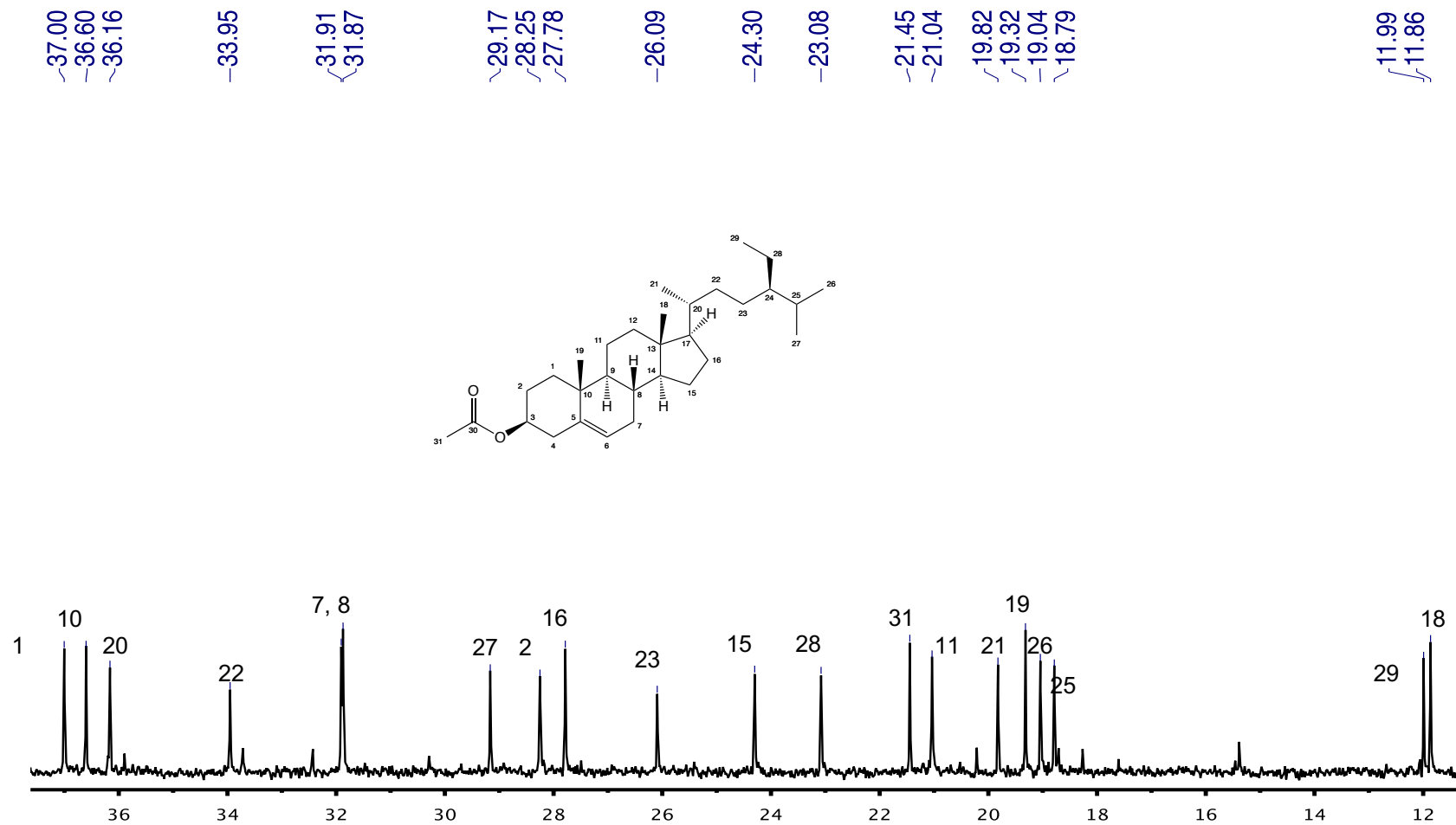
Figure 5.31 ^{13}C NMR spectrum (100MHz, CDCl$_3$) of β-sitosteryl acetate (5a) - expansion
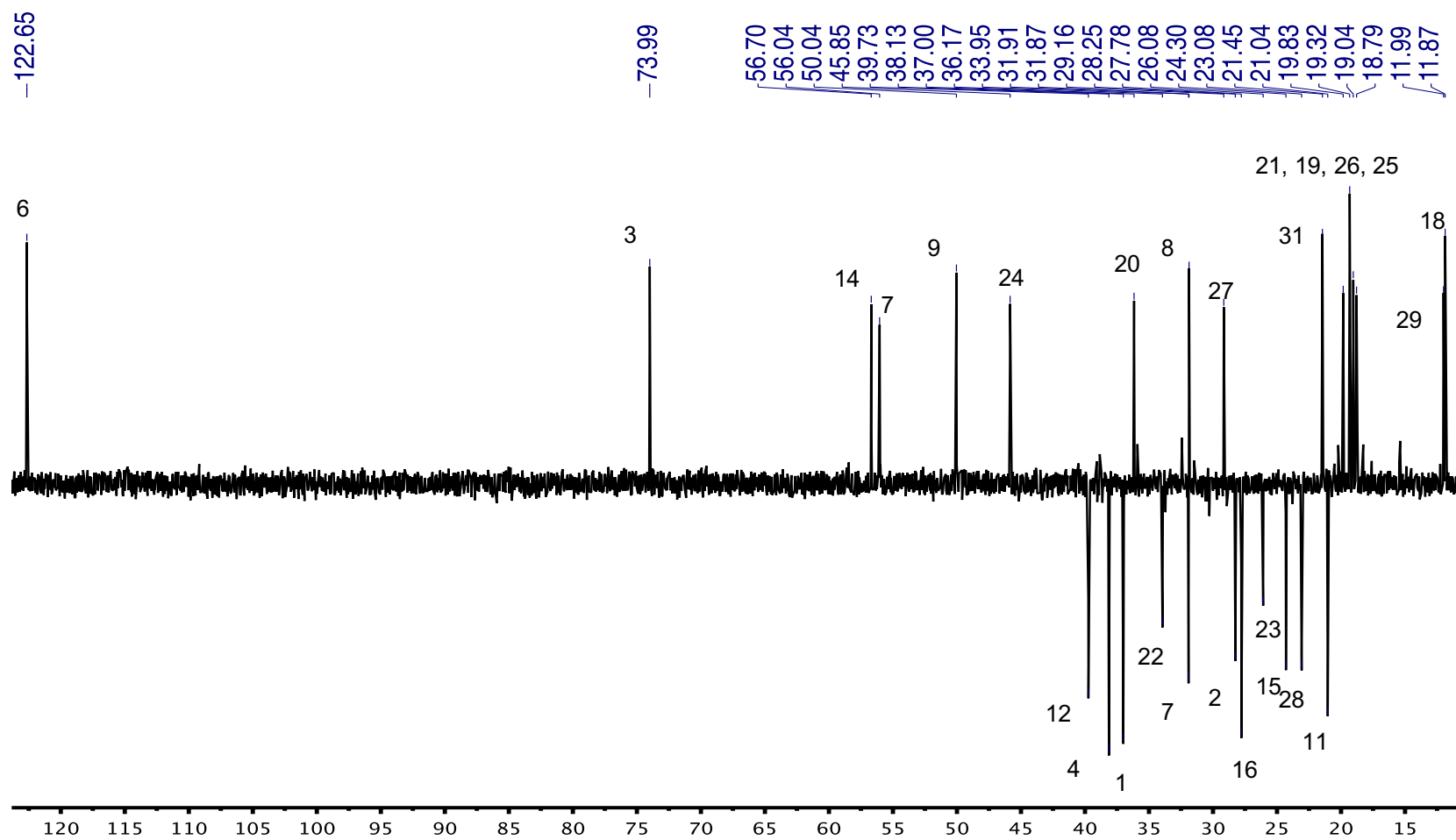
Figure 5.32 [1]D DEPT135 spectrum (100MHz, CDCl$_3$) of β-sitosteryl acetate (5a)

5.1.4 The chloroform/methanol (1:1) extraction

The second extract was made with chloroform/methanol (1:1) using the previously defatted vegetal material. This mixture of solvents, being of medium polarity, has the ability of extracting a broader spectrum of metabolites then the single solvents should have. Some of those metabolites comprehend polar terpenoids compounds, coumarins, lignans, alkaloids, polyphenolic compounds, glycosylated compounds and sugars. So, this maceration had the objective of extracting the majority of the natural products, intended as secondary metabolites of the plant. The molecules that were isolated from the fractionation of this extract were seven: compound 6 to 12 and their physical, chemical and spectroscopic properties are described in the next paragraphs.

5.1.4.1 Physic and spectroscopic data of heneicosane (6)
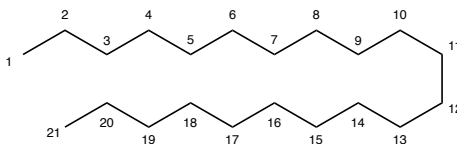
Figure 5.33 Structure of heneicosane (6)

The alkane 6 (Figure 5.33) precipitated as a white amorphous solid. It is soluble in $CHCl_3$ and hexane but less soluble in other nonpolar solvents and it always needs to be heated to be solubilized completely. The compound had mp of 43-45°C and its molecular formula is $C_{21}H_{44}$.

^{1}H NMR (400 MHz, $CDCl_3$) δ (ppm): 0.88 (t, J=6.7 Hz, 3H), 1.25 (s, 37H). ^{13}C NMR (100MHz, $CDCl_3$) δ (ppm): 14.14 (2CH_3), 22.71 (C-2 and C-19), 29.38 (C-4 and C-17), 29.68 (C-5 and C-16), 29.72 (11C), 31.95 (C-3 and

C-18). GC-MS R_t (min): 71.609; (EI) m/z: 296 ($M^{+\bullet}$), 57 (100%), 71 (85%), 85 (75%), 43 (40%).

5.1.4.1.1 Structural elucidation of heneicosane (6)

The mass spectrum of compound 6 (Figure 5.34) showed the classic pattern of a long chain alkane, with differences of 14 Da between almost all the peaks. The molecule identification was confirmed by confrontation with the NIST database.
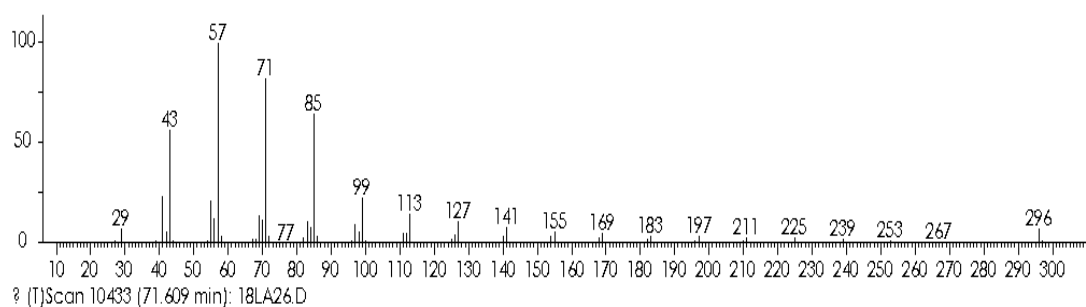
Figure 5.34 EI/MS spectrum of heneicosane (6)

The ^{1}H NMR spectrum (Figure 5.35) showed signals typical of long chain alkane, with a upfield triplet at 0.88 ppm (*J*=6.7 Hz, 6H, 2Me) that integer for the terminal methyl groups and a more downfield singlet that integer for the other 36 protons (1.25 ppm), typical of long chains of CH_2. The absence of any other signal showed that the molecule was an alkane with no substituents or ramifications. The ^{13}C NMR spectrum (Figure 5.36) also showed a long chain alkane molecule pattern with very few signals in the downfield region and a lot of signals in the upfield region of the spectrum. A intense signal at 29.72 ppm corresponds to the majority of the CH_2 of the molecule (10C). Then there were a series of signal which were relative to two carbons each and started with the

104

two methyl groups at 14.14 ppm and continued with the carbons following up the chain at 22.71 ppm (C-2 and C-19), 29.38 ppm (C-4 and C-17), 29.68 ppm (C-5 and C-16) and 31.95 ppm (C-3 and C-18). The absence of other signals was indicative of an alkane molecule.
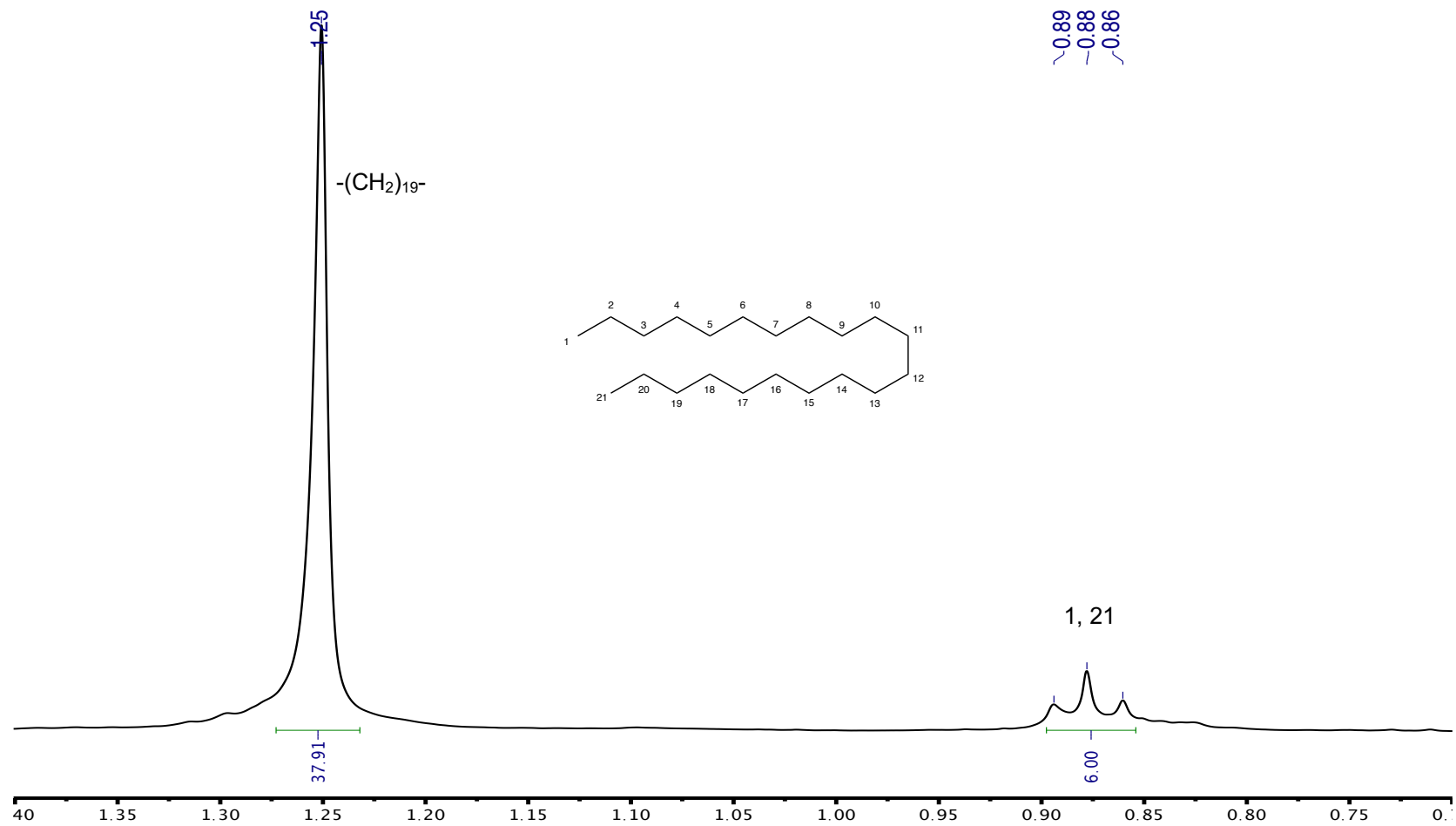
Figure 5.35 ^{1}H NMR spectrum (400MHz, CDCl$_3$) of heneicosane (6)
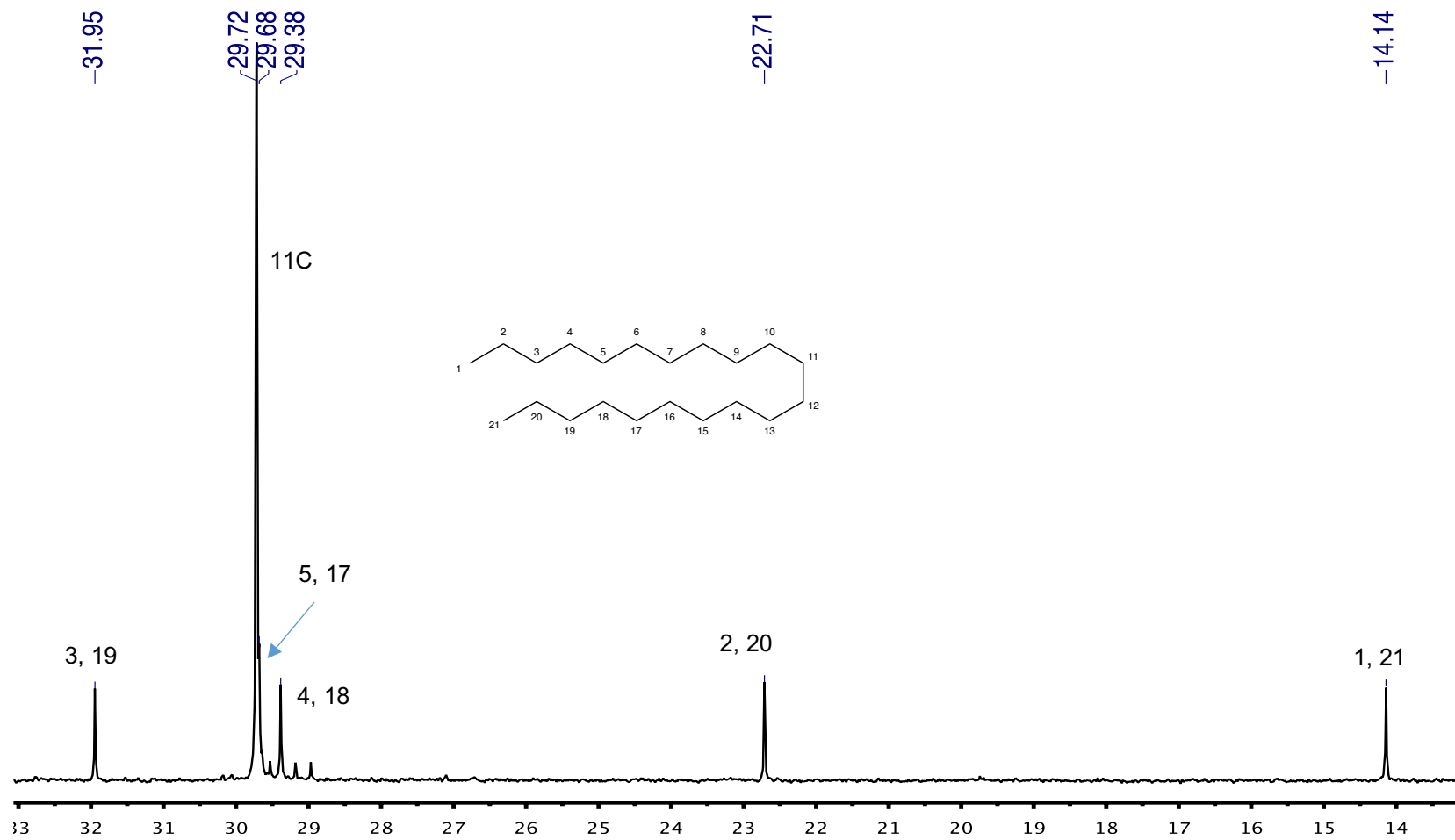
Figure 5.36 ^{13}C NMR spectrum (100MHz, CDCl$_3$) of heneicosane (6)

5.1.4.2 Physic and spectroscopic data of triacontanol (7)
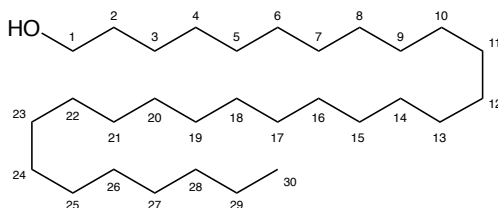
Figure 5.37 Structure of triacontanol (7)

The alcohol (Figure 5.37) crystallizes in small flat crystals flakes with a chromium shade, but once it was completely dry it looked like an amorphous white solid with the consistence of plastic. It resulted to be completely insoluble in the majority of solvents but slightly soluble in pyridine, with a higher solubility when the solvent was heated up. The compound has mp of 77-78°C and its molecular formula is $C_{30}H_{62}O$.

^{1}H NMR (400 MHz, Py-5d) δ (ppm): 0.87 (t, *J*=6.5 Hz, 3H), 1.33 (s, 53H), 1.52 (p, *J*=7.1 Hz, 2H), 1.75 (p, *J*=6.8 Hz, 2H), 3.87 (t, *J*=6.5 Hz, 2H). ^{13}C NMR (100MHz, Py-5d) δ (ppm): 13.99 (CH_3), 22.67 (C-25), 26.31 (C-24), 29.34 (C-23), 29.74 (C-2), 31.87 (23C), 33.56 (C-3), 61.92 (C-1).

5.1.4.2.1 Structural elucidation of triacontanol (7)

The EI mass spectrum of the alcohol has the classic long chain alkane molecule pattern, like the ones already mentioned in this section. But looking at the spectrum is noticeable at first sight that it's missing the molecular ion. This is not uncommon in EI spectra were most of the time the energy is too high for the molecule to bear and it is fragmented completely. In any case the

first peak of m/z of 420 is exactly 18 Da lighter than the molecular ion would have been (438 m/z). The mass spectrum is showed in figure 5.38.
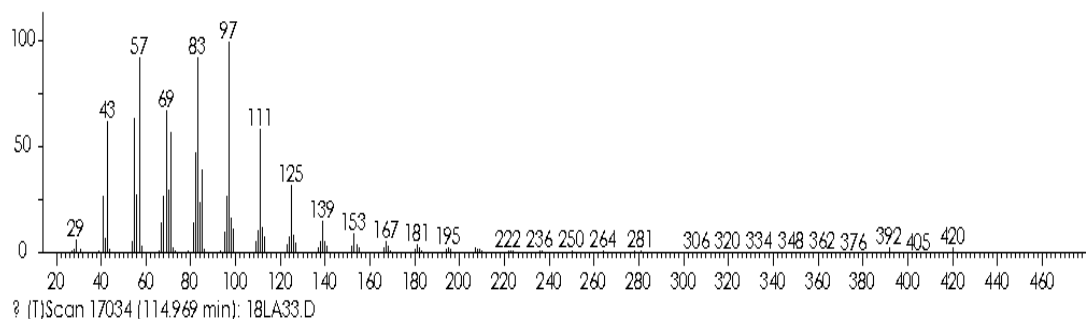
Figure 5.38 EI/MS of triacontanol (7)

The ^{1}H NMR spectrum (Figure 5.39) showed signals typical of long chain alcohol, with a upfield triplet at 0.87 ppm (J=6.5 Hz, 3H, Me) that integer for the terminal methyl group and a more downfield singlet that integer for the other 64 protons (1.33 ppm), typical of long chains of CH_2. Then two pentaplets at 1.52 ppm (*J*=7.1 Hz, 2H, H-3) and 1.75 ppm (*J*=6.8 Hz, 2H, H-2) followed by a triplet at 3.87 ppm (*J*=6.5 Hz, 2H, H-1), which are indicative of the presence of an oxygen attached to a long chain of carbons. The absence of any other signal showed that the oxygen doesn't have any substituent and that the molecule is in fact an alcohol. The ^{13}C NMR spectrum (Figure 5.40) also showed a long chain alcohol molecule pattern with very few signals in the downfield region and a lot of signals in the upfield region of the spectrum. A very intense signal at 29.73 ppm corresponds to the majority of the CH_2 of the molecule. But the signal that was decisive to characterize the molecule was the one at 61.92 ppm relative to the carbon attached to the oxygen which is characteristic of alcohols.
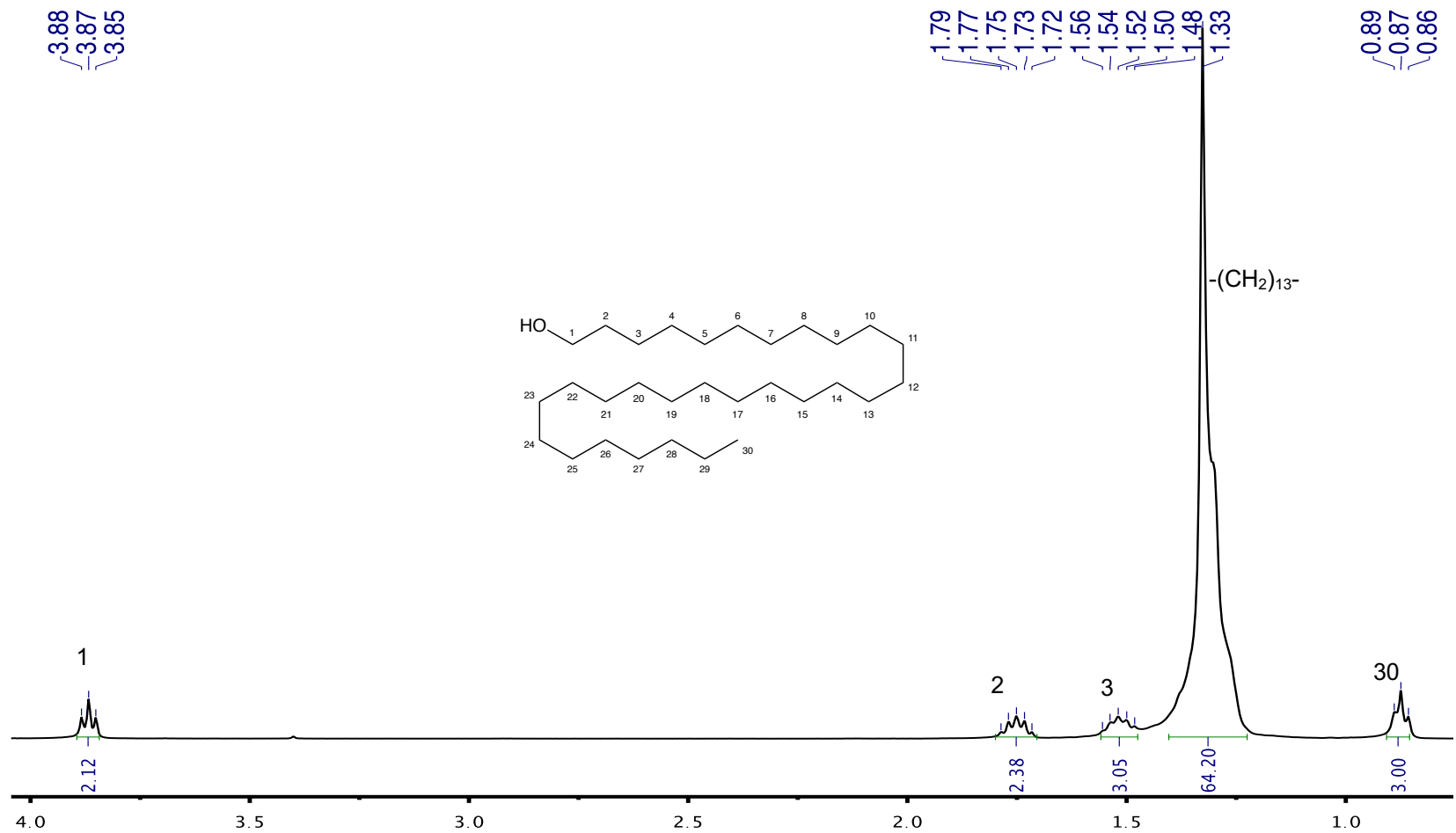
Figure 5.39 ^{1}H NMR spectrum (400MHz, Py-5d) of triacontanol (7)
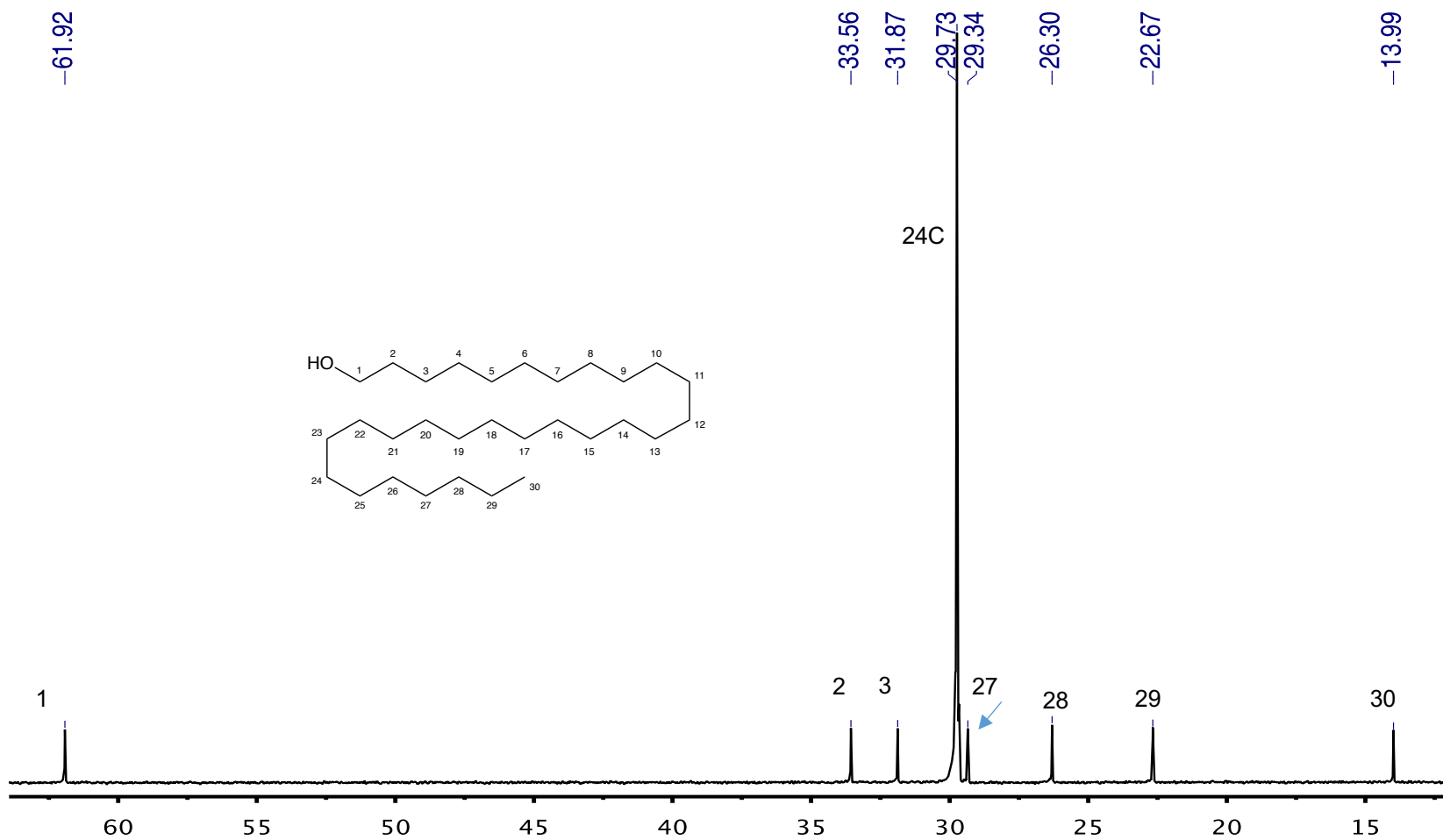
Figure 5.40 ^{13}C NMR spectrum (100MHz, Py-5d) of triacontanol (7)

5.1.4.3 Physic and spectroscopic data of *p*-coumaric acid (8)
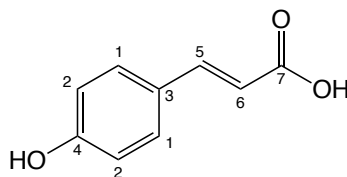
Figure 5.41 Structure of *p*-coumaric acid (8)

Compound 8 (Figure 5.41) present itself as a white yellowish amorph solid which precipitate in hexane and cold chloroform. It was soluble in acetone, and insoluble in nonpolar solvents, and it reveal under the UV light (254 and 365 nm) as a dark spot. Also, after staining with ceric sulfate it was observed as a dark spot on the TLC. It has mp of 213-215 °C and molecular formula of $C_9H_8O_3$.

^{1}H NMR (400 MHz, acetone) δ (ppm): 6.35 (d, *J*=15.9 Hz, 1H), 6.95 (d, J=8.7 Hz, 2H), 7.57 (d, *J*=8.7 Hz, 2H), 7.63 (d, *J*=15.9 Hz, 1H). ^{13}C NMR (100MHz, acetone) δ (ppm): 114.90 (C-6), 115.79 (C-2), 126.19 (C-3), 129.99 (C-1), 144.67 (C-5), 159.61 (C-4), 167.35 (C-7).

5.1.4.3.1 Structural elucidation of *p*-coumaric acid (8)

The ^{1}H NMR spectrum (Figure 5.42) showed signals typical of phenyl propionic acids, with only four downfield doublets. The signals are part of two AB/AX not correlating systems, clearly visible from the roof effect from which each couple of signals is affected. The first comprehends a doublet at 6.35 ppm (*J*=15.9 Hz, 1H) and the most downfield signal at 7.63 ppm (d, *J*=15.9 Hz, 1H). The coupling constant J of 15.9 Hz found in these signals also reveals the *trans* configuration of the doble bond of molecule. The second system

contains the more intense doublets at 6.95 (J=8.7 Hz, 2H) and at 7.43 (J=8.7 Hz, 2H) which are characteristic of p substituted aromatic ring that still retains a symmetry axis. The ^{13}C NMR spectrum (Figure 5.43) showed a phenyl propionic molecule pattern with very few signals all in the downfield region. The most typical signals were at 114.90 ppm and 144.67 ppm for the olefinic carbons and at 115.79 ppm and 129.99 ppm for the aromatic carbons. The latter integrate for two nuclei each, corresponding to the two pairs of symmetric Sp^2 carbons of the ring. The signals at 126.19 ppm and at 159.61 ppm are produced by the tetrasubstituted carbon bonded of the olefin and to the hydroxyl group respectively. The less shielded signal at 167.35 ppm belongs instead to the Sp^2 carbon of the carbonyl group. All The 2D NMR spectra also confirmed the identity of the molecule (Figure 5.44 to 5.46), particularly the ^{1}H-^{1}H NOESY spectrum (Figure 5.47) confirmed the spatial configuration of the olefin.
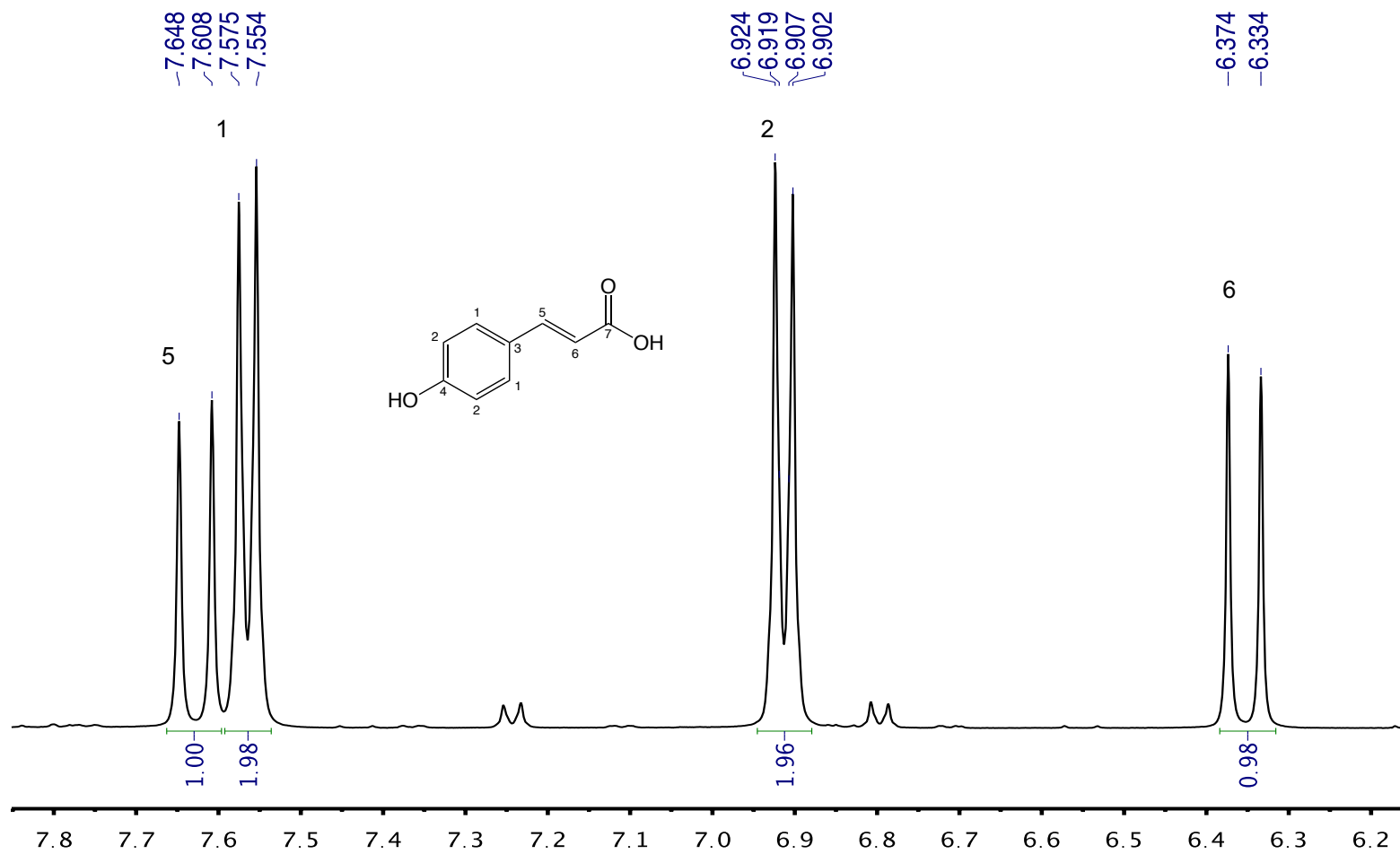
Figure 5.42 ^{1}H NMR spectrum (400MHz, Acetone-6d) of *p*-coumaric acid (8)
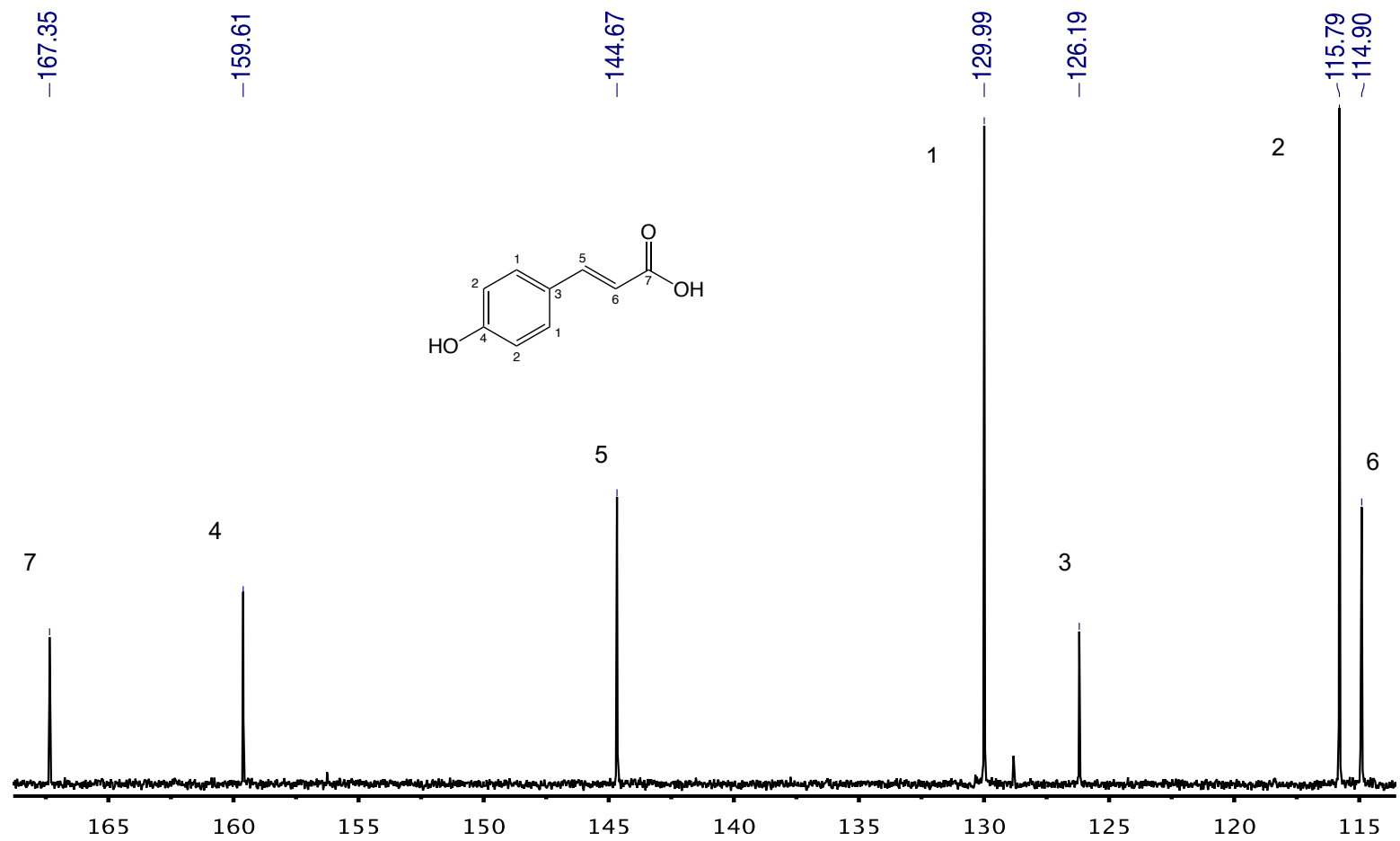
Figure 5.43 ^{13}C NMR spectrum (100MHz, Acetone-6d) of *p*-coumaric acid (8)
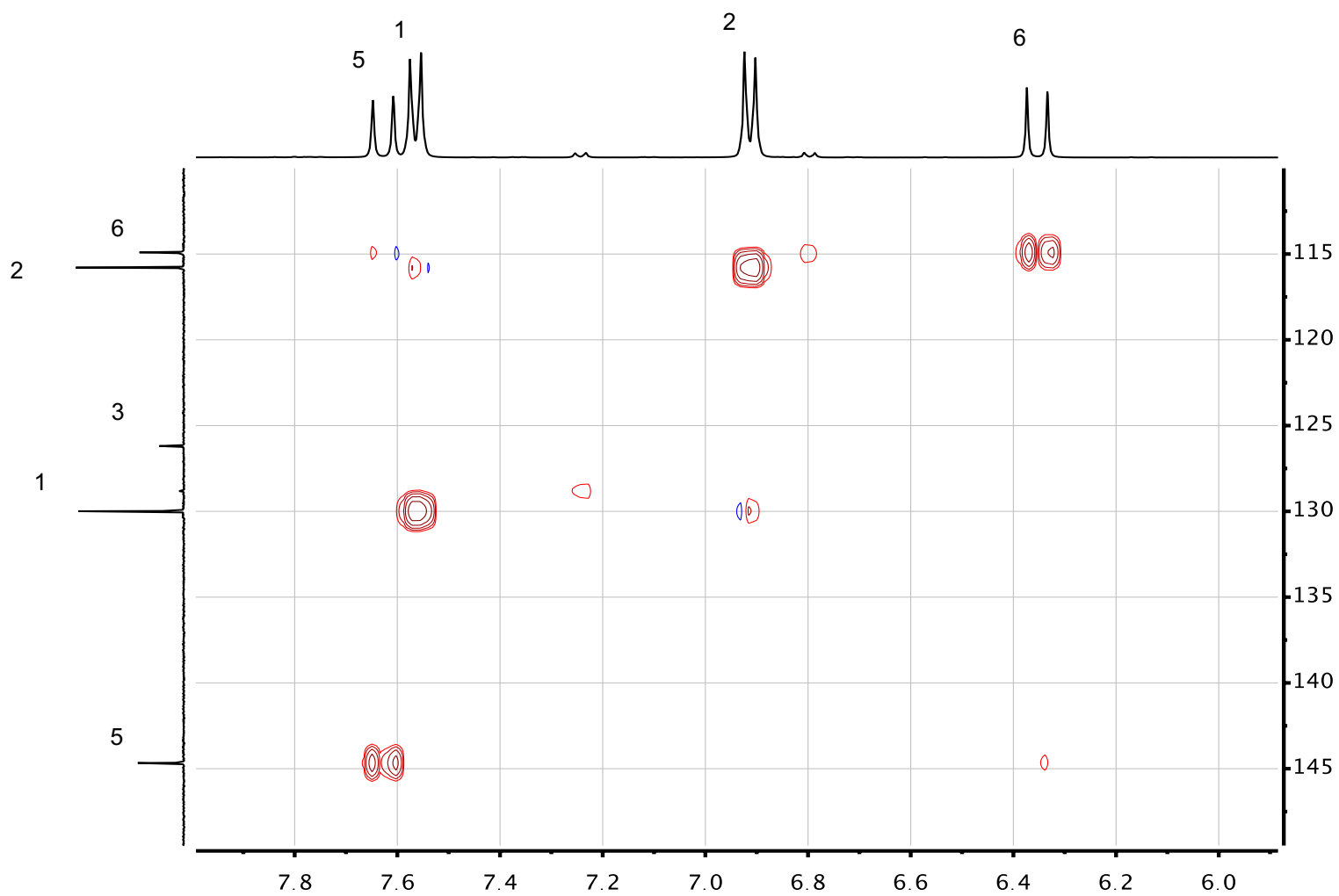
Figure 5.44 ^{1}H-^{13}C HSQC NMR spectrum (400MHz, Acetone-6d) of *p*-coumaric acid (8)
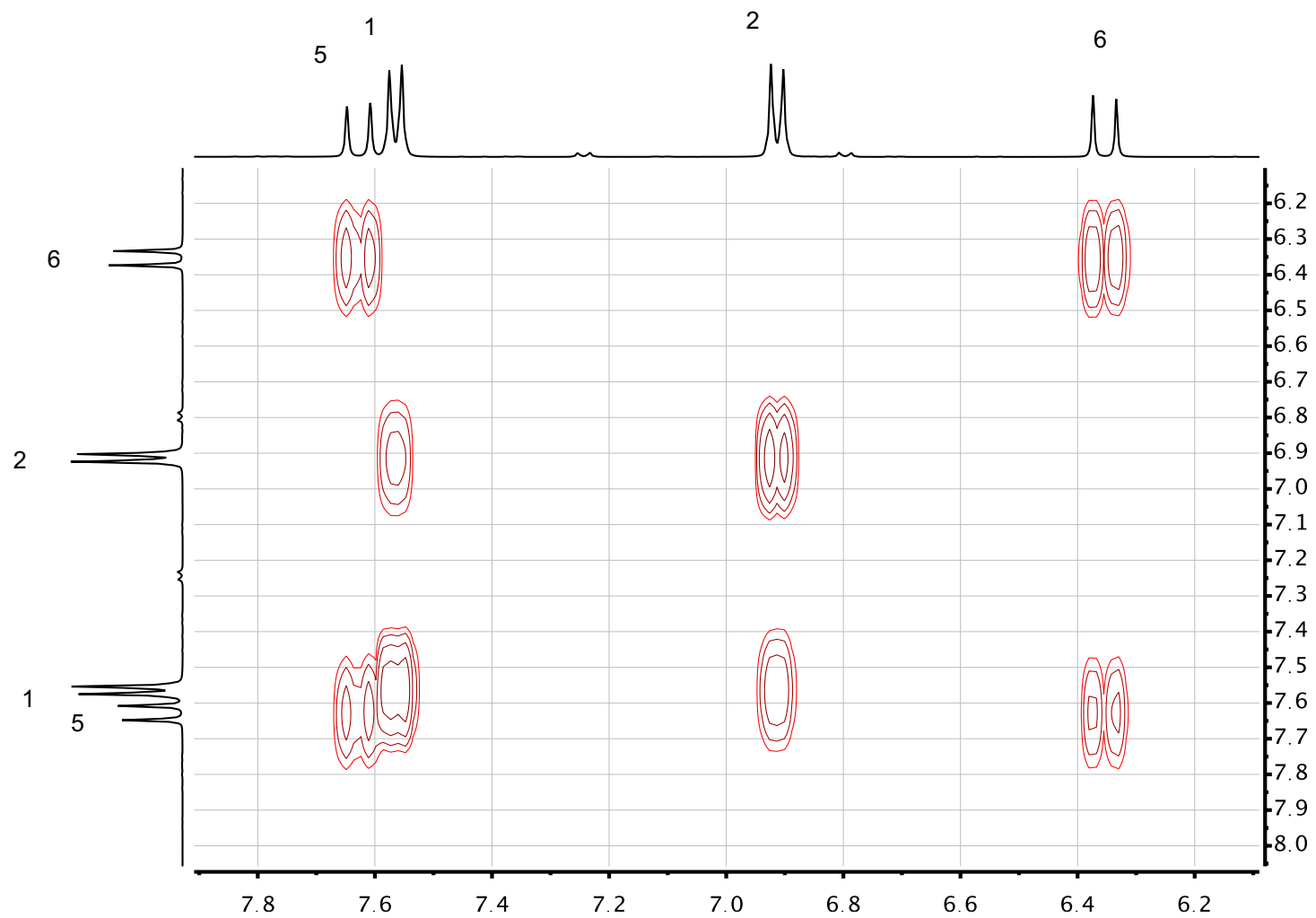
Figure 5.45 ^{1}H-^{1}H COSY NMR spectrum (400MHz, Acetone-6d) of *p*-coumaric acid (8)
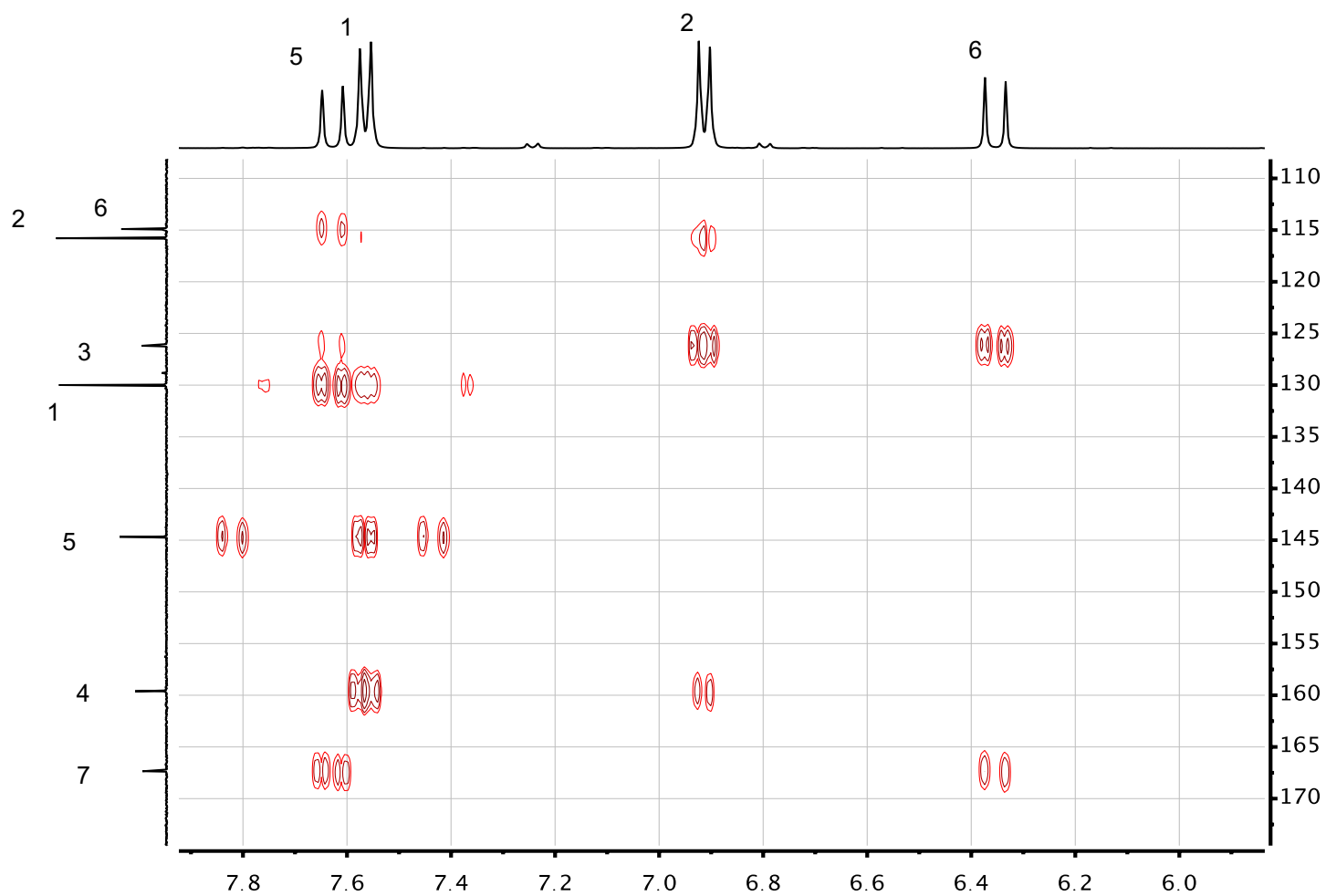
Figure 5.46 ^{1}H-^{13}C HMBC NMR spectrum (400MHz, Acetone-6d) of *p*-coumaric acid (8)
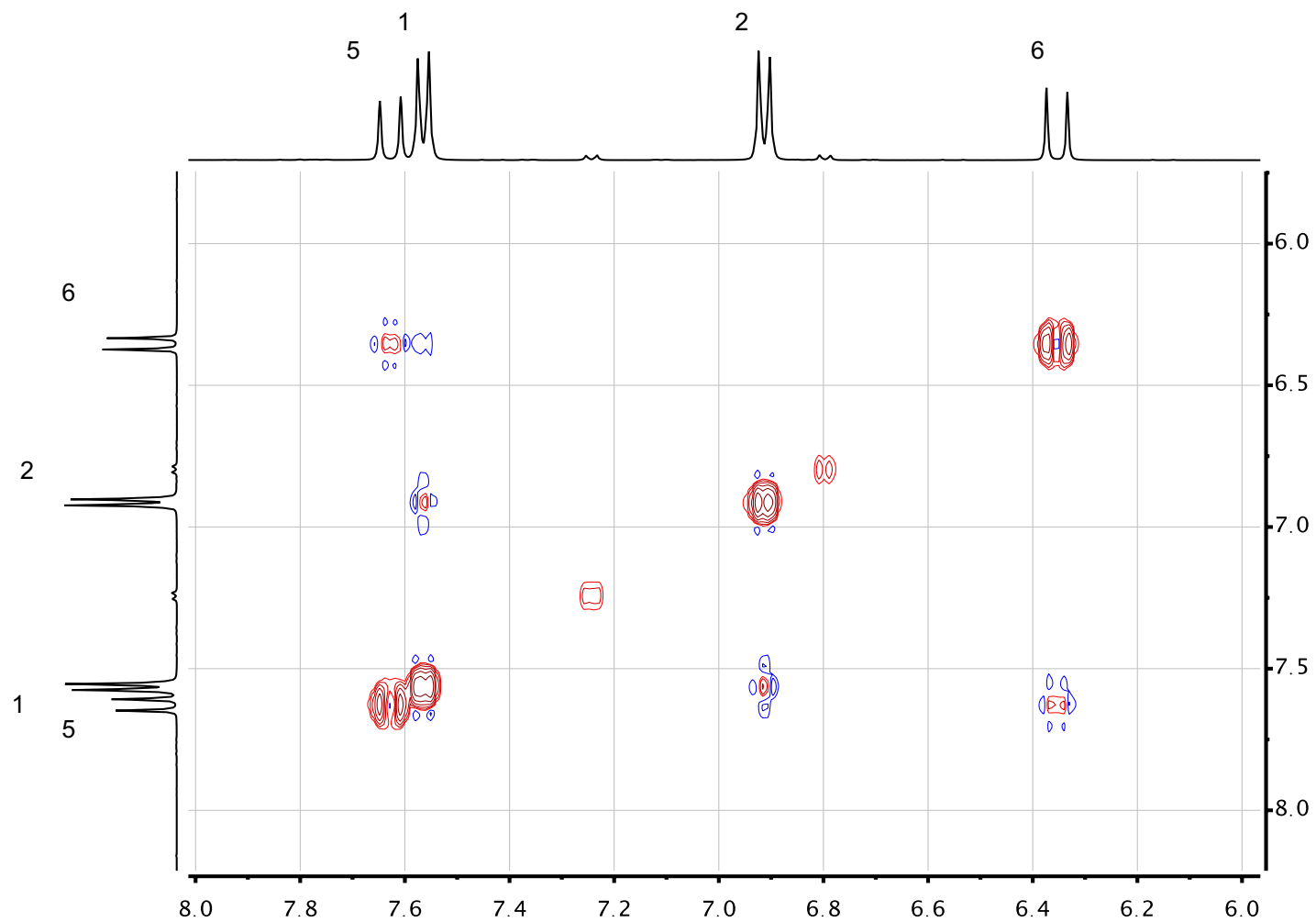
Figure 5.47 ^{1}H-^{1}H NOESY NMR spectrum (400MHz, Acetone-6d) of *p*-coumaric acid (8)

5.1.4.4 Physic and spectroscopic data of margaric acid (9)
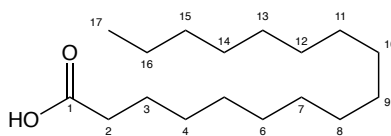
Figure 5.48 Structure of margaric acid (9)

Compound 9 (Figure 5.48) present itself as a rose amorphous solid which precipitate in chloroform. It was found to be soluble in pyridine, and insoluble in nonpolar solvents. It was observed as a dark spot on a TLC after staining with ceric sulfate. It has mp of 80-82 °C and molecular formula $C_{17}H_{34}O_2$.

^{1}H NMR (400 MHz, Py-5d) δ (ppm): 0.87 (t, *J*=7.2 Hz, 3H), 1.33 (s, 22H), 1.42 (q, *J*=7.5 Hz, 4H), 1.83 (t, *J*=7.6 Hz, 2H), 2.55 (t, *J*=7.5 Hz, 2H). ^{13}C NMR (100MHz, Py-5d) δ (ppm): 14.04 (CH$_3$), 22.70 (C-17), 25.43 (C-16), 29.38 (C-15), 29.48 (C-14), 29.60 (C-13), 29.69 (C-12), 29.76 (7C), 31.89 (C-3), 34.67 (C-2), 175.75 (C-1).

5.1.4.4.1 Structural elucidation of margaric acid (9)

The ^{1}H NMR spectrum (Figure 5.49) showed signals typical of a carboxylic acid, with only few upfield signals. Much like the other identified carboxylic acids from this plant the principal signals are the ones from the long carbon chain. At 0.87 ppm (t, *J*=7.2 Hz) a typical signal of CH$_3$ at the end of the chain, followed by a singlet at 1.33 ppm which integer for 22 hydrogens, then there are three signals at 1.42 ppm (q, *J*=7.5 Hz, 4H), 1.83 ppm (t, *J*=7.6 Hz, 2H), 2.55 ppm (t, *J*=7.5 Hz, 2H), which are the protons next to the

carboxylic group and are characteristic of acids. The ^{13}C NMR spectrum (Figure 5.50) showed a carboxylic acid pattern. The signals for the characterization of the molecule were the one at 29.76 ppm which is the sum of seven carbons of the molecule, typical of a long chain of carbons, and the one at 175.75 ppm indicative of a free carboxylic acid.
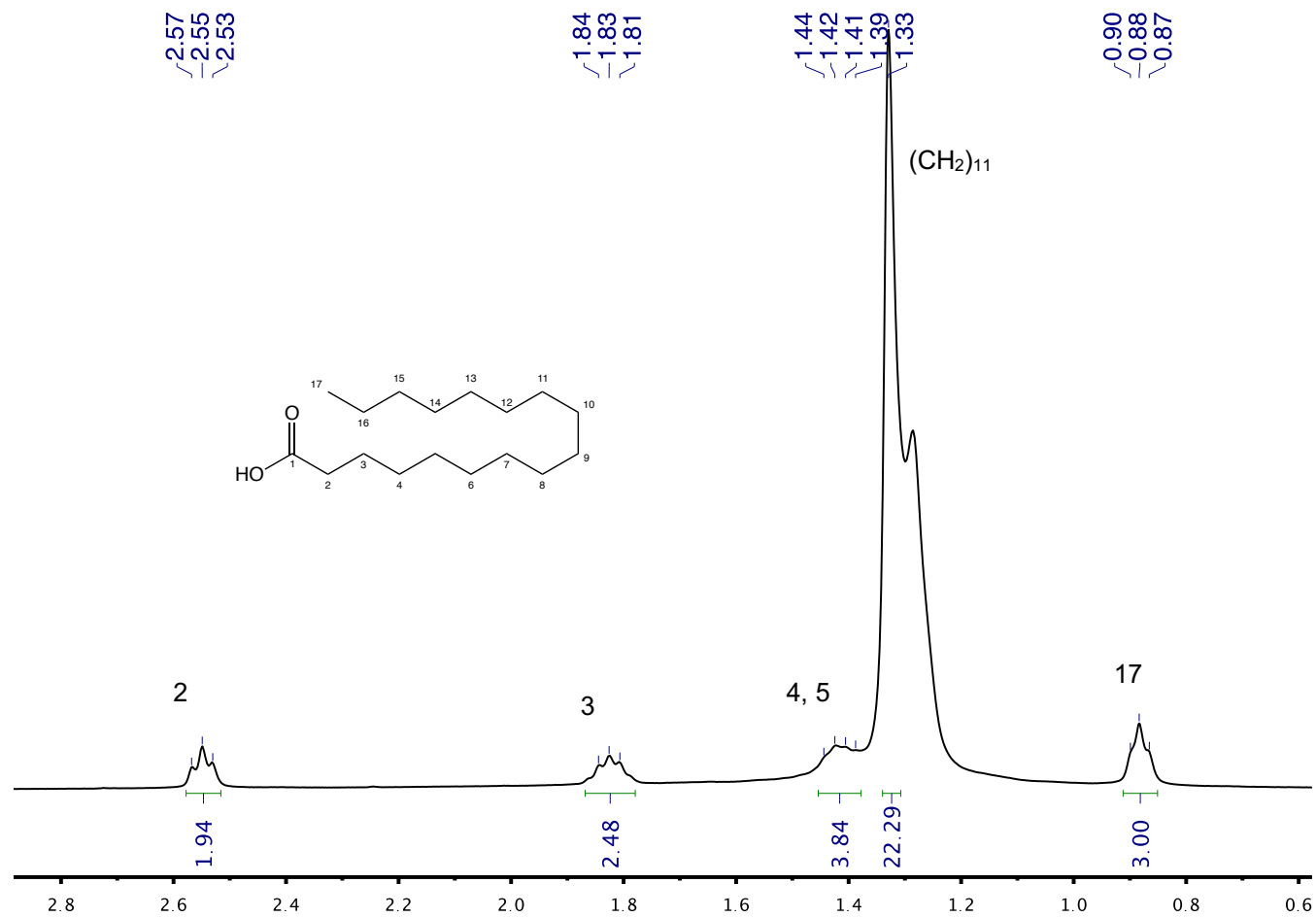
Figure 5.49 ^{1}H NMR spectrum (400MHz, Py-5d) of margaric acid (9)
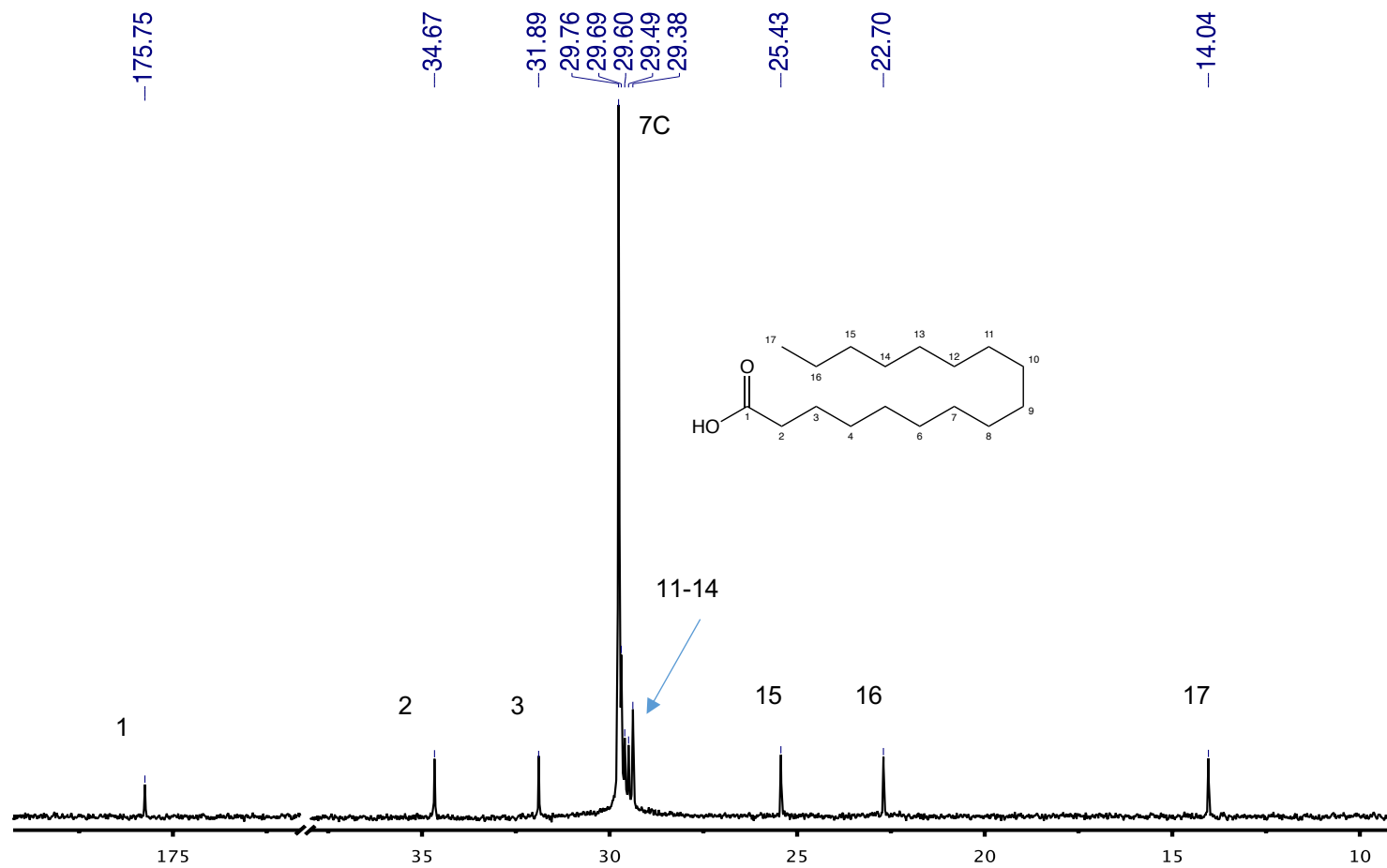
Figure 5.50 ^{13}C NMR spectrum (100MHz, Py-5d) of margaric acid (9)

5.1.4.5 Physic and spectroscopic data of caffeic acid (10)
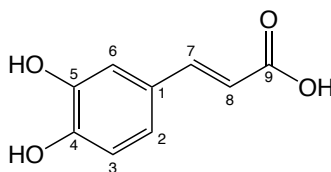
Figure 5.51 Structure of caffeic acid (10)

Compound 10 (Figure 5.51) is a greenish amorph solid which precipitate in chloroform. It was soluble in methanol, and insoluble in less polar solvents. It was visible under the UV light at 254 and 365 nm as a dark spot, it was observed as a brown spot on a TLC after staining with ceric sulfate. It has mp of 225-227 °C and molecular formula of $C_9H_8O_4$. The identity of the molecule was confirmed by the literature (*98*).

^{1}H NMR (400 MHz, MeOD) δ (ppm): 6.20 (d, *J*=15.9 Hz, 1H), 6.67 (d, 8.2Hz, 1H), 6.85 (dd, *J*=8.3, 2.1 Hz, 1H), 6.95 (d, *J*=2.1 Hz, 1H), 7.50 (d, *J*=15.9 Hz, 1H). ^{13}C NMR (100MHz, Py-5d) δ (ppm): 113.31 (C-8), 113.77 (C-6), 115.09 (C-3), 121.61 (C-2), 126.27 (C-1), 145.42 (C-5), 145.96 (C-7), 148.28 (C-4), 167.60 (C-9).

5.1.4.5.1 Structural elucidation of caffeic acid (10)

The ^{1}H NMR spectrum (Figure 5.52) showed signals typical of phenyl propionic acids, with only four downfield doublets. Two of the signals are part of AX system. It comprehends two doublets one at 6.20 ppm (*J*=15.9 Hz, 1H) and the other at 7.50 ppm (d, *J*=15.9 Hz, 1H). The coupling constant *J* of 15.9 Hz found in these signals revealed the *trans* configuration of the molecule. The

other signals comprehend two doublets at 6.67 ppm (J=8.2 Hz, 2H) and at 6.95 ppm (J=2.1 Hz, 2H) which are for the protons in position 3 and 6 respectively, and a doublet of a doublet at 6.85 ppm (dd, J=8.3, 2.1 Hz, 1H) due to the proton in position 2. The larger coupling constant generated by the vicinal proton H_3 and the smaller one produced by the H_6. The five signals are typical of an aromatic ring non-symmetrically substituted, and one of the substituents is an olefin. The ^{13}C NMR spectrum (Figure 5.53) showed a phenyl propionic molecule pattern with very few signals in the downfield region. The first typical signals were the two of similar intensities at 113.31 ppm and 145.96 ppm for the olefinic carbons and at 126.27 ppm, 145.42 and 148.28 ppm for the aromatic quaternary carbons, which were also spotted for their lower intensity. The less shielded signal at 167.60 ppm belongs instead to the Sp^2 carbon of a free carbonyl group. The remaining signals were attributed to the aromatic carbons. 2D NMR experiments were used to confirm the identity of the molecule (Figure 5.54 to 5.55), particularly the ^1H-^1H NOESY spectrum (Figure 5.56) confirmed the special configuration of the olefin.
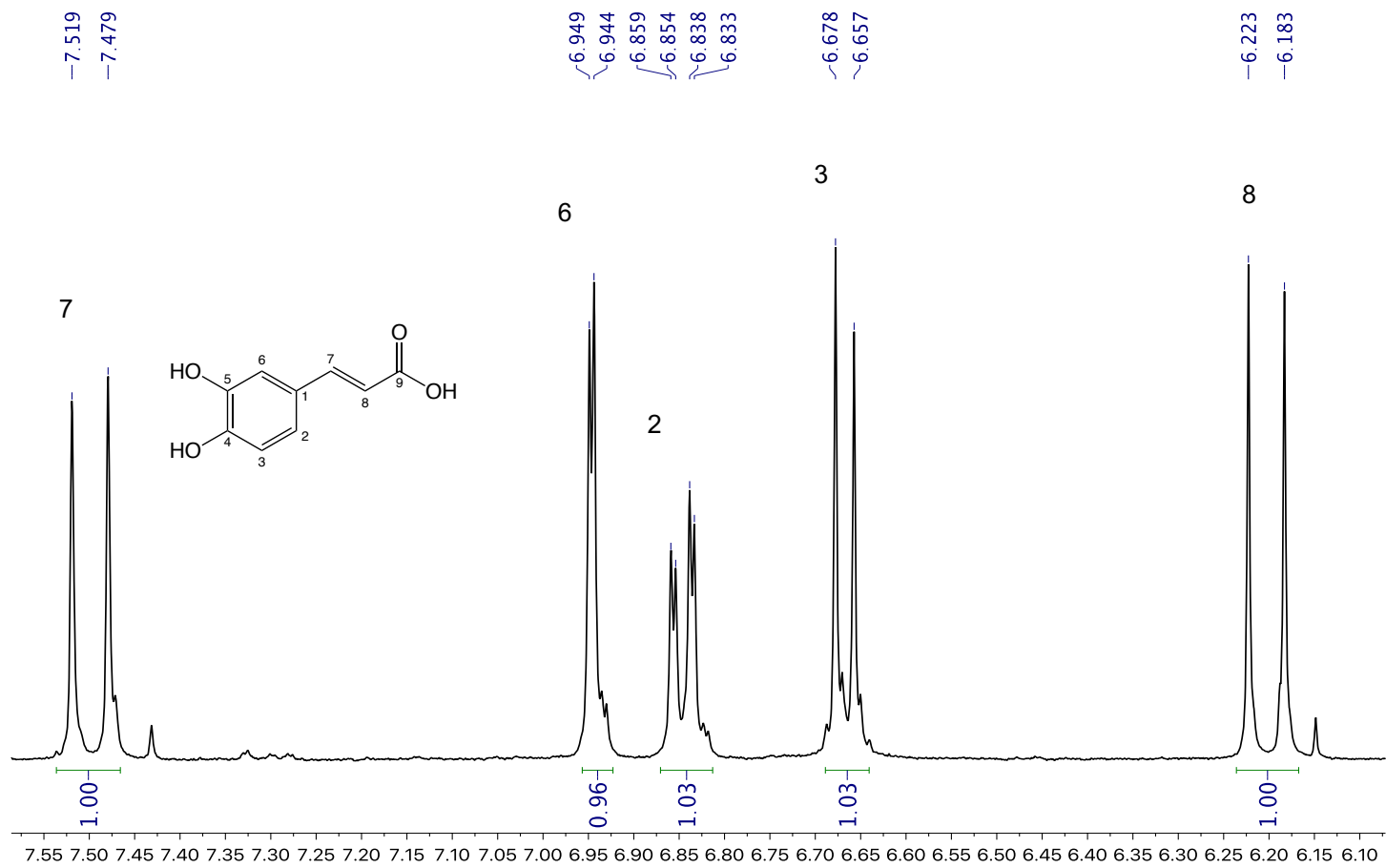
Figure 5.52 ^{1}H NMR spectrum (400MHz, MeOD) of caffeic acid (10)
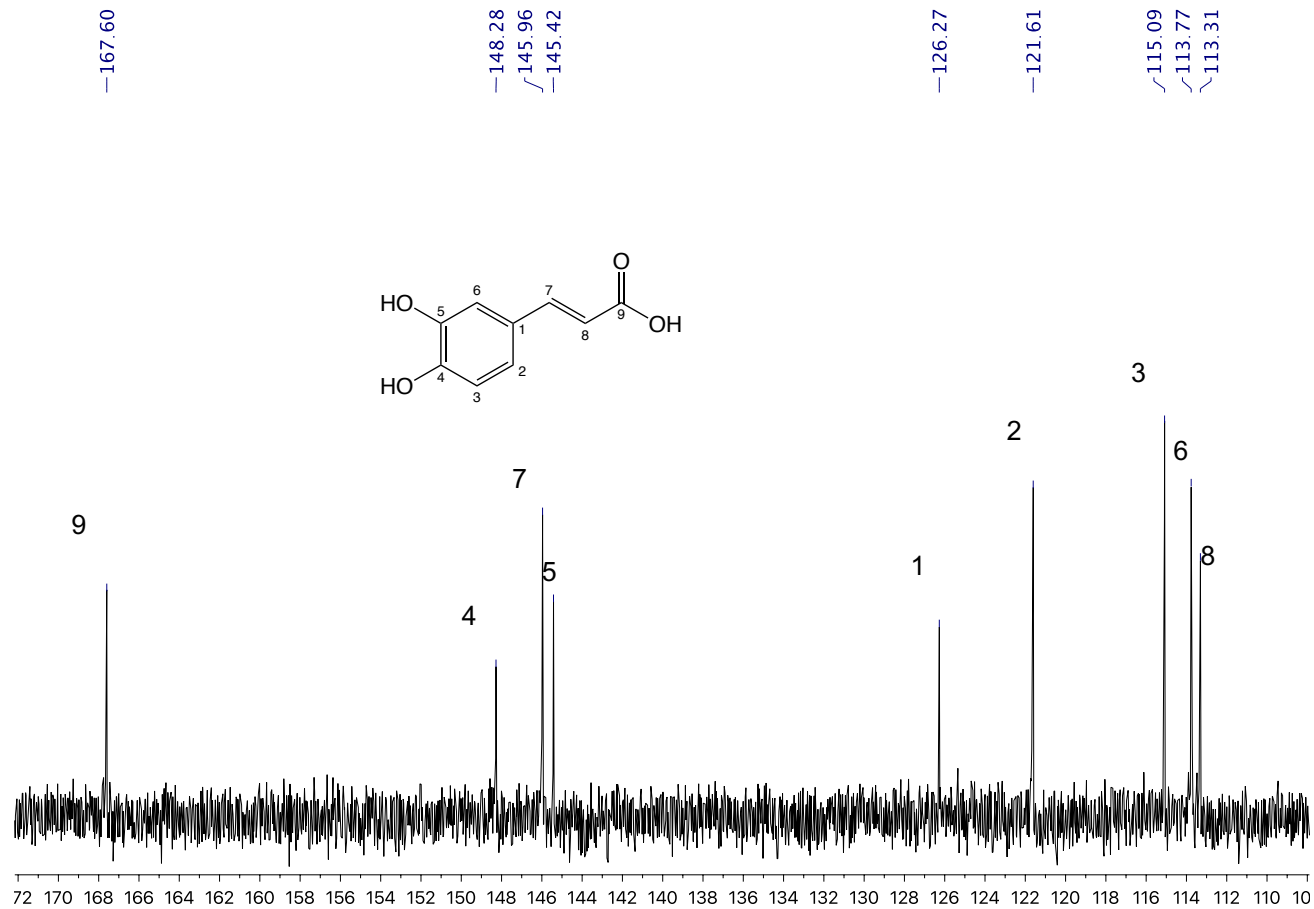
Figure 5.53 ^{13}C NMR spectrum (100MHz, MeOD) of caffeic acid (10)
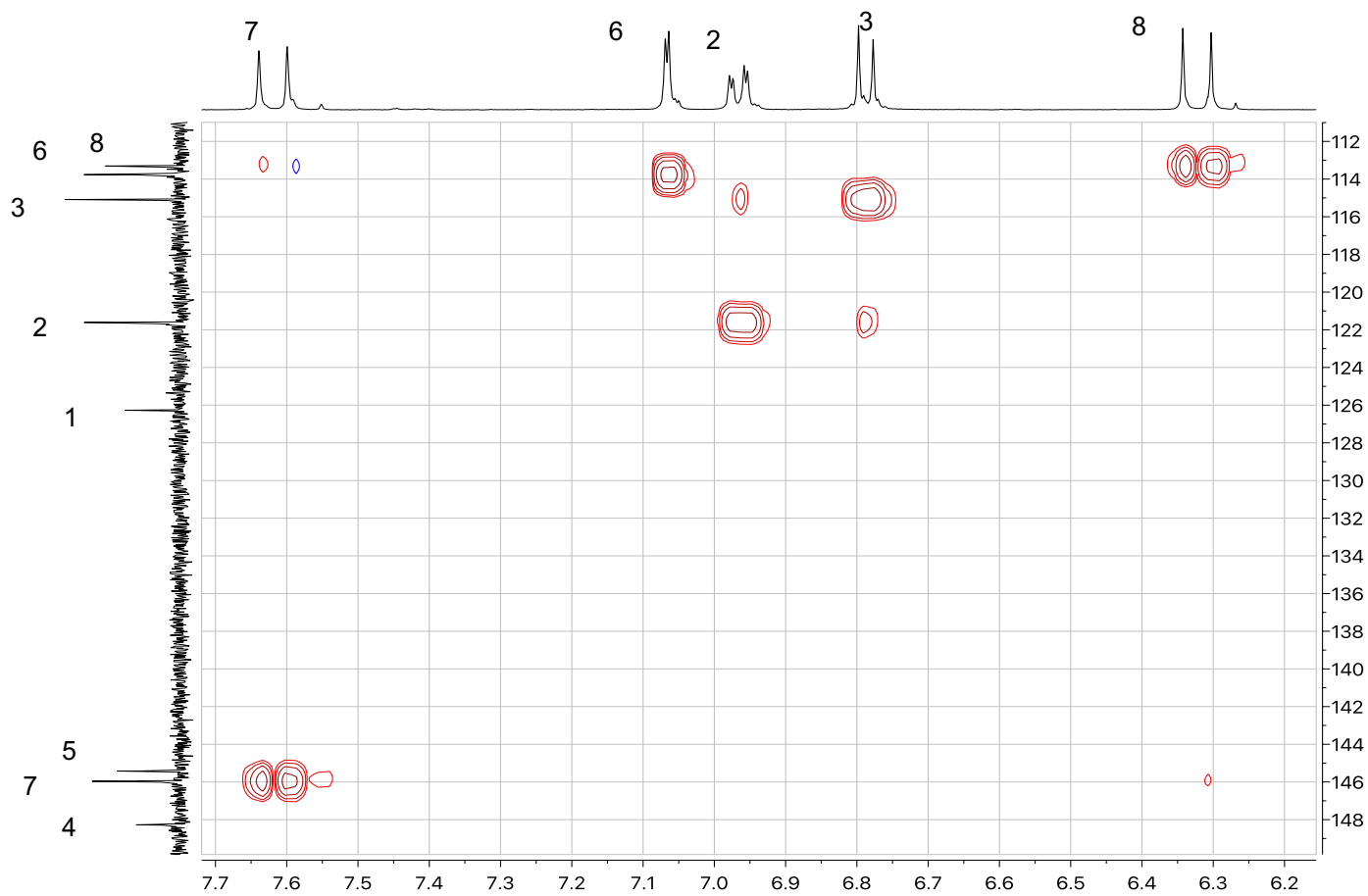
Figure 5.54 ^{1}H-^{13}C HSQC NMR spectrum (400MHz, MeOD) of caffeic acid (10)
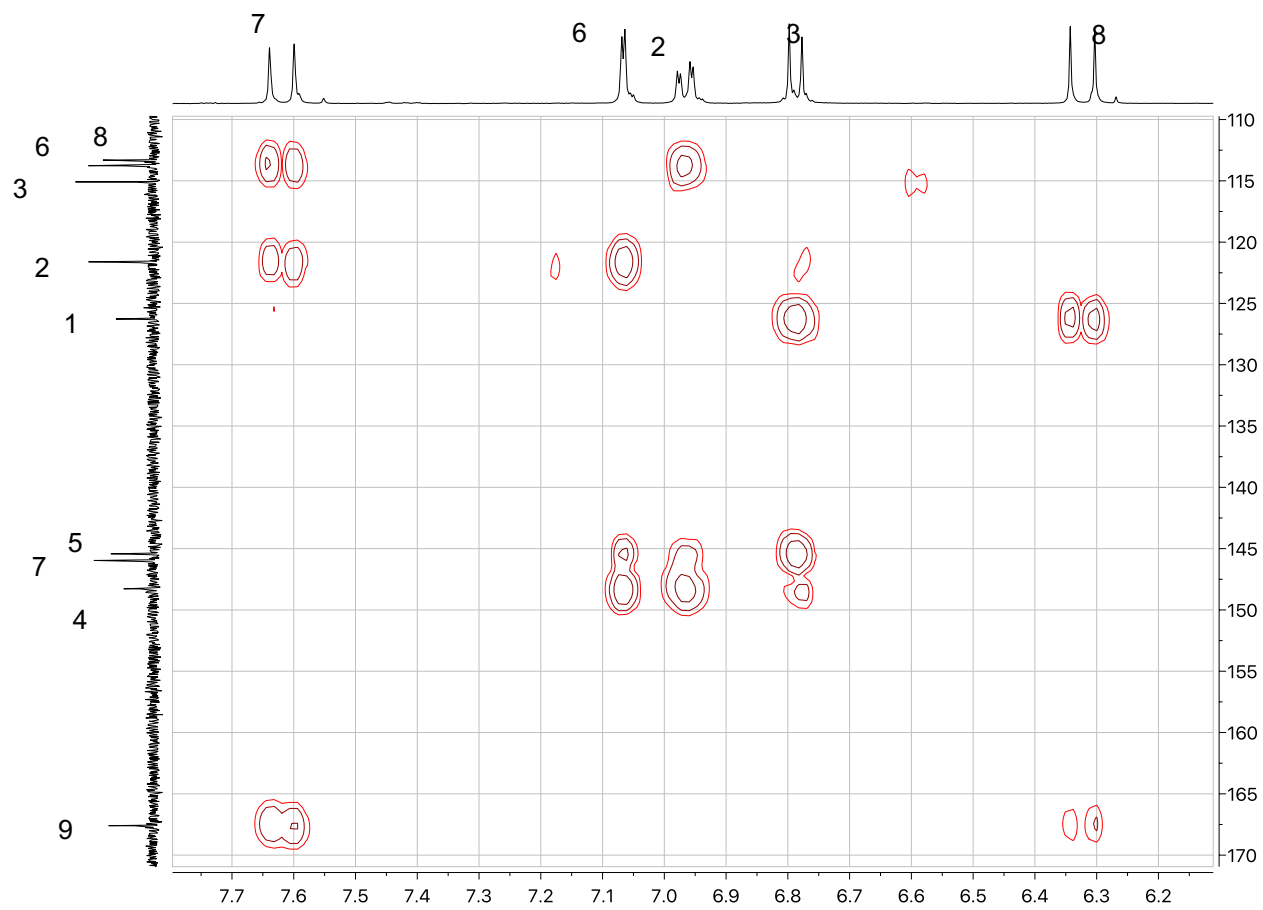
Figure 5.55 ^{1}H-^{13}C HMBC NMR spectrum (400MHz, MeOD) of caffeic acid (10)
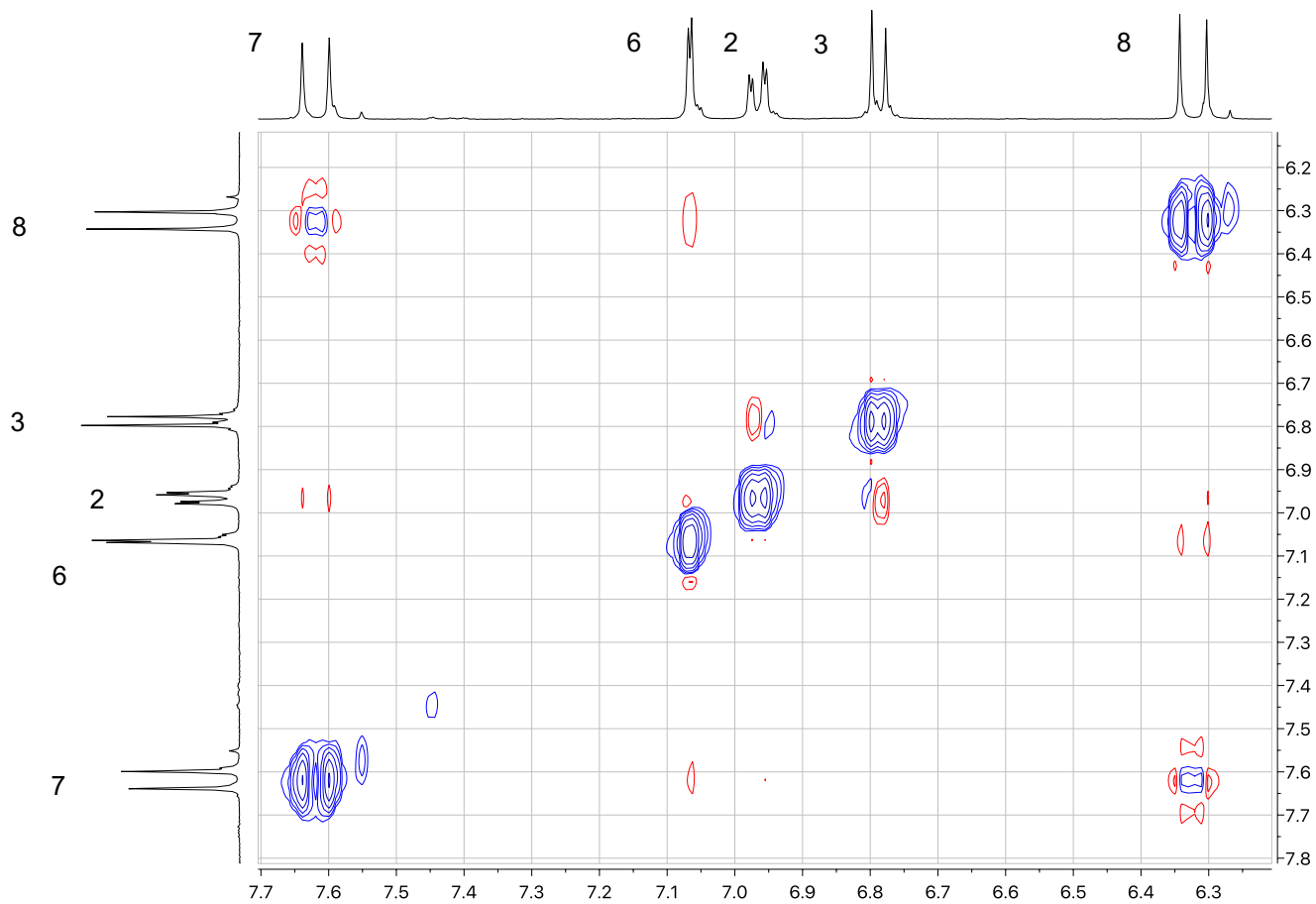
Figure 5.56 ^{1}H-^{1}H NOESY NMR spectrum (400MHz, MeOD) of caffeic acid (10)

5.1.4.6 Physic and spectroscopic data of daucosterol (11)
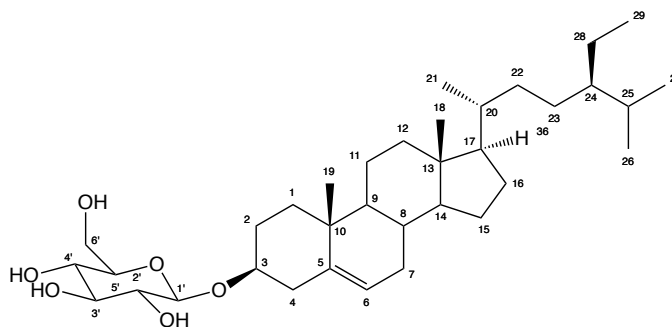
Figure 5.57 Structure of daucosterol (11)

The glycoside 11 (Figure 5.57) crystalized into the CC (needle-shaped crystals) when a 100% EtOAc mobile phase was reached, then it solubilized when 90:10 EtOAc/MeOH passed through the column. It was recovered as a crystalline solid washed several times with MeOH, sonicating it for 15 minutes each time until the solid was white. It was soluble in pyridine (Py) and partially soluble in hot MeOH (over 50°C). The compound did not reveal under the UV light, it has mp > 280°C and molecular formula of $C_{35}H_{60}O_6$.

The following spectral data of compound 11 was also confronted with the literature (Table 5.4).

^{1}H NMR (400 MHz, CDCl$_3$) δ (ppm): 0.67 (s, 3H), 0.88 (d, J=7.7 Hz, 3H), 0. 89 (t, J=8.1 Hz, 3H), 0.90 (d, J=8.1 Hz, 3H), 0.95 (s, 3H), 1.00 (d, J=6.7 Hz, 3H), 2.49 (brt, J=12.5 Hz, 1H), 2.75 (m, 1H), 3.96 (m, 1H), 4.02 (m, 2H), 4.10 (brt, J=8.0 Hz, 1H), 4.32 (t, J=8.2 Hz, 1H), 4.33 (t, J=8.2 Hz, 1H), 4.45 (dd, J=11.9, 5.1 Hz, 1H), 4.60 (brd, J=11.6 Hz, 1H), 5.01 (d, J=7.7 Hz, 1H), 5.37 (d, J=4.7 Hz, 1H). ^{13}C NMR (100MHz, CDCl$_3$) δ (ppm): 11.76 ppm (C-18), 11.95 ppm (C-29), 18.80 ppm (C-21), 19.00 ppm (C-19), 19.21 (C-26), 19.77 ppm (C-27), 21.07 (C-11), 23.18 (C-28), 24.30 (C-15), 26.17 (C-23), 28.33 (C-16), 29.21 (C-25), 30.04 (C-2), 31.84 (C-8), 31.96 (C-7), 33.99 (C-22), 36.18

(C-20), 36.71 (C-10), 37.26 (C-1), 39.73 (C-12), 39.12 (C-4), 42.26 (C-13), 45.82 (C-24), 50.12 (C-9), 56.02 (C-17), 56.61 (C-14), 62.62 (C-6'), 71.47 (C-4'), 75.13 (C-2'), 77.86 (C-3), 78.28 (C-5'), 78.40 (C-3'), 102.36 (C-1'), 121.70 (C-6), 140.68 (C-5).

5.1.4.6.1 Structural elucidation of daucosterol (11)

The ^{1}H NMR spectrum (Figure 5.58) showed signals typical of a steroid, with signals in the upfield region. They are given for the protons of the aliphatic hydrogens of the four rings of the molecule. The most important and easy to recognize are the signals of the CH_3, which were very intense: the singlet at 0.67 ppm (3H, Me-18), the doublet at 0.88 ppm (J=7.7 Hz, 3H, Me-27), the doublet at 0.90 ppm (J=8.1 Hz, 3H, Me-26), the triplet at 0.89 (J=8.1 Hz, 3H, Me-29), the doublet of 1.00 ppm (J=6.7 Hz, 3H, Me-21) and the singlet at 0.95 ppm (3H, Me-19). Other signals of the sterol were found at downfield: the broad triplet at 2.49 ppm (J=12.5 Hz, 1H, H-4a), a multiplet at 2.75 ppm that integer for one proton (H-4b). The molecule also presented protons relative to a sugar molecule which correspond to glucose according to the values of the J-coupling between the hydrogens of the sugar. These signals were a multiplet at 4.08 ppm (H-5'), and a broad triplet at 4.10 ppm (J=8.0 Hz, 1H, H-2'), then was observed a complex signal composed by two different triplets falling very close to each other at 4.32 ppm (J=8.2 Hz, 1H, H-3') and 4.33 ppm (J=8.2 Hz, 1H, H-4') respectively. These signals were followed by a doublet of doublet at 4.45 ppm (dd, J=11.9, 5.1 HZ, 1H, H-6b'), a doublet at 4.60 ppm (J=11.6 HZ, 1H, H-6a') and broad doublet relative to the anomeric proton at 5.01 ppm (J=7.7 Hz, 1H, H-1'). It was also observed a broad signal of low intensity at

6.53 ppm that was assigned to one hydroxyl group of the sugar. Then follow another multiplet that integer for another proton at 3.96 ppm (H-3), which was relative to the proton germinal to the hydroxyl group of the aglycone, and the most shielded signal of the vinylic hydrogen at 5.37 ppm (d, *J*=4.7 Hz, 1H, H-6).

The ^{13}C NMR spectrum (Figure 5.59) also showed a glycosilated steroid pattern: a quaternary carbon at 140.68 ppm (C-5) and a vinylic carbon at 121.70 ppm (C-6) correspond to the presence of the double bond and its position in the molecule was confirmed by the HMBC correlations between H-3 and C-5). Also, it was observed a carbon at 102.36 ppm (C-1'), characteristic of anomeric carbons in hexose sugars. The position of the glycosylation in the molecule was confirmed by the HMBC correlations between H-3 and C-1' and vice versa between H-1' and C-3. Then there is the carbon directly attached to the hydroxyl group at 77.86 ppm (C-3), which also was important to confirm the presence of a hydroxyl group. This signal was surrounded by the others signals relative to the carbon skeleton of the sugar: 78.40 ppm (C-3'), 78.28 ppm (C-5'), 75.13 ppm (C-2'), 71.47 ppm (C-4') and 62.62 ppm (C-6'). In the downfield region, there were the signals of the steroid rings and lateral chain (Figure 5.60) particularly the methyl carbons at 11.76 ppm (C-18), 11.95 ppm (C-29), 18.80 ppm (C-21), 19.00 (C-18) 19.21 ppm (C-26) and 19.77 ppm (C-27). The 1D DEPT135 spectrum (Figure 5.61) was useful to discriminate between the carbons of the aglycone and the sugar. The assigned signals were confirmed with the literature (*96*).

The molecule was also analyzed using 2D NMR experiments: ^{1}H-^{1}HCOSY, ^{1}H-^{13}C HSQC, ^{1}H-^{13}C HMBC (Figure 5.62) and [1]H-^{1}H NOESY

(Figure 5.63). 2DNMR spectra confirmed the structure of the molecule and the stereocenters configuration (NOESY). Particularly, COSY and HSQC experiments were important for determination of correlations between hydrogens and their positions in the molecule skeleton, as well as to assign all the carbons of the compound. The position of the double bond was deduced by confronting the ^{13}C NMR spectral assignation obtained experimentally from the HMBC and ^{13}C DEPT experiments with those of literature. The assignation of C-6 was reported to be at 121.70 ppm, this carbon is farther from the OH than C-4. Therefore, if the double bond was between this carbon and C-5 its shift would have been at higher frequencies (at least of 10 ppm) then the 122.0 ppm given experimentally. Instead carbon C-5 is certain to be the part of the double bond, since its shift was found at 141.0 ppm which is characteristic of tetrasubstituted Sp^2 carbons. Also, no proton attached to this carbon is found in the ^1H NMR spectrum, this signal if present is easily spotted for its high multiplicity and shift.

Table 5.4 Spectroscopic data of daucosterol (11)

n	^{1}H NMR (400 MHz, Py) δ (ppm), (*96*)	^{1}H NMR (400 MHz, Py) δ (ppm), 11	^{13}C NMR (100MHz, Py) δ (ppm), (*96*)	^{13}C NMR (100MHz, Py) δ (ppm), 11
1	-	-	37.6	37.26
2	-	-	30.3	30.04
3	3.97 m	3.96 m	78.3	77.86
4a	2.38 m	2.49 (brt, *J*=12.5 Hz, 1H)	39.4	39.12
4b	2.63 m	2.75 m		
5	-	-	141.0	140.68
6	-	5.37 (psd, *J*=4.7 Hz, 1H)	122.0	121.70
7	-	-	32.2	31.96
8	-	-	32.1	31.84
9	-	-	50.4	50.12
10	-	-	37.0	36.71
11	-	-	21.4	21.07
12	-	-	40.0	39.73
13	-	-	42.6	42.26
14	-	-	57.0	56.61
15	-	-	24.6	24.30
16	-	-	28.7	28.33
17	-	-	56.3	56.02
18	0.66 s	0.67 s	12.0	11.76
19	0.94 s	0.95 s	19.3	19.00
20	-	-	36.5	36.18
21	0.99 d	1.00 (d, *J*=6.7 Hz, 3H)	19.1	18.80
22	-	-	34.3	33.99
23	-	-	26.4	26.17
24	-	-	46.1	45.82
25	-	-	29.5	29.21
26	0.90 d	0.90 (d, *J*=8.1 Hz, 3H)	19.5	19.21
27	0.87 d	0.88 (d, *J*=7.7 Hz, 3H)	20.1	19.77
28	-	-	23.4	23.18
29	0.89 t	0.89 (t, *J*=8.1 Hz, 3H)	12.2	11.95
1'	4.95 d	5.01 (d, *J*=7.7 Hz, 1H)	102.6	102.36
2'	4.08 t	4.10 (bt, *J*=8.0 Hz, 1H)	75.4	75.13
3'	4.28 t	4.32 (t, *J*=8.2 Hz, 1H)	78.7	78.40
4'	4.31 t	4.33 (t, *J*=8.2 Hz, 1H)	71.7	71.47
5'	4.03 m	4.02 m	78.5	78.28
6'a	4.59 dd	4.60 (bd, *J*=11.6 HZ, 1H)	62.9	62.62
6'b	4.42 dd	4.45 (dd, *J*=11.9, 5.1 HZ, 1H)		
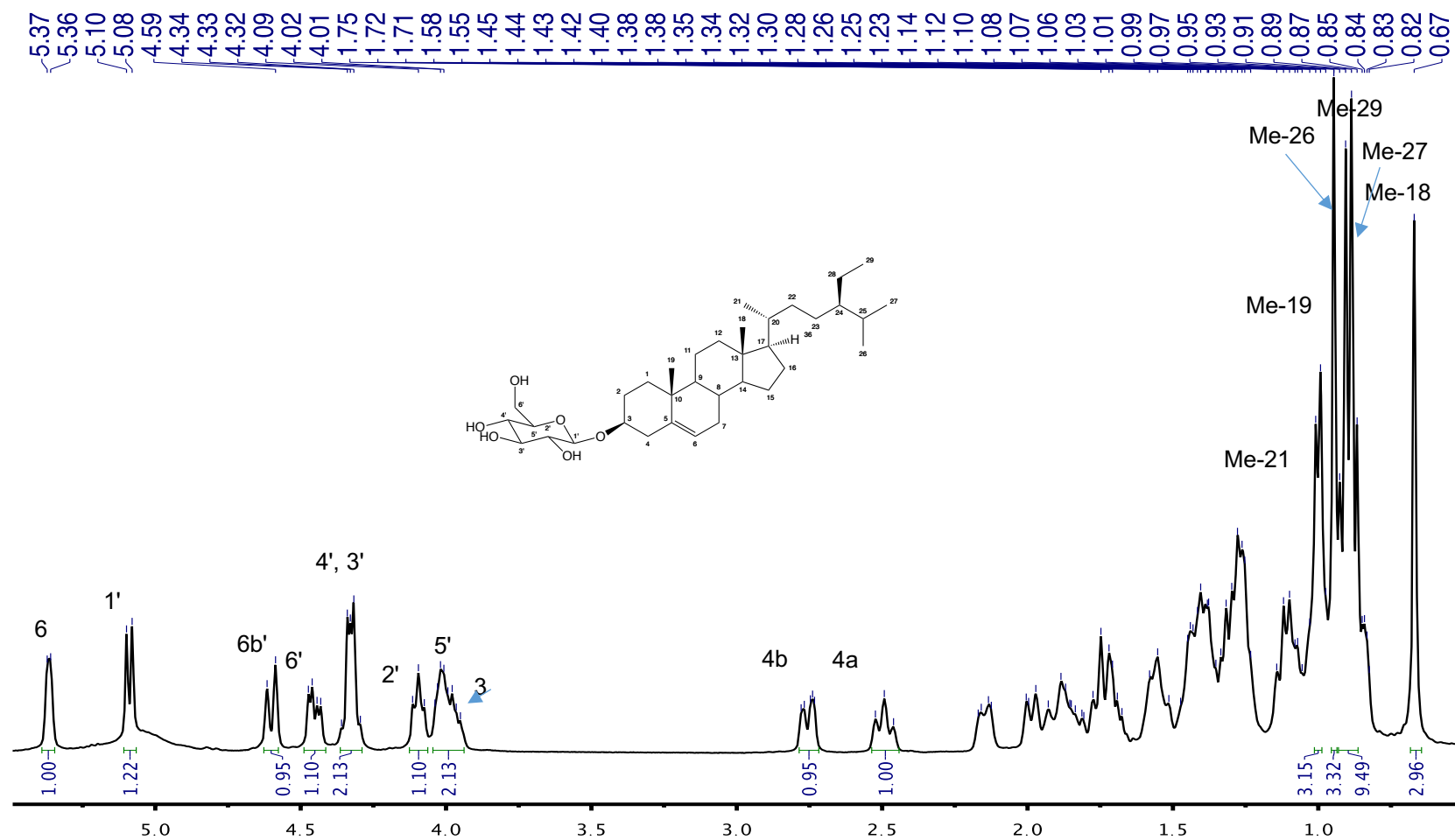
Figure 5.58 ^{1}H NMR spectrum (400MHz, Py-5d) of daucosterol (11)
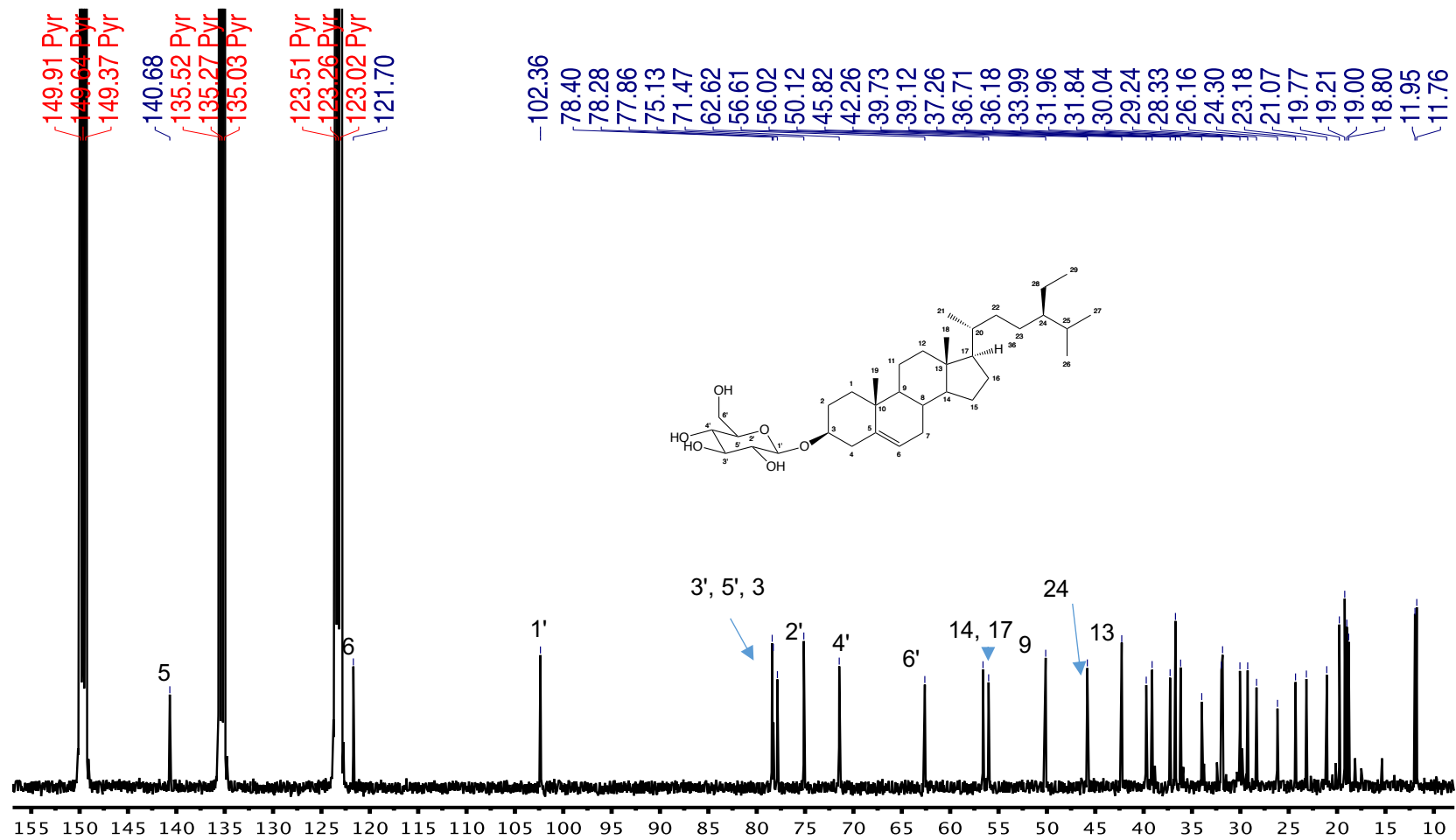
Figure 5.59 ^{13}C NMR spectrum (100MHz, Py-5d) of daucosterol (11)
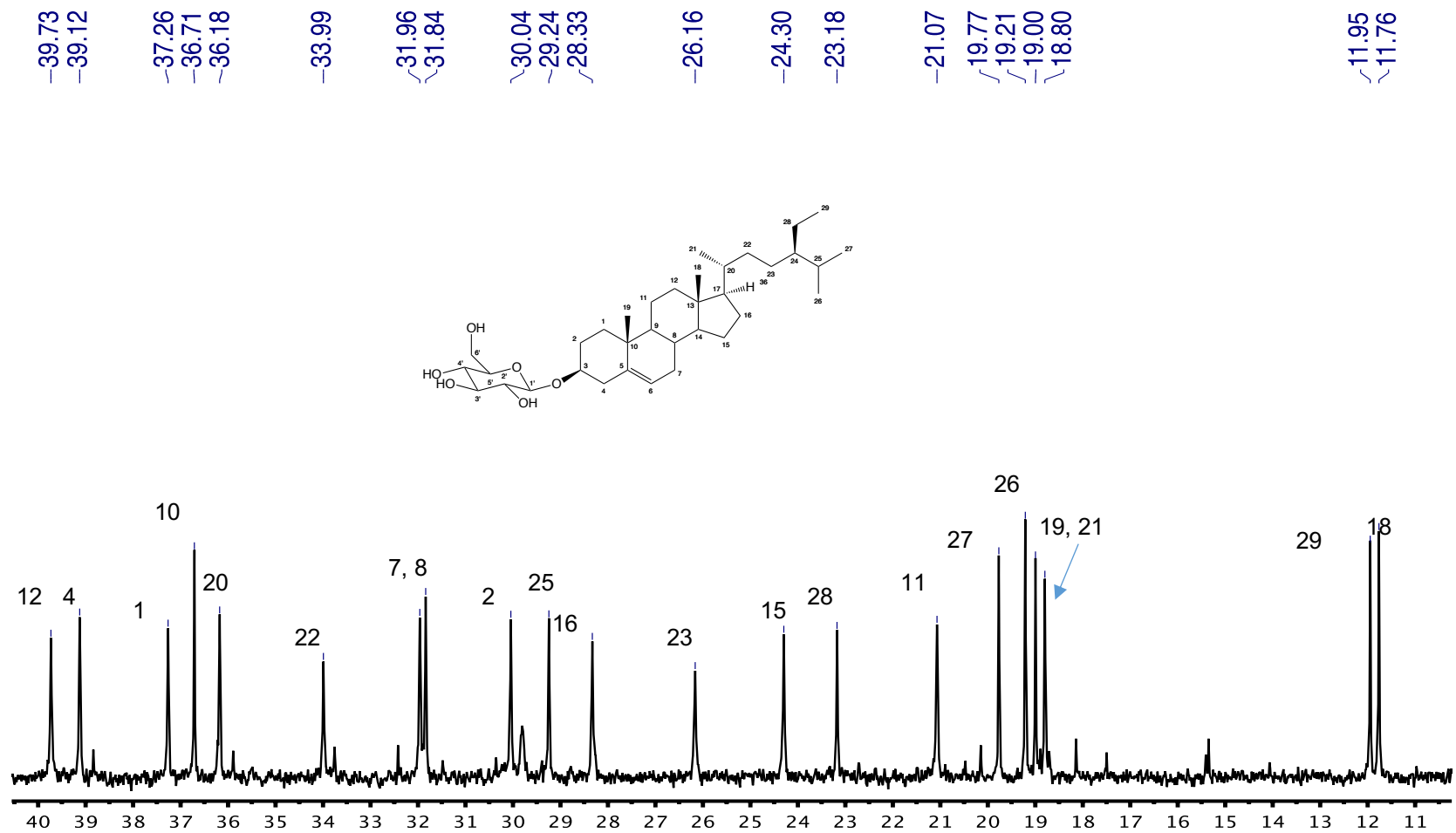
Figure 5.60 ^{13}C NMR spectrum (100MHz, Py-5d) of daucosterol (11) - expansion
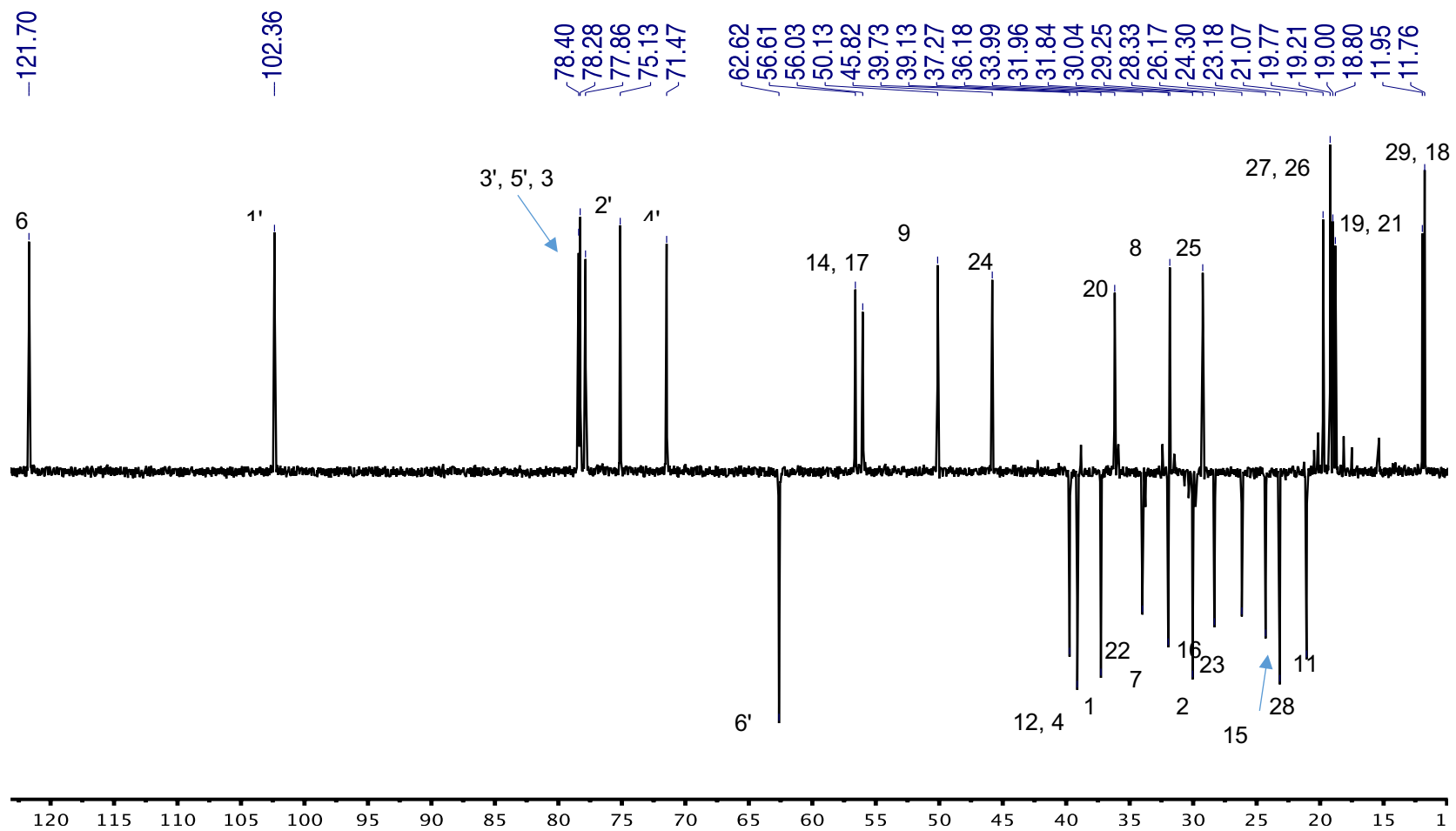
Figure 5.61 [1]D DEPT135 spectrum (100MHz, Py-5d) of daucosterol (11)
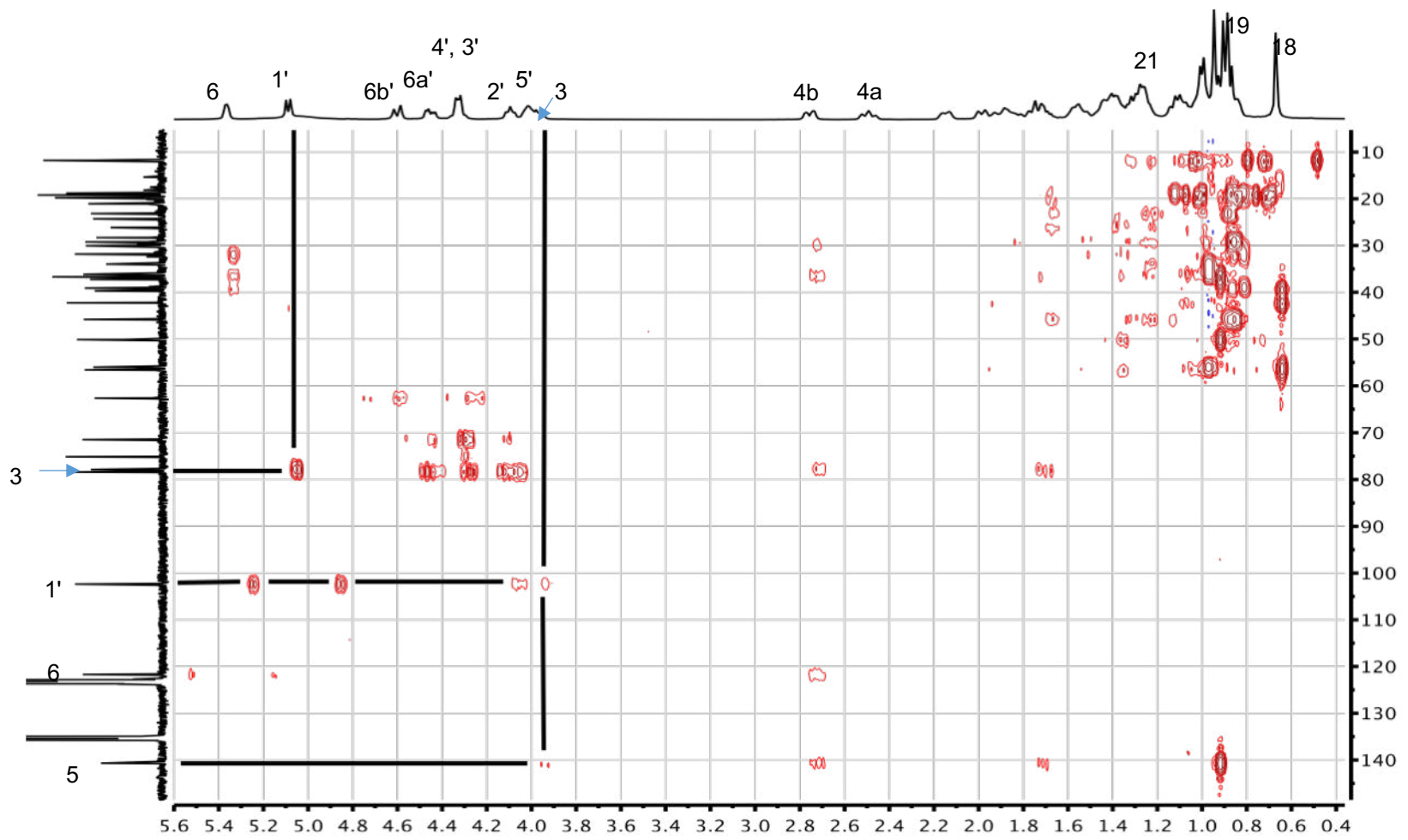
Figure 5.62 ^{1}H-^{13}C HMBC spectrum (400MHz, Py-5d) of daucosterol (11)
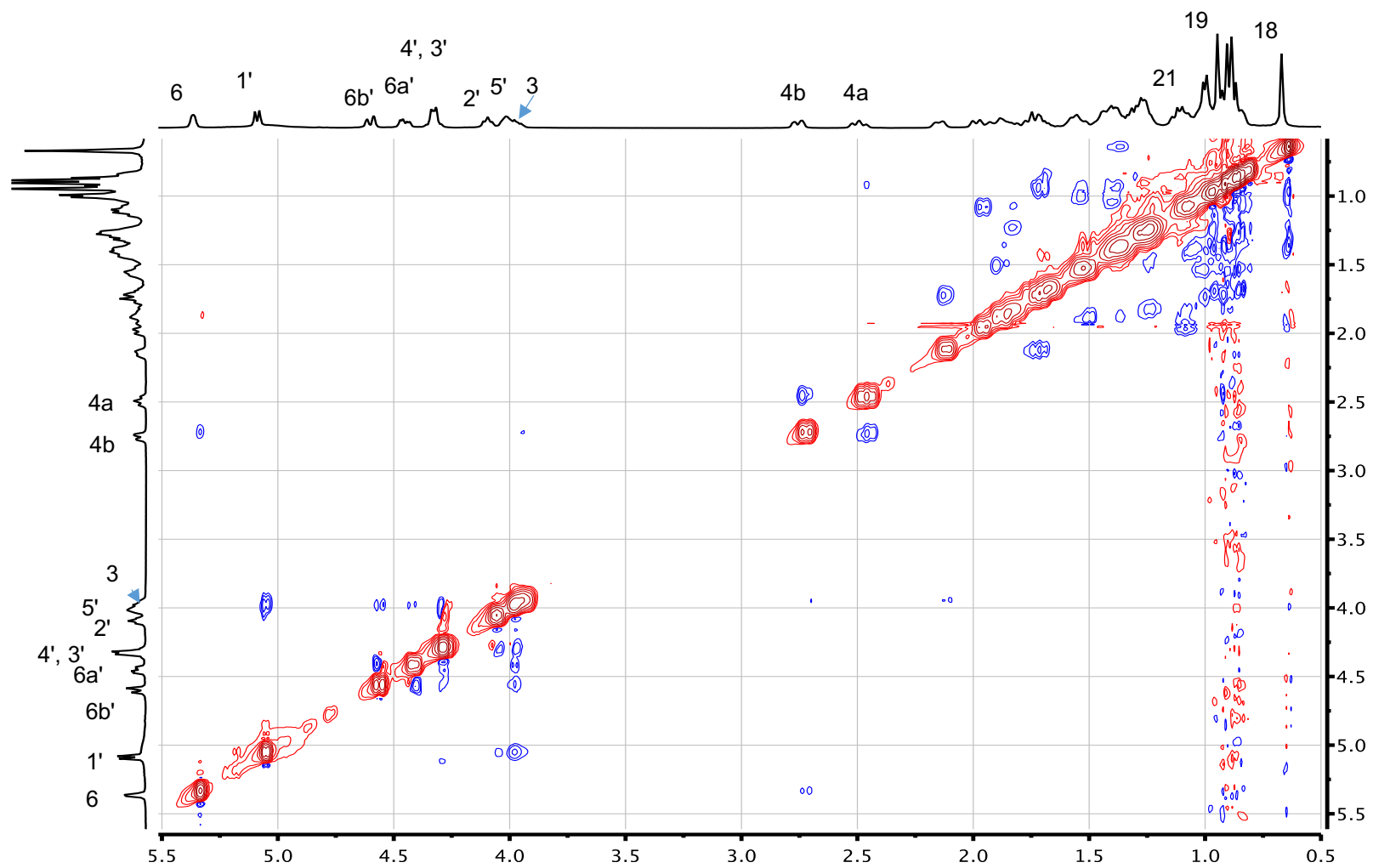
Figure 5.63 ^{1}H-^{1}H NOESY spectrum (400MHz, Py-5d) of daucosterol (11)

5.1.4.7 Physic and spectroscopic data of daucosteryl tetracetate (11a)
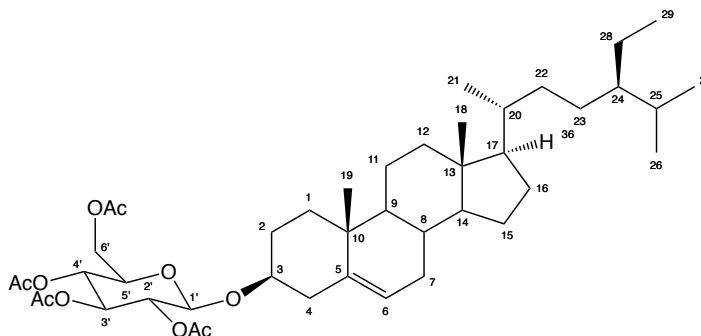
Figure 5.64 Structure of daucosteryl tetracetate (11a)

Compound 11a (Figure 5.64) is a white crystalline solid which crystalize in $CHCl_3$ into needle shaped crystals. It was soluble in $CHCl_3$, and insoluble in polar solvents, unlike the natural product (11) which was only soluble in pyridine, from which it was derived, and it does not reveal under the UV light. It has mp of 166-168 °C and molecular formula of $C_{43}H_{68}O_{10}$. The following spectral data of compound 11a was also confronted with the literature (Table 5.5).

^1H NMR (400 MHz, $CDCl_3$) δ (ppm): 0.69 (s, 3H), 0.83 (d, J=6.0 Hz, 3H), 0.85 (d, J=8.2 Hz, 3H), 0.86 (t, J=7.5 Hz, 3H), 0.94 (d, J=6.3 Hz, 3H), 1.01 (s, 3H), 2.03 (s, 3H), 2.04 (s, 3H), 2.07 (s, 3H), 2.10 (s, 3H), 3.51 (dq, J=11.2, 5.9 Hz, 1H), 3.70 (ddd, J=10.6, 4.8, 2.5 Hz, 1H), 4.13 (dd, J=12.3, 2.5 Hz, 1H), 4.28 (dd, J=12.3, 4.7 Hz, 1H), 4.61 (d, J=8.0 Hz, 1H), 4.98 (t, J=8.8 Hz, 1H), 5.10 (t, J=9.7 Hz, 1H), 5.23 (t, J=9.6 Hz, 1H), 5.38 (psd, J=4.9 Hz, 1H). ^{13}C NMR (100MHz, $CDCl_3$) δ (ppm): 11.86 ppm (C-18), 11.99 ppm (C-29), 18.79 ppm (C-21), 19.04 ppm (C-27), 19.37 ppm (C-19), 19.83 (C-26), 20.63 (Me-6'), 20.66 (Me-4'), 20.74 (Me-3'), 20.78 (Me-2'), 21.05 (C-11), 23.07 (C-28), 24.30 (C-15), 26.06 (C-23), 28.25 (C-16), 29.15 (C-25), 29.45 (C-2),

31.87 (C-8), 31.91 (C-7), 33.94 (C-22), 36.14 (C-20), 36.72 (C-10), 37.20 (C-1), 38.92 (C-12), 39.74 (C-4), 42.33 (C-13), 45.84 (C-24), 50.17 (C-9), 56.05 (C-17), 56.76 (C-14), 62.11 (C-6'), 68.54 (C-4'), 71.49 (C-2'), 71.69 (C-5'), 72.92 (C-3'), 80.09 (C-3), 99.64 (C-1'), 122.17 (C-6), 140.35 (C-5), 169.31 (CO-6'), 169.41 (CO-4'), 170.36 (CO-3'), 170.71 (CO-2').

5.1.4.7.1 Structural elucidation of daucosteryl tetracetate (11a)

The ^{1}H NMR spectrum (Figure 5.65) showed signals typical of a steroid, with a lot of signals in the upfield region. The first signals are the CH$_3$ of the aglycone: the singlet at 0.68 ppm (3H, Me-19), the doublet at 0.81 ppm (J=6.9 Hz, 3H, Me-27), the doublet at 0.83 ppm (J=7.4 Hz, 3H, Me-26), the triplet at 0.84 (J=7.4 Hz, 3H, Me-29), the doublet of 0.92 ppm (J=6.6 Hz, 3H, Me-21) and the singlet at 1.01 ppm (3H, Me-18). The spectra showed also four signals relative to the methyl groups of the acetylated sugar: 2.03 ppm (s, 3H, Me-6'), 2.04 ppm (s, 3H, Me-4'), 2.07 ppm (s, 1H, Me-3') and 2.10 ppm (s, 3H, Me-2'). Other signals in the downfield region are the double quartet at 3.51 ppm (J=11.2, 5.9 Hz, 1H, H3), which corresponds to the proton germinal to the glucosyl group. Followed by the signals relative to the hydrogens of the glucose: 3.70 ppm (ddd, J=10.6, 4.8, 2.5 Hz, 1H, H-5'), 4.13 ppm (dd, J=12.3, 2.5 Hz, 1H, H-6a'), 4.28 ppm (dd, J=12.3, 4.7 Hz, 1H, H-6b'), 4.61 ppm (d, J=8.0 Hz, 1H, H-1'), 4.96 ppm (t, J=8.8 Hz, 1H, H-2'), 5.08 ppm (t, J=9.7 Hz, 1H, H-4') and 5.21 ppm (t, J=9.6 Hz, 1H, H-3'). The most shielded signal of the spectrum is the one relative to the vinylic hydrogen at 5.35 ppm (pd, J=5.5, 1.9 Hz, 1H, H-6). The ^{13}C NMR spectrum (Figure 5.66) also showed a steroid pattern with very few signals in the downfield region: first the carbonyl groups

of the four acetyl groups at 170.71 ppm (CO-2'), 170.36 ppm (CO-3'), 169.41 ppm (CO-4') and at 169.31 ppm (CO-6'), these signals confirmed the acetylation of the molecule. A quaternary carbon at 140.35 ppm (C-5), and the vinylic carbon at 122.17 ppm (C-6). The following signals were those related to the carbons of the sugar and the carbon of aglycone directly attached to the hydroxyl group: 99.64 ppm (C-1'), 80.09 (C-3), 72.92 ppm (C-3'), 71.69 ppm (C-5'), 71.49 ppm (C-2'), 68.54 ppm (C-4') and 62.11 ppm (C-6'). In contrast, in the upfield region, there were a lot of signals which were all relative to the protons of the steroid rings and lateral chain. Especially simple to recognize were the methyl carbons at 11.86 ppm (C-18), 11.99 ppm (C-29), 18.79 ppm (C-21), 19.04 ppm (C-27), 19.37 ppm (C-19) and 19.83 ppm (C-26). These signals are the most shielded of the spectrum and are characteristic of steroid molecules (Figure 5.67). It was also taken a 1D DEPT135 spectrum (Figure 5.68) which was useful to discriminate the CH_2 from the CH and CH_3. The assigned signals were also confirmed from the literature (*96*). The molecule was also analyzed using 2D NMR experiments: ^1H-^1H COSY, ^1H-^{13}C HSQC, ^1H-^{13}C HMBC and ^1H-^1H NOESY.

Table 5.5 Spectroscopic data of daucosteryl tetracetate (11a)

n	¹H NMR (400 MHz, Py) δ (ppm), (*96*)	¹H NMR (400 MHz, Py) δ (ppm), 11a	¹³C NMR (100MHz, Py) δ (ppm), (*96*)	¹³C NMR (100MHz, Py) δ (ppm), 11a
1	-	-	37.2	37.20
2	-	-	29.4	29.45
3	3.49 m	3.51 (dq, dq, *J*=11.2, 5.9 Hz, 1H)	80.1	80.09
4	-	-	38.1	38.92
5	-	-	140.3	140.35
6	5.37 m	5.38 (psd, *J*=4.9 Hz, 1H)	122.2	122.17
7	-	-	31.8	31.87
8	-	-	31.9	31.91
9	-	-	50.01	50.17
10	-	-	36.57	36.72
11	-	-	21.0	21.05
12	-	-	39.7	39.74
13	-	-	42.3	42.33
14	-	-	56.7	56.76
15	-	-	24.3	24.30
16	-	-	28.2	28.25
17	-	-	56.0	56.05
18	0.67 s	0.69 s	11.8	11.86
19	0.99 s	1.01 s	19.4	19.37
20	-	-	36.1	36.14
21	0.93 d	0.94 (d, *J*=6.3 Hz, 3H)	18.8	18.79
22	-	-	33.9	33.94
23	-	-	26.0	26.06
24	-	-	45.8	45.84
25	-	-	29.1	29.15
26	0.84 d	0.85 (d, *J*=8.2 Hz, 3H)	19.8	19.83
27	0.82 d	0.83 (d, *J*=6.0 Hz, 3H)	19.0	19.04
28	-	-	23.1	23.07
29	0.85 t	0.86 (t, *J*=7.5 Hz, 3H)	12.0	11.99
1'	4.59 d	4.61 (d, *J*=8.0 Hz, 1H)	99.7	99.64
2'	4.96 t	4.98 (t, *J*=8.8 Hz, 1H)	71.5	71.49
3'	5.21 t	5.23 (t, *J*=9.6 Hz, 1H)	72.9	72.92
4'	5.08 t	5.10 (t, *J*=9.7 Hz, 1H)	68.5	68.54
5'	3.69 ddd	3.70 (ddd, *J*=10.6, 4.8, 2.5 Hz, 1H)	71.7	71.69
6'a	4.13 dd	4.13 (dd, *J*=12.3, 2.5 Hz, 1H)	62.1	62.11
6'b	4.26 dd	4.28 (dd, *J*=12.3, 4.7 Hz, 1H)		
CO2'	-	-	170.7	170.71
CO3'	-	-	170.4	170.36
CO4'	-	-	169.4	169.41
CO6'	-	-	169.3	169.31
Me2'	2.09 s	2.10 s	20.8	20.78
Me3'	2.05 s	2.07 s	20.7	20.74
Me4'	2.03 s	2.04 s	20.6	20.66
Me6'	2.01 s	2.03 s	20.6	20.63
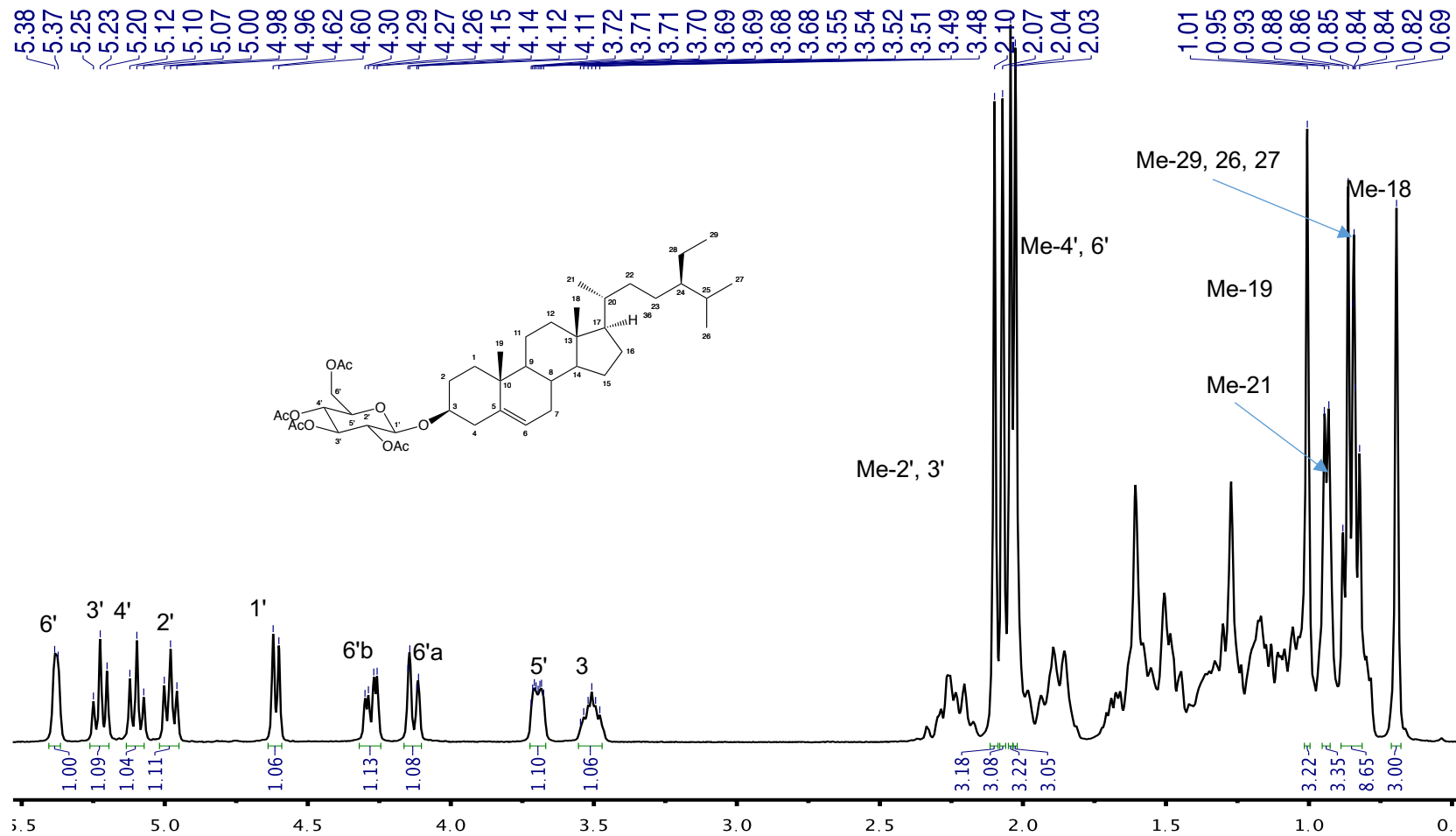
Figure 5.65 ^{1}H NMR spectrum (400MHz, CDCl$_3$) of daucosteryl tetracetate (11a)
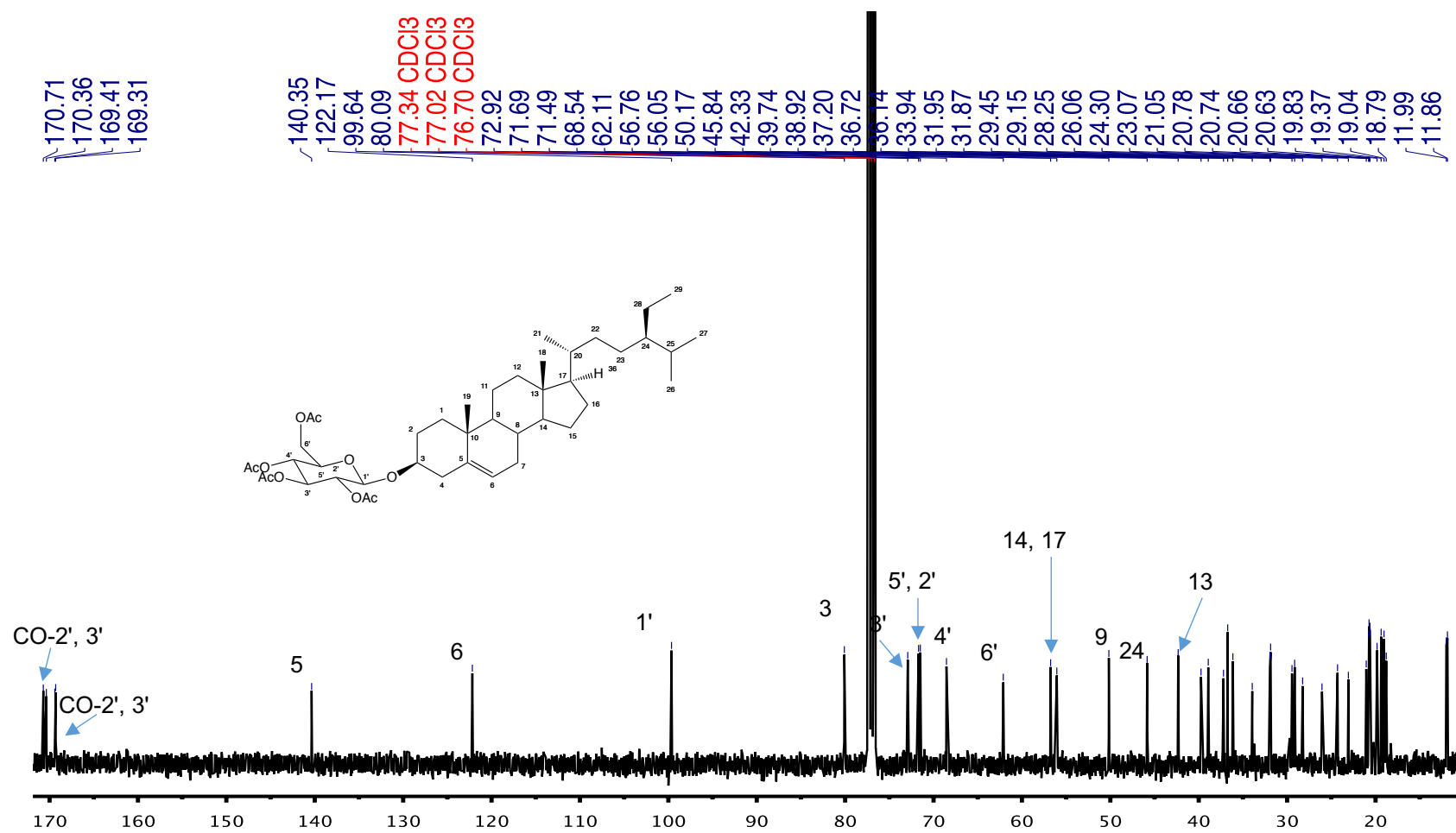
Figure 5.66 ^{13}C NMR spectrum (100MHz, CDCl$_3$) of daucosteryl tetracetate (11a)
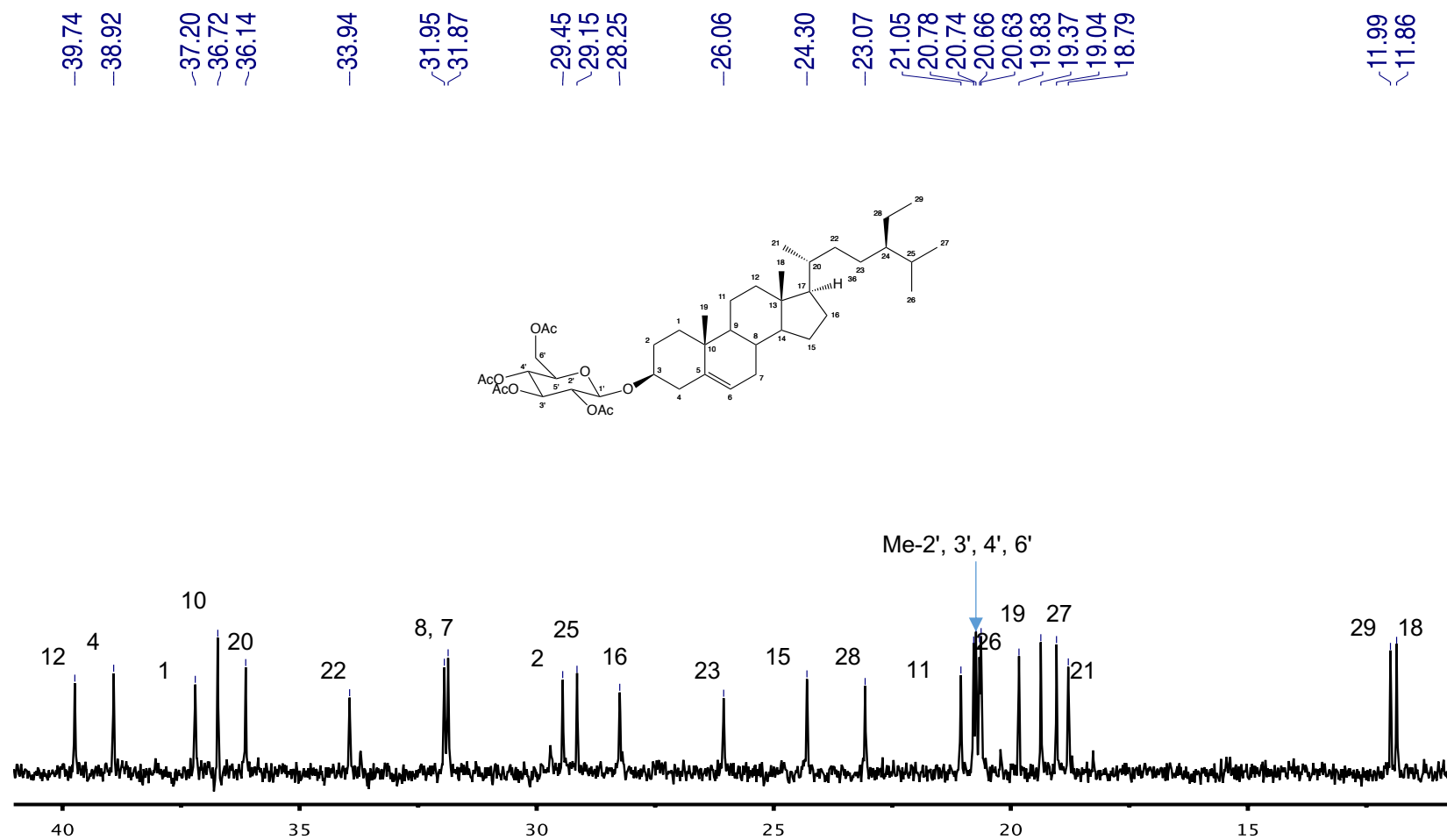
Figure 5.67 ^{13}C NMR spectrum (100MHz, CDCl$_3$) of daucosteryl tetracetate (11a) - expansion
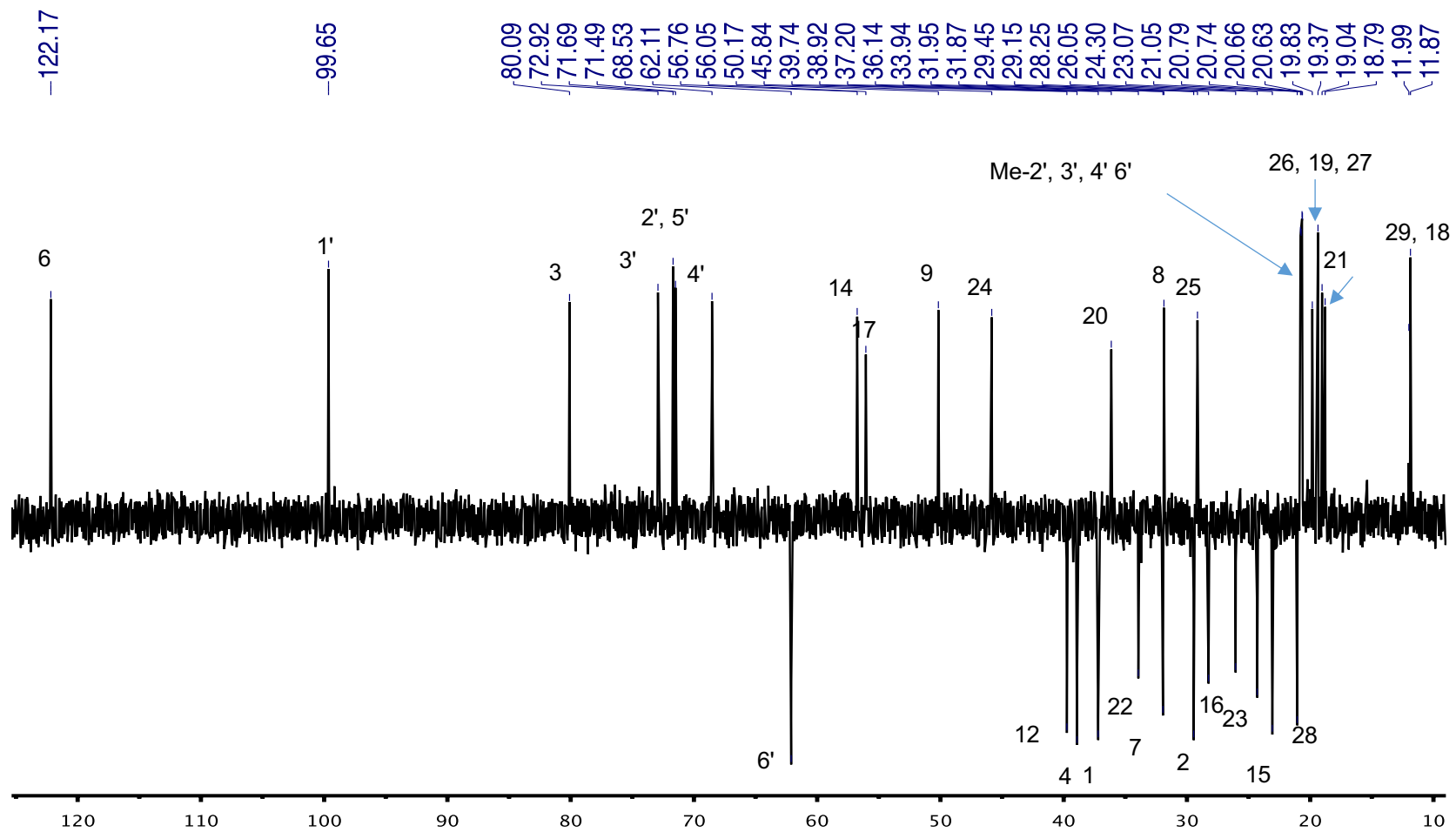
Figure 5.68 [1]D DEPT135 spectrum (100MHz, CDCl$_3$) of daucosteryl tetracetate (11a)

5.1.4.8 Isolation and purification of KCl (12)

This inorganic compound was partially soluble in H_2O and needed to be heated in order to achieve complete solubilization. On the other hand, it resulted to be completely insoluble in any organic solvent and it had mp higher than 300°C and its molecular formula is KCl. Also its high concentration in the leaves tissues is probably evidence of the halophilic nature of the plant (99). Since CAM plants are not usually halophites, *H. glomerata* might be a rare example of this class of organisms (100–102).

5.1.4.8.1 Structural elucidation of KCl (12)

The IR spectrum (Figure 5.69) of the molecule showed very few signals in general and between 1800 and 2300 cm^{-1} the spectrum shows a very high noise. This absence of signals and the high background noise it's due to the nature of the compound itself, lacking vibrating covalent bonds and being very crystalline.
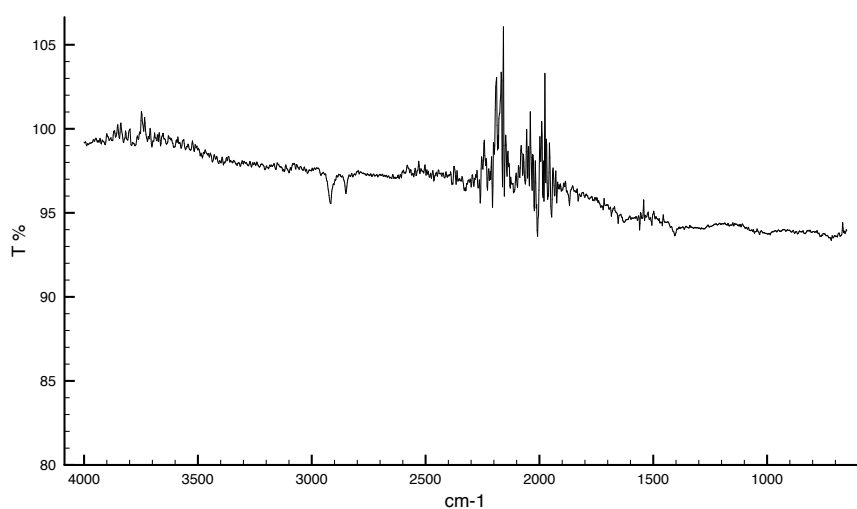
Figure 5.69 IR spectrum of KCl (12)

That is one of the first evidences that shown that the molecule was in fact an inorganic compound. Also, the ^{1}H NMR spectrum and the ^{13}C NMR spectrum didn't show any signals related to organic molecules, so the compound was confirmed to be an inorganic molecule or mixture of compounds. The X-ray analysis of the compound shows a diffractogram of an ionic compound, as shown in the figure 5.70. By confrontation with the data base of the equipment was confirmed the identity of the molecule as KCl.
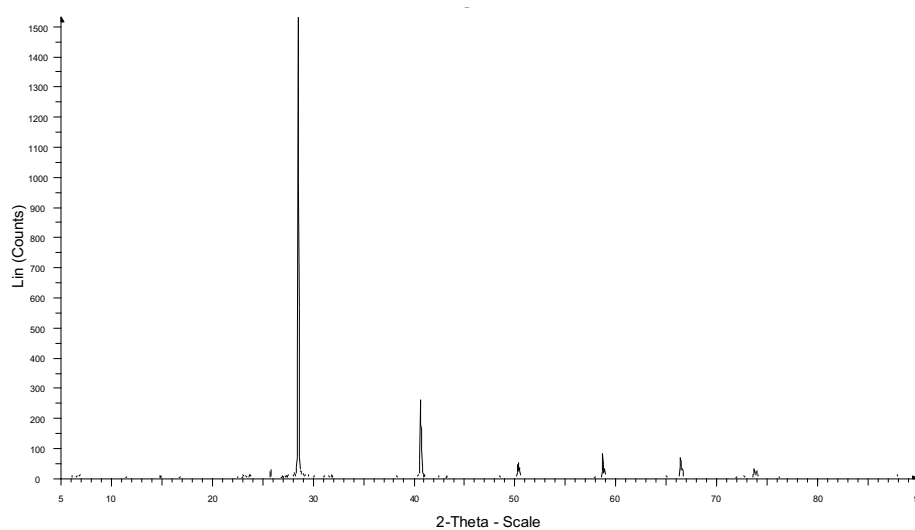
Figure 5.70 X-ray diffractogram of KCl (12)

5.1.5 The aqueous macerations

The last solvent used in the extraction of *H. glomerata* vegetal material was distilled water. The latter was first used on freshly collected aerial parts of the plant and secondly on the material which was already macerated with the organic solvents. Meanwhile the roots were extracted only dried and after maceration with the organic solvents. Due to the high polarity of water the target compounds of this process are mainly polyhydroxylated compounds. Some examples of target molecules are sugars, poly glycosylated flavonoids, free AA, and polyphenols in general. This maceration had the goal of extracting all the metabolites more polar than those extracted with the organic solvents. Also, the water extraction of the fresh material was performed in order to extract compounds that may be sensible of oxidation processes and or decomposition derived from the drying process. Some of these compounds might be vitamins, nucleic acids and nucleosides, AA and small peptides among others.

The components of these extracts were not isolated through column chromatography but were identified by equipment with higher perfor-mance, such as UPLC-MS and HPLC-MS. The bioassay-directed fractionation of one of leaf aqueous extracts was carried out for the identification of antibacterial compounds. This fractionation was performed using a flash column chromatography (FC) apparatus already described in the material and equipment chapter.

5.1.6 GC-MS analysis

5.1.6.1 Hexane extract

Abundance
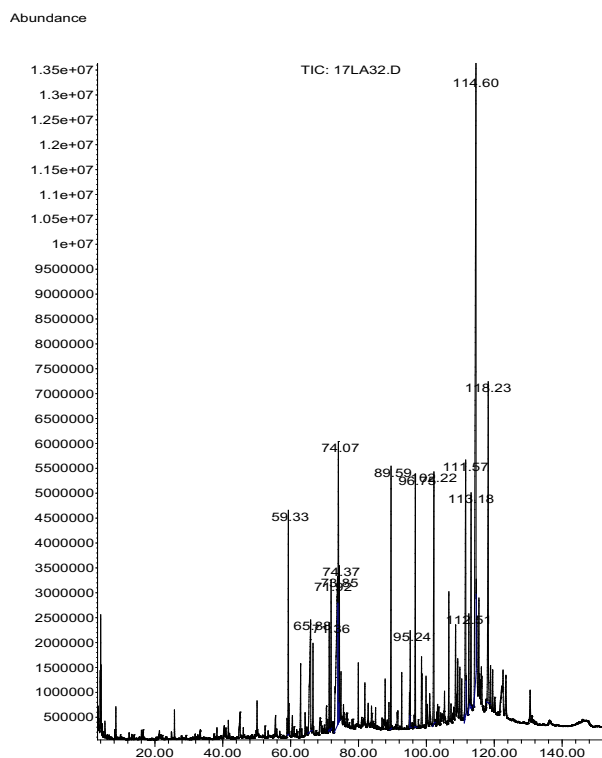
Figure 5.71 Chromatogram obtained from the GC analysis

The objective of this analysis was to characterize the major components of the extract, even compounds that were not isolated using CC, to have a wider view of the composition of the extract itself and to give a first justification of the use of the plant as antibacterial and anticancer ethnical medicine. In the figure 5.71 is reported the chromatogram of the hexane extract obtained from GC analysis. The phytochemicals found in the extract (Table 5.6) were mainly steroids which make the 43.56 % of the extract, in minor quantities were also found fatty acids, saturated (6.02%) and unsaturated (11.84%) and two ethyl esters of unsaturated fatty acids (10.15%). Were also present long chain alkanes (9.13%) a dialcohol with a 30 carbons chain (3.94%), a diterpene (2.44%) and a ketone derivate from the oxidation of the phytol (3.76%). It was calculated the relative retention indices for all the compounds (last column of the Table 5.6), which is the retention time (RT) of a compound normalized to retention times of adjacently eluting n-alkanes. Retention times vary with the individual chromatographic system

153

(column length, film thickness, diameter, carrier gas velocity and pressure, and void time), the retention indices are quite independent of these parameters and allow comparing values measured by different analytical laboratories under varying conditions.

Table 5.6 Results of the GC-MS analysis for the hexane extract

t_R (min)	Compound	Abundance (%)	Retention index
59.332	Phyton	3.758	609.00
65.881	Palmitic acid (C16:0)	6.018	1320.35
71.359	Heneicosane	1.704	1773.38
71.918	Phytol	2.444	2030.54
73.842	Linoleic acid (C18:2 $\Delta^{9,12}$)	11.835	890.34
74.072	Ethyl linoleate	7.712	1005.84
74.368	Ethyl oleate	2.434	1154.49
89.601	Unknown	4.572	-
95.243	Heptacosane	1.483	2175.52
96.747	Unknown	4.595	-
102.219	Nonacosane	5.941	2386.47
111.573	Campesterol	7.625	2414.05
112.512	Stigmasta-5,22-dien-3-ol	1.939	203.14
113.157	1,30-triacontanediol	3.937	915.26
114.601	β-sitosterol	25.470	2509.50
118.227	Stigmast-4-en-3-one	8.532	3393.00

Between the identified compounds there are some that are reported in the literature for their biological activity, such as: campesterol, stigmasterol, stigmastan-4-en-3-one, β-sitosterol, phytol, γ-linoleic acid, oleic acid and palmitic acid. The reported activities for these compounds effectively explain the use of the plant in folk medicine in the treatment of cancer and bacterial infections.

From the compounds isolated through CC, the major components β-sitosterol and nonacosane were found also in the GC-MS analysis. They have

concentrations, which represent together more than the 30% of the extract composition. The other isolated compounds were not identified in the GC-MS analysis due to instrumental limitation and low volatilization of isolated compounds. In addition, some compounds were not identified because of its quantity and their absence in the NIST library.

Comparing the compounds identified by GC-MS with the literature we found some similitudes with the reported phytochemicals from the Bromeliaceae family (*41*).

The more prominent sterol of the hexane extract was the β-sitosterol, which is reported to be present in the family and the genus (*67*, *68*); the other steroids were also reported in the plant's family. Concerning, phytol, phytone, the other n-alkanes, the saturated and unsaturated fatty acids and their derivatives as well as the di-alcohol, there are no reports in the literature of the presence of these molecules either the genus or family of *Hechtia glomerata*.

Identified hydrocarbons, heneicosane, heptacosane and nonacosane, together with 1,30-triacontadienol are derivatives of the reduction of long chain fatty acids (LCFAs) or very long chain fatty acids (VLCFAs) (*103*), and they are involved in the plant biosynthesis of esters and waxes (*104*). The terpenoid phyton is a derivative of phytol which itself derives from the metabolism of chlorophyll and the mevalonate/acetate biosynthetic route. Phytosterols campesterol, stigmasterol and β-sitosterol can be synthesized from the same biosynthetic route. They are the most common phytosterols in plants (*105*) and their quantity in the plants dependent on the plant's metabolism and vitality (*106*).

5.1.6.2 GC-MS analysis of some isolated compounds from CHCl₃/MeOH extract

Some isolated compounds such as 1-7 and semisynthetic compounds 5a and 4m were found to contain some minor contaminats thus they were analized by GC-MS. Table 5.7 shows results of analysis of each sample run in the same conditions, therefore they were pooled into one table.

Table 5.7 Results of the GC-MS analysis for the isolated and derivatized compounds

t_R (min)	Compound	Hexane (%)	C/M* (%)
10.580	Octanal	0.06	-
16.144	Nonanal	0.07	-
21.431	1-Dodecene	-	0.78
25.918	2-(E)-Decenal	0.10	-
34.148	1-Tetradecene	-	2.54
45.946	1-Hexadecene	-	1.47
50.143	Unknown	-	0.02
56.817	12-Methyltetradecanic acid (C14:0, anteiso)	0.24	-
58.400	Pentadecanoic acid (C15:0)	1.44	-
58.419	Isopropyl myristate	0.02	-
62.006	n-Nonadecane	0.11	-
62.183	Palmitoleic acid (C16:1, Δ^9)	0.45	-
65.054	Trachylobane	0.07	-
63.700	Palmitic acid (C16:0)	15.05	-
66.440	5-(E)-Eicosene	0.10	-
66.748	14-Methylpalmitic acid (C17:0, iso)	1.90	-
66.755	n-Eicosane	0.19	-
67.261	2-Hexyl-cyclopropaneoctanoic acid	0.55	-
67.497	Kaur-16-ene	0.11	-
68.036	Margaric acid (C18:0)	0.50	-
69.632	$Trans$-vaccenic acid (C18:1, Δ^{11})	0.35	-
71.366	n-Heneicosane	2.02	7.87
74.374	Nonadecenoic acid (C19:1, Δ^{13})	1.09	-
74.861	Oleic acid (C18:1, Δ^9)	0.45	-
75.701	n-Docosane	0.43	1.57
79.872	Gondonic acid (C20:1, Δ^{11})	0.49	-

Table 5.7 Results of the GC-MS analysis for the isolated and derivatized compounds

(Continued)

t_R (min)	Compound	Hexane (%)	C/M* (%)
80.162	*n*-Tricosane	-	6.62
83.689	Cyclotetracosane	0.09	-
84.004	*n*-Tetracosane	0.37	1.20
87.591	12-(Z)-Pentacosene	0.04	-
88.005	*n*-Pentacosane	1.60	4.10
89.528	Unknown	-	1.78
91.381	9-Hexacosene	0.42	2.44
91.676	*n*-Hexacosane	0.42	1.37
95.033	12-(*Z*)-heptacosene	0.33	-
95.243	*n*-Heptacosane	2.26	7.12
98.909	Cycloocatacosane	-	13.71
99.040	*n*-Octacosane	-	3.22
101.871	Nonacosanol	0.13	-
102.055	Dotriacontenol	-	0.13
102.298	*n*-Nonacosane	5.33	30.72
105.313	1-Triacontanol	-	1.82
105.497	*n*-Triacontane	1.63	2.75
108.545	Hentriacontane	1.42	8.78
110.896	Ergosterol	0.79	-
111.573	Campesterol	13.93	-
112.512	Stigmasterol	4.18	-
112.867	Hentriacontanol	0.09	-
113.175	1,30-Triacontanediol	0.09	-
115.146	β-Sitosterol	40.74	-
115.921	(3β,5α)-Ergostanol	0.32	-

* C/M: CHCl$_3$/MeOH extract

A total of 51 compounds were identified from the analysis, most of which were part of the hexane extract, since the majority of the analyzed samples came from this extract. For the hexane extract the most abundant components were the sterols (59.96 %) even though they were just 5 different molecules. The second most abundant group comprehended the fatty acids

(FAs) with a 22.51 %. The unsaturated fatty acids (UFAs) were found in a lower concentration (2.84 %) than the saturated fatty acids (SAFAs; 19.67 %). The hydrocarbons were also abundant among these compounds (16.78 %), with the alkanes reaching the 15.87 % and the alkenes the 0.90 %. The other classes of compounds with low concentration represented less than the 1 % of the identified components. They include 3 long chain alcohols, 3 aldehydes, 2 terpenoids and 1 ester of SAFA. The aldehydes, octanal, nonanal and 2-(*E*)-decenal can be considered as derivatives of the reduction of the FAs or further oxidation of hydrocarbons. These types of metabolites are produced by the plants when they undergo oxidative stress derived from pollution or pests (*107*). Two terpenoid compounds identified were trachylobane and kaur-16-ene. These trachylobane and kaurane diterpenoids are considered to be intermediates in the biosynthesis of plant growth hormones gibberellins (*108*).

On the other hand, compounds identified from samples 6 and 7 obtained from the $CHCl_3$/MeOH extract were mainly hydrocarbons (70.31 %) composed by 65.03 % of alkanes and a 5.28 % of alkenes. The other components identified were two alcohols, dotriacontanol and triacontanol (1.95 %) as well as two unknown compounds (1.80 %).

5.2 Metabolomic study

5.2.1 UPLC-QTOF-MS analysis
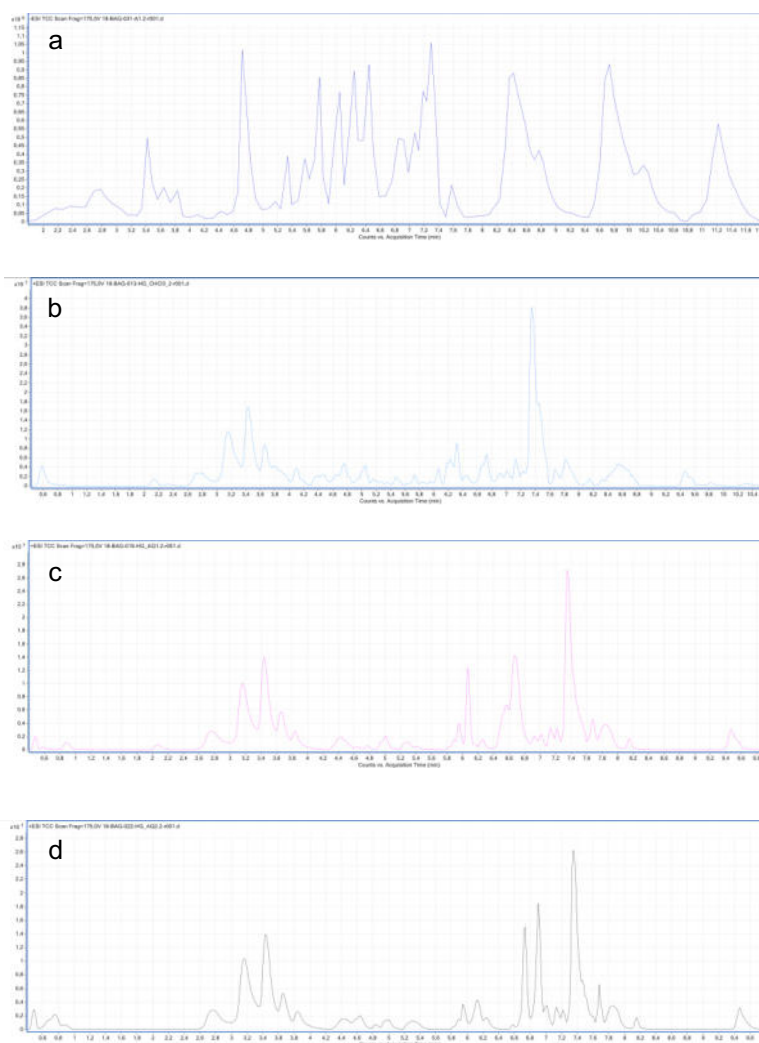
Figure 5.72 Chromatograms: a) Hexane extract; b) CHCl₃/MeOH extract; c) Dry aqueous extract; d) Fresh aqueous extract

Results of UPLC separation are reported in figure 5.72 which shows chromatograms for the four extracts: hexane (a), CHCl₃/MeOH (b), dried aqueous (c) and fresh aqueous (d) extracts. A total of 226 metabolites were identified from the analysis: 42 from the hexane extract, 117 from the CHCl₃/MeOH extract, 115 from the dry aqueous extract and 55 from the fresh aqueous extract. The composition of each extract was consistent with the

polarity of the solvent used in the maceration. At the same time extracts shared some similarities. Figure 5.73 showed the percentage of metabolites shared among extracts and the ones that were specific for each of them.
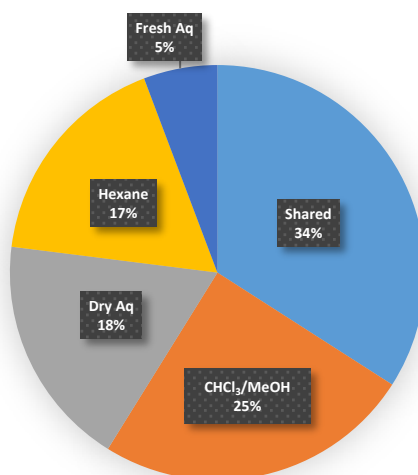
Figure 5.73 Percentage of metabolites in each extract

33 compounds were identified in dry aqueous and CHCl$_3$/MeOH extracts. 21 compounds were identified in the CHCl$_3$/MeOH and both aqueous extracts. 17 compounds were found in both aqueous extracts. Two compounds in fresh aqueous and hexane extracts. Two compounds in hexane and aqueous extracts. Two compounds were found in all extracts. Only one compound was found to be part of hexane and CHCl$_3$/MeOH extracts. One compound was part of both the CHCl$_3$/MeOH and fresh aqueous extracts. A total of 79 shared compounds representing the 34% of the entire metabolome. The total metabolomic profile of *H. glomerata* comprises 38% flavonoids and stilbenes, 31% terpenes and steroids, 15% phenolic acids and derivatives, 10% fatty acids and hydrocarbons, 6% nitrogen containing compounds (Figure 5.74).
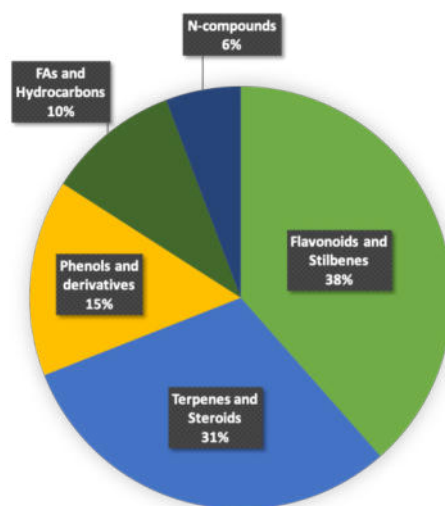
Figure 5.74 Metabolomic profile of *H. glomerata* Zucc.

Hexane extract resulted to be mostly composed by non-polar metabolites as predicted by the hydrophobicity of the maceration solvent (full extract composition is reported in table 5.8). Its profile consisted mainly of terpenes and steroids (67%), and the second most abundant group consisted of fatty acids and hydrocarbons (26%). The two minority groups of compounds are nitrogen-containing compounds (5%), and flavonoids and stilbenes (2%), the latter with only one compound. The most abundant molecules of the hexane extract were phytol, β-sitosterol, campesterol, stigmasterol and tillandsinone (Figure 5.75a). The first compound is phytol whit the higher concentration among them and it is a diterpene which can take part in the synthesis of chlorophylls and it is also produced in their breakdown (*150*). Its high concentration is justified for the need of leaf photosynthesizing pigments. In fact, another product of their metabolism, pheophorbide A was found among the identified compounds. Figure 5.75b described the production of phytol from chlorophyll A (1), and its catabolism is catalyzed by the enzyme chlorophyllase (a).

Table 5.8 Metabolites identified from the Hexane exract by UPLC-QTOF-MS analysis

t_R (min)	Compound	MW (g/mol)	Chemical Formula	Class
0.8886	Ethyl behenate	368.3654	$C_{24}H_{48}O_2$	FA and Hydrocarbons
1.4800	5Z,8Z,11Z,14Z,17Z,20Z-Tricosahexaenoic acid (C23:6, $\Delta^{5,8,11,14,17,20}$)	342.0951	$C_{23}H_{34}O_2$	FA and Hydrocarbons
2.2010	17,20-Hexacosadienoic acid (C26:6, $\Delta^{23,20,17,14,11,8}$)	392.3650	$C_{26}H_{48}O_2$	FA and Hydrocarbons
2.4490	Pristanic acid	298.5110	$C_{19}H_{38}O_2$	Terpenes and Steroids
2.5100	23-*trans*-*p*-Coumaroyloxytormentic acid	650.3840	$C_{39}H_{54}O_8$	Terpenes and Steroids
2.7630	Phytenic acid (*cis*-γ 3-)	310.5220	$C_{20}H_{38}O_2$	Terpenes and Steroids
2.8510	13-Hydroxyoctadecadienoic acid	309.1025	$C_{18}H_{15}NO_4$	FA and Hydrocarbons
2.8520	α-Tocopherol	430.3534	$C_{29}H_{50}O_2$	Terpenes and Steroids
2.9860	(3β,5ξ,9β)-24-Methyl-9,19-cyclolanost-25-en-3-yl formate	468.7700	$C_{36}H_{52}O_2$	Terpenes and Steroids
3.3860	Hexyl stearate	368.3650	$C_{24}H_{48}O_2$	FA and Hydrocarbons
3.4970	Rosilic acid	300.2660	$C_{18}H_{36}O_3$	FA and Hydrocarbons
3.7350	Avenasterol (δ5-)	412.2100	$C_{29}H_{48}O$	Terpenes and Steroids
3.7810	Stigmasta-5,22-dien-3-β-ol	412.2590	$C_{29}H_{48}O_1$	Terpenes and Steroids
3.9760	Phytanoic acid	312.5380	$C_{20}H_{40}O_2$	Terpenes and Steroids
4.4050	Stearic acid (C18:0)	284.0000	$C_{18}H_{38}O_2$	FA and Hydrocarbons
4.5170	Nonacosene	406.4539	$C_{29}H_{58}$	FA and Hydrocarbons
4.7220	Cafesterol	316.0766	$C_{20}H_{28}O_3$	Terpenes and Steroids
4.7960	Tillandsinone	466.7900	$C_{33}H_{54}O$	Terpenes and Steroids
4.8750	Isopropyl Palmitate	298.5110	$C_{19}H_{38}O_2$	FA and Hydrocarbons
5.1220	Stigmasterol 3-stearate	678.6320	$C_{47}H_{82}O_2$	Terpenes and Steroids
5.1800	24-hydroxy-β-amyrin	442.7280	$C_{20}H_{50}O_2$	Terpenes and Steroids
5.3150	(5α)-Ergostane	386.7100	$C_{28}H_{50}$	Terpenes and Steroids
5.5430	(5ξ,8ξ,9ξ,13ξ)-Pimar-15-en-19-oic acid	304.2020	$C_{20}H_{32}O_2$	Terpenes and Steroids
5.5680	Catechin 4'-methyl ether	304.0950	$C_{16}H_{16}O_6$	Flavonoids and Stilbenes

Table 5.8 Metabolites identified from the Hexane exract by UPLC-QTOF-MS analysis (Continued)

t_R (min)	Compound	MW (g/mol)	Chemical Formula	Class
5.6440	Funtumine	317.2699	$C_{21}H_{35}NO$	N-compounds
5.7047	1,21-Heneicosanediol	328.3340	$C_{21}H_{44}O_2$	FA and Hydrocarbons
5.9100	Phytol	296.5390	$C_{20}H_{40}O$	Terpenes and Steroids
5.9630	(+)-δ-Tocopherol	402.3490	$C_{27}H_{46}O_2$	Terpenes and Steroids
5.9820	β-Sitosterol	414.1020	$C_{29}H_{50}O$	Terpenes and Steroids
6.2600	Antheraxanthin	584.8850	$C_{40}H_{56}O_3$	Terpenes and Steroids
6.4600	Stigmasterol	412.0365	$C_{29}H_{48}O$	Terpenes and Steroids
6.4740	Brassicasterol	398.3549	$C_{28}H_{46}O$	Terpenes and Steroids
6.5450	Campesterol	400.9756	$C_{28}H_{48}O$	Terpenes and Steroids
7.1270	Bixin aldehyde	348.4862	$C_{24}H_{28}O_2$	Terpenes and Steroids
7.1460	Ergosterol	396.4537	$C_{29}H_{44}O$	Terpenes and Steroids
7.3000	Protopanaxatriol	476.7420	$C_{30}H_{52}O_4$	Terpenes and Steroids
7.6180	Kahweol	314.1880	$C_{20}H_{26}O_3$	Terpenes and Steroids
7.6190	16-*O*-Methylcafestol	330.4680	$C_{21}H_{30}O_3$	Terpenes and Steroids
7.7760	Royleanone-4	344.1604	$C_{20}H_{24}O_5$	Terpenes and Steroids
8.7060	*N*-Acetyl-Phytosphingosine	359.3030	$C_{20}H_{41}NO_4$	N-compounds
9.4130	Tricin	330.1676	$C_{17}H_{14}O_7$	Flavonoids and Stilbenes
9.5230	Erythrodiol	442.3811	$C_{30}H_{50}O_2$	Terpenes and Steroids

From this enzymatic reaction is produced the chlorophyllide A (2) which is then metabolized by the Mg-dechetalase (b), into pheophorbide A (3). The whole process occurs in the chloroplast.
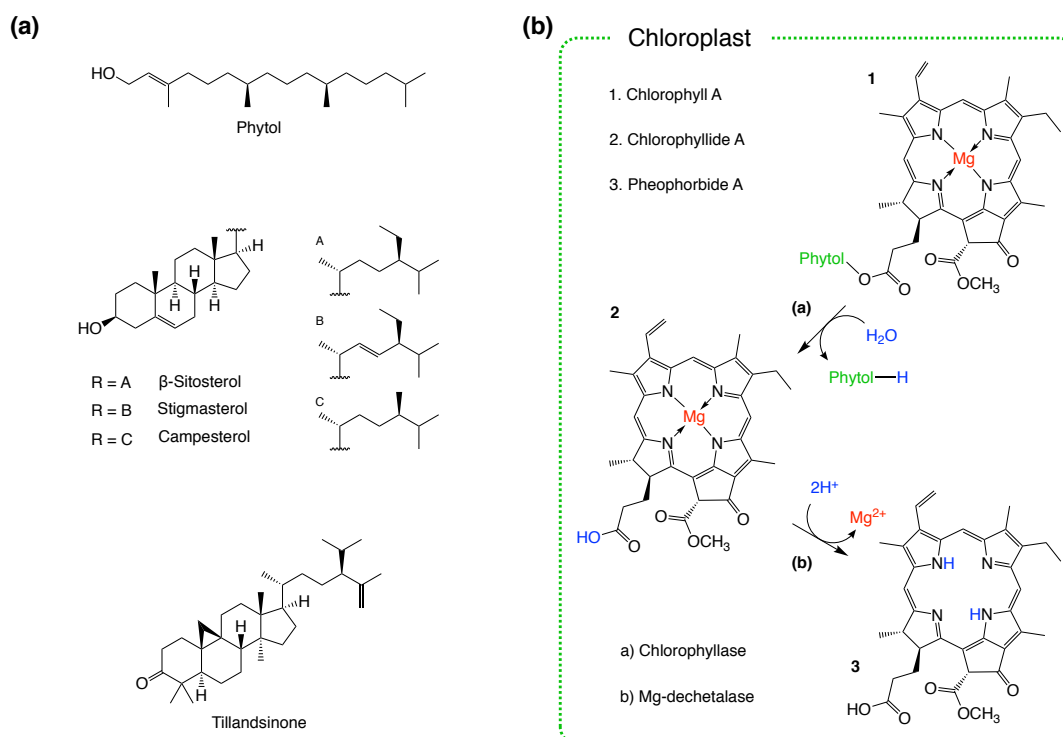
Figure 5.75 Major components of the hexane extract (a); Phytol production from chlorophyll A degradation in the Chloroplast

Production of phytol throughout the chlorophyll degradation is also linked to the biosynthesis of tocopherols and tocotrienols. They are part of height compounds known as vitamin E, which are membrane component essential for its integrity. These liposoluble molecules are potent antioxidants and radical scavenging agents produced in contrast of oxidative stress. α- and δ-tocopherol were identified within the metabolome of *H. glomerata* and their structure and biosynthesis are reported in figure 5.76. The synthesis of

tocopherols takes place inside the chloroplast and can follow straight way the degradation of chlorophyll. The phytol produced in the catabolism is first phosphorylated to phytyl monophosphate (PMP) by the phytol kinase 1 (PK1). The latter first is decarboxylated and the generated negative charge drives the attack to the phytol and the formation of the 2-methyl-6-phytyl-1,4-benzoquinol (MPBQ).
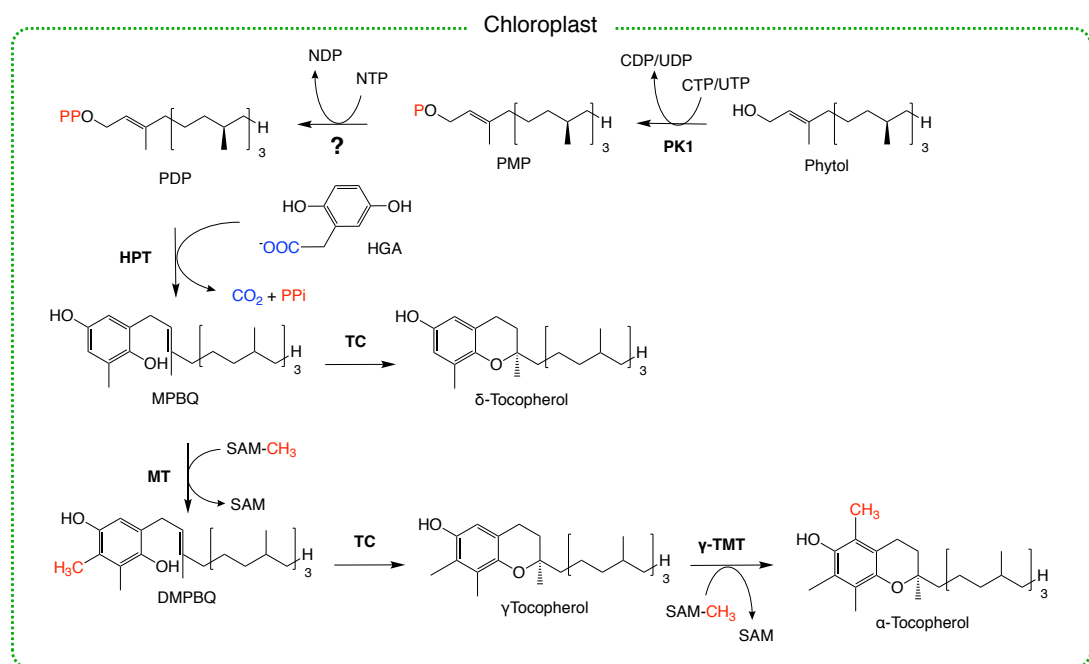
Figure 5.76 Biosynthesis of α-, γ-, and δ-tocopherol from phytol

This last reaction is catalyzed by the enzyme homogentisate phytyltransferase (HPT), and its byproducts are carbon dioxide and pyrophosphate (PPi). The MPBQ can either be cyclized by the tocopherol cyclase (TC) into δ-tocopherol or it can be methylated by a methyl transferase. The cosubstrate used in this reaction is S-adenosylmethionine (SAM) and the product is the 2,3-dimethyl-6-phytyl-1,4-benzoquinol (DMPBQ). Throughout the cyclization of this intermediate by TC, the γ-tocopherol is then synthesized

165

and its methylation at the position 5 produces α-tocopherol. This last modification is catalyzed by the enzyme γ-tocopherol methyltransferase (γ-TMT) (*151*). The three sterols: β-sitosterol, campesterol, and stigmasterol are well known and widely spread among all plant species. Membrane of plants' cells has a diversified lipid composition with these three sterols being predominant over all the others. The ratio between these compounds in the plant tissues is specific of plants species, for example the ratio between β-sitosterol and campesterol is determined by the sterol methyltransferases (SMT) activities. The enzymes that catalyze the methylation at position 24 of side chain. Also, the regulation of the ratio and composition of sterols seems to be a very important element of different cellular processes. In fact, it determines the totality of cell's functions and the vitality of the plant (*106*). Functions of sterols within the plant's cells, a part of being constitutively essential for plant's cellular membrane are numerous. For instance, they are precursors of plant hormones (brassinosteroids), which regulate plants development and growth. They are also part of the transmembrane signal transduction, throughout the formation of specific lipid rafts. These act like microdomains on the surface of the membrane and are used by signaling enzyme complexes as anchoring platforms (152, 153). Tillandsinone one the major components of the hexane extract is a sterol reported for the first time in genus *Tillandsia*, from *T. fasciculata* (*154*). These types of steroids with uncommon isopropyl side chains are usually rare in terrestrial plants. They are found in marine sponges such as the *Aplysnia* species (*155*). There are reports of this unusual steroid in the species *Nervilia purpurea* (Orchideaceae) and *Viola formosana* (Violaceae) (*156*, *157*). Tillandsinone could be used as

biomarker between *H. glomerata* and its family. It is also a sign of a close phylogenetic correlation of *H. glomerata* and *T. fasciculata*.

In contrast to the hexane extract, the CHCl$_3$/MeOH extract is mainly composed by flavonoids and stilbenes (43%). The terpenes and steroids (26%) represent the second biggest group of molecules, followed by the phenols and their derivatives (19%). The last two minority classes of compounds are represented by the non-polar compounds such as fatty acids and hydrocarbons (8%) as well as nitrogen containing compounds (4%). The complete composition of this extract is reported in table 5.9. Among the most abundant compounds of this extract are piceatannol, spinacetin, resveratrol, luteolin and daucosterol (Figure 5.77). Piceatannol, is a stilbene which is produced by the cyclization of a polyketide (phenylpropanoid pathway) starting from a molecule of caffeoyl-CoA. It was also successfully synthetized by the hydroxylation of resveratrol molecule at the position 5, throughout an enzymatic reaction catalyzed by a flavin-dependent monooxygenase (HpaBC) (*158*). Piceatannol shares the same biosynthetic pathway as resveratrol, changing only the starting point, which in this case is *p*-coumaroyl-CoA (5.77B). The synthesis of both piceatannol and resveratrol, the coenzyme A has three acetyl subunits obtained from three molecules of malonyl-CoA. Through this elongation process the polyketide precursor to the products is synthesized. The enzyme involved in the synthesis of piceatannol is still not being elucidated, but it is believed to be the pinosylvin synthase. Instead for the resveratrol is well known the enzyme responsible for the cyclization of its precursor, which is resveratrol synthase (RS).

Table 5.9 Metabolites identified from the CHCl₃/MeOH exract by UPLC-QTOF-MS analysis

t_R (min)	Compound	MW (g/mol)	Chemical Formula	Class
3.2660	Fustin-7-rhamnoside	434.1218	$C_{21}H_{22}O_{10}$	Flavonoids and Stilbenes
3.4180	Epicatechin 3-*O*-(4-methylgallate)	456.1036	$C_{23}H_{20}O_{10}$	Flavonoids and Stilbenes
3.4180	Cnidimol 7-glucoside	438.0930	$C_{21}H_{26}O_{10}$	Phenols and derivatives
3.4180	Ursolic acid	456.1037	$C_{30}H_{48}O_3$	Terpenes and Steroids
3.5680	Salviaflaside methyl ester	536.1523	$C_{25}H_{28}O_{13}$	Phenols and derivatives
3.6530	(17α, 23*S*)-Epoxy-28, 29-dihydroxy-27-norlanost-8-ene-3, 24-dione	472.3179	$C_{29}H_{44}O_5$	Terpenes and Steroids
3.6680	6'''-*O*-Sinapoylsaponarin	800.2157	$C_{38}H_{40}O_{19}$	Flavonoids and Stilbenes
3.6880	Dulxanthone G	414.1322	$C_{22}H_{22}O_8$	Phenols and derivatives
3.8650	Heliangine	362.4170	$C_{20}H_{26}O_6$	Terpenes and Steroids
4.0880	Syringaresinol	418.4370	$C_{22}H_{26}O_8$	Phenols and derivatives
4.0960	Khellol glucoside	408.1084	$C_{19}H_{20}O_{10}$	Phenols and derivatives
4.1320	Pelargonidin 3-*O*-[β-*D*-Glucopyranosyl-(1-2)-[4-hydroxycinnamoyl-(-6)]-β-*D*-glucopyranoside](*E*-) 5-*O*-β-*D*-glucopyranoside	903.2545	$C_{42}H_{47}O_{22}$	Flavonoids and Stilbenes
4.1480	Isovitexin 2"-*O*-[4-hydroxy-(*E*)-cinnamoyl-(-6)-β-*D*-glucopyranosyl] 4'-*O*-β-*D*-glucopyranoside	902.2466	$C_{42}H_{46}O_{22}$	Flavonoids and Stilbenes
4.1750	(*E*)-Oxyresveratrol 3'-*O*-β-*D*-glucoside	406.1271	$C_{20}H_{22}O_9$	Flavonoids and Stilbenes
4.2830	(-)-Medicocarpin	432.1428	$C_{22}H_{24}O_9$	Phenols and derivatives
4.4700	γ-L-Glutamyl-*S*-(2-carboxy-1-propyl)cysteinylglycine	393.0000	$C_{14}H_{23}N_3O_8S$	N-compounds
4.4780	3, 5, 8-Trihydroxy-3', 4', 7-trimethoxyflavone	360.0854	$C_{18}H_{16}O_8$	Flavonoids and Stilbenes
4.5800	4-Methoxybenzenepropanol 1-(2-sulfoglucoside)	408.1086	$C_{16}H_{24}O_{10}S$	Phenols and derivatives
4.7290	Glabrol	392.2000	$C_{25}H_{28}O_4$	Flavonoids and Stilbenes
4.8460	Cyanidin 3-(6"-malonyl)-laminaribiose	679.4050	$C_{30}H_{33}O_{19}$	Flavonoids and Stilbenes
4.9390	Phytolaccagenic acid 3-*O*-glucose(1"->3')arabinose	810.4400	$C_{42}H_{66}O_{15}$	Terpenes and Steroids
4.9620	3-*O*-Methylrosmarinic acid	374.1009	$C_{19}H_{18}O_8$	Phenols and derivatives

Table 5.9 Metabolites identified from the CHCl₃/MeOH exract by UPLC-QTOF-MS analysis (Continued)

t$_R$ (min)	Compound	MW (g/mol)	Chemical Formula	Class
5.0220	Hispaglabridin A	392.1120	$C_{25}H_{28}O_4$	Flavonoids and Stilbenes
5.0520	2, 4, 6-Phenanthrenetriol 2-*O*-β-*D*-glucoside	388.1167	$C_{20}H_{20}O_8$	Phenols and derivatives
5.0530	8-Hydroxy-4'-methoxypinoresinol	388.1520	$C_{21}H_{24}O_7$	Flavonoids and Stilbenes
5.0540	Kaempferol 3-*O*-rhamnoside	431.3700	$C_{21}H_{19}O_{10}$	Flavonoids and Stilbenes
5.0760	9, 10, 13-trihydroxy-11-octadecenoic acid	330.2400	$C_{18}H_{34}O_5$	FA and Hydrocarbons
5.0970	Sinapoylquinic acid	398.2430	$C_{18}H_{22}O_{10}$	Phenols and derivatives
5.1110	(*Z*)-4', 6-Dihydroxyaurone 6-glucoside	416.1112	$C_{21}H_{20}O_9$	Flavonoids and Stilbenes
5.3300	Petunidin	317.2930	$C_{16}H_{13}O_7$	Flavonoids and Stilbenes
5.4230	Hydroxymethyl glutathione	336.2285	$C_{20}H_{32}O_4$	N-compounds
5.5100	Glycyrrhizin	822.9420	$C_{42}H_{62}O_{16}$	Terpenes and Steroids
5.5440	Sarsasapogenin	416.3290	$C_{27}H_{44}O_3$	Terpenes and Steroids
5.5500	γ-L-Glutamyl-γ-L-glutamyl-L-methionine	407.1347	$C_{15}H_{25}N_3O_8S$	N-compounds
5.6190	Piceatannol 4'-glucoside	406.3870	$C_{20}H_{22}O_9$	Flavonoids and Stilbenes
5.7240	3, 8-Dihydroxy-6-methoxy-7(11)-eremophilen-12, 8-olide	296.1625	$C_{16}H_{24}O_5$	Terpenes and Steroids
5.8010	(ent-15β)-15, 19-Dihydroxy-7-trachylobanone	318.2175	$C_{20}H_{30}O_3$	Terpenes and Steroids
5.8090	(ent-6α, 7α, 16αH)-6, 7, 17-Trihydroxy-19-kauranoic acid	352.2233	$C_{20}H_{32}O_5$	Terpenes and Steroids
5.9450	6-tuliposide A	278.1519	$C_{11}H_{18}O_8$	FA and Hydrocarbons
5.9460	2-Hydroxyenterodiol	318.1444	$C_{18}H_{22}O_5$	Phenols and derivatives
5.9510	10-hydroperoxy-8*E*, 12*Z*-octadecadienoic acid	312.2289	$C_{18}H_{32}O_4$	FA and Hydrocarbons
6.0550	β-Sitostanol	416.4018	$C_{29}H_{52}O$	Terpenes and Steroids
6.0600	Pregna-5,16,20-triene-3β,20-diol diacetate	398.2431	$C_{25}H_{34}O_4$	Terpenes and Steroids
6.1500	2''-*O*-*trans*-*p*-Coumaroylastragalin	594.1369	$C_{30}H_{26}O_{13}$	Flavonoids and Stilbenes
6.1520	Daucosterol	576.8600	$C_{35}H_{60}O_6$	Terpenes and Steroids
6.3010	Quercetin 3-(6''-acetylgalactoside)-7- rhamnoside	652.1640	$C_{29}H_{32}O_{17}$	Flavonoids and Stilbenes

Table 5.9 Metabolites identified from the CHCl₃/MeOH exract by UPLC-QTOF-MS analysis (Continued)

t_R (min)	Compound	MW (g/mol)	Chemical Formula	Class
6.3010	(15α, 20R)-Dihydroxypregn-4-en-3-one 20-[glucosyl-(1-4)-6-acetyl-glucoside]	698.3495	$C_{35}H_{54}O_{14}$	Terpenes and Steroids
6.3270	Cirsimaritin	314.2463	$C_{17}H_{14}O_6$	Flavonoids and Stilbenes
6.3460	Peonidin	300.1339	$C_{18}H_{20}O_4^+$	Flavonoids and Stilbenes
6.3650	Gliricidin	300.0630	$C_{16}H_{12}O_6$	Flavonoids and Stilbenes
6.3770	Guanosine pentaphosphate	598.1230	$C_{10}H_{12}N_5O_{17}P_4$	N-compounds
6.4260	5-*p*-Coumaroylquinic acid	338.2444	$C_{16}H_{18}O_8$	Phenols and derivatives
6.4320	5-enolpyruvoyl-shikimate 3-phosphate	320.2332	$C_{20}H_{32}O_3$	Phenols and derivatives
6.4450	Herbacetin 7-(6''-quinoylglucoside)	638.1480	$C_{28}H_{30}O_{17}$	Flavonoids and Stilbenes
6.4610	Trihydroxycinnamoyl quinic acid	370.0900	$C_{16}H_{18}O_{10}$	Phenols and derivatives
6.4700	Corchorosol A	536.2981	$C_{29}H_{44}O_9$	Terpenes and Steroids
6.5620	Cyclopassifloside II	682.4273	$C_{37}H_{62}O_{11}$	Terpenes and Steroids
6.8030	Pelargonidin 3-rutinoside-5-(maronoyl)glucoside	827.2244	$C_{36}H_{43}O_{22}$	Flavonoids and Stilbenes
6.8060	1-Caffeoylquinic acid	354.2742	$C_{16}H_{18}O_9$	Phenols and derivatives
6.8820	1-Hydroxy-1-phenyl-3-octadecanone	360.3012	$C_{24}H_{40}O_2$	FA and Hydrocarbons
6.9270	Kaempferol 3-(2''-galloyl-α-L- arabinopyranoside)	570.2872	$C_{27}H_{22}O_{14}$	Flavonoids and Stilbenes
6.9990	Apigenin 7-*O*-(6''-malonyl-apiosyl-glucoside)	650.5380	$C_{29}H_{30}O_{17}$	Flavonoids and Stilbenes
7.0210	Malvin	655.6110	$C_{29}H_{35}O_{17}$	Flavonoids and Stilbenes
7.0910	Hecogenin	430.6290	$C_{27}H_{42}O_4$	Terpenes and Steroids
7.1000	Phytolaccagenic acid 3-*O*-hexose	678.4020	$C_{37}H_{58}O_{11}$	Terpenes and Steroids
7.1190	Methyl *cis*-dihydrojasmonate	626.2747	$C_{13}H_{22}O_3$	FA and Hydrocarbons
7.1460	Phytolaccagenic acid 3-*O*-glycoside	678.4000	$C_{37}H_{58}O_{11}$	Terpenes and Steroids
7.1850	Piceid	390.2785	$C_{20}H_{22}O_8$	Flavonoids and Stilbenes
7.2600	Tricin	330.1676	$C_{17}H_{14}O_7$	Flavonoids and Stilbenes
7.3000	Pedunculagin	782.5720	$C_{35}H_{26}O_{21}$	Phenols and derivatives

Table 5.9 Metabolites identified from the CHCl₃/MeOH exract by UPLC-QTOF-MS analysis (Continued)

t_R (min)	Compound	MW (g/mol)	Chemical Formula	Class
7.3450	Kaempferol 3-triglucoside-7-rhamnoside-*p*-coumaroyl	1064.3030	$C_{48}H_{56}O_{27}$	Flavonoids and Stilbenes
7.3450	1,3-*O*-Dicaffeoylglycerol	416.1100	$C_{21}H_{20}O_9$	Phenols and derivatives
7.3470	Spinacetin 3-*O*-glucosyl-(1->6)-[apiosyl(1->2)]-glucoside	802.6840	$C_{34}H_{42}O_{22}$	Flavonoids and Stilbenes
7.3480	Hexosyl-hexosyl-soyasapogenol E	780.4702	$C_{42}H_{68}O_{13}$	Terpenes and Steroids
7.3480	3,7,3'-*O*-triglucopyranosyl-dephinidine	789.6703	$C_{33}H_{41}O_{22}^{+}$	Flavonoids and Stilbenes
7.3860	Quercetin-3-Galactoside-6"-Rhamnoside-3'''-Rhamnoside	770.7220	$C_{34}H_{42}O_{20}$	Flavonoids and Stilbenes
7.3860	Hederagenin 3-*O*-hexose-pentose	766.4500	$C_{41}H_{66}O_{13}$	Terpenes and Steroids
7.3910	Cyanidin 3-sambubioside	743.6401	$C_{32}H_{39}O_{20}$	Flavonoids and Stilbenes
7.4150	Quercetin 3-*O*-glucosyl-rhamnosyl-glucoside	772.6620	$C_{33}H_{40}O_{21}$	Flavonoids and Stilbenes
7.4150	1-Sinapoyl-2-feruloylgentiobiose	724.6603	$C_{33}H_{40}O_{18}$	Phenols and derivatives
7.4190	Luteolin-7-rutinoside	592.5522	$C_{28}H_{32}O_{14}$	Flavonoids and Stilbenes
7.4270	Pheophorbide A	592.2691	$C_{35}H_{36}N_4O_5$	N-compounds
7.4270	(*Z*)-13-Oxo-9-octadecenoic acid	296.2344	$C_{18}H_{32}O_3$	FA and Hydrocarbons
7.4490	Diosmin	608.2641	$C_{28}H_{32}O_{15}$	Flavonoids and Stilbenes
7.4600	(3*Z*)-Phycocyanobilin	586.2824	$C_{33}H_{38}N_4O_6$	N-compounds
7.5100	2-(2-Methylbutanoyl)-9-(3-methyl-2*E*-pentenoyl)-2β, 9α-dihydroxy-4*Z*, 10(14)-oplopadien-3-one	430.2695	$C_{26}H_{38}O_5$	Terpenes and Steroids
7.5420	Tricin 7-*O*-(6"-(*E*)-sinapoyl)-β-*D*-glucopyranoside	698.1800	$C_{34}H_{34}O_{16}$	Flavonoids and Stilbenes
7.6670	Glycyrrhetinic acid 3-*O*-glucuronide	646.8180	$C_{36}H_{54}O_{10}$	Terpenes and Steroids
7.6780	Bavachalcone	338.3193	$C_{21}H_{22}O_4$	Phenols and derivatives
7.6780	Dihexosyl luteolin sulfate	690.1101	$C_{27}H_{30}O_{19}S$	Flavonoids and Stilbenes
7.7070	Cholic acid	408.2878	$C_{24}H_{40}O_5$	Terpenes and Steroids
7.7310	Bixin aldehyde	348.4862	$C_{24}H_{28}O_2$	Terpenes and Steroids
7.7760	Cinnamtannin B1	864.6147	$C_{45}H_{36}O_{18}$	Flavonoids and Stilbenes

Table 5.9 Metabolites identified from the CHCl$_3$/MeOH exract by UPLC-QTOF-MS analysis (Continued)

t$_R$ (min)	Compound	MW (g/mol)	Chemical Formula	Class
7.8020	Galloylquinic acid isomer	800.2203	C$_{38}$H$_{40}$O$_{19}$	Flavonoids and Stilbenes
7.8270	Cyanidin 3,5,3'-tri-O-glycoside	773.5953	C$_{33}$H$_{41}$O$_{21}$$^+$	Flavonoids and Stilbenes
7.8380	Kaempferol 3,7,4'-O-triglucoside	772.6580	C$_{33}$H$_{40}$O$_{21}$	Flavonoids and Stilbenes
7.8380	Hederagenin 3-O-glucose(1"->3')galactose	796.4622	C$_{42}$H$_{68}$O$_{14}$	Terpenes and Steroids
7.8380	Theaflavin 3-O-gallate	716.6043	C$_{36}$H$_{28}$O$_{16}$	Flavonoids and Stilbenes
7.8460	α-Hederin	750.9671	C$_{41}$H$_{66}$O$_{12}$	Terpenes and Steroids
7.8470	Spinacetin 3-O-glucosyl-(1->6)-glucoside	670.5711	C$_{29}$H$_{34}$O$_{18}$	Flavonoids and Stilbenes
7.8690	Luteolin 7-O-(2-apiosyl-6-malonyl)-glucoside	666.5380	C$_{29}$H$_{30}$O$_{18}$	Flavonoids and Stilbenes
7.8760	Petunidin 3-O-(6-O-acetyl)-glucoside	521.5890	C$_{24}$H$_{25}$O$_{13}$$^+$	Flavonoids and Stilbenes
7.9010	Piceatannol 4'-glucoside	406.3870	C$_{20}$H$_{22}$O$_9$	Flavonoids and Stilbenes
8.0220	16β-16-Hydroxy-3-oxo-1, 12-oleanadien-28-oic acid	468.3210	C$_{30}$H$_{44}$O$_4$	Terpenes and Steroids
8.1270	Rutin	610.1534	C$_{27}$H$_{30}$O$_{16}$	Flavonoids and Stilbenes
8.2080	Luteolin 7-(6"-malonylneohesperidoside)	680.5680	C$_{30}$H$_{32}$O$_{18}$	Flavonoids and Stilbenes
8.2320	Aloesol 7-glucoside	396.1759	C$_{20}$H$_{28}$O$_8$	Phenols and derivatives
8.2480	1-caffeoyl-3-ferulylglycerol	430.2700	C$_{22}$H$_{22}$O$_9$	Phenols and derivatives
8.2820	γ-Tocotrienol	411.2230	C$_{28}$H$_{42}$O$_2$	Terpenes and Steroids
8.2890	2-Deoxybrassinolide	464.3488	C$_{28}$H$_{48}$O$_5$	Terpenes and Steroids
8.4670	Epiafzelechin 3-O-gallate	426.7290	C$_{22}$H$_{18}$O$_9$	Flavonoids and Stilbenes
8.8560	3-O-glucopyranosyl-6,3',5'-trimethoxy-3,5,7,4'-tetrahydroxyflavone	538.4601	C$_{24}$H$_{26}$O$_{14}$	Flavonoids and Stilbenes
9.4010	Zeaxanthin	568.8811	C$_{40}$H$_{56}$O$_2$	Terpenes and Steroids
9.4010	Ananaflavoside B	536.3871	C$_{25}$H$_{28}$O$_{13}$	Flavonoids and Stilbenes
10.1580	Isochlorogenic acid b	514.4831	C$_{26}$H$_{26}$O$_{11}$	Phenols and derivatives
10.1580	Cyanidin 3,5-O-diglucoside	611.5280	C$_{27}$H$_{31}$O$_{16}$$^+$	Flavonoids and Stilbenes

Stilbenes have a wide range of functions in plants, one of them is to protect the plant from infection and environmental stress (*159*). In fact they are involved in the inducible and constitutive defenses of the plant against fungal pathogens, nematodes and herbivores (*160*).
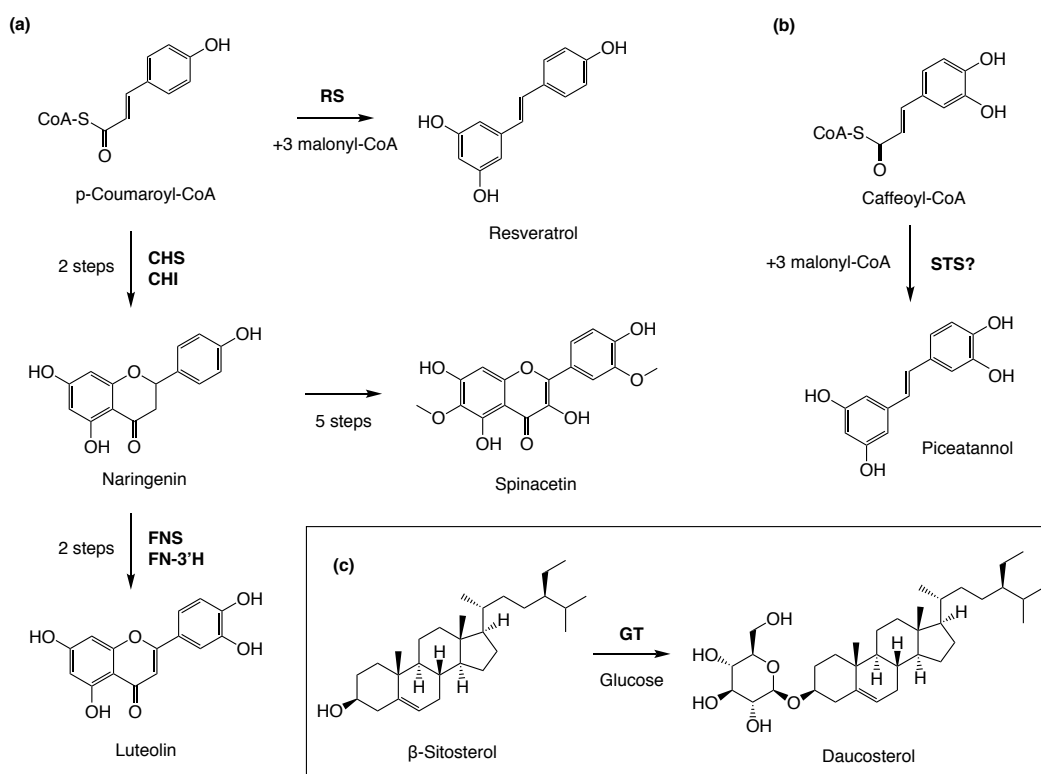
Figure 5.77 Biosynthetic pathway schematization of resveratrol, spinacetin and luteolin (a), piceatannol (b), daucosterol (c)

Spinacetin and luteolin are two flavonoids and they also come from the phenylpropanoid pathway. In fact, both of them and resveratrol share the same precursors, with just few enzymatic steps of cyclization, isomerization, hydroxylation and methylation differences (Figure 5.77a) (*161*). From *p*-coumaroyl-CoA, there are three enzymatic steps: the naringenin chalcone synthesis from the polyketide, catalyzed by the chalcone synthase (CHS), the cyclization of chalcone into naringenin by the chalcone isomerase (CHI), the oxidation of naringenin to apigenin by the enzyme flavone synthase (FNS) and

the hydroxylation of the apigenin into luteolin by the flavone 3' hydroxylase (FN-3'H). The biosynthesis can also diverge with the modification of naringenin, through 5 steps of consecutive oxidation, hydroxylation and methylation. These modifications are operated by various enzymes, many of which are isoforms of the cytochrome P450 (*162, 163*). Among flavonoids functions include antioxidant and radical scavenging activity, to protect the plant from oxidative stress. Flavonoids are involved in process of detoxification since they can stimulate the seeds' germination and can act as signaling molecules. Some flavonoids are antibiotics to protect the plant from infection (*164*). The last compound is the daucosterol (eleutheroside A), a monoglycosylic saponin derivative of β-sitosterol (Figure 5.77C). It is synthesized throughout the glucosylation of the sterol in position 3 by a glucose transferase (GT). Its high concentration is well justified by the aglycone which is also very abundant in the hexane extract. The glycosyl derivatives of sterols have shown to be crucial in seed development even though their function as part of the cellular membrane is still unclear (*165*).

The $CHCl_3$/MeOH extract is very similar to dry aqueous extract mainly for their flavonoids and stilbenes (44%). Also, terpenes and steroids are abundant (24%), followed by the phenols and their derivatives (18%). The less concentrated classes of molecules are fatty acids and hydrocarbons (7%), and nitrogen containing compounds (6%). The identified components of the dry aqueous extract are listed in table 5.10. Some of the most abundant compounds are the same as the previous extract, being spinacetin and resveratrol the highest in concentration, followed by delphinidine, daucosterol, oleanolic acid, ananaflavoside B and kaempferol.

Table 5.10 Metabolites identified from the dry aqueous exract by UPLC-QTOF-MS analysis

t_R (min)	Compound	MW (g/mol)	Chemical Formula	Class
2.8660	Syringin	372.1440	$C_{17}H_{24}O_9$	Phenols and derivatives
3.1550	Caffeic acid *O*-glucoside	342.1000	$C_{15}H_{18}O_9$	Phenols and derivatives
3.6530	Prunin	434.1200	$C_{21}H_{22}O_{10}$	Flavonoids and Stilbenes
3.8130	Stigmasta-5,22-dien-3-β-ol	412.2590	$C_{29}H_{48}O_1$	Terpenes and Steroids
4.1490	Pallidol	454.2830	$C_{28}H_{22}O_6$	Flavonoids and Stilbenes
4.1600	5-Heneicosylresorcinol	404.3654	$C_{27}H_{48}O_2$	Flavonoids and Stilbenes
4.6090	1-Octen-3-yl primeveroside	422.2123	$C_{19}H_{34}O_{10}$	FA and Hydrocarbons
4.6560	Aloesol 7-glucoside	396.3890	$C_{19}H_{24}O_9$	Phenols and derivatives
4.7710	Delphinidin 3-sophoroside 5-glucoside	789.6700	$C_{33}H_{41}O_{22}^+$	Flavonoids and Stilbenes
4.9390	Azukisaponin III	810.9750	$C_{42}H_{66}O_{15}$	Terpenes and Steroids
5.0230	Phytyl monophosphate	374.1947	$C_{18}H_{30}O_8$	Terpenes and Steroids
5.0970	Sinapoylquinic acid	398.2430	$C_{18}H_{22}O_{10}$	Phenols and derivatives
5.4000	S-sinapyl-L-cysteine-L-glycine	370.4200	$C_{16}H_{22}N_2O_6S$	N-compounds
5.5100	Glycyrrhizin	822.9420	$C_{42}H_{62}O_{16}$	Terpenes and Steroids
5.5440	Sarsasapogenin	416.3290	$C_{27}H_{44}O_3$	Terpenes and Steroids
5.7240	3, 8-Dihydroxy-6-methoxy-7(11)-eremophilen-12, 8-olide	296.1625	$C_{16}H_{24}O_5$	Terpenes and Steroids
5.7370	Chlorogenic acid	354.0950	$C_{16}H_{18}O_9$	Phenols and derivatives
5.9450	6-tuliposide A	278.1519	$C_{11}H_{18}O_8$	FA and Hydrocarbons
5.9460	2-Hydroxyenterodiol	318.1444	$C_{18}H_{22}O_5$	Phenols and derivatives
5.9990	Daidzin	416.3820	$C_{21}H_{20}O_9$	Flavonoids and Stilbenes
5.9990	Tylactone	394.2719	$C_{23}H_{38}O_5$	FA and Hydrocarbons
6.0230	Symphytine	381.2167	$C_{20}H_{31}NO_6$	N-compounds
6.0520	2"-*O*-*trans*-*p*-Coumaroylastragalin	594.1369	$C_{30}H_{26}O_{13}$	Flavonoids and Stilbenes

Table 5.10 Metabolites identified from the dry aqueous exract by UPLC-QTOF-MS analysis (Continued)

t_R (min)	Compound	MW (g/mol)	Chemical Formula	Class
6.1500	3-Caffeoylpelargonidin 5-glucoside	595.1427	$C_{30}H_{27}O_{13}^{+}$	Flavonoids and Stilbenes
6.1500	Daucosterol	576.8600	$C_{35}H_{60}O_6$	Terpenes and Steroids
6.1520	*p*-Coumaroyl-feruloylglycerol	414.1300	$C_{22}H_{22}O_8$	Phenols and derivatives
6.3200	Peonidin	300.1339	$C_{18}H_{20}O_4^{+}$	Flavonoids and Stilbenes
6.3460	Coumaric acid glucoside	326.2990	$C_{15}H_{18}O_8$	Phenols and derivatives
6.3570	Gliricidin	300.0630	$C_{16}H_{12}O_6$	Flavonoids and Stilbenes
6.3650	Digalloylglucose	483.3830	$C_{20}H_{20}O_{14}$	Phenols and derivatives
6.3720	Guanosine pentaphosphate	598.1230	$C_{10}H_{12}N_5O_{17}P_4$	N-compounds
6.3770	Epicatechin 3-*O*-gallate	442.3262	$C_{22}H_{18}O_{10}$	Flavonoids and Stilbenes
6.4210	Herbacetin 7-(6"-quinoylglucoside)	638.1480	$C_{28}H_{30}O_{17}$	Flavonoids and Stilbenes
6.4450	Tetramethylquercetin	358.3165	$C_{19}H_{18}O_7$	Flavonoids and Stilbenes
6.4740	3-*O*-(Glcb1-4Galb)-(25*R*)-12-oxo-5α-spirostan-3β-ol	770.4450	$C_{40}H_{66}O_{14}$	Terpenes and Steroids
6.5610	Cyclopassifloside II	682.4273	$C_{37}H_{62}O_{11}$	Terpenes and Steroids
6.5620	4-Glycosyloxycinnamoylcholine	412.2034	$C_{20}H_{30}NO_8$	Phenols and derivatives
6.5650	Cusparine	307.1227	$C_{19}H_{17}NO_3$	N-compounds
6.5690	Kaempferol 3-*O*-rutinoside	594.1590	$C_{27}H_{30}O_{15}$	Flavonoids and Stilbenes
6.5730	All-trans-Carophyll yellow	460.3375	$C_{32}H_{44}O_2$	Terpenes and Steroids
6.7530	Kaempferol 3-*O*-(6"-acetyl-galactoside) 7-*O*-rhamnoside	636.5550	$C_{29}H_{32}O_{16}$	Flavonoids and Stilbenes
6.7570	Epimedin A	838.2901	$C_{39}H_{50}O_{20}$	Flavonoids and Stilbenes
6.7600	Pelargonodin 3-rutinoside *p*-coumaric	725.2100	$C_{36}H_{37}O_{16}$	Flavonoids and Stilbenes
6.7600	Proanthocyanin monogallate	728.8290	$C_{36}H_{56}O_{15}$	Flavonoids and Stilbenes
6.7610	1, 28-Dicaffeoyloctacosanediol	750.5083	$C_{46}H_{70}O_8$	Phenols and derivatives
6.7610	1,26-Hexacosanediol diferulate	750.4604	$C_{46}H_{70}O_8$	Phenols and derivatives
6.7610	Sinapoyl choline dehydro dimer-isomer	618.3223	$C_{40}H_{58}O_5$	N-compounds

Table 5.10 Metabolites identified from the dry aqueous exract by UPLC-QTOF-MS analysis (Continued)

t_R (min)	Compound	MW (g/mol)	Chemical Formula	Class
6.7660	Pelargonidin 3-rutinoside-5-(maronoyl)glucoside	827.2244	$C_{36}H_{43}O_{22}$	Flavonoids and Stilbenes
6.8060	1-Caffeoylquinic acid	354.2742	$C_{16}H_{18}O_9$	Phenols and derivatives
6.8820	1-Hydroxy-1-phenyl-3-octadecanone	360.3012	$C_{24}H_{40}O_2$	FA and Hydrocarbons
6.9920	3-(2-Heptenyloxy)-2-hydroxypropyl undecanoate	356.2943	$C_{21}H_{40}O_4$	FA and Hydrocarbons
6.9990	Apigenin 7-*O*-(6''-malonyl-apiosyl-glucoside)	650.5380	$C_{29}H_{30}O_{17}$	Flavonoids and Stilbenes
7.0210	Malvin	655.6110	$C_{29}H_{35}O_{17}$	Flavonoids and Stilbenes
7.0910	Hecogenin	430.6290	$C_{27}H_{42}O_4$	Terpenes and Steroids
7.1000	Phytolaccagenic acid 3-*O*-hexose	678.4020	$C_{37}H_{58}O_{11}$	Terpenes and Steroids
7.1270	Epicatechin 3-*O*-(3-*O*-methylgallate)	456.2491	$C_{23}H_{20}O_{10}$	Flavonoids and Stilbenes
7.1600	Apigetrin glycoside	622.4901	$C_{27}H_{26}O_{17}$	Flavonoids and Stilbenes
7.1620	Piceid	390.2785	$C_{20}H_{22}O_8$	Flavonoids and Stilbenes
7.2600	Cyanidin 3,5,3'-tri-*O*-glucoside	773.6700	$C_{33}H_{41}O_{21}^+$	Flavonoids and Stilbenes
7.2750	Tricin	330.1676	$C_{17}H_{14}O_7$	Flavonoids and Stilbenes
7.3000	Kaempferol-3-Rhamnoside-4''-Rhamnoside-7-Rhamnoside	724.2210	$C_{33}H_{40}O_{18}$	Flavonoids and Stilbenes
7.3370	Kaempferol 3-triglucoside-7-rhamnoside-*p*-coumaroyl	1064.3030	$C_{48}H_{56}O_{27}$	Flavonoids and Stilbenes
7.3450	1,3-*O*-Dicaffeoylglycerol	416.1100	$C_{21}H_{20}O_9$	Phenols and derivatives
7.3470	Undecaprenyl phosphate mannose	1008.7100	$C_{61}H_{101}O_9P$	Terpenes and Steroids
7.3470	Oleanolic acid 3-*O*-glucose(1''->3')arabinose	750.4600	$C_{41}H_{66}O_{12}$	Terpenes and Steroids
7.3480	Spinacetin 3-*O*-glucosyl-(1->6)-[apiosyl(1->2)]-glucoside	802.6840	$C_{34}H_{42}O_{22}$	Flavonoids and Stilbenes
7.3480	Hexosyl-hexosyl-soyasapogenol E	780.4702	$C_{42}H_{68}O_{13}$	Terpenes and Steroids
7.3480	Peonidin 3-sophoroside-5-glucoside	787.2301	$C_{34}H_{43}O_{21}$	Flavonoids and Stilbenes
7.3500	3,7,3'-*O*-triglucopyranosyl-dephinidine	789.6703	$C_{33}H_{41}O_{22}^+$	Flavonoids and Stilbenes
7.3860	Hederagenin 3-*O*-hexose-pentose	766.4500	$C_{41}H_{66}O_{13}$	Terpenes and Steroids
7.3910	Prenyl caffeate	248.1049	$C_{14}H_{16}O_4$	Phenols and derivatives

177

Table 5.10 Metabolites identified from the dry aqueous exract by UPLC-QTOF-MS analysis (Continued)

t_R (min)	Compound	MW (g/mol)	Chemical Formula	Class
7.4150	Cyanidin 3-sambubioside	743.6401	$C_{32}H_{39}O_{20}$	Flavonoids and Stilbenes
7.4169	Quercetin 3-*O*-glucosyl-rhamnosyl-glucoside	772.6620	$C_{33}H_{40}O_{21}$	Flavonoids and Stilbenes
7.4190	1-Sinapoyl-2-feruloylgentiobiose	724.6603	$C_{33}H_{40}O_{18}$	Phenols and derivatives
7.5420	2-(2-Methylbutanoyl)-9-(3-methyl-2*E*-pentenoyl)-2β, 9α-dihydroxy-4*Z*, 10(14)-oplopadien-3-one	430.2695	$C_{26}H_{38}O_5$	Terpenes and Steroids
7.6060	Qurcetin-3-(dicaffeoyl)sophorotrioside-7-glucoside	1274.3220	$C_{57}H_{62}O_{33}$	Flavonoids and Stilbenes
7.6670	Tricin 7-*O*-(6"-(*E*)-sinapoyl)-β-*D*-glucopyranoside	698.1800	$C_{34}H_{34}O_{16}$	Flavonoids and Stilbenes
7.6780	Bavachalcone	338.3193	$C_{21}H_{22}O_4$	Phenols and derivatives
7.7310	Cholic acid	408.2878	$C_{24}H_{40}O_5$	Terpenes and Steroids
7.7760	Bixin aldehyde	348.4862	$C_{24}H_{28}O_2$	Terpenes and Steroids
7.7950	Dimer proanthocyanin monogallate	729.1511	$C_{37}H_{29}O_{16}$	Flavonoids and Stilbenes
7.8010	Trihydroxycinnamoylquinic acid	370.0910	$C_{16}H_{18}O_{10}$	Phenols and derivatives
7.8020	Cinnamtannin B1	864.6147	$C_{45}H_{36}O_{18}$	Flavonoids and Stilbenes
7.8270	Galloylquinic acid isomer	800.2203	$C_{38}H_{40}O_{19}$	Flavonoids and Stilbenes
7.8370	Agavoside B	754.6861	$C_{34}H_{42}O_{19}$	Terpenes and Steroids
7.8370	(3β,9β,12α,16α,24*E*)-12,16-Trihydroxy-9,19-cyclolanost-24-en-26-oic acid-3-diglucopyranoside	796.9912	$C_{42}H_{68}O_{14}$	Terpenes and Steroids
7.8380	Cyanidin 3,5,3'-tri-*O*-glycoside	773.5953	$C_{33}H_{41}O_{21}^{+}$	Flavonoids and Stilbenes
7.8389	Kaempferol 3,7,4'-*O*-triglucoside	772.6580	$C_{33}H_{40}O_{21}$	Flavonoids and Stilbenes
7.8400	Hederagenin 3-*O*-glucose(1"->3')galactose	796.4622	$C_{42}H_{68}O_{14}$	Terpenes and Steroids
7.8460	Theaflavin 3-*O*-gallate	716.6043	$C_{36}H_{28}O_{16}$	Flavonoids and Stilbenes
7.8470	α-Hederin	750.9671	$C_{41}H_{66}O_{12}$	Terpenes and Steroids
7.8690	Spinacetin 3-*O*-glucosyl-(1->6)-glucoside	670.5711	$C_{29}H_{34}O_{18}$	Flavonoids and Stilbenes
7.8740	Luteolin 7-sulfate-3'-rutinoside	674.5790	$C_{27}H_{30}O_{18}S$	Flavonoids and Stilbenes

Table 5.10 Metabolites identified from the dry aqueous exract by UPLC-QTOF-MS analysis (Continued)

t_R (min)	Compound	MW (g/mol)	Chemical Formula	Class
7.8760	Luteolin 7-*O*-(2-apiosyl-6-malonyl)-glucoside	666.5380	$C_{29}H_{30}O_{18}$	Flavonoids and Stilbenes
7.9010	Petunidin 3-*O*-(6-*O*-acetyl)-glucoside	521.5890	$C_{24}H_{25}O_{13}^+$	Flavonoids and Stilbenes
7.9880	Filfiline	389.3672	$C_{26}H_{47}NO$	N-compounds
8.0220	Piceatannol 4'-glucoside	406.3870	$C_{20}H_{22}O_9$	Flavonoids and Stilbenes
8.1850	Peonidin 3-rhamnoside	447.3610	$C_{22}H_{23}O_{10}^+$	Flavonoids and Stilbenes
8.2280	Myricetin 3,3'-digalactoside	642.5190	$C_{27}H_{30}O_{18}$	Flavonoids and Stilbenes
8.2320	Luteolin 7-(6''-malonylneohesperidoside)	680.5680	$C_{30}H_{32}O_{18}$	Flavonoids and Stilbenes
8.2380	Kaempferol-3-sophoroside-Per-*O*-methoxy-cinnamoyl	890.2522	$C_{41}H_{46}O_{22}$	Flavonoids and Stilbenes
8.2460	Delphinidin 3-rutinoside-5-galactoside	773.2100	$C_{33}H_{41}O_{21}$	Flavonoids and Stilbenes
8.2480	Aloesol 7-glucoside	396.1759	$C_{20}H_{28}O_8$	Phenols and derivatives
8.2670	Spinasaponin A	794.9760	$C_{42}H_{66}O_{14}$	Terpenes and Steroids
8.2820	1-caffeoyl-3-ferulylglycerol	430.2700	$C_{22}H_{22}O_9$	Phenols and derivatives
8.3390	Luteolin 7-*O*-(2-apiosyldiacetyl) glucoside	664.1600	$C_{30}H_{32}O_{17}$	Flavonoids and Stilbenes
8.3410	Luteolin 7-*O*-diglucuronide	638.4850	$C_{27}H_{26}O_{18}$	Flavonoids and Stilbenes
8.4670	2-Deoxybrassinolide	464.3488	$C_{28}H_{48}O_5$	Terpenes and Steroids
8.8560	Epiafzelechin 3-*O*-gallate	426.7290	$C_{22}H_{18}O_9$	Flavonoids and Stilbenes
8.8890	Dolichyl *D*-xylosyl phosphates	572.3482	$C_{30}H_{52}O_8P$	Terpenes and Steroids
9.4010	3-*O*-glucopyranosyl-6,3',5'-trimethoxy-3,5,7,4'-tetrahydroxyflavone	538.4601	$C_{24}H_{26}O_{14}$	Flavonoids and Stilbenes
9.4080	Zeaxanthin	568.8811	$C_{40}H_{56}O_2$	Terpenes and Steroids
9.4170	(3β, 16α, 21β, 22α)-12-Oleanene-3, 16, 21, 23, 28-pentol-22-angeloyloxy-23-al	586.3835	$C_{35}H_{54}O_7$	Terpenes and Steroids
10.1580	Ananaflavoside B	536.3871	$C_{25}H_{28}O_{13}$	Flavonoids and Stilbenes
10.1600	Isochlorogenic acid B	514.4831	$C_{26}H_{26}O_{11}$	Phenols and derivatives

Delphinidine, ananaflavoside B and kaempferol are an anthocyanidin, a flavone and a flavonol, respectively. The biosynthesis of these molecules could follow the synthesis of luteolin, in the hierarchy of the pathway (Figure 5.78). The ananaflavoside B could be synthetized from subsequent hydroxylations, methylations and glycosylation of luteolin.
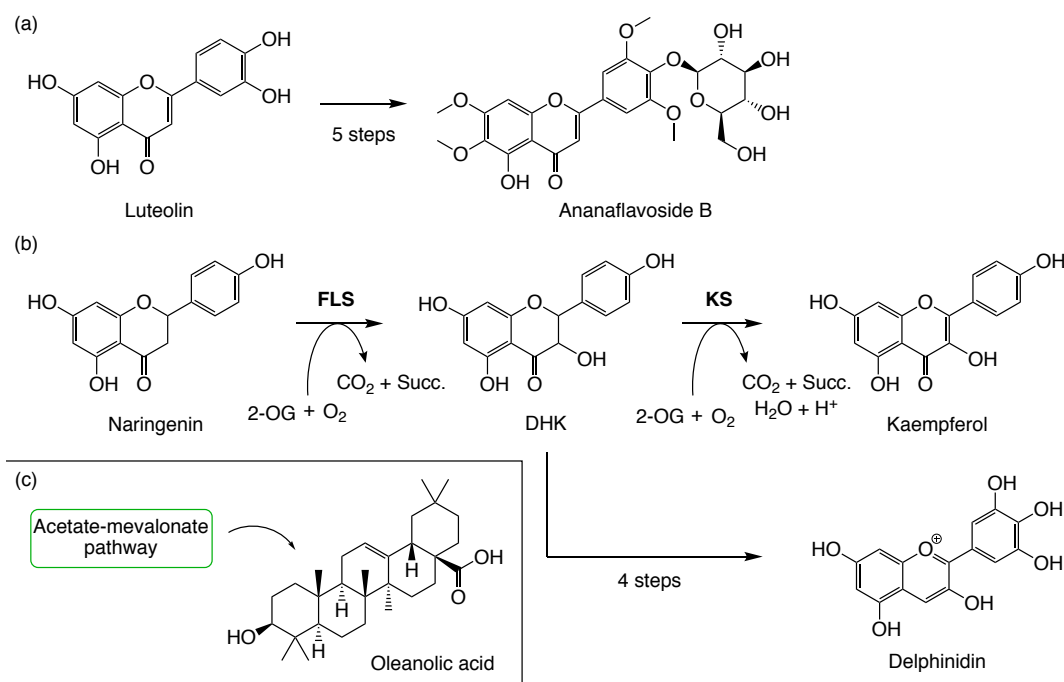
Figure 5.78 Biosynthetic pathway schematization of ananaflavoside B (a), kaempferol and delfinidine (b), and oleanolic acid (c)

A hydroxylation at position 3 of naringenin by the flavonol synthase (FLS), result in dihydrokaempferol (DHK). Then kaempferol is synthesized by the kaempferol synthase (KS), throughout a double bond between the carbons 2 and 3, the oxidation process consumes oxygen and 2-oxoglutarate (2-OG) and produces a proton, water, carbon dioxide and succinate (Succ.). Instead delphinidin biosynthesis starts from the DHK with four steps including oxidation and hydroxylation (*164*). Anthocyanidins functions are mostly pigmentation of plant's tissues, as well as antioxidant and radical scavenging

actions. Anthocyanidins protect plants from abiotic stressors using many mechanisms of protection (sunscreen, antioxidant and metalchelating). Anthocyanins could delay senescence in plants by mineral deficency (*166*).

Oleanolic acid is a pentacyclic triterpenoid metabolite related to betulinic acid, its biosynthesis involves the acetate-mevalonate pathway. It differentiates from the steroids synthesis by the special arrangement imposed by the enzyme β-amyrin synthase (AS1) on the squalene molecule during the cyclization. This terpenoid compound is often found together with one of its derivatives, the ursolic acid (Figure 5.79), identified also in the plant metabolome. Oleanolic acid and ursolic acid are mostly found in plants' epicuticular waxes where they exert the activity of barrier against pathogens and water loss. They are also the precursor to many triterpenoid saponins which serve as well as defense to herbivores or pathogens and as allelopathic agents (*167*).
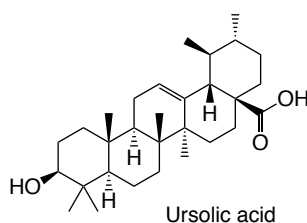
Ursolic acid

Figure 5.79 Structure of ursolic acid

Very closely to dry aqueous extract, the fresh aqueous extract is composed mainly by flavonoid and stilbenes, which are more than half of extract (58%). Terpenes and steroids (18%), phenols and their derivatives (13%) are also abundant in the extract. The lesser components are fatty acids and hydrocarbons (7%), and the nitrogen containing compounds (4%). This extract composition its fully represented in table 5.11.

Table 5.11 Metabolites identified from the fresh aqueous exract by UPLC-QTOF-MS analysis

t_R (min)	Compound	MW (g/mol)	Chemical Formula	Class
1.9670	3, 8-Diglucosyldiosmetin	624.1670	$C_{28}H_{32}O_{16}$	Flavonoids and Stilbenes
2.9860	5,7-Dihydroxy-6-methoxyisoflavone 7-O-rhamnoside	430.1264	$C_{22}H_{22}O_9$	Flavonoids and Stilbenes
4.7710	Stigmasta-5,22-dien-3-β-ol	412.2590	$C_{29}H_{48}O_1$	Terpenes and Steroids
5.0230	Delphinidin 3-sophoroside 5-glucoside	789.6700	$C_{33}H_{41}O_{22}^+$	Flavonoids and Stilbenes
5.5430	Phytyl monophosphate	374.1947	$C_{18}H_{30}O_8$	Terpenes and Steroids
5.9450	Catechin 4'-methyl ether	304.0950	$C_{16}H_{16}O_6$	Flavonoids and Stilbenes
6.1520	6-tuliposide A	278.1519	$C_{11}H_{18}O_8$	FA and Hydrocarbons
6.3460	Daucosterol	576.8600	$C_{35}H_{60}O_6$	Terpenes and Steroids
6.3560	Peonidin	300.1339	$C_{18}H_{20}O_4^+$	Flavonoids and Stilbenes
6.3770	Glabridin	324.1300	$C_{20}H_{20}O_4$	Flavonoids and Stilbenes
6.4210	Guanosine pentaphosphate	598.1230	$C_{10}H_{12}N_5O_{17}P_4$	N-compounds
6.4420	Epicatechin 3-O-gallate	442.3262	$C_{22}H_{18}O_{10}$	Flavonoids and Stilbenes
6.4740	Chlorogenoquinone	352.1502	$C_{18}H_{24}O_7$	Phenols and derivatives
6.5730	Tetramethylquercetin	358.3165	$C_{19}H_{18}O_7$	Flavonoids and Stilbenes
6.6430	Kaempferol 3-O-rutinoside	594.1590	$C_{27}H_{30}O_{15}$	Flavonoids and Stilbenes
6.7140	Luteolin 7-(2''-apiosylglucoside)	580.1430	$C_{26}H_{28}O_{15}$	Flavonoids and Stilbenes
6.7610	Ergosterol endoperoxide	428.3110	$C_{28}H_{44}O_3$	Terpenes and Steroids
6.7630	Proanthocyanin monogallate	728.8290	$C_{36}H_{56}O_{15}$	Flavonoids and Stilbenes
6.7650	1, 28-Dicaffeoyloctacosanediol	750.5083	$C_{46}H_{70}O_8$	Phenols and derivatives
6.7660	1,26-Hexacosanediol diferulate	750.4604	$C_{46}H_{70}O_8$	Phenols and derivatives
7.1270	Epicatechin 3-O-(3-O-methylgallate)	456.2491	$C_{23}H_{20}O_{10}$	Flavonoids and Stilbenes
7.1600	Piceid	390.2785	$C_{20}H_{22}O_8$	Flavonoids and Stilbenes
7.2600	Cyanidin-3-O-(2''-O-β-xylopyranosyl-β-glucopyranoside)-5-O-β-glucopyranoside	743.6400	$C_{32}H_{39}O_{20}$	Flavonoids and Stilbenes

Table 5.11 Metabolites identified from the fresh aqueous exract by UPLC-QTOF-MS analysis (Continued)

t_R (min)	Compound	MW (g/mol)	Chemical Formula	Class
7.2740	Tricin	330.1676	$C_{17}H_{14}O_7$	Flavonoids and Stilbenes
7.3000	Kaempferol 3-triglucoside-7-rhamnoside-*p*-coumaroyl	1064.3030	$C_{48}H_{56}O_{27}$	Flavonoids and Stilbenes
7.3450	Oleanolic acid 3-*O*-glucose(1"->3')arabinose	750.4600	$C_{41}H_{66}O_{12}$	Terpenes and Steroids
7.3480	Spinacetin 3-*O*-glucosyl-(1->6)-[apiosyl(1->2)]-glucoside	802.6840	$C_{34}H_{42}O_{22}$	Flavonoids and Stilbenes
7.3491	Hexosyl-hexosyl-soyasapogenol E	780.4702	$C_{42}H_{68}O_{13}$	Terpenes and Steroids
7.3500	3-*O*-rutinosyl-3'-*O*-glucopyranosyl cyanidin	757.6710	$C_{33}H_{41}O_{20}^+$	Flavonoids and Stilbenes
7.3820	Quercetin-3-Galactoside-6"-Rhamnoside-3'''-Rhamnoside	770.7220	$C_{34}H_{42}O_{20}$	Flavonoids and Stilbenes
7.3860	3,7,3'-*O*-triglucopyranosyl-dephinidine	789.6703	$C_{33}H_{41}O_{22}^+$	Flavonoids and Stilbenes
7.3880	Hederagenin 3-*O*-hexose-pentose	766.4500	$C_{41}H_{66}O_{13}$	Terpenes and Steroids
7.3910	Prenyl caffeate	248.1049	$C_{14}H_{16}O_4$	Phenols and derivatives
7.4130	Cyanidin 3-sambubinoside-5-rhamnoside	727.2100	$C_{32}H_{39}O_{19}$	Flavonoids and Stilbenes
7.5550	Peonidin 3-sophoroside	625.1771	$C_{28}H_{33}O_{16}^+$	Flavonoids and Stilbenes
7.7760	Bixin aldehyde	348.4862	$C_{24}H_{28}O_2$	Terpenes and Steroids
7.8010	Trihydroxycinnamoylquinic acid	370.0910	$C_{16}H_{18}O_{10}$	Phenols and derivatives
7.8020	Cinnamtannin B1	864.6147	$C_{45}H_{36}O_{18}$	Flavonoids and Stilbenes
7.8270	Galloylquinic acid isomer	800.2203	$C_{38}H_{40}O_{19}$	Flavonoids and Stilbenes
7.8370	Agavoside B	754.6861	$C_{34}H_{42}O_{19}$	Terpenes and Steroids
7.8740	Luteolin 7-sulfate-3'-rutinoside	674.5790	$C_{27}H_{30}O_{18}S$	Flavonoids and Stilbenes
7.8760	Luteolin 7-*O*-(2-apiosyl-6-malonyl)-glucoside	666.5380	$C_{29}H_{30}O_{18}$	Flavonoids and Stilbenes
7.9010	Petunidin 3-*O*-(6-*O*-acetyl)-glucoside	521.5890	$C_{24}H_{25}O_{13}^+$	Flavonoids and Stilbenes
8.0220	Piceatannol 4'-glucoside	406.3870	$C_{20}H_{22}O_9$	Flavonoids and Stilbenes
8.1850	Peonidin 3-rhamnoside	447.3610	$C_{22}H_{23}O_{10}^+$	Flavonoids and Stilbenes
8.2280	Myricetin 3,3'-digalactoside	642.5190	$C_{27}H_{30}O_{18}$	Flavonoids and Stilbenes
8.2990	Aloesol 7-glucoside	396.1759	$C_{20}H_{28}O_8$	Phenols and derivatives

Table 5.11 Metabolites identified from the fresh aqueous exract by UPLC-QTOF-MS analysis (Continued)

t_R (min)	Compound	MW (g/mol)	Chemical Formula	Class
8.3020	Delphinidin 3-rutinoside 5-glucoside	773.6690	$C_{33}H_{41}O_{21}^+$	Flavonoids and Stilbenes
8.3410	Myricitrin glucoside	464.0954	$C_{21}H_{20}O_{12}$	Flavonoids and Stilbenes
8.8560	Luteolin 7-*O*-diglucuronide	638.4850	$C_{27}H_{26}O_{18}$	Flavonoids and Stilbenes
9.4010	Epiafzelechin 3-*O*-gallate	426.7290	$C_{22}H_{18}O_9$	Flavonoids and Stilbenes
9.4100	3-*O*-glucopyranosyl-6,3',5'-trimethoxy-3,5,7,4'-tetrahydroxyflavone	538.4601	$C_{24}H_{26}O_{14}$	Flavonoids and Stilbenes
10.1580	Zeaxanthin	568.8811	$C_{40}H_{56}O_2$	Terpenes and Steroids
10.1600	Ananaflavoside B	536.3871	$C_{25}H_{28}O_{13}$	Flavonoids and Stilbenes
10.2100	Isochlorogenic acid b	514.4831	$C_{26}H_{26}O_{11}$	Phenols and derivatives

High quantity of polyphenols and antioxidant compounds found in *H. glomerata* could due to adaptation of plant to arid environments. It is known that plants that use the Crassulacean Acid Metabolism (CAM) to survive water availability limitation are able to save H_2O molecules minimizing their photorespiration (*168*). A CAM plant produced oxygen inside its tissues during the day, even if its production is minimized. That's why polyphenols and antioxidant molecules in general might have an important role in preventing the oxidative stress produced by the Calvin cycle. The most constitutive molecules of the fresh aqueous extract are practically the same as the dry one. They are spinacetin, resveratrol, delphinidin, cyanidin and luteolin. With the only exception of cyanidin all the compounds are already present in the other extracts. Cyanidin is an anthocyanidin that can be produced from the same pathway of the flavonols, starting from DHK.
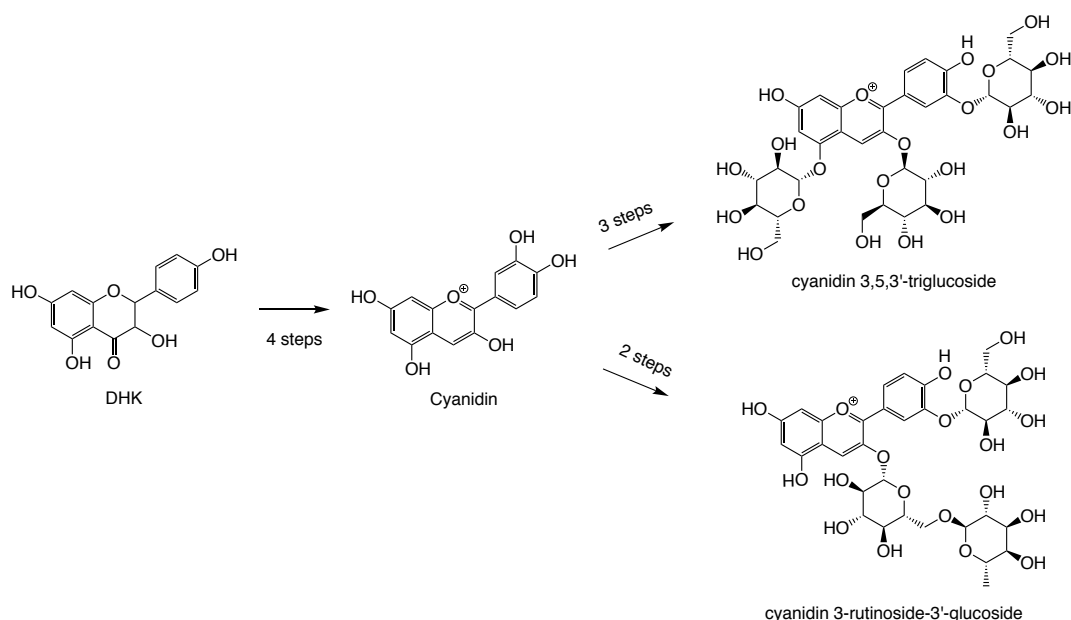
Figure 5.80 Biosynthetic pathway schematization of cyanidin, cyanidin 3,5,3'-triglucoside and cyanidin 3-rutinoside-3'-glucoside from dihydrokaempferol (DHK)

Its synthesis is the conjunction of four enzymatic steps which comprehend hydroxylation, oxidation and two steps of reduction. Cyanidin was found to be present in various glycosylated forms in plant's metabolome. Two of them: cyanidin 3,5,3'-triglucoside and cyanidin 3-rutinoside-3'-glucoside are known to cause scarlet coloration in some *Bromeliaceae* plants (*169*). Biosynthesis and glycosylated derivatives of cyanidin are reported in figure 5.80. Among other abundant components of fresh aqueous extract are isoscoparin and isochlorogenic acid (Figure 5.81). The first one is a C-glycosylflavone, which has C-C bond between a glucose molecule and the C-6 of the flavone. This class of flavonoids are synthesized by the plant like other flavonoids (*170*). Instead the isochlorogenic acid is a phenylpropionate derivative of quinic and caffeic acid, in a 1:2 ratio. This molecule is an antioxidant that to protect the plant, and its metabolism is tress induced (*171*). All the metabolites identified by UPLC-QTOF-MS in *H. glomerata* extracts are reported in table 5.8.

Isoscoparin

Isochlorogenic acid B
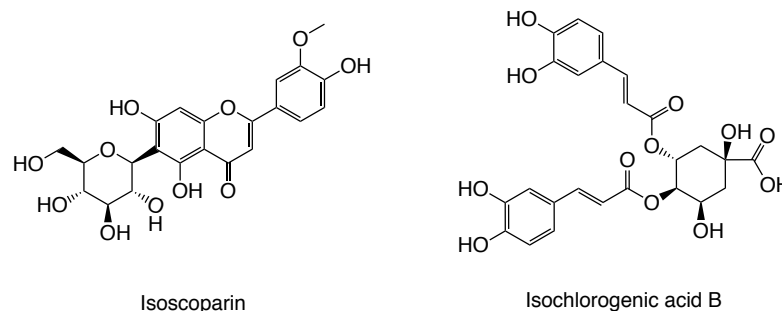
Figure 5.81 Structure of isoscoparin (left) and isochlorogenic acid B (right)

5.2.2 Statistical analysis

5.2.2.1 Principal components analysis (PCA)

The parameter used for PCA analysis was the relative abundance of each component in every extract. From PCA plots was possible to notice the difference in composition between the four extracts. The 2D plot (Figure 5.82) showed this difference against the principle coordinates (PC) 1 and 2, in which PC1 displays a higher percent of difference than the PC2 (79.1 % and 14.4 % respectively).
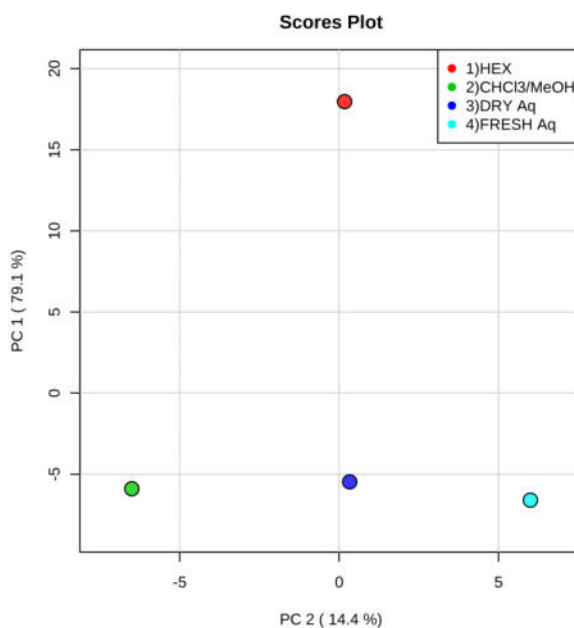
Figure 5.82 2D plot of the PCA analysis

The closest the extracts appear in the plots the similar the extracts are. The plots contain various components expressed in percentage, representing the variation of the calculated scores for each compound. The hexane extract was the most different, as shown by its distance in the 2D plot from the other three extracts. This is due to its different composition mainly of non-polar

187

compounds which were extracted by the hexane during the maceration. The CHCl₃/MeOH and the aqueous extracts were almost aligned in PC1, having the dry aqueous extract in between the other two, meaning that they have a similar composition. In the PC2 the three extracts are instead separated, the aqueous extracts were slightly closer to each other because their composition was more similar, due to the polarity of the solvent used in the maceration. Similarities and differences of extracts were also visible from the chromatograms (Figure 5.71). In this sense it was clearly visible that hexane extract was the most different of the four. The same differences were also visible from the 3D PCA and loading plots in figure 5.83.
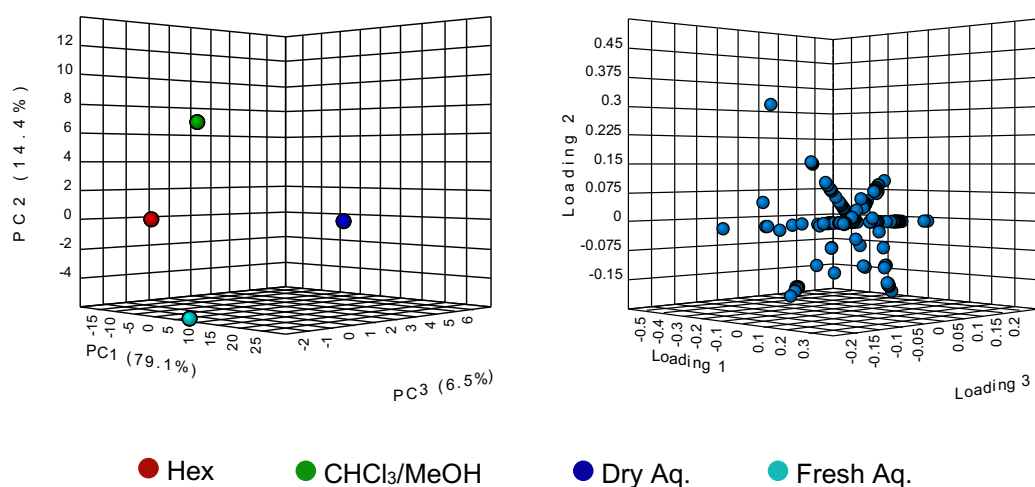
Figure 5.83 3D plot (left) and loading plot (right) of the PCA analysis

The 3D plot showed an extra coordinate the PC3 which had the lower percentage of difference (6.5 %). This allowed interpret the plot base on the phase of the vectors that go from the origin of the axes to the points that represent each extract. If the vectors (points) were close to each other (small angle) they correlate. If they were out of phase (90°) it means that they non-

correlated and if they were at 180° it means that components were anti-correlated. It was visible that vectors of CHCl₃/MeOH and aqueous extracts were out of phase of 90° from the vector of the hexane extract. This underlined a lack of correlation among the data represented in the vectors which are the components of each extract and confirmed that the most difference was found in the hexane extract composition. The 3D loading plot showed this difference more in each compound, where the ones that find themselves close to each other correlated in the same way. If they were aligned on the same vector it means they are part of the same extract. If components were in between the vectors they shared among the extracts.

5.2.2.2 Hierarchical clustering analysis
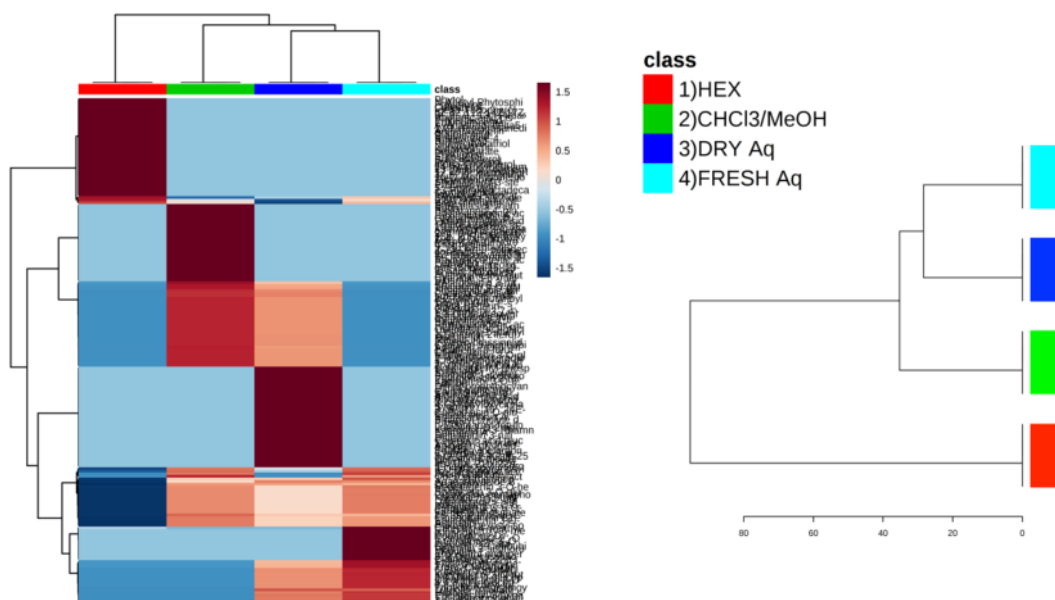
Figure 5.84 Hierarchical clustering analysis: Heatmap (left) and dendrogram (right) of the components of the extracts of *H. glomerata*

It was performed ANOVA and t-test test on the data collected form the UPLC-QTOF-MS analysis of the leaf extracts. Results are shown in heatmap

(Figure 5.84). The t-test shows the presence of specific component in each extract using hotter colors while using colder colors for its absence. It also showed the shared compounds which allow a graphical visualization of the composition and differences of the extracts. Other representation of the correlation between the extracts is the dendrogram. Results showed that hexane extract has the higher significance difference (P>0.05), followed by the CHCl$_3$/MeOH which is more similar to dry aqueous and fresh aqueous extracts. Figure 5.85 showed classes of compounds responsible for the main differences between the extracts. The same module of MeboAnalyst was used for features and compound's classes.
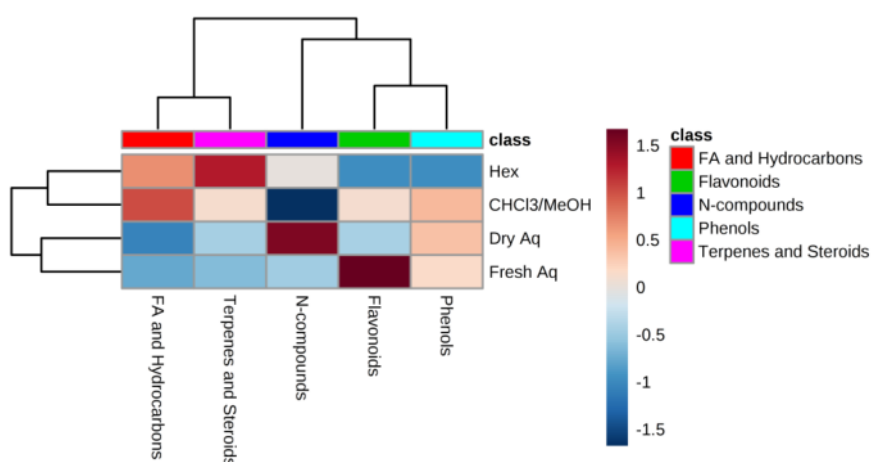
Figure 5.85 Principle classes of compounds found in each extract

Figure 5.85 shows the principle classes of compounds which are divided in two main groups in base of their abundance in the extracts, and this fits also with their polarity. Result confirms that extracts have different compositions based on the type of solvent used in the maceration. This is due to the fact that a polar solvent will extract more polar compounds than a non-

polar one and vice versa, explaining why is more difficult to find all the compounds in the same type of extract.

5.2.2.3 Pathway analysis

Figure 5.86 showed that metabolic biosynthetic pathways of *H. glomerata* with the higher impact on its metabolome are flavone and flavonol (1.00), phenylpropanoid (0.46), steroid (0.39), flavonoid (0.34), diterpenoid (0.34) and fatty acids (0.27).
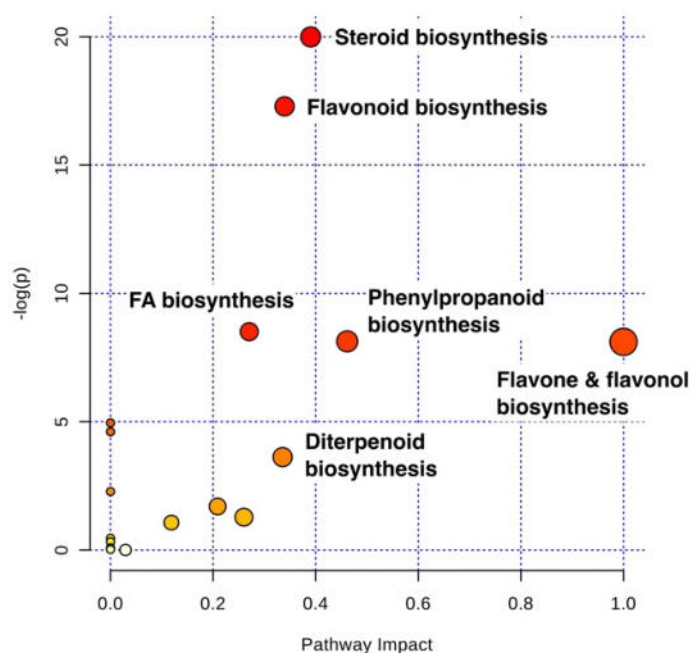
Figure 5.86 Pathway analysis

These principal pathways are correlated to the flavonoids, HCA derivatives, terpenes, steroids and FAs content of the plant. The lower impact pathways are mostly enhancing some specific process for some compounds, such as linoleic and arachidonic acid metabolism or FAs elongation in

mitochondria but they are mainly derived from the same principal classes of metabolites (See table 5.12).

The identified pathways have been reported for some plants of the family of Bromeliaceae such as *A. comosus*, where the terpenes biosynthesis (diterpenes, triterpenes and carotenoids), FAs biosynthesis (esters) and polyphenols biosynthesis have been investigated (*224*). For *A. comosus* var. *bracteatus* where also reported a 5,825 unigenes which were mapped to a total of 117 pathways responsible for the biosynthesis of terpenes and phenylpropanoid compounds (*225*).

Table 5.12 Results of pathway analysis of *H. glomerata*

Pathway	Tot	Exp	Hits	Raw p	-log (p)	Holm adjust	FDR	Imp
Steroid biosynthesis	28	2.64	15	2.08E-09	2.00E+01	1.73E-07	1.73E-07	0.39
Flavonoid biosynthesis	37	3.48	16	3.11E-08	1.73E+01	2.55E-06	1.29E-06	0.34
Fatty acid biosynthesis	47	4.42	13	2.02E-04	8.51E+00	1.64E-02	4.98E-03	0.27
Phenylpropanoid biosynthesis	31	2.92	10	2.94E-04	8.13E+00	2.35E-02	4.98E-03	0.46
Flavone and flavonol biosynthesis	8	0.75	5	3.00E-04	8.11E+00	2.37E-02	4.98E-03	1.00
Linoleic acid metabolism	5	0.47	3	7.05E-03	4.96E+00	5.50E-01	9.75E-02	0.00
Arachidonic acid metabolism	10	0.94	4	9.98E-03	4.61E+00	7.68E-01	1.18E-01	0.00
Diterpenoid biosynthesis	19	1.79	5	2.68E-02	3.62E+00	1.00E+00	2.78E-01	0.34
Stilbenoid biosynthesis	6	0.56	2	1.02E-01	2.28E+00	1.00E+00	9.45E-01	0.00
Terpenoid backbone biosynthesis	24	2.26	4	1.83E-01	1.70E+00	1.00E+00	1.00E+00	0.21
Phenylalanine metabolism	11	1.04	2	2.77E-01	1.28E+00	1.00E+00	1.00E+00	0.26
Terpenoid-quinone biosynthesis	22	2.07	3	3.43E-01	1.07E+00	1.00E+00	1.00E+00	0.12
Fatty acid elongation in mitochondria	13	1.22	1	7.25E-01	3.21E-01	1.00E+00	1.00E+00	0.00
Porphyrin and chlorophyll metabolism	33	3.11	1	9.64E-01	3.72E-02	1.00E+00	1.00E+00	0.00
Fatty acid metabolism	37	3.48	1	9.76E-01	2.46E-02	1.00E+00	1.00E+00	0.00
Carotenoid biosynthesis	37	3.48	1	9.76E-01	2.46E-02	1.00E+00	1.00E+00	0.00
Purine metabolism	55	5.18	1	9.96E-01	3.79E-03	1.00E+00	1.00E+00	0.03

Plants are stimulated to produce large amount of flavonoids when they are under environmental stress like excessive coldness, (the plant was collected during the winter) or after physical damage (*226*). Sun light and dryness can also affect flavonoids production, which accumulate in the tissues directly exposed solar radiation. Instead the biosynthesis of HCAs seems not to be affected by these environmental stresses (*227*). Soil salinity is another variable that can affect plants phenolic composition, producing the increase of antioxidants concentration (*228*).

5.3 Biological assays

5.3.1 Antibacterial activity of *H. glomerata* Zucc.

Table 5.13 reports the leaf extracts antibacterial activity, showing that the CHCl$_3$/MeOH extract was active against the sensible strains of *S. aureus* with a MIC of 62.5 µg/mL and *E. faecium* with a MIC of 125 µg/mL, showing selectivity for the gram-positive bacteria. The other extracts resulted non-active against all the sensible bacterial strains. Also, hexane, CHCl$_3$/MeOH and aqueous root extracts were tested against the same sensitive bacterial strains giving null activity.

Table 5.13 Activity of *H. glomerata* leaf extracts against sensible bacteria

Extract	MIC (µg/mL)				
	S. aureus	*E. faecium*	*P. aeruginosa*	*E. coli*	*K. Pneumoniae*
Hexane	>500	>500	>500	>500	>500
C/M*	125	62.5	>500	>500	>500
Dry Aq.	>500	>500	>500	>500	>500
Fresh Aq.	>500	>500	>500	>500	>500

* C/M: CHCl$_3$/MeOH extract.

Table 5.14 showed results for leaf and root extracts of *H. glomerata* and some isolated and derivatized compounds against resistant bacteria. Leaves hexane and aqueous extracts (fresh and dry) were somehow active against *E. coli* producer of ESBL, and the three strains of *K. pneumoniae* resistant to oxacillins, producer of ESBL, and NDM-1 +, with MIC value of 500 µg/mL each. This is could be due to their complex composition, which does not allow a good concentration of active components.

Table 5.14 Activity of *H. glomerata* leaf and root extracts and some isolated compounds and their semi-synthetic derivatives against resistant bacteria

Leaf extract	MIC (µg/mL)								
	MRSA*	**LRSE***	**VREF***	**CRAB***	**CRPA***	**ECPE***	**KPPN***	**KPPE***	**ORKP***
Hexane	>500	>500	>500	>500	>500	500	500	500	500
C/M*	>500	>500	>500	>500	>500	>500	>500	>500	>500
Dry Aq.	>500	>500	>500	>500	>500	500	500	500	500
Fresh Aq.	>500	>500	>500	>500	>500	500	500	500	500
Root extract									
Hexane	>500	>500	>500	>500	>500	>500	>500	>500	>500
C/M*	>500	500	>500	500	500	>500	>500	>500	>500
Aqueous	>500	>500	>500	>500	>500	>500	>500	>500	>500
Compounds									
β-Sitosterol	>200	200	200	200	200	>200	200	>200	>200
β-Sit. Ac.	>200	200	200	100	200	200	>200	200	>200
Daucosterol	>200	200	200	200	200	>200	>200	>200	>200
Dauco. Tetr.	>200	>200	200	200	200	>200	>200	>200	>200
*p*CA*	>200	>200	>200	>200	>200	>200	>200	>200	>200
CA*	>200	>200	>200	>200	>200	>200	>200	>200	>200
Levofloxacin	12.5	6.25	100	12.5	0.78	25	100	0.78	>200

* C/M: CHCl$_3$/MeOH extract; MRSA: Methicillin resistant *S. aureus*; LRSE: Linezolid resistant *S. epidermidis*; VREF: Vancomycin resistant *E. faecium*; CRAB: Carbapenem resistant *A. baumannii*; CRPA: Carbapenem resistant *P. aeruginosa*; ECPE; *E. coli* producer of ESBL; KPPN: *K. pneumoniae* producer of NDM-1+; KPEP: *K. pneumoniae* producer of ESBL; ORKP: Oxacillin resistant *K. pneumoniae*; *p*CA: *p*-Coumaric acid; CA: Caffeic acid.

Leaf CHCl$_3$/MeOH extract showed null activity against all resistant strains tested. It is possible that the activity of this extract was masked or inhibited by other compounds present in this extract that's why the extract did not show activity. Antibacterial activity of extracts against sensible and resistant bacteria could due to the genetic mutations that bacteria have to undergo in order to gain its resistance. Mutation changes have to be compensated by the bacteria resulting in changes in their metabolic processes and therefore genetic expression (*229*). These modifications can generate new metabolic pathways and alternative mechanisms of action and hence resistant bacteria might show activity even if sensible strains did not show any.

Roots raw extracts like the leaves' extracts, resulted to be generally non-active against the selected resistant bacterial strains. The CHCl$_3$/MeOH extract was the only one which displayed low activity against *S. epidermidis* linezolid resistant, *A. baumannii* and *P. aeruginosa* both carbapenems resistant (Table. 5.11). Other extracts give null activity against the tested resistant strains. Because much like the previously tested extracts, their active components do not reach a useful concentration in the working solution. This is also in agreement with the ethnical use of *H. glomerata*, because the leaves are used in folk medicine whereas the roots are used as food source. On the other hand, the activity of some pure compounds (Table 5.14) against sensitive bacteria have been reported in the literature (*230, 231*). β-Sitosterol showed weak activity (MIC 200 µg/ml) against *S. epidermidis* (linezolid), *E. faecium* (vancomycin), *A. baumannii* (carbapenems), *P. aeruginosa* (carbapenems), and *K. pneumoniae* (NDM-1 +). β-Sitosterol acetate displayed weak activity (MIC 200 µg/ml) towards *S. epidermidis* (linezolid), *E. faecium*

(vancomycin), *P. aeruginosa* (carbapenems), *E. coli* (ESBL) and *K. pneumoniae* (ESBL) whereas against *A. baumannii* (carbapenems) had a moderate activity (MIC 100 μg/ml). Daucosterol gave activity (MIC 200 μg/ml) against *S. epidermidis* (linezolid), *E. faecium* (vancomycin), *A. baumannii* (carbapenems), and *P. aeruginosa* (carbapenems). Daucosterol acetylated had activity (MIC 200 μg/ml) towards *E. faecium* (vancomycin), *A. baumani* (carbapenems) and *P. aeruginosa* (carbapenems). Activity of phytocompounds and their semisynthetic derivatives towards resistant bacteria was weak, the most active tested compound was β-sitosterol acetate, with a MIC of 100 μg/mL against *A. baumannii* (carbapenems). In the literature the compound has shown to have some activity on the growth of various bacterial strains, such as *S. aureus*, *E. coli* and *K. pneumoniae*, reporting halos of inhibition (*232*). β-Sitosterol was the second most active of the compounds, respecting what reported in the literature and having no activity at its highest concentration against *S. aureus*, *E. coli* and two strains of *K. pneumoniae*. The other bacteria were susceptible at 200 μg/mL of the compound which is still too high concentration to consider the molecule active. Daucosterol and its tetraacetate derivative gave almost the same results of antibacterial activity. Chemical structure of these molecules is larger than their aglycones so physical barriers of bacteria could create difficulties of compounds to reach the cytoplasm and exert their effect. It is know that some of them (especially the gram-positive ones) produce biofilms which have the ability to stop undesirable compounds to reach the bacteria, and protect it. *A. baumannii*, it resulted to be sensible to the acetylated β-sitosterol but not β-sitosterol. It is possible that acetylated sterol crossess the cytoplasmic membrane of bacteria

due to its increased lipophilicity compared with its non-acetylated parent. On the other hand, both daucosterol and its derivative resulted inefficient in any of the tested bacterial strains. It is also ought to mention that the bacterial strains were very resistant, needing sometimes very high concentrations of levofloxacin which resulted above the ones reported. For example, the concentrations used for levofloxacine in the assays wer not enough to kill *K. pneumoniae* resistant to oxacillins, showing the high resistance of the strain.

5.3.2 Antibacterial screening of dry aqueous extract fractions

Six fractions were tested against four resistant bacterial strains that resulted sensible to the aqueous extracts (Table 5.11). Results of screening show that fractions were inactive against the bacteria at the maximum tested concentration (500 µg/mL). This could be explained by a probable loss of activity of the extract during time, even if stored at -20 °C. In addition, its fractionation throughout the flash chromatographer could speed up the extract degradation. To prove this hypothesis the fractions were reunited and tested again. A sample of aqueous extract that was not fractionated was tested also. None of the tested samples showed any activity.

5.3.3 Cytotoxicity assay of *H. glomerata*'s raw extracts

Cytotoxicity of organic leaf extracts resulted much higher than the aqueous extracts (Figure 5.87). Cytotoxic activity (IC_{50}) of organic extracts was in the range of 24 to 49 µg/mL against cancer cell lines tested. Whereas the IC_{50} value for the aqueous extracts were 49 – 93 µg/mL.
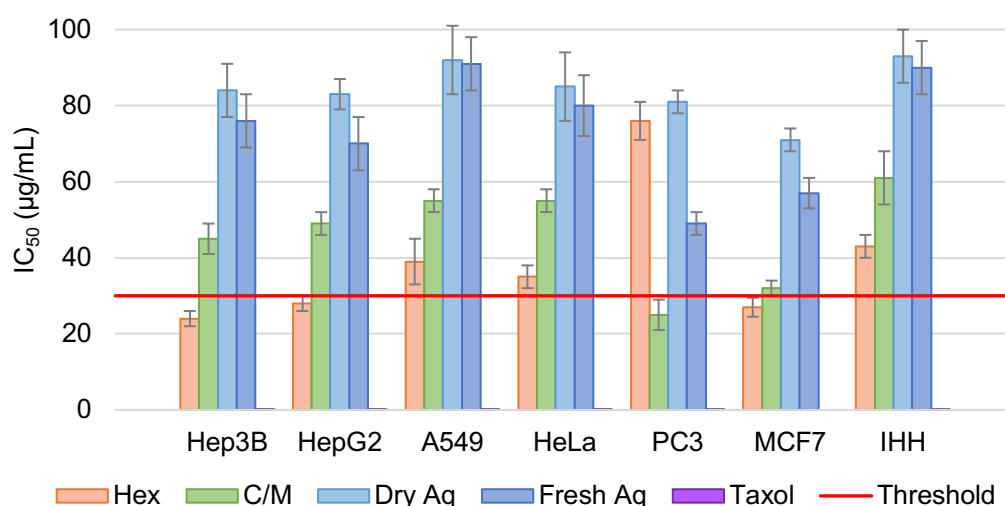
Figure 5.87 Cytotoxic effect (IC_{50}) of *H. glomerata*'s leaf extracts against Hep3B, HepG2, A549, HeLa, PC3, MCF7 and IHH cell lines. *Paclitaxel was used as positive control showing IC_{50} of 6.4±2.1, 7±3.4, 21.5±3.4, 8.5±1.7, 13.2±3 and 59.8±6.8 ng/mL respectively for the tested cell lines, with exception of MCF7 for which was not determined. The hexane (Hex), $CHCl_3$/MeOH (C/M), dry aqueous (Dry Aq) and fresh aqueous (Fresh Aq) extracts were considered active when their IC_{50} was below the threshold (red line) was set to 30 µg/mL.

The most cytotoxic active extract was the hexane, having IC_{50} values $\leq$ 30 µg/mL against Hep3B, MCF7 and HepG2 tumor cell lines. The lower IC_{50} reported for this extract were against Hep3B (24 ± 2 µg/mL), MCF7 (27 ± 2.5 µg/mL) and HepG2 (28 ± 2 µg/mL). The second most affected cell lines were HeLa and A549 with IC_{50} 40 µg/mL, showing a low activity. Instead, no activity was observed for PC3 cell line (IC_{50}: 76 ± 5 µg/mL), which resulted less affected than the IHH cells (IC_{50}: 43 ± 3 µg/mL). The $CHCl_3$/MeOH extract was the second most active extract, with an IC_{50} of 25 ± 4 µg/mL against the PC3 cell line. Lower cytotoxicity was observed against the MCF7 cell line with an IC_{50} of 32 ± 2 µg/mL. Dry aqueous extract showed low cytotoxic activity with IC_{50} values $\geq$ 80 µg/mL for the cancer cell lines tested. The fresh aqueous extract had only two IC_{50} values $\leq$ 60 µg/mL these were with PC3 and MCF7 cell lines, therefore it was considered inactive.

There is no remarkable selectivity between the cancer cell lines and immortalized normal hepatocytes (IHH). The higher selectivity was obtain with the chloroform/methanol extract were the lowest IC_{50} was 55 ± 3 µg/mL and the IHH had an IC_{50} is of 61 ± 7 µg/mL.

Selectivity index (SI) of extracts was calculated (Table 5.15). Some degree of selectivity of organic extracts for cancerous cells is clearly visible from the calculations especially the $CHCl_3$/MeOH extract resulted remarkably more cytotoxic for PC3 and MCF7 cancer cells.

Table 5.15 SI calculated for the extracts

Extract	Hep3B	HepG2	A549	HeLa	PC3	MCF7
Hexane	1.79±0.15	1.54±0.11	1.10±0.17	1.23±0.11	0.57±0.04	1.59±0.15
C/M*	1.36±0.12	1.24±0.08	1.11±0.06	1.11±0.06	2.44±0.39	1.91±0.12
Aq. 1*	1.11±0.09	1.12±0.05	1.01±0.10	1.09±0.12	1.15±0.04	1.31±0.06
Aq. 2*	1.18±0.11	1.29±0.13	0.99±0.08	1.13±0.11	1.84±0.11	1.58±0.11

* C/M: $CHCl_3$/MeOH extract; Aq. 1: dry Aqueous extract; Aq. 2: Fresh aqueous extract.

Difference in activity observed between the organic and the aqueous extracts could due to the size and polarity of their molecules (Rule of 5) rather than their qualitative nature. Some compouns from the aqueous extracts may contain multiple sugar molecules in order to stay in solution or multiple polar functional groups which could not allow them to cross the cellular membrane (*233*). If only few molecules can reach the cytoplasm, then the concentration they achieve will not be sufficient to cause a toxic effect on the cell. It would be easer for the cell to get rid of the toxic component by their deactivation or by pumping them to the extra cellular space (*234*). The identified compounds from the hexane extract justify its activity, in fact its active principle seems to

be the β-sitosterol which reaches the highest concentration among the extract's components.

The polarity of solvent mixture in CHCl$_3$/MeOH extract allows it to have a broader set of compounds. This means that the components in this extract has a higher probability to have the correct characteristics to exert a pharmacological activity from a Lipinski rule point of view. Among the isolated compounds there are some that might be responsible or at least take part in the extract biological activity.

Table 5.16 shows the results of the cytotoxicity of the root extracts of *H. glomerata*. Unfortunately, only the hexane extract showed some activity against PC3 cells (IC$_{50}$ = 73.29 ± 6.76 µg/mL). Although an inhibition of cell growth is clearly present, the IC$_{50}$ value is too high to consider the extract active (*78*). The low activity displayed by the root hexane extract is probably explainable by its high content in lipids. It is probably that saponifiable and non-saponifiable fats might be damaging the cellular membrane.

Table 5.16 IC$_{50}$ values (µg/mL) of the root extracts against the cancer cell lines

Root extract	IC$_{50}$ (µg/mL)						
	Hep3B	**HepG2**	**A549**	**HeLa**	**PC3**	**MCF7**	**IHH**
Hexane	N/A	>200	N/A	129.6±11.79	73.26±6.76	>100	N/A
C/M*	N/A	>200	N/A	>200	>100	>100	N/A
Aqueous	N/A	>200	N/A	>200	>100	>100	N/A
Control	**IC$_{50}$ (ng/mL)**						
Paclitaxel	6.4±2.1	7±3.4	21.5±3.4	8.5±1.7	13.2±3	ND	59.8±6.8

* C/M: CHCl$_3$/MeOH extract.

5.3.4 ANOVA analysis of cytotoxicity results

Results of cytotoxic activity of leaves extracts were also submitted to a single factor analysis of variance (One-Way ANOVA), the summary of the parameters used in the calculations is given in table 5.17. Results of ANOVA calculations are reported in table 5.18.

Table 5.17 Parameters of the ANOVA calculation

Groups	Count	Sum	Average	Variance
Hexane	7	272	38.8571429	315.142857
CHCl$_3$/MeOH	7	322	46	172.333333
Dry Aqueous	7	589	84.1428571	54.1428571
Fresh Aqueous	7	513	73.2857143	251.904762

Analysis of calculated values showed a significant variation among the considered variables. The F value (16.4795967) resulted much higher than the F$_{crit}$ (3.00878657) demonstrating that at least one of the extracts is part of a completely different population when compared to the others. Also, the P-value (4.9964×10^{-6}) resulted a 10^{-4} factor smaller than the selected α value (0.05), also stating the non-null hypothesis for the cytotoxicity results.

Table 5.18 Result of the ANOVA calculation

Variation	SS	df	MS	F	P-value	F crit
Between Groups	9807.7143	3	3269.2381	16.4795967	4.9964E-06	3.00878657
Within Groups	4761.1429	24	198.380952	-	-	-
Total	14568.857	27	-	-	-	-

The t-test results (Table 5.19) showed that the $CHCl_3$/MeOH and the hexane extracts gave the most similar results in cytotoxicity.

Table 5.19 Result of the t-test calculation

Confronted extracts	P(T<=t) two-tail
Hexane vs $CHCl_3$/MeOH	0.40879635
Hexane vs Dry Aqueous	4.352×10^{-5}
Hexane vs Fresh Aqueous	0.00241639
$CHCl_3$/MeOH vs Dry Aqueous	2.1778×10^{-5}
$CHCl_3$/MeOH vs Fresh Aqueous	0.00434225
Dry Aqueous vs Fresh Aqueous	0.12652051

Their P-value was 0.408796346 which is almost ten times greater than the selected α level. When confronted with the aqueous extracts cytotoxicity the organic extracts resulted producing a low P-value in the range of 2×10^{-3} – 2×10^{-5}. Instead the dry and fresh aqueous extracts resulted to be similar to each other having a P-value (0.126520506) greater than the selected α level.

5.3.5 Reported biological activity of compounds identified by GC-MS in the $CHCl_3$/MeOH extract

Some of identified compounds from the tested extracts have already been reported in the literature as bioactive. For example it has been reported that phytol has activity against eight bacterial and eight fungal strains, showing a strong antibacterial activity with MICs between 3 and 38 µg/mL, against *Bacillus cereus*, *Micrococcus luteus*, *Listeria monocytogenes*, *P. aeruginosa*, *Salmonella typhimurium*, *E. coli*, *Enterobacter cloacae* and *Micrococcus flavus* (*109*). Phytol has also been reported to exert cytotoxic activity against various

types of cancer cell lines and normal immortalized cells giving variable results. It was found to be modestly active against MCF7, HeLa, A549, and PC3 cells, with IC_{50} ranging between 1.13 ± 0.05 µg/mL and 9.98 ± 0.25 µg/mL (*110*). Diterpenoids trachylobane and kaur-16-ene are also part of a family of bioactive compounds, reported as antibacterial (*111*), and both of them are also reported having cytotoxic effects (*112*). Regarding stigmasterol and campesterol there are just few reports of these sterols tested as pure compounds, but there are various reports of the biological activity of their mixture and derivatives. For example, their acetylated derivatives shown to have antibacterial activity against *S. aureus*, *E. coli*, *P. aeruginosa* and *Klebsiella* among other bacteria (*113*). β-Sitosterol and daucosterol which are very high in concentration are instead reported to have no antibacterial properties against *E. coli*, *S. aureus* and *K. pneumoniae* (MIC >500 µg/mL) (*114*). β-Sitosterol was also reported to have various activities, such as cytotoxicity against cancer cells like MCF7, A549, PC3, HeLa and HepG2. Their IC_{50} were 29.53 µg/mL, 78 µg/mL, 30.85 µg/mL, 170.60 µg/mL and 21.98 µg/mL respectively, showing a moderate inhibition of the cellular growth on the cancer cell lines (*115–118*). The glycosylated derivative of β-sitosterol which is already been reported in the literature as biologically active, having mild toxic effect on PC3 cells with an IC_{50} of 31.9 ± 0.054 µg/mL (*119*). The glycosylated sterol is also capable of stimulate the Wnt/β-catenin signalization and therefore inhibit the proliferation, migration and invasion of hepatocellular carcinoma (HCC) cells. Against HepG2 the molecule showed a very low cytotoxicity with an IC_{50} of 251 µg/mL and against Hep3B resulted to have a medium inhibitory concentration higher than 20 µg/mL (*120, 121*).

Stigmasterol is reported to have cytotoxic activity against Hela and A549 cell lines with IC_{50} of 5.04 µg/mL and 4.28 µg/mL respectively (*122*). *p*-Coumaric acid is instead reported to have a contradictory antibacterial activity. Lou *et al*. found that the acid has an effect against Gram–positive bacteria such as *S. aureus* (MIC: 20 µg/mL) and Gram–negative bacteria like *E. coli* (MIC: 80 µg/mL). It was also reported that this molecule has a double damage mechanism of action comprehending an increase in the membrane permeability and binding on the phosphate anion of the DNA of the bacteria (*123*). Instead other works the activity against *S. aureus* was reported lower (MIC: 625 µg/mL) or completely absent for both *p*-coumaric acid and caffeic acid (MIC > 1 µg/mL) against *S. aureus*, *S. epidermidis* and against *E. coli* among other bacteria (*124*). Caffeic acid and *p*-coumaric acid have also been reported to be active when tested against cancer cell lines. Da Silva *et al*. found that caffeic acid has a stronger effect than *p*-coumaric acid on HEp2 cells, having an IC_{50} of 244.12 µg/mL and 561.86 µg/mL respectively (*125*). The two phenolic acids are also known to have antimutagenic activity and affect the viability of numerous tumor cell lines, such as A549, HepG2 and MCF7 among others, showing IC_{50} between 164.05 and 180.16 µg/mL or lower (*124, 126*). Cytotoxic activity of caffeic acid is also reported against PC3 cells with an IC_{50} of 32 µg/mL (*127*). Other biological activities of some of the identified components of the plant *H. glomerata* are reported in table 5.20.

Table 5.20 Reported activity for the compounds identified from the hexane extract

Compound	Biological activity	Source	Reference
Stigmasterol	Chemopreventive effect in skin carcinoma; *in vitro* antioxidant activity; anti-osteoarthritic; antimutagenic activity; cytotoxic, antibacterial, antifungal, antimycobacterial	*Azadirachta indica, Clerodendrum inerme* linn., *Gleditsia sinensi, Talium paniculatum*	(*128–132*)
Stigmasterol glycoside	Antibacterial: *Aspergillus niger*	*Melochia umbellata*	(*133*)
Stigmasteryl acetate	Antibacterial: *S. albus, S. aureus, S. uridans, E. coli, P. pyocyanea, Klebsiella*	*A. tricolor, A. squamosal, A. alliceum*	(*113*)
Stigmastan-4en-3-one	Antimycobacterial; antiplasmodial	*Cenchrus setiserum, Erythrina stricta*	(*134, 135*)
β-Sitosterol	Antimutagenic activity; antioxidant and Anibacterial[1]; antiproliferative, induces apoptosis[2]; cytotoxic, antibacterial, antifungal, antimycobacterial	*Gleditsia sinensi, Vitex agnus, Talium paniculatum*	(*131, 132, 136, 137*)
β-Sitosteryl acetate	Antibacterial: *S. albus, S. aureus, S. uridans, E. coli, P. pyocyanea, Klebsiella*	*A. tricolor, A. squamosal, A. alliceum*	(*113*)
Campesterol	Anti-inflamatory; antiangiogenic; cytotoxic, antibacterial, antifungal, antimycobacterial	*Lupezia racemose, Chrysantenum coronarium* L., *Talium paniculatum*	(*132, 138, 139*)
Phytol	Anticancer[3]; antibacterial[4]; anticancer activity	*Gracilona edulis, Aster yumena*	(*140–142*)
γ-Linoleic	Antiproliferative; antimycobacterial; anibacterial: FabI, MR-*S. aureus, H. pylori, mycobacteria*	*Amischotolype hispida*	(*143–145*)
Oleic acid	Antimycobacterial: *M. tuberculosis*; anibacterial: FabI, MR-*S. aureus, H. pylori, mycobacteria*	-	(*146, 147*)
Palmitic acid	Antimycobacterial; promotion of melanoma cells growth	*Amischotolype hispida*	(*144, 148*)
UFA, SAFA and linolenic acid	Anibacterial: FabI, MR-*S. aureus, H. pylori, mycobacteria*	-	(*149*)

[1]In *Bacillus subtilis, S. aureus, S. epidermis, E. faecalis, E. coli*; [2]In colon, breast, prostate, liver, stomach cancer; [3]In MCF-7, human colon carcinoma; [4]In *P. aeruginosa*.

5.3.6 Reported biological activities of the major components identified by UPLC-QTOF-MS

Biological activities of major components of *H. glomerata* were investigated in the literature. The biological activities of phytol, β-sitosterol, campesterol, stigmasterol and daucosterol were already discussed in paragraph 5.3.5. Instead no biological activity was found reported in the literature for the steroid tillandsinone.

Oleanolic and ursolic acids are well known cytotoxic agents. It has been reported the mechanism of action of oleanolic acid, which is the induction of p53 dependent apoptosis throughout the ERK/JNK/AKT Pathway (*172*). Instead the ursolic acid, much like the daucosterol, mediates the Wnt/β-catenin signaling, inducing apoptosis in PC3 cells (*173*). It is reported that the mixture of oleanolic and ursolic acid has moderate inhibitory activity against MCF7 cell line, with an IC_{50} of 23.97 µg/mL (*174*). Oleanolic acid alone was also found to have cytotoxic effects on HepG2, MCF7 and A549 cell lines with medium inhibitory concentrations of 36.87 ± 1.14 µg/mL, 26.19 ± 1.45 µg/mL and 19.50 ± 1.72 µg/mL respectively (*175*). In other reports the terpenoid acid was reported to have high toxicity on Hep3B and PC3 cells with IC_{50} lower than 3.65 µg/mL and of 2.97 µg/mL respectively after 48 hours of exposition (*176*). Mild effects were shown on HeLa with IC_{50} higher than 100 µg/mL (*177*). These triterpenoid acids have also antibacterial properties on *S. mutans, S. sobrinus* (MICs of 2 µg/mL), *S. pneumoniae* (MIC of 16 µg/mL), methicillin-sensitive and methicillin-resistant *S. aureus* (MIC of 8 µg/mL and 64 µg/mL, resp.), *Bacillus subtilis* (MIC of 8 µg/mL), *B. cereus* and *E. faecalis* (MIC of 6.25–8.00 µg/mL), *E. faecium* (MIC of 8 µg/mL), and *P. aeruginosa* (MIC of

256 µg/mL). It was found that oleanolic acid alters the synthesis of DnaK in *E. coli*, producing a heat-shock response in this species. Also, both oleanolic and ursolic acid inhibit peptidoglycan turnover in *L. monocytogenes*, affecting the cellular wall of bacteria (*178*).

Biological activities of resveratrol include anticancer and chemopreventive. The pathways to exert its chemopreventive activity are various, such as the Fas receptor (CD95) signaling, apoptosis, NFκB, phosphoinositol 3-kinases/protein kinase B (PI3Ks/Akt), sirtuin 1 (SIRT1) and Wnt. It was found that miRNA is also a target of resveratrol blocking the process of translation (*179*). Resveratrol was tested for a minimum of 48h and maximum of 96h against HepG2, and Hep3B cells giving an IC_{50} ranges of 32.48 ± 14.58 µg/mL and 34.57 ± 17.43 µg/mL; and 28.9 ± 17.07 µg/mL and 51.14 ± 24.87 µg/mL respectively for the two cell lines (*180*). Against PC3 cells resveratrol is reported to be very active, with IC_{50} of 11.0 µg/mL (*181*), instead it produces a weaker inhibition over MCF7cells, with IC_{50} values of 213 µg/mL. The reported mechanism of action on MCF7 cells was associated with the modulation of phophorilated Akt and Caspase 9 (*182*). Resveratrol against HeLa cells had also a good antiproliferative activity with an IC_{50} of 67.8 ± 9.2 µg/mL and a very good cytotoxic activity against A549 cells with an IC_{50} of 5.82 µg/mL (*183*). The stilbene has potential antibacterial agent, having multiple interesting antibacterial properties, like the inhibition of the electron transport chain (ETC), cleavage of DNA molecules, inhibition of cell division by preventing the formation of the Z-ring, and the antibiofilm activity. Resveratrol was tested against different types of foodborne pathogens including *S. aureus*, *B. cereus*, *B. subtilis*, and *L. monocytogenes*, *E. coli*

O157:H7, *Salmonella Typhimurium*, *Vibrio cholerae*, *Campylobacter jejuni*, *Campylobacter coli*, *Arcobacter butzleri,* and *Arcobacter cryaerophilus*. The MICs range of resveratrol against the Gram-positive bacteria was between 0.625 and 521 µg/mL, and for the Gram-negative bacteria between 16.5 and 260 µg/mL (*184*). In another report, resveratrol was tested against six Gram-positive bacteria including *B. cereus* (ATCC 11778), *S. aureus* (ATCC 25923), methicillin-sensible *S. aureus* (MSSA), methicillin-resistant *S. aureus* (MRSA), and *E. faecalis* (ATCC 29212); and seven Gram-negative bacteria: *E. coli* (ATCC 25922), *E. coli* (clinical), *K. pneumoniae* (ATCC 13883), *K. pneumoniae* (clinical), *S. typhimurium* (ATCC 13311), *P. aeruginosa* (ATCC 27853), *P. aeruginosa* (clinical). The MICs range for the Gram-positive bacteria was 50-200 µg/mL with *B. cereus* being the most affected, instead all the Gram-negative bacteria resulted to have a MIC higher than 400 µg/mL (*185*). Antibacterial properties of resveratrol were also tested against three strains of *Propionibacterium acnes* giving IC_{50} of 73 µg/mL (*186*). It is clear that resveratrol is mainly active against Gram-positive bacteria.

Among the biological activities of piceatannol there are anti-inflammatory (NFκB), antimutagenic, and antiproliferative (cytotoxic, proapoptotic activity and hormesis) activities. The cytotoxic and proapoptotic activity were tested against prostate cancer cells (PC3, IC_{50}: 25 µg/mL), liver cancer cells (HepG2; IC_{50} > 200 µg/mL) and cervix cancer cells (HeLa, IC_{50}: 50 µg/mL). It is reported that piceatannol has antitumor effect in animals and also antileishmanial, antiplasmodial, and antibacterial activities. The latter activity was tested against three strains *P. acnes* (IC_{50}: 123 µg/mL) (*186*),

Salmonella infantis (IC$_{92}$: 244.24 µg/mL), *L. monocytogenes* (IC$_{84}$: 61.06 µg/mL), *Candida tropicalis* (IC$_{30}$: 61.06 µg/mL) (*187*).

Spinacetin, luteolin and kaempferol are reported as a good antioxidant agents, with comparable activities (*188*). Spinacetin is also able to suppress mast cells activation and passive cutaneous anaphylaxis in a murine model, showing its anti-inflammatory and antiallergenic activity (*189*). This molecule is a promising hepatoprotective agent (*190*). It is reported that a glycosylated derivative of the flavonol (Spinacetin 3-*O*-gentiobioside) has cytotoxic effect against HepG2 cells reaching the 69% of inhibition with 3 mM treatment for 48 hours (*191*). Luteolin and kaempferol and their derivatives exerted antiviral and antibacterial activity. The last activity was exhibited against MRSA, vancomycin-resistant enterococci (VRE) and *Burkholderia cepacia*, with MICs of 512 µg/mL or higher. More toxic results were obtained for luteolin against *E. coli*, *K. pneumoniae* and *P. aeruginosa* (ATCC) having MICs of 125 µg/mL for all strains (*192*). Luteolin has multiple biological effects, such as anti-inflammation, anti-allergy and anticancer and these activities might be related to each other. The flavone was active against MCF7, HeLa, A549, Hep3B and HepG2 cell lines having, after 48 hours of treatment, IC$_{50}$ of 9.41 µg/mL, 2.17 µg/mL, 4.29 µg/mL, 4.31 µg/mL and 2.92 µg/mL, respectively (*193–195*). Luteolin was tested against PC3 cells for 24, 48 and 72 hours and the average IC$_{50}$ obtained was of 9.0 µg/mL (*196*). The therapeutic cytotoxicity of the molecule is due to the inhibition of suppression of cell survival pathways, stimulation of apoptosis pathways, and also can block the angiogenesis process and the tumor growth *in vivo* (*197, 198*). Kaempferol was tested against different bacterial strains, including *B. cereus*, *B. subtilis* and *S. aureus*

having inhibition of bacteria growth (*199*). This flavonol has antineoplastic (anti-angiogenesis, antiproliferative, apoptosis) activity against HeLa and other cancerous cell lines with an IC_{50} of 42.1 ± 3.2 µg/mL (*200*). It was reported that it has antioxidant, anti-inflammatory and antitumor activity on HepG2 with IC_{50} of 30.92 ± 0.05 µg/mL (*201*). Kaemferol was active against MCF7, A549, Hep3B and PC-3 cell lines having IC_{50} of 90.82 ± 4.2 µg/mL, 35.80 ± 0.4 µg/mL, 40 µg/mL and 41.98 µg/mL, respectively (*202–204*).

Biological activity of ananaflavoside B is not deeply studied due to the scarce publications found, but in one report the flavone glycoside and its isomer ananaflavoside C are reported to be produced by plants used in the Nigerian ethnomedicine. In particular they might be involved in the hypoglycemic activity of their extracts and thus in the management of diabetes using traditional methods (*205*).

Delphinidin and cyanidin, like most of the anthocyanidins and anthocyanins, are known to be potent antioxidant and antiradical agents as well as for their interaction with DNA (*206*). 3-O-Sabubioside derivatives have been found to inhibit the Angiotensin Converting Enzyme (ACE), as part of the aqueous extract of *Hibiscus sabdariffa* calyces (*207*). Delphinidin was tested for its cytotoxic activitiy against MCF7 (*208*), A549 (*209*), PC3 (*210*) and HeLa (*211*) cell lines showing IC_{50} of 120 µg/mL, >80 µg/mL, 90 µg/mL and 37.9 ± 15.3 µg/mL, respectively. Cyanidin had a good cytotoxic activity against MCF7 cells with an IC_{50} of 13.55 µg/mL after 48 hours exposition (*208*). Some of its glycosylated derivatives are also reported in the literature having a number of biological activities, such has cytotoxic or antiproliferative effect on different cell lines (*212–214*). Cyanidin-3-glycoside and various delphinidin derivatives

were also isolated from antibacterial extracts of pomegranate fruit (*215*) and Chilean blackberry (*216*).

No inhibitory concentration was found for isoscoparin against cell lines under study, but it was reported that some its glycosylated derivatives are active against bacterial neuramidase (*217*). The flavone-C-glycoside was found to be part of the components of the cytotoxic plant *Gentiana farreri* Balf. (*218*). Isochlorogenic acid B was reported to have an IC_{50} of 160.10 μg/mL against MCF7 cells (*219*), however no other study of cytotoxicity for this compound was found in the literature. Ethyl acetate extract of chicory roots was found to be compose by a mixture of chlorogenic and isochlorogenic acid and have antibacterial activity against 21 bacterial strains, being more active than the positive control (*220*).

The IC_{50} found in the literature for the major compounds identified from the UPLC-QTOF-MS analysis of *H. glomerata*'s leaf extracts are reported in table 5.21.

Table 5.21 Reported IC_{50} (µg/mL) of the major components against the cell lines in analysis.

Compound	Class	Extract*	Hep3B	HepG2	A549	HeLa	PC3	MCF7	Ref
Phytol	Terpene	Hex	-	-	7.30	1.99	9.98	1.13	(*110*)
β-Sitosterol	Steroid	Hex	-	-	78	170.60	30.85	140	(*115–117*)
Daucosterol	Steroid	C/M; AqD; AqF	>20	251	17.46	-	31.9	-	(*119–121, 221*)
Stigmasterol	Steroid	Hex	-	-	4.28	5.04	-	-	(*122*)
Campesterol	Steroid	Hex	-	-	-	>100	-	-	(*222*)
Tillandsinone	Steroid	Hex	-	-	-	-	-	-	-
Oleanolic acid	Steroid	C/M; AqD; AqF	<3.65	36.87	19.50	>100	2.97	26.19	(*175–177, 223*)
Resveratrol	Stilbene	C/M; AqF	34.57	32.48	5.82	15.48	0.23	14.84	(*180–183*)
Piceatannol	Stilbene	C/M	-	>48.85	-	12.21	6.11	-	(*186*)
Luteolin	Flavonoid	C/M; AqD; AqF	4.31	2.92	4.29	2.17	9.0	9.41	(*193–196*)
Spinacetin	Flavonoid	C/M; AqD; AqF	-	-	-	-	-	-	-
Kaempferol	Flavonoid	C/M; AqD; AqF	40	30.92	35.80	42.1	41.98	90.82	(*200–204*)
Ananaflavoside B	Flavonoid	C/M; AqD; AqF	-	-	-	-	-	-	-
Delphinidine	Flavonoid	AqD; AqF	-	-	>24.26	11.49	27.29	36.39	(*208–211*)
Cyanidin	Flavonoid	C/M; AqD; AqF	-	-	-	-	-	13.55	(*208*)
Isoscoparin	Flavonoid	C/M; AqD; AqF	-	-	-	-	-	-	-
Isochlorogenic acid B	Polyphenol	C/M; AqD; AqF	-		-	-	-	160.10	(*219*)

*Hex: hexane extract; C/M: $CHCl_3$/MeOH (1:1) extract; AqD: dry aqueous extract; AqF: fresh aqueous extract.

5.3.7 Biodirected study of the CHCl₃/MeOH extract pooled fractions

5.3.7.1 Antibacterial screening of the CHCl₃/MeOH extract pooled fractions

Due to activity displayed by the CHCl₃/MeOH extract against the sensible strains *S. aureus* and *E. faecium*, it was decided to perform a screening of antibacterial activity of macro-fractions of the extract. Results of the screening are reported in table 5.22, where is shown that fraction 1, 3 and 8 the only active ones.

Table 5.22 Screening of the CHCl₃/MeOH extract fractions

Fractions	MIC (µg/mL)	
	S. aureus ATCC 25923	*E. faecium* ATCC 29212
1	200	200
2	>200	>200
3	100	50
4	>200	>200
5	>200	>200
6	>200	>200
7	>200	>200
8	100	100

Fraction 1 resulted active against both sensible strains *S. aureus* and *E. faecium* at the maximum tested concentration of 200 µg/mL. Its activity is probably due to its high composition of hydrocarbons and lipids, since this is the less polar extract fraction and probably retains most of the composition of hexane extract. Fraction 3 was also active against both strains with MIC values of 100 and 50 µg/mL for *S. aureus* and *E. faecium,* respectively. The composition of this fraction is shown in the next paragraph and the

antibacterial results shows a higher sensitivity of *E. faecium* of fraction components. Fraction 8 also had activity against both strains with MICs of 100 µg/mL, this fraction is the most polar and probably contains glycosylated compounds such as saponins and other polyphenols which have already been reported to have antimicrobial activity. Its composition could resemble that aqueous extracts in which various active compounds have been identified from the metabolomic study.

5.3.7.2 Composition of pooled fraction 1

Twelve compounds were identified in GC-MS analysis of fraction 1, almost all of them are long chain saturated alkanes with the exception of two terpenoids. The identified volatile compounds are reported in Table 5.23.

The most abundant compound is nonacosane (44 %) which was also found very abundant in the GC-MS analysis of the hexane extract. Other abundant compounds are cerotic acid (17 %), tetratriacontane (13 %) and octacosane (11 %). The alkanes are common in plants and are part of their waxes and have a protective function over the leaves tissues (*104*, *235*). These compounds are not reported as bioactive, but they could be damaging the cellular membrane and biofilms of the bacteria causing a lower proliferation. Because of this effect, in the whole extract these lipophilic molecules could allow a better penetration of other phytochemicals with antibacterial activity into the bacteria cytoplasm. The sterol or diterpene and the carotenoid could also have some antibacterial activity, but they are in very low concentration (<1 %). This could explain the mild activity of this fraction against both *S. aureus* and *E. faecium*.

These results are not exhaustive and still leave some of the components as unclear or unknown.

Table 5.23 GC-MS analysis of pooled fraction 1 of *H. glomerata* leaves' CHCl$_3$/MeOH extract

t$_R$ (min)	Compound	% area
31.074	Heneicosane	1.10
31.835	Saturated long chain alkane I	1.30
32.075	Sterol or diterpene	0.28
32.184	Saturated long chain alkane II	0.69
32.510	Pentacosane	2.49
32.825	Tetratetracontane	2.17
33.134	Octacosane	10.60
33.426	Cerotic acid	17.06
33.574	Carotenoid	0.33
33.735	Nonacosane	44.29
34.009	Saturated long chain alkane III	6.25
34.295	Tetratriacontane	13.44

All the compounds were identified using the NIST 08 mass spectral database.

That's why it was decided to methylate the fraction and repeat the analysis to better volatilize its constituents in GC-MS analysis. Results showed eight compounds identified from this second analysis (table 5.24). The main components of fraction were methyl undecanoate (37 %) and a linoleic acid ester (36 %). The other components were mainly alkanes, the most abundant being nonacosane (15 %) being a total of 21 % of the fraction. A fatty alcohol: ceryl alcohol (2 %) was identified. As already mention lipids such as alkanes and FAs could take part in the activity of the fraction against the sensible bacteria through the debilitation of the plasmatic membrane. Linoleic acid like other UFAs and their derivatives are reported to have antibacterial activity (*236*).

Table 5.24 GC-MS analysis of the methylated pooled fraction 1 of *H. glomerata* leaves'
CHCl₃/MeOH extract

t_R (min)	Compound	% area
35.265	Methyl undecanoate	36.717
88.287	Bis(2-hethylhexyl) phthalate	2.605
93.962	Heptacosane	2.065
97.312	Ceryl alcohol*	1.986
97.450	Octacosane	1.072
100.964	Nonacosane	14.946
107.283	Hentriacontane	4.783
132.120	Linoleic acid ester*	35.827

The majority of the compounds were identified using the NIST 08 mass spectral database. *Compounds identified manually or tentatively (Lipid Maps).

To complete analysis of fraction 1 it was also analyzed by HPLC-QTOF-MS (Table 5.25). A total of 105 compounds were identified from the analysis: 56 FAs and derivatives (50 %), 14 steroids (20 %), seven polyphenols (15 %), 15 terpenoids (9 %), five N-compounds (2 %), and two alkenes (1 %). Six compounds (3 %) were not identified and are still unknown.

FAs and derivatives were the most abundant class of metabolites which is in agreement with the low polarity of the fraction and extract. They are thirty-one FAs (29 %), seven esters (7 %), eight oxidation products (5 %), one aldehyde (4%), four ketones (3 %), three alcohols (1 %), and two diacids (1 %). From identified FAs twenty-three were UFAs (28 %) while eight were SAFAs (14 %), these last ones were mostly VLCFAs. As mentioned before FAs and especially UFAs such as linoleic acid are reported to have antibacterial activity against Gram-positive bacteria (*149*), which could partially justify the activity of the fraction against the two sensitive bacteria.

Table 5.25 HPLC-QTOF-MS analysis of pooled fraction 1 of the CHCl₃/MeOH extract of *H. glomerata*

t_R (min)	Compound	Molecular formula	m/z	Experimental mass	Calculated mass	Error (ppm)	Area %	Ref
0.290	Dodecadienyl acetate	$C_{14}H_{24}O_2$	225.1379	-	224.1776	-	1.52	a
0.301	Betaine aldehyde	$C_5H_{12}NO$	102.0915	102.0921	102.0919	1.76	0.66	b
0.301	Pentanamide	$C_5H_{11}NO$	102.0915	101.0842	101.0841	1.79	0.66	b
0.301	2-Methyl-2-butenal	C_5H_8O	102.0916	84.0575	-	-	3.69	c
0.378	Unknown	-	107.0129	-	-	-	0.83	-
0.389	2,3,4-Trimethoxybenzoic acid	$C_{10}H_{12}O_5$	213.0782	-	212.0685	-	0.33	c
0.389	Benzyl nicotinate	$C_{13}H_{11}NO_2$	213.0782	213.0789	213.0790	-0.56	0.40	b
0.411	16-Hydroxy hexadecanoic acid	$C_{16}H_{32}O_3$	272.2324	272.2328	272.2351	-8.50	0.77	b
0.411	16-Oxo-palmitate	$C_{16}H_{30}O_3$	270.2164	270.2168	270.2195	-9.84	0.67	b
0.422	*N*1,*N*8-Diacetylspermidine	$C_{11}H_{23}N_3O_2$	252.1674	229.1770	229.1790	-9.00	0.33	b
0.422	Unknown	-	233.1023	-	-	-	0.35	-
0.422	12-(2,3-Dihydroxycyclopentyl)-2-dodecanone	$C_{17}H_{32}O_3$	284.2334	284.2338	284.2351	-4.67	0.67	b
0.433	Sterebin D	$C_{18}H_{30}O_3$	294.2184	294.2189	294.2195	-1.85	0.36	b
0.433	6-Oxabicyclo[3.1.0]hexane-2-undecanoic acid methyl ester	$C_{17}H_{30}O_3$	282.2174	282.2178	282.2195	-5.98	0.48	b
0.433	Miyristic acid (C14:0)	$C_{14}H_{22}N_2O_2$	268.2004	-	250.1908	-	0.52	c
0.433	2-Methoxy-hexadecanoic acid	$C_{17}H_{34}O_3$	286.2494	286.2498	286.2508	-3.64	0.87	b
0.444	Phytyl acetate	$C_{22}H_{42}O_2$	339.1528	-	338.3185	-	0.45	c
0.444	Dimorphecolic acid	$C_{18}H_{32}O_3$	296.2343	296.2346	296.2351	-1.77	0.36	b
0.444	Catelaidic acid (C22:1, Δ^{11})	$C_{16}H_{22}N_2O_6$	339.1528	-	338.3185	-	0.45	c
0.444	Oleic acid (C18:1, Δ^9)	$C_{18}H_{34}O_2$	283.2200	-	282.2559	-	0.51	a
0.444	18-Hydroxyoleate	$C_{18}H_{33}O_3$	298.2503	-	297.2435	-	0.73	a
0.444	Linoleic acid (C18:2, $\Delta^{9,12}$)	$C_{18}H_{32}O_2$	281.1917	280.2402	262.1681	-2.57	0.48	a
0.444	Oxo-oleate	$C_{18}H_{31}O_3$	296.2343	-	295.2279	-	0.39	c

Table 5.25 HPLC-QTOF-MS analysis of pooled fraction 1 of the CHCl₃/MeOH extract of *H. glomerata* (Continued)

t_R (min)	Compound	Molecular formula	m/z	Experimental mass	Calculated mass	Error (ppm)	Area %	Ref
0.444	Erucic acid (C22:1, Δ^{13})	$C_{16}H_{19}NO_6$	339.1528	-	338.3185	-	0.45	c
0.444	12*R*-hydroxy-9*Z*-octadecenoic acid	$C_{18}H_{34}O_3$	298.2503	298.2508	298.2508	-0.11	0.73	b
0.477	Hexadecene	$C_{16}H_{32}$	288.2668	-	224.2504	-	0.40	b
0.488	(*R*)-10-Hydroxystearic acid	$C_{18}H_{36}O_3$	300.2661	300.2671	300.2664	2.12	0.64	b
0.565	2-Oxophytanic acid	$C_{20}H_{38}O_3$	326.2833	326.2838	326.2821	5.09	0.30	b
0.576	Methylsuberic acid	$C_9H_{16}O_4$	189.1100	-	188.1050	-	0.70	a
0.598	Unknown	-	233.1020	-	-	-	0.38	-
0.598	Unknown	-	233.1018	-	-	-	0.48	-
0.609	Hexadecenoic acid (C16:1, Δ^2)	$C_{16}H_{30}O_2$	255.1313	-	254.2246	-	0.19	c
0.653	Geranate derivative I	-	167.9716	-	-	-	0.53	c
0.653	Geranate derivative II	-	167.9716	-	-	-	0.56	c
0.675	Gadoleic acid (C20:1, Δ^9)	$C_{20}H_{38}O_2$	328.2990	-	310.2872	-	0.36	c
0.731	Undecanedioic acid	$C_{11}H_{20}O_4$	217.1467	-	216.1362	-	0.61	c
0.819	Heptadecenoic acid (C17:1, Δ^{10})	$C_{17}H_{32}O_2$	345.1592	-	268.2402	-	0.58	c
0.819	Heptadecanedione	$C_{17}H_{32}O_2$	345.1592	-	268.2402	-	0.71	c
0.819	Heptadecenoic acid isomer	$C_{17}H_{32}O_3$	345.1592	-	268.2402	-	0.64	c
0.830	Margaroleic acid (C17:1 Δ^9)	$C_{17}H_{32}O_2$	269.1885	-	268.2402	-	0.60	a
0.885	Anethole	$C_{10}H_{12}O$	148.9966	-	148.0888	-	4.47	d
0.973	Pentacosanoic acid (C25:0)	$C_{25}H_{50}O_2$	383.2803	-	382.3811	-	0.17	c
1.105	Methyl cinnamate	$C_{10}H_{10}O_2$	163.0159	162.0088	162.0681	-	4.24	c
1.105	Chavicol	$C_9H_{10}O$	135.0130	-	134.0732	-	0.95	c
1.105	3-(4-Methoxyphenyl)-2-propenal	$C_{10}H_{10}O_2$	163.0159	-	162.0681	-	4.24	c
1.150	Unknown	-	326.1027	-	-	-	0.61	-
1.150	Hydroxycinnamate derivative	$C_{15}H_{18}O_8$	326.1027	326.1026	326.1002	7.58	0.61	b

Table 5.25 HPLC-QTOF-MS analysis of pooled fraction 1 of the CHCl₃/MeOH extract of *H. glomerata* (Continued)

t_R (min)	Compound	Molecular formula	m/z	Experimental mass	Calculated mass	Error (ppm)	Area %	Ref
1.150	Unknown	-	326.1027	-	-	-	0.61	-
1.172	Lignoceryl alcohol	$C_{24}H_{50}O$	355.0748	-	354.3862	-	0.55	c
1.172	Ucriol	$C_{20}H_{32}O_3$	321.1354	-	320.2351	-	0.03	c
1.172	Gallic acid derivative	$C_{13}H_{16}O_{10}$	350.1055	332.0751	332.0743	2.23	trace	b
1.172	Kaurene isomer	$C_{20}H_{28}O_4$	333.0953	-	332.1988	-	0.55	c
1.194	Tangeraxanthin	$C_{34}H_{44}O_2$	485.3489	-	484.3341	-	0.26	c
1.502	Farnesal	$C_{15}H_{24}O$	468.3912	-	220.1827	-	0.57	c
1.569	Nonacosene	$C_{29}H_{58}$	407.3388	-	406.4539	-	0.65	a
1.646	Tetracosatrienoic acid (C24:3, $\Delta^{15,18,21}$)	$C_{24}H_{42}O_2$	363.3119	-	362.3185	-	1.63	a
1.646	Tetracosatrienoic acid isomer	$C_{24}H_{42}O_3$	363.3119	-	362.3185	-	1.63	a
1.646	kaurenoic acid derivative	$C_{20}H_{30}O_2$	385.2942	-	302.2246	-	0.51	c
1.899	24-Methylcycloart-23-en-3β-yl acetate	$C_{33}H_{54}O_2$	482.4072	482.4076	482.4124	-9.93	0.64	b
2.065	Montanic acid (C28:0)	$C_{28}H_{56}O_2$	425.2894	-	424.4280	-	0.31	c
2.087	Nonacosanol	$C_{29}H_{60}O$	425.2894	-	424.4644	-	0.31	c
2.087	Citronellic acid	$C_{10}H_{18}O_2$	171.1165	-	170.1307	-	0.43	a
2.098	5β-Cholestane-3α,7α,12α,26-tetrol	$C_{27}H_{48}O_4$	459.3421	436.3585	436.3553	7.42	trace	b
2.175	Eicosanediol	$C_{20}H_{42}O_2$	378.3310	-	314.3185	-	0.52	b
2.175	Cholest-5-ene	$C_{27}H_{46}$	388.3947	370.3609	370.3600	2.53	0.01	b
2.285	Docosatetraenoic acid (C22:4, $\Delta^{4,7,10,13}$)	$C_{22}H_{36}O_2$	333.2999	-	332.2715	-	1.26	a
2.285	Methyl acetyl ricinoleate	$C_{21}H_{38}O_4$	355.2828	354.2755	354.2770	-4.31	0.57	b
2.285	Hexadecanone derivative	$C_{22}H_{36}O_2$	333.2999	-	332.2715	-	1.26	c
3.013	Triacontapentaenoic acid (C30:5)	$C_{30}H_{50}O_2$	443.2586	-	442.3811	-	0.08	a
3.697	Ethyl oleate	$C_{20}H_{38}O_2$	310.3091	-	310.2872	-	2.58	c
4.083	(9E)-Valenciaxanthin	$C_{27}H_{40}O_3$	413.3068	412.2996	412.2977	4.39	0.68	b

t_R (min)	Compound	Molecular formula	m/z	Experimental mass	Calculated mass	Error (ppm)	Area %	Ref
4.259	Boviquinone 4	$C_{26}H_{36}O_4$	413.2688	412.2615	412.2614	0.25	1.27	b
4.336	Nutriacholic acid	$C_{24}H_{38}O_4$	413.2689	390.2794	390.2770	6.21	1.98	b
4.336	Caleic acid (C18:3, $\Delta^{3,9,12}$)	$C_{18}H_{30}O_2$	279.1553	-	278.2246	-	1.84	a
4.336	Octadecatrienoic acid isomer I	$C_{18}H_{30}O_2$	279.1553	-	278.2246	-	1.84	a
4.336	Octadecatrienoic acid isomer II	$C_{18}H_{30}O_3$	279.1553	-	278.2246	-	1.84	a
4.336	Decatrienoic acid (C10:3, $\Delta^{2,4,6}$)	$C_{10}H_{14}O_2$	167.0120	-	166.0994	-	2.76	a
4.336	Octadecatrienoic acid isomer III	$C_{18}H_{30}O_3$	279.1553	-	278.2246	-	1.84	a
4.347	7α,12β-Dihydroxy-5β-cholan-24-oic Acid	$C_{24}H_{40}O_4$	392.2901	392.2904	392.2927	-5.86	1.40	b
4.358	But-3-en-2-one	C_4H_6O	71.0498	-	70.0419	-	0.78	c
4.369	Linolenyl myristate	$C_{32}H_{58}O_2$	475.2390	-	474.4437	-	0.37	a
4.369	Myristyl linolenate	$C_{32}H_{58}O_3$	475.2390	-	474.4437	-	0.37	a
4.446	Oleic acid derivative	$C_{24}H_{44}O_6$	429.2427	-	428.3138	-	0.80	a
4.446	Stigmasterol derivative I	$C_{29}H_{48}O_2$	429.2427	-	428.3654	-	0.73	a
4.446	Stigmasterol derivative II	$C_{29}H_{48}O_3$	429.2427	-	428.2311	-	0.69	a
4.579	7α,12β-Dihydroxy-5β-cholan-24-oic Acid	$C_{24}H_{40}O_4$	393.2993	392.2921	392.2927	-1.55	0.33	b
4.590	24-methyl-5Z,9Z-pentacosadienoic acid	$C_{26}H_{48}O_2$	393.2992	-	392.3654	-	0.31	a
5.064	Phytal	$C_{20}H_{38}O$	312.3250	294.2912	294.2923	-3.66	2.13	b
5.715	Pentadecylic acid (C15:0)	$C_{15}H_{30}O_2$	243.1874	-	242.2246	-	0.98	a
5.715	Isopentadecylic acid (C15:0, iso)	$C_{15}H_{30}O_3$	243.1874	-	242.2246	-	0.98	a
5.748	Carboceric acid (C27:0)	$C_{27}H_{54}O_2$	411.3495	-	410.4124	-	2.18	a
5.748	25-Azacholesterol	$C_{26}H_{45}NO$	388.3574	387.3495	387.3501	-1.51	0.01	b
5.957	Hexacosatrienoic acid (C26:3)	$C_{26}H_{46}O_2$	390.3739	-	390.3498	-	0.01	a
5.957	Hexacosatrienoic acid derivative	$C_{26}H_{52}O_3$	412.3530	-	412.3916	-	2.16	a
8.019	9,9-Dimethoxy-nonanoic acid	$C_{11}H_{22}O_4$	219.1626	-	218.1518	-	0.37	b

Table 5.25 HPLC-QTOF-MS analysis of pooled fraction 1 of the $CHCl_3$/MeOH extract of *H. glomerata* (Continued)

t_R (min)	Compound	Molecular formula	m/z	Experimental mass	Calculated mass	Error (ppm)	Area %	Ref
11.691	4α-Methylfecosterol	$C_{29}H_{48}O$	412.3674	412.3682	412.3705	-5.70	0.39	b
11.702	(3β,22*E*,24*R*)-23-Methylergosta-5,7,22-trien-3-ol	$C_{29}H_{46}O$	411.3642	410.3569	410.3549	4.89	1.33	b
13.477	Campesterol derivative	$C_{28}H_{44}O_2$	412.3527	-	412.3341	-	4.96	c
13.477	(24*R*)-Ergost-4-ene-3,6-dione	$C_{28}H_{44}O_2$	435.3249	412.3343	412.3341	0.52	trace	b
13.477	Ergostanol derivative	$C_{29}H_{46}O$	411.3492	-	410.3549	-	6.19	c
13.477	Glycerol triundecanoate	$C_{36}H_{68}O_6$	619.4907	596.5022	596.5016	1.03	0.62	b
13.488	(3*S*,3'*S*,5*R*,5'*R*,6*R*)-3,6-Epoxy-5,6-dihydro-3',5,8'-trihydroxy-β,κ-caroten-6'-one	$C_{40}H_{56}O_5$	616.4080	616.4152	616.4128	3.96	trace	b
13.488	Phthioceranic acid (C37:0)	$C_{43}H_{86}O_2$	635.4649	-	634.6628	-	1.15	a
13.488	Linoleic acid derivative	$C_{20}H_{33}O_2$	652.5182	-	-	-	trace	c
13.488	Episteryl palmitoleate	$C_{44}H_{74}O_2$	635.4649	-	634.5689	-	1.15	a

[a]Lipidmaps; [b]METLIN; [c]FooDB; [d]PhytoHub.

Some FAs have been reported to have antibacterial activities against different strains of bacteria and mycobacteria. The mechanism of action involved in their bacteria toxicity has been shown to involve the inhibition of the bacterial enzyme enoyl-acyl carrier protein reductase (FabI) (*236*).

Identified steroids were derivative of cycloartenol, cholestanol, stigmasterol, campesterol, fecosterol, episterol and ergosterol. These sterols are part of the leaf cuticle, and/or derivatives of the metabolism of more abundant steroids, like cholestanol which is a derivative of the metabolism of campesterol (*237*). Some of them could also be a sign of infection, such as fecosterol and episterol (*238*). Some of them, like cycloartenol, stigmasterol, campesterol and ergosterol derivatives have already been reported as bioactive against bacteria (*113*, *132*, *138*, *139*, *239*, *240*). Among the polyphenols five were phenyl propene derivatives and two were benzoic acid derivatives. From the first category of phytocompounds anethole, methyl cinnamate and 3-(4-Methoxyphenyl)-2-propenal are the most abundant. They are mainly found in plants' essential oils, and have demonstrated antibacterial and antimicrobial activity (*241*). The terpenoids were also abundant but only few reached a concentration higher than 1 % of the fraction 1. In general, various kauranes, xanthins and phytol derivatives have been identified, the last one being the most abundant and active. The identified terpenoids such as monoterpenes, sesquiterpenes, diterpenes, and triterpenes are employed by plants for a variety of functions. They regulate plant growth and development, and are used for specialized chemical interactions and protection with the abiotic and biotic environment (*242*). The most abundant of identified terpenoids is phytal (2 %) which is been reported as a drug

resistance reversal agent derivative of phytol, showing reduction of resistance on *E. coli* strains (*243*). Other identified compounds were the nitrogenated compounds from which the most interesting is a betalain aldehyde already reported in the family of Bromeliads (*41*). Only two alkenes: hexadecene and nonacosene were identified despite the non-polar nature of the fraction. This can be explained by the sample treatment needed for the HPLC technique, which does not allow the solubilization and therefore the analyzation of non-polar compounds. Composition of this fraction partially explains its activity against the two Gram-positive sensitive bacteria.

5.3.7.3 Composition of pooled fraction 3

Pooled fraction 3 was analyzed by HPLC-QTOF-MS in both positive and negative modes, identifying 28 components reported in table 5.26. The major identified components were phenolic acids (PAs) derivatives (57 %), including: hydroxycinnamic acids (HCAs) derivatives (46 %), coumarins (10 %) and benzoic acid derivatives (1 %). Other components were flavonoids (31 %) a pigment (6 %) and two unknown compounds (6 %). The antibacterial activity of this fraction is partially justified from its composition. Some of the compounds are reported as bioactive or are similar in structure to other antibacterial compounds. Among the HCAs derivatives are the two phenylpropyl coumarates: 3-(4-hydroxyphenyl) propyl coumarate and 3-(4-hydroxyphenyl-5-methoxy) propyl coumarate.

Their structure is very similar to the caffeic acid phenethyl ester (CAPE), a propolis component which, along with its derivatives, is already reported to have antibacterial activity.

Table 5.26 HPLC-QTOF-MS analysis of pooled fraction 3 of the CHCl₃/MeOH extract of *H. glomerata*

t_R (min)	Compound	Calculated formula	Negative (m/z)	Positive (m/z)	Fragments	Error (ppm)	Area (%)	Ref.
1.001	Protocatechuic acid	$C_7H_6O_4$	153.0189	-	[M-H]⁻: 109	-2.61	0.69	(*244*)
1.732	Salicylic acid	$C_7H_6O_3$	137.0239	-	[M-H]⁻: 93	-3.65	0.60	a, b
3.129	Caffeic acid	$C_9H_8O_4$	179.0342	-	[M-H]⁻: 135	-4.47	0.18	a
4.416	2-*O*-*p*-coumaroylglycerol	$C_{12}H_{14}O_5$	237.0768	239.0917	[M-H]⁻: 119, 145, 163; [M+H]⁺: 147, 119	5.48; 1.25	3.92	(*244*)
4.737	*p*-Coumaric acid	$C_9H_8O_3$	163.04	-	[M-H]⁻: 119	-0.61	3.79	(*245*)
4.990	1-*O*-*p*-coumaroylglycerol	$C_{12}H_{14}O_5$	237.0767	-	[M-H]⁻: 119, 145, 163	-0.42	10.52	c
6.000	Prunin	$C_{21}H_{22}O_{10}$	433.1141	-	ND	0.23	0.02	m
6.741	Dicaffeoyl glycerol	$C_{21}H_{20}O_9$	415.1044	417.1176	[M-H]⁻: 253, 161, 179, 135, 237 [M+H]⁺: 163, 145, 164, 237	-0.96; 2.17	11.11	(*43*)
7.063	Caffeoyl coumaroyl glycerol	$C_{21}H_{20}O_8$	399.1102	401.1221	[M-H]⁻: 163, 253, 119, 145, 135, 235, 179; [M+H]⁺: 147, 163, 145, 119	-2.49; 4.26	2.64	m
7.158	Feruloyl coumaroyl glycerol isomer	$C_{22}H_{20}O_8$	-	413.1222	[M+H]⁺: 163, 177, 145, 320	-2.18	0.28	(*43*)
7.363	Feruloyl caffeoyl glycerol isomer	$C_{22}H_{22}O_9$	429.1199	431.1322	[M-H]⁻: 134, 193, 253, 235 [M+H]⁺: 177, 145, 163	-3.48; 1.86	1.78	m
7.378	Naringenin	$C_{15}H_{12}O_5$	271.0615	-	[M-H]⁻: 151, 119	1.11	0.36	a, c
7.514	Naringenin derivative	$C_{24}H_{20}O_8$	-	437.1215	[M+H]⁺: 437, 177, 251, 147, 243, 221	-3.66	1.81	e
7.572	Synapoyl derivative	$C_{18}H_{18}O_8$	-	363.1077	[M+H]⁺: 183, 207, 175, 168	0.83	2.77	e
7.608	Homoeriodictyol	$C_{16}H_{14}O_6$	301.0715	-	[M-H]⁻: 151	-1.33	0.43	b
7.767	Unknown	$C_{26}H_{46}O_6$	-	455.3339	[M+H]⁺: 239	-6.15	3.01	-
7.772	Diosmetin or chrysoeriol	$C_{16}H_{12}O_6$	299.0568	-	[M-H]⁻: 284	2.34	0.83	b

Table 5.26 HPLC-QTOF-MS analysis of pooled fraction 3 of the CHCl$_3$/MeOH extract of *H. glomerata* (Continued)

t_R (min)	Compound	Calculated formula	Negative (m/z)	Positive (m/z)	Fragments	Error (ppm)	Area (%)	Ref.
7.837	Chlorophyll derivative	NA	-	843.2336	[M+H]$^+$: 843, 555, 844, 597, 556	ND	6.29	e
8.088	Unknown	C$_{21}$H$_{18}$O$_5$	-	-	[M+H]$^+$: 349, 351, 207, 193	-	3.46	-
8.014	Coumarin isomer	C$_9$H$_6$O$_2$	-	147.0438	[M+H]$^+$: 91, 119, 147, 65	-2.04	2.57	m
8.168	Coumarin derivative	C$_{20}$H$_{22}$O$_6$	-	359.1488	[M+H]$^+$: 147, 119	-0.28	7.18	m
8.215	3-(4-Hydroxyphenyl) propyl coumarate	C$_{18}$H$_{18}$O$_4$	297.1151	-	[M-H]$^-$: 119, 145, 163 [M+H]$^+$: 107, 147, 135	6.39; 1.34	6.08	m
8.297	3-(4-Hydroxyphenyl-3-methoxy) propyl coumarate	C$_{19}$H$_{20}$O$_5$	327.1255	-	[M-H]$^-$: 163, 119, 145, 177, 133, 312, 299	5.20	2.46	m
8.370	Kaempferol or cyanidin derivative	C$_{18}$H$_{16}$O$_7$	-	345.097	[M+H]$^+$: 345, 312, 329, 330, 287	0.29	2.30	e
8.508	Isorhamnetin derivative	C$_{19}$H$_{18}$O$_8$	-	375.1076	[M+H]$^+$: 375, 342, 245, 317, 360	0.53	13.48	e
9.156	Demethylnobiletin	C$_{20}$H$_{20}$O$_8$	-	389.1227	[M+H]$^+$: 389, 356, 331, 373, 359, 374	-1.03	4.90	d
9.342	Tetramethylquercetin	C$_{19}$H$_{18}$O$_7$	-	359.1127	[M+H]$^+$: 359, 326, 343, 360, 344, 301	0.56	1.54	m
9.992	Keampferol or quercetin derivative	C$_{24}$H$_{38}$O$_4$	-	391.2843	[M+H]$^+$: 149, 57, 71	0.00	4.97	e

[a]METLIN; [b]MassBank; [c]In-house database; [d]FooDB; [e]ReSpect; [m]Manual

The bacteril strains reported to be sensitive to CAPE are *S. aureus*, *Bacillus subtilis*, and *P. aeruginosa* (MICs: 62.5-125 µg/mL, 125-250 µg/mL, and 125-250 µg/mL, respectively) (*246*). The flavonoid quercetin and its derivatives are also reported to have antibacterial activity. For example its methylated derivative showed inhibition against MRSA (*247*). Inhibition of bio-film formation and growth of *E.coli* was also observed after incubation with extracts rich in quercetin derivatives or with the extracted pure molecules (*248*).

Some derivatives of kaempferol are also reported to have activity against both Gram-positive and Gram-negative bacteria. Reporting MICs in the range of 32-256 µg/mL for *S. aureus* and *P. aeruginosa* (*249*). Other flavonoids like cyanidin, isorhamnetin and diosmetin could also take part in the whole antibacterial activity (*250*).

5.3.7.4 Composition of pooled fraction 8

Data obtained from the analysis of pooled fraction 8 are showed in table 5.27. The dentified components were 16 including: eight HCAs (71 %), three flavonoids (7 %), three sugar derivatives (12 %) and two benzoic acid derivatives (10 %). The majority of the compounds were shared with fraction 3 which in part explains the antibacterial activity of this fraction. The components responsible for this fraction activity are probably the glycerol derivatives of caffeic acid, which represent the most abundant metabolites. Glycerol derivatives of caffeic acid comprise caffeoyl glycerol, 1-*O*-*p*-coumaroyl glycerol, 2-*O*-*p*-coumaroyl glycerol, dicaffeoyl glycerol, caffeoyl coumaroyl glycerol and feruloyl caffeoyl glycerol.

Table 5.27 HPLC-QTOF-MS analysis of pooled fraction 8 of *H. glomerata* $CHCl_3$/MeOH extract

t_R (min)	Compound	Calculated formula	Negative (m/z)	Fragments	Error (ppm)	Area (%)	Ref.
0.516	Sucrose	$C_{12}H_{22}O_{11}$	341.1081	179, 89, 119, 101, 161	-2.35	8.83	(*251*)
0.517	Quinic acid	$C_7H_{12}O_6$	191.0555	191, 85	-3.14	0.81	a
0.517	Trihydroxybutanoic acid	$C_4H_8O_5$	135.0293	75, 71, 115, 59, 135, 57, 45	-4.44	0.50	b
0.519	Tetrahydroxypentanoic acid	$C_5H_{10}O_6$	165.0395	75, 59	-6.06	1.05	b
0.977	Protocatechuic acid	$C_7H_6O_4$	153.0185	109	-5.23	5.12	(*244*), c
3.839	Caffeoyl glycerol	$C_{12}H_{14}O_6$	253.0705	161, 135, 253, 179	-5.14	14.22	(*43*)
4.309	2-*O*-*p*-coumaroyl glycerol	$C_{12}H_{14}O_5$	237.0765	145, 119, 163	-1.27	0.96	(*244*)
4.768	*p*-Coumaric acid	$C_9H_8O_3$	163.0398	119	-1.84	10.23	a
4.883	1-*O*-*p*-coumaroyl glycerol	$C_{12}H_{14}O_5$	237.0758	145, 119, 163	-4.22	6.24	a
5.802	Prunin	$C_{21}H_{22}O_{10}$	433.1127	161, 135, 253	-3.00	0.25	a, d
5.917	Quercetin-3-*O*-rutinoside	$C_{27}H_{30}O_{16}$	609.1434	300, 609	-4.43	0.23	a, d
6.064	Ferulic acid	$C_{10}H_{10}O_4$	193.0496	161, 134, 135	-5.18	1.41	a
6.836	Dicaffeoyl glycerol	$C_{21}H_{20}O_9$	415.1016	253, 161, 179, 135, 237	-4.58	37.82	(*43*)
7.065	Kaempferol	$C_{15}H_{10}O_6$	285.0395	NA	-3.51	0.03	a
7.295	Caffeoyl coumaroyl glycerol isomer	$C_{21}H_{20}O_8$	399.1072	163, 253, 119, 145, 135, 235, 179	-3.26	9.64	m
7.410	Feruloyl caffeoyl glycerol	$C_{22}H_{22}O_9$	429.1178	134, 193, 253, 235	-3.03	2.66	m

[a]In-house database; [b]FooDB; [c]METLIN; [d]MassBank; [m]Manual

228

p-Coumaric acid and protocatechuic acid are reported in good concentrations, and they might also take part in the antibacterial activity of this fraction. The identified flavonoids: quercetin and kaempferol, are reported to have antibacterial or antimicrobial effects. On the other hand, the presence of sugar derivatives might be affecting the growth of the bacteria enhancing their proliferation and therefore lowering the whole antibacterial effect.

5.3.7.5 Cytotoxicity screening of the CHCl$_3$/MeOH extract pooled fractions

Since the CHCl$_3$/MeOH extract resulted to have a good activity against PC3 and MCF7 cell lines, and because of its wider composition it was decided to test its fractions. They were screened against both cell lines in order to find out which fraction was the most active and, in this way, perform a biodirected study for the identification of cytotoxic compounds. The results of the screening are reported in figure 5.88.

MCF7 cells resulted to be sensible to both pooled fractions 3 and 4, at concentrations of 100 µg/mL (47.4 ± 3.9 % and 12.7 ± 1.9 %, viability percentage, respectively) and pooled fraction 4 at 50 µg/mL (33.5 ± 7.9 %, viability percentage) (Figure 5.88A). PC3 cells was sensible to pooled fraction 2, 3 and 4 at 100 µg/mL (33.8 ± 3.5 %, 25.4 ± 1.7 % and 15.8 ± 1.9 %, viability percentage respectively), while pooled fraction 4 at 50 µg/mL (48.8 ± 7.2 %, viability percentage) (Figure 5.88B).
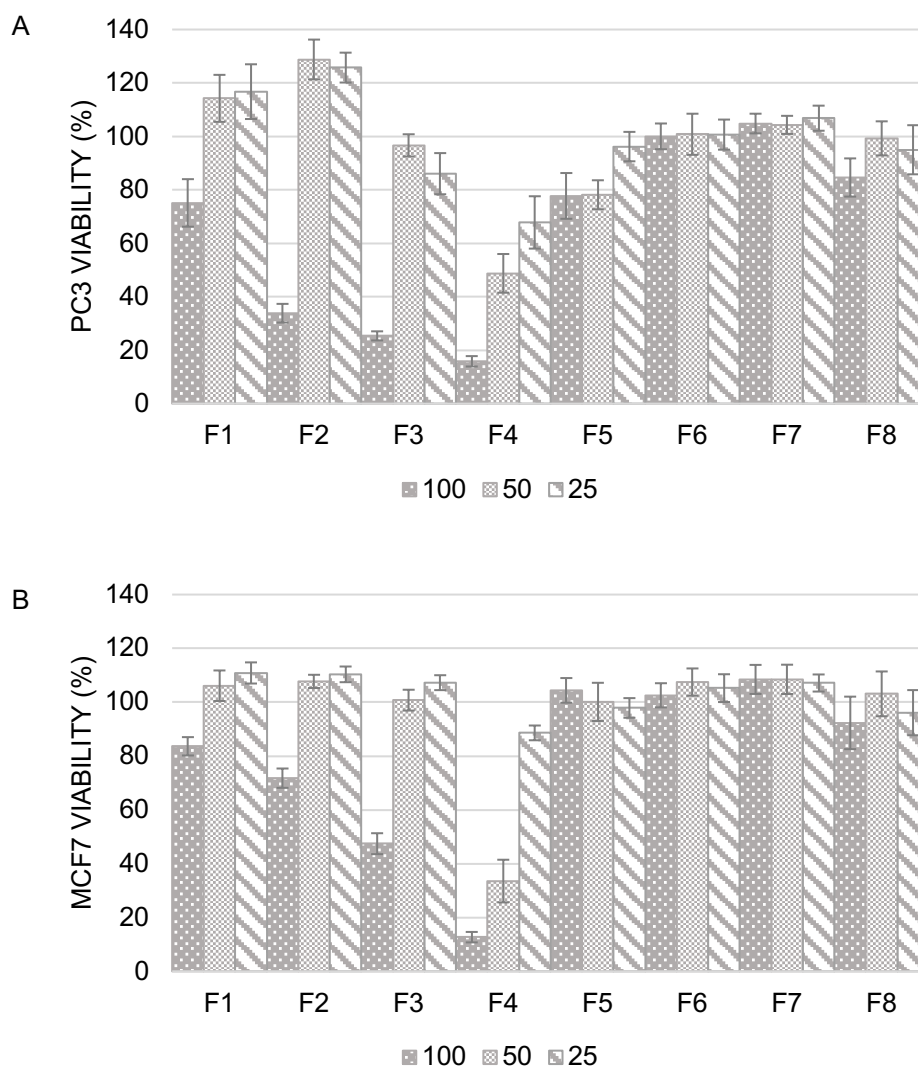
Figure 5.88 Viability for PC3 (A) and MCF7 (B) cells after 48h treatment with 100, 50 and 25 µg/mL of the macro-fractions of the CHCl₃/MeOH extract.

Results showed selectivity of pooled fractions 3 and 4 for both prostate and breast cancer cells pointing out their bioactive composition. Their contiguity also suggest that the active compounds must be shared among these two fractions and therefore implying a possible similitude in structure and properties of their components.

5.3.7.6 Composition of pooled fraction 4

Pooled fraction 4 was analyzed by UPLC-QTOF-MS, in both positive and negative mode identifying 22 compounds (Table 5.28), 16 compounds are shared with pooled fraction 3. The majority of them were PAs derivatives (56 %), including HCAs derivatives (45 %), coumarins (6 %), and benzoic acid derivatives (2 %) and a lignan: syringaresinol (3 %). It was also identified four flavonoids (27 %), a pigment (4 %) and a FA: palmitoleic acid (3 %) while two compounds is still unknown (10 %).

From identified compounds the cytotoxic activity of the fraction is partially explained. Phenolic compounds of extract are known to have the ability to form reactive oxygen species (ROs) in the culture medium, such as H_2O_2 that take part in the fraction toxicity (*252*). As already mentioned, caffeic acid and its derivatives are already been reported as part of the extract of other plants of family of Bromeliads taxonomically related to the genus *Hechtia* and to have cytotoxic activity on cancer cells. The same is reported for the CAPE to exert a potent and specific inhibition of nuclear transcription factor NF-kappa B (*253*). CAPE also inhibit the PI3K/Akt signaling pathway lowering cell survival (*254*). The majority of identified flavonoids in this fraction were already reported in the metabolomic profile of the plant (Section 5.2). Their biological activity was also investigated in the literature and already reported in the same section. The only new molecule is the demethylnobiletin, but its activity against cancer is still unknown.

Table 5.28 HPLC-QTOF-MS analysis of pooled fraction 4 of the CHCl₃/MeOH extract of *H. glomerata*

t_R(min)	Compound	Calculated formula	Negative (m/z)	Positive (m/z)	Fragments	Error (ppm)	Area (%)	Ref.
1.001	Protocatechuic acid	$C_7H_6O_4$	153.0189	-	[M-H]⁻: 109	-2.61	0.89	(*244*)
1.732	Salicylic acid	$C_7H_6O_3$	137.0239	-	[M-H]⁻: 93	-3.65	0.86	a, b
3.129	Caffeic acid	$C_9H_8O_4$	179.0342	-	[M-H]⁻: 135	-4.47	0.24	a
4.416	2-*O*-*p*-coumaroylglycerol	$C_{12}H_{14}O_5$	237.0768	239.0917	[M-H]⁻: 119, 145, 163; [M+H]⁺: 147, 119	5.48; 1.25	7.22	(*244*)
4.737	*p*-Coumaric acid	$C_9H_8O_3$	163.04	-	[M-H]⁻: 119	-0.61	6.05	(*245*)
4.990	1-*O*-*p*-coumaroylglycerol	$C_{12}H_{14}O_5$	237.0767	-	[M-H]⁻: 119, 145, 163	-0.42	12.18	c
5.384	Unknown	NA	-	275.1307	[M+H]⁺: 79, 197, 179, 135	ND	3.84	m
6.561	Dicaffeoyl glycerol isomer	$C_{21}H_{20}O_9$	-	417.117	[M+H]⁺: 163, 145, 237	-2.40	3.50	c
6.741	Dicaffeoyl glycerol	$C_{21}H_{20}O_9$	415.1044	417.1176	[M-H]⁻: 253, 161, 179, 135, 237 [M+H]⁺: 163, 145, 164, 237	-0.96; 2.17	14.53	(*43*)
7.063	Caffeoyl coumaroyl glycerol	$C_{21}H_{20}O_8$	399.1102	401.1221	[M-H]⁻: 163, 253, 119, 145, 135, 235, 179 [M+H]⁺: 147, 163, 145, 119	-2.49; 4.26	3.66	m
7.514	Naringenin derivative	$C_{24}H_{20}O_8$		437.1215	[M+H]⁺: 437, 177, 251, 147, 243, 221	-3.66	2.22	e
7.569	Malvidin	$C_{17}H_{14}O_7$	-	331.0805	[M+H]⁺: 331, 315, 298, 273, 281	-2.11	3.83	e
7.837	Chlorophyll derivative	NA	-	843.2336	[M+H]⁺: 843, 555, 844, 597, 556	ND	10.32	m
8.013	Unknown	$C_{19}H_{18}O_9$	-	391.1019	[M+H]⁺: 391, 361, 389, 375, 358	-1.28	2.70	m
8.014	Coumarin isomer	$C_9H_6O_2$	-	147.0438	[M+H]⁺: 91, 119, 147, 65	-2.04	1.84	m
8.168	Coumarin derivative	$C_{20}H_{22}O_6$	-	359.1488	[M+H]⁺: 147, 119	-0.28	5.32	m
8.215	3-(4-Hydroxyphenyl) propyl coumarate	$C_{18}H_{18}O_4$	297.1151	-	[M-H]⁻: 119, 145, 163 [M+H]⁺: 107, 147, 135	6.39; 1.34	4.33	m

Table 5.28 HPLC-QTOF-MS analysis of pooled fraction 4 of the CHCl3/MeOH extract of *H. glomerata* (Continued)

t_R(min)	Compound	Calculated formula	Negative (m/z)	Positive (m/z)	Fragments	Error (ppm)	Area (%)	Ref.
8.297	3-(4-Hydroxyphenyl-3-methoxy) propyl coumarate	$C_{19}H_{20}O_5$	327.1255	-	[M-H]⁻: 163, 119, 145, 177, 133, 312, 299	5.20	3.02	m
8.370	Kaempferol or cyanidin derivative	$C_{18}H_{16}O_7$	-	345.097	[M+H]⁺: 345, 312, 329, 330, 287	0.29	3.37	e
8.784	Palmitoleic acid	$C_{16}H_{30}O_2$	-	255.2318	[M+H]⁺: 69, 67, 83, 55, 81, 97, 95, 71, 43, 135, 93, 121, 107, 97, 149, 67, 109	-0.39	1.71	m
9.156	Demethylnobiletin	$C_{20}H_{20}O_8$	-	389.1227	[M+H]⁺: 389, 356, 331, 373, 359, 374	-1.03	5.74	d
9.453	Syringaresinol	$C_{21}H_{22}O_9$	-	419.1342	[M+H]⁺: 419, 389, 371, 420, 390	1.19	2.63	m

[a]METLIN; [b]MassBank; [c]In-house database; [d]Foodb; [e]ReSpect; [m]Manual.

5.3.7.7 Cytotoxicity of *p*-coumaric acid and caffeic acid

Since *p*-Coumaric and caffeic acid were isolated from the active fractions of the $CHCl_3$/MeOH extract they were tested for their cytotoxic activity against MCF7 and PC3 cell (Table 5.29). Caffeic acid was the most active showing IC_{50} of 68.8 ± 12.2 and 91.5 ± 5.3 µg/mL against PC3 and MCF7 respectively. Instead *p*-coumaric acid showed an IC_{50} of 179.9 ± 31.6 µg/mL for PC3 cells, but no activity was shown towards MCF7.

Caffeic acid resulted extremely sensible to the ambience conditions once dissolved in the culture medium change the colour of the medium signalling of its decomposition. This kind of behaviour was already described for the molecule as the formation of reactive oxygen species (ROs) (*255*).

Table 5.29 Cytotoxic activity of *p*-coumaric and caffeic acid

Compound	IC_{50} (µg/mL)	
	MCF7	PC3
p-Coumaric acid	>100	179.9 ± 31.6
Caffeic acid	91.5 ± 5.3	68.8 ± 12.2

It is important to point out that the high standard deviation obtained in some cases from the assays is probably due to random fluctuation in the cellular growth. This caused some of the experiments to be inconsistent and to somehow affect results of experiments.

5.4 Microarray analysis

5.4.1 Genetic expression of PC3 cells treated with *p*-coumaric acid

Genes (35,764) were monitored during the microarray analysis of PC3's RNA, and a total of 25,606 genes gave a variation of Zscore. Figure 5.89 showes the fluorescence observed from the chip after hybridization. Green fluorescence is given by the genes expressed for the treated cells, red fluorescence comes from the genes expressed for the control, and the yellow fluorescence is given by both treated and untreated cells.

Figure 5.89 Fluorescence emitted by the hybridized H35K chip: treated cells (green), untreated cells (reed) and both (yellow)

The up or down-regulated genes represent the response of PC3 cells to the *p*CA treatment. From the observed genes 16,936 had a Zscore < +1 and > -1, while 2751 had a Zscore ≤ +1.5 and ≥ +1, and finally 1524 and 424 had a Zscore ≥ +1.5 and ≥ +2 respectively. Instead 2706 had a Zscore ≥ -1.5 and ≤ -1, while 1689 and 394 had a Zscore ≤ -1.5 and ≤ -2 respectively. The dispersion plot of the obtained genes is reported in figure 5.90. These results

were submitted to a statistical evaluation in order to assess their divergence

from the house-keeping genes (Zscore = 0).
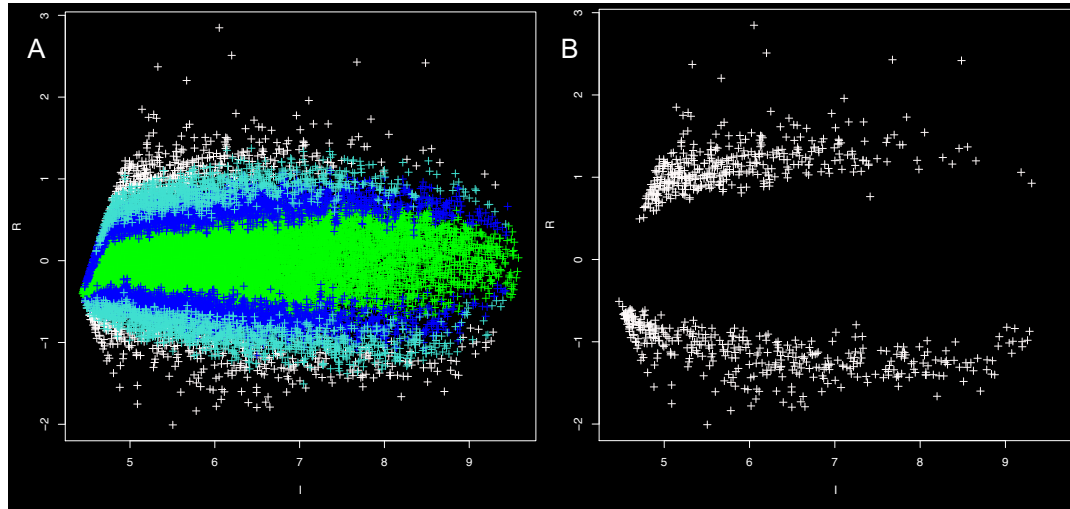
Figure 5.90 A) Dispersion plot of all monitored genes: -1< Zscore <+1 (green crosses); +1≤ Zscore ≥+1.5 and -1.5≤ Zscore ≤-1 (blue crosses); Zscore ≥ +1.5 and ≤ -1.5 (light blue crosses); Zscore ≥ +2 and ≤ -2 (white crosses). B) Dispersion plot of genes with Zscore ≥ +2 and ≤ -2

Since the genes with Zscore ≥ +2 and ≤ -2 (white crosses) are the most

different (P>0.05) from the data mainstream, they represent the most relevant

change in the cellular genetic expression. For this reason and for simplicity,

only these genes will be considered in the data analysis. The dispersion plot

obtained from the statistical analysis of all genes based on their Zscore is

showed in figure 7.88. See appendix for the full lists of genes with Zscore ≥ +2

and ≤ -2.

5.4.2 Bioinformatics analysis

Selected lists of genes were submitted to DAVID bioinformatics web

database. This recognized 230 up-regulated genes and 201 down-regulated

genes. The functional annotation results of the up-regulated and down-

regulated genes were grouped in clusters based on the class of proteins they encoded. This way the principal characteristics of the identified genes and the pathways they affected were highlighted.

5.4.2.1 Up-regulated genes

The principal identified up-regulated genes are involved in the regulation of transcription, protein activation, DNA-binding. Most of these genes encode for Zn-fingers or for protein kinases and are found in the nucleus. Other genes regulate angiogenesis, ubiquitination, protein conjugation, and cell adhesion. Certain genes also regulate cellular stress-related processes, such as stress and inflammation responses, DNA repair, cell survival and also cellular proliferation. Some of the most interesting clusters of genes are reported in figure 5.91.
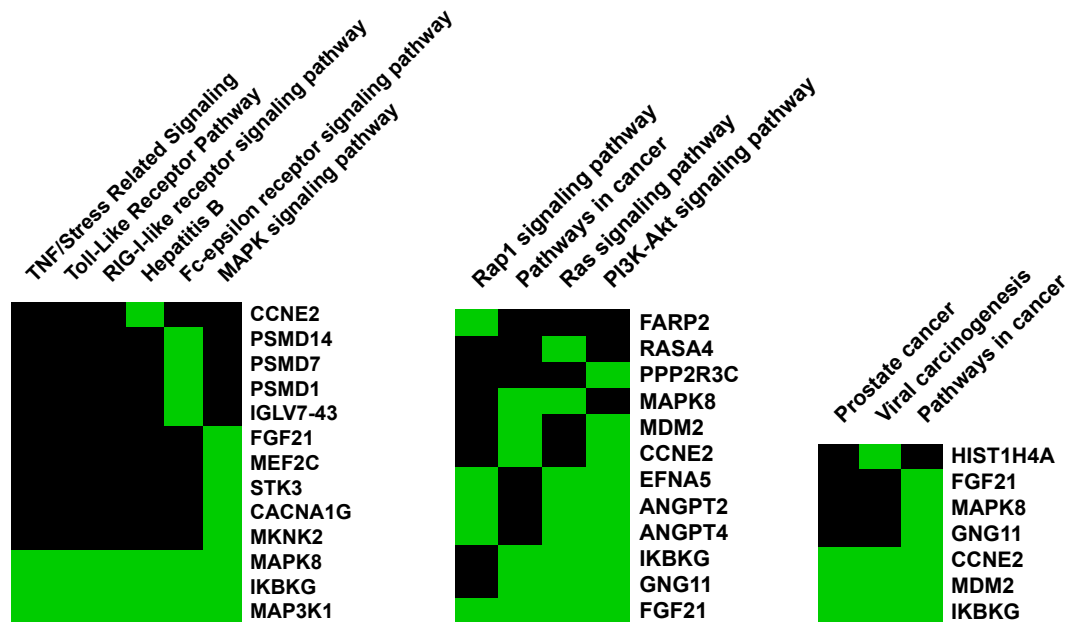
Figure 5.91 Most interesting up-regulated genes clusters (Enrichment Score > 1)

From the project point of view, the most important genes of these clusters are the inhibitor of nuclear factor κ B kinase regulatory subunit γ (IKBKG/NEMO), the mitogen activated protein kinase 8 (MAPK8/JNK1), the mitogen activated protein 3 kinase 1 (MAP3K1/MEKK1), the proto oncogene MDM2, the angioproteins 2 and 4 (ANGPT2/4), the Ras GTPase-activating protein 4 (RASA4), Ser/Thr kinase 3 (STK3), cyclin E2 (CCNE2), voltage-dependent T-type Ca channel subunit α-1G (CACNA1G), G protein subunit γ 11 (GNG11), ephrin-A5 (EFNA5), myocyte enhancer factor 2C (MEF2C), MAP kinase-interacting Ser/Thr-protein kinase 2 (MKNK2) and Ser/Thr-protein phosphatase 2A regulatory subunit B" subunit γ (PPP2R3C).

IKBKG encodes a protein also known as NEMO a Zn-finger which is essential in the modulation of the NF-kB signalization pathway. In fact, this protein is the regulatory subunit of the IKK core complex and phosphorylates the NF-kB inhibitor deactivating it. This activates many signalization pathways such as inflammation, immunity, differentiation, cell growth, tumorigenesis and apoptosis (*256*). MAPK8 or JNK1 is a Ser/Thr kinase involved in various biological processes like cell proliferation, differentiation, migration, transformation and programmed cell death. It was reported that, in cancer, this protein pathway to cell apoptosis is stimulated by antioxidant compounds like flavonoids (*257*). MAP3K1 also known as MEKK1 is a protein kinase part of a transduction cascade that activates the ERK and MAPK8 pathways. It is also involved in the activation of the kinases of CHUK and IKBKB which are part of the NF-kB pathway (*258, 259*). MDM2 is a ubiquitin ligase that mediates the ubiquitination of p53 and consequently its proteasome degradation. Furthermore, it inhibits p53-mediated cell cycle arrest and apoptosis by

binding its transcriptional activation domain (*260*). The RING type region of the MDM2 protein is a Zn-finger that if mutated causes the loss of the ubiquitination activity of this protein (*261*). ANGPT2 is a glycoprotein which can interact with the vascular endothelial growth factor (VEGF) to facilitate endothelial cells migration and proliferation. This protein can induce the loosening of the cell-matrix contact and cause consequent apoptosis and vascular regression (*262*). ANGPT4 is also a glycoprotein and is the main ligand of the transmembrane receptor protein Tyr-kinase (TEK/TIE2) activator. It also promotes endothelial cell survival, migration and angiogenesis (*263*). RASA4 or CAPRI encodes for Ras, a Ca^{2+}-dependent GTPase activating protein which regulates the Ras-MAPK pathway (*264*). This is also known as MAPK/ERK cascade, can be involved in many cellular processes based on the cellular context. These processes comprise cell growth, adhesion, survival and differentiation through the regulation of transcription, translation and cytoskeletal rearrangements (*265*). STK3/MST2 is a stress activated, pro-apoptotic Ser/Thr-kinase. This protein may also take part in the activation of the oncoprotein YAP1 which in turns migrate in the nucleus and regulates the expression of genes important for cell proliferation, death and migration (*266*). G1/S-specific Cyclin E2 is essential for the regulation of late G1 and early S cellular phase. It regulates cyclin-dependent Ser/Thr kinase binding and activity, it is also involved in cell division and initiation of DNA replication (*267*). Another important function of this protein is telomere maintenance which include: maintain proper telomeric long and structure, replicate and repair the telomeric DNA sequences (*268*). CACNA1G is a low-voltage-activated (LVA) channel which mediates the entrance of Ca^{2+} ions into the cytoplasm. It is in

fact involved in a variety of Ca-dependent processes among which are gene expression, cell motility, growth, division, and death (*269*). Guanin nucleotide-binding protein subunit γ is a G protein involved in several transmembrane signaling systems. The γ chain is required for GTPase activity and regulates cellular senescence (*267, 270*). Ephrin-A5 is glycophos-phatidylinositol (GPI) -bound ligand for Eph-receptors, which are Tyr-kinase crucial for cell migration, repulsion, adhesion (*271*). MEF2C is a transcription factor part of a family of proteins that are associated with the development of many diseases. It is associated with various pathways of signalization such as Ca^{2+} signaling, MAP kinase signaling, Wnt signaling, PI3K/AKT signaling among others (*272*). The Wnt pathway regulates the development in many cancer types (*273*), while the PI3K/AKT pathway components are responsible for the regulation of cell survival, cell cycle progression and cellular growth. These signalization pathways are usually altered in cancer (*274*). MKNK2 is Ser/Thr-kinase that could play a role in the response to environmental stress, and is also involved in the phosphorylation of the eukaryotic initiation factor 4E (eIF4E) which promotes tumorigenesis and prostate cancer progression (*275, 276*). MKNK2 is also implicated in the pro-survival response in drug resistance (*277*). PPP2R3C is Ca^{2+}-binding Ser/Thr-kinase regulatory subunit, and it is part of a phosphatase protein complex that inhibits the function of P-glycoprotein/ABCB1. The latter is a molecule involved in cancer multidrug resistance (*278*).

5.4.2.1.1 Affected pathways

The analyzed clusters reported some pathways in which the up-regulated genes are found (Table 5.30). The majority of these affected pathways correspond to cancer-related biological processes.

Table 5.30 Pathways affected by the selected up-regulated genes

Term	Count	%	Genes
Epstein-Barr virus infection	6	2.61	PSMD14, PSMD1, IKBKG, MDM2, MAPK8, PSMD7
Ras signaling pathway	8	3.48	IKBKG, GNG11, EFNA5, MAPK8, FGF21, ANGPT2, ANGPT4, RASA4
MAPK signaling pathway	8	3.48	MEF2C, MAP3K1, IKBKG, MKNK2, CACNA1G, MAPK8, FGF21, STK3
PI3K-AKT signaling pathway	9	3.91	CCNE2, IKBKG, MDM2, GNG11, EFNA5, FGF21, ANGPT2, ANGPT4, PPP2R3C
Ubiquitin mediated proteolysis	5	2.17	UBE2A, MAP3K1, MDM2, MID1, UBE2U
Proteasome	3	1.30	PSMD14, PSMD1, PSMD7
Prostate cancer	3	1.30	MDM2, CCNE2, IKBKG
Pathways in cancer	6	2.61	MAPK8, MDM2, CCNE2, IKBKG, GNG11, FGF21
Rap1 signaling pathway	5	2.17	FARP2, EFNA5, ANGPT2, ANGPT4, FGF21
Toll-like receptors pathway	3	1.30	MAPK8, IKBKG, MAP3K1
TNF/stress related signaling	3	1.30	MAPK8, IKBKG, MAP3K1
RIG-I-like receptor pathway	3	1.30	MAPK8, IKBKG, MAP3K1
Hepatitis B	4	1.75	MAPK8, IKBKG, MAP3K1, CCNE2
Fc-ε receptor signaling pathway	7	3.05	MAPK8, IKBKG, MAP3K1, PSMD14, PSMD7, PSMD1, IGLV7-43

The pathways were identified by DAVID bioinformatics in the KEGG database.

Among the most important pathways affected by the *p*CA treatment are the PI3K/AKT signaling pathway (Figure 5.92). In this pathway nine genes were upregulated in response to the treatment: FGF21, ANGPT2, ANGPT4, EFNA5, GNG11, MDM2, IKBKG, CCNE2 and PPP2R3C.
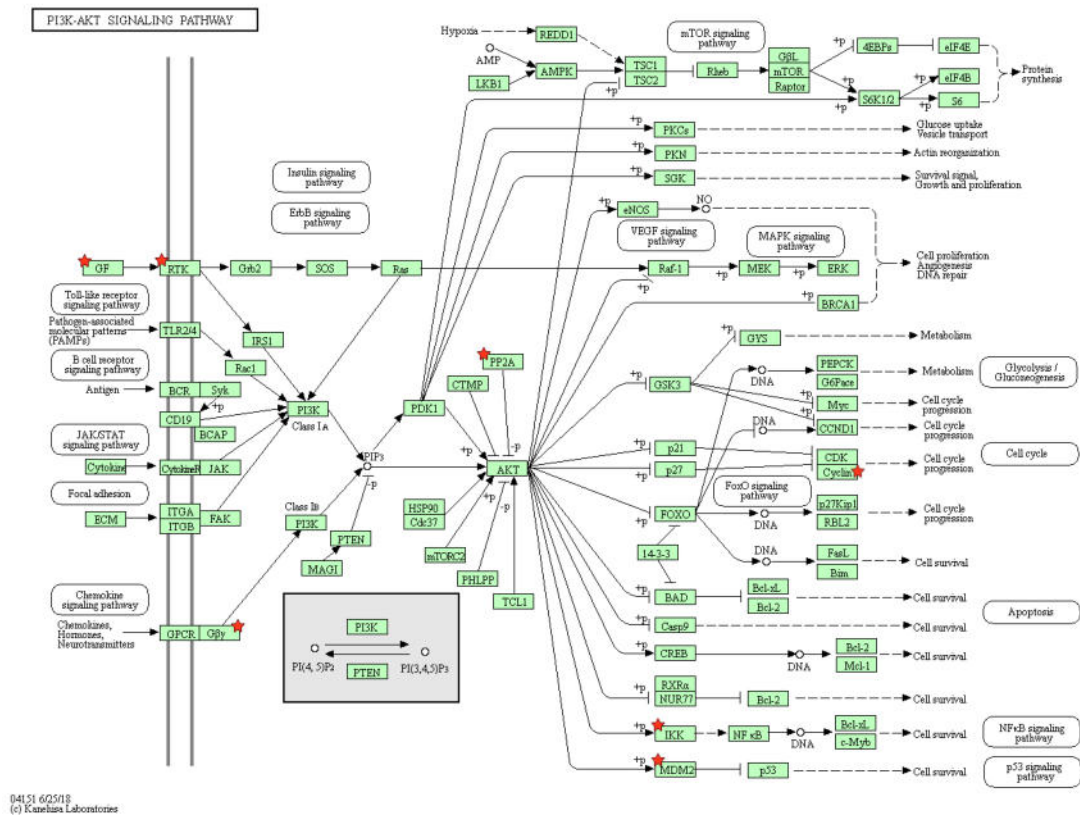
Figure 5.92 PI3K/AKT signalling pathway: GF) FGF21, ANGPT2, ANGPT4, EFNA5; RTK) FGF21; Gβγ) GNG11; MDM2) MDM2; IKK) IKBKG; Cyclin) CCNE2; PP2A) PPP2R3C. The up-regulated components of the pathway are marked with a red star.

As already mentioned, this pathway is involved in the regulation of cell survival, cell cycle progression and cellular growth. Some of the reported genes are found upstream of the pathway like FGF21, ANGPT2/4, EFNA5, GNG11 and PPP2R3C. These proteins are able to control the pathway in a general way, affecting a wider variety of components and processes. The effect of their up regulation could be reflected in any of the signalization outcome, form cell metabolism and nutrients uptake to cell survival and proliferation. Instead other genes like MDM2, IKBKG and CCNE2 are found more downstream of the pathway. MDM2 is involved in the p53 signaling pathway, while IKBKG regulates the NF-kB signaling pathway and therefore in cell survival. Finally, CCNE2 affects the cell cycle progression.

242

Another identified pathway is the MAPK signaling pathway, which contains eight up-regulated genes: FGF21, CACNA1G, MKNK2, IKBKG, MAP3K1, STK3, MAPK8 and MEF2C (Figure 5.93).
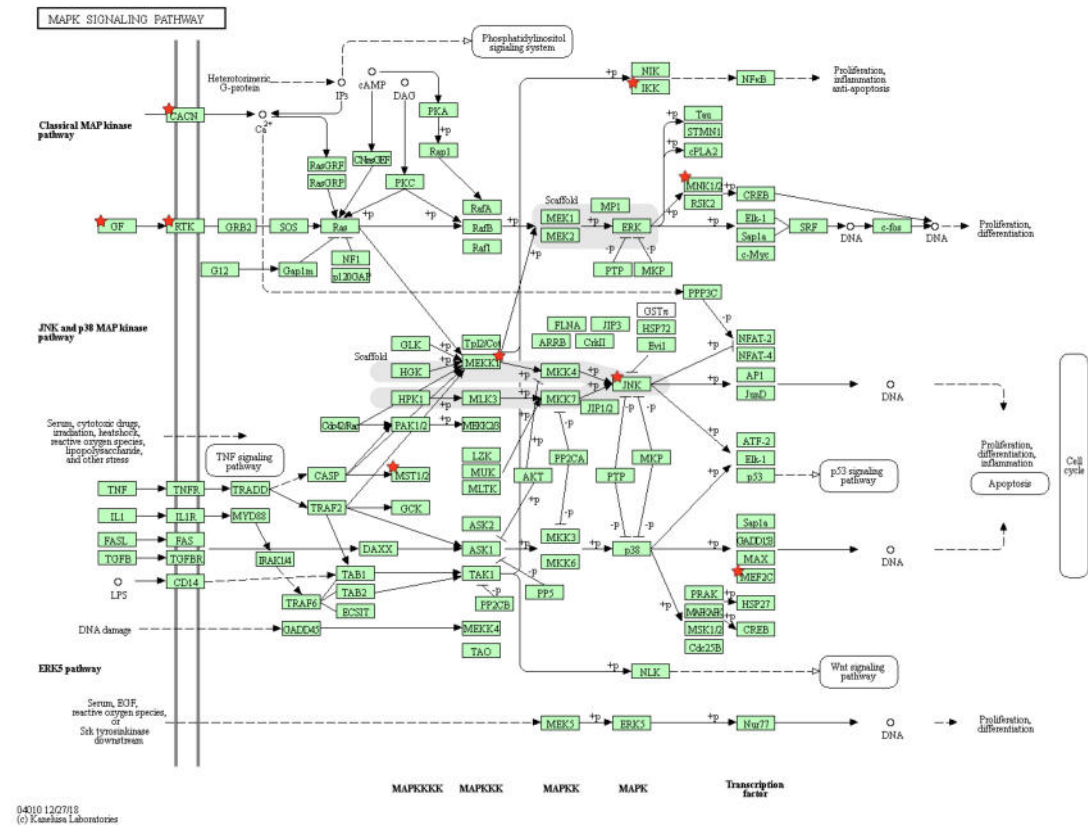
Figure 5.93 MAPK signalling pathway: GF, RTK) FGF21; CACN) CACNA1G; MNK1/2) MKNK2; IKK) IKBKG; MEKK1) MAP3K1; MST1/2) STK3; JNK) MAPK8; MEF2C) MEF2C. The up-regulated components of the pathway are marked with a red star.

The affected genes found most upstream in this pathway are FGF21 and CACNA1G. In this signalization route these genes seem to be associated with cell proliferation, differentiation and inflammation. But these might also activate other pathways like the phosphatidylinositol signaling system and the Ras signaling pathway. Meanwhile STK3, MAP3K1, MAPK8, IKK and MKNK2 are kinases involved in the in the phosphorylation and therefore activation/inactivation of other components of the pathway. Of these proteins

243

the ones reported more downstream can also interact with both kinases and transcription factors. For example, IKBKG can activate NF-κB and MKNK2 activates CREB which regulate cell proliferation, differentiation, inflammation and anti-apoptotic processes. Instead MEF2C is a transcription factor which may be activated indirectly by MAPK8, MAP3K1 and all the peripheral membrane proteins. This protein directly interacts with DNA and regulates apoptosis and cell cycle. The same outcome can be obtained by MAPK8. The Ras signaling pathway is also among the treatment affected pathways, comprising eight up-regulated genes: FGF21, ANGPT2, ANGPT4, EFNA5, GNG11, RASA4, IKBKG and MAPK8 (Figure 5.94).
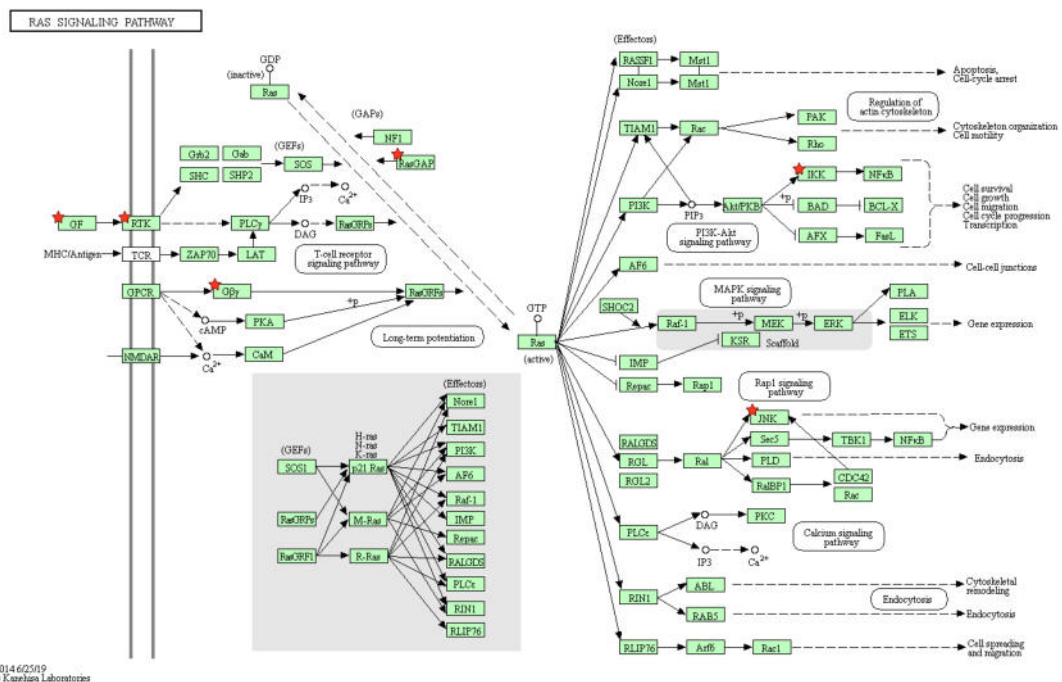
Figure 5.94 Ras signalling pathway: GF) FGF21, ANGPT2, ANGPT4, EFNA5; RTK) FGF21; Gβγ) GNG11; RasGAP) RASA4; IKK) IKBKG; JNK) MAPK8. The up-regulated components of the pathway are marked with a red star.

The same genes as the past two pathways are reported upstream of the actual one: FGF21, ANGPT2, ANGPT4, EFNA5. Instead GNG11 in this

case is implicated in the regulation of the Ras activator RasGRPs that activates Ras which is the central node of this pathway. Another important overexpressed component of the Ras pathway is RasGAP which is a protein that also regulates de activity of Ras. In fact, this protein is able to switch Ras off through the activation of GTPase which changes Ras from GTP-bound to GDP-bound. Meanwhile, MAPK8 is involved in the regulation of gene expression and IKBKG in cell survival, growth, migration, cell cycle progression and transcription.

Other important pathways affected by the *p*CA are the pathways in cancer, in which six genes were found up-regulated: GNG11, MDM2, CCNE2, FGF21, IKBKG and MAPK8 (Figure 5.95).
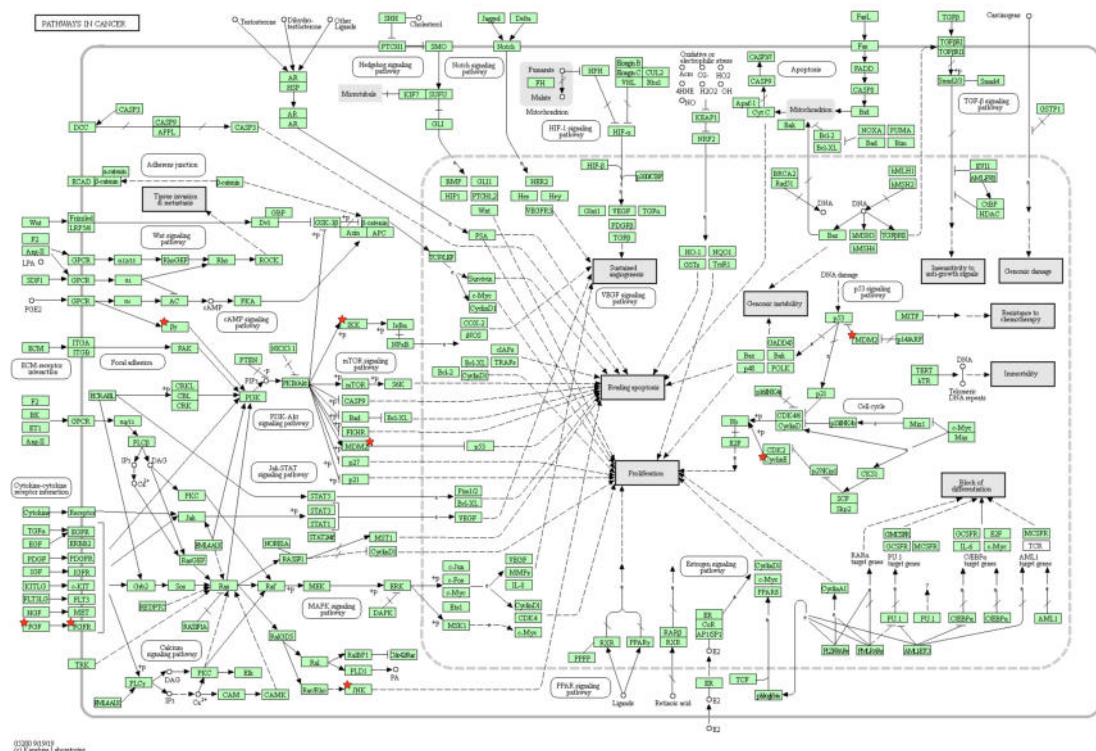
Figure 5.95 Pathways in cancer: GF) FGF21, ANGPT2, ANGPT4, EFNA5; RTK) FGF21; Gβγ) GNG11; RasGAP) RASA4; IKK) IKBKG; JNK) MAPK8. The up-regulated components of the pathway are marked with a red star.

Of these genes the most upstream are growth factors (GF) and GF receptors like FGF21. These proteins could also indirectly activate Ras which in turns could activate MAPK8 and lead to the cell evasion from apoptosis. Meanwhile In this pathway GNG11 is reported to regulate the activity of PI3K and consequently IKBKG and MDM2 which cause the apoptosis evasion. Also, the activity of MDM2 can be derived from DNA damage and reparation, while cyclin E2 is responsible for cellular proliferation.

The last affected pathway that was considered interesting is the prostate cancer pathway. Only three genes of this path were found up-regulated: MDM2, IKBKG and CCNE2 (Figure 5.96).
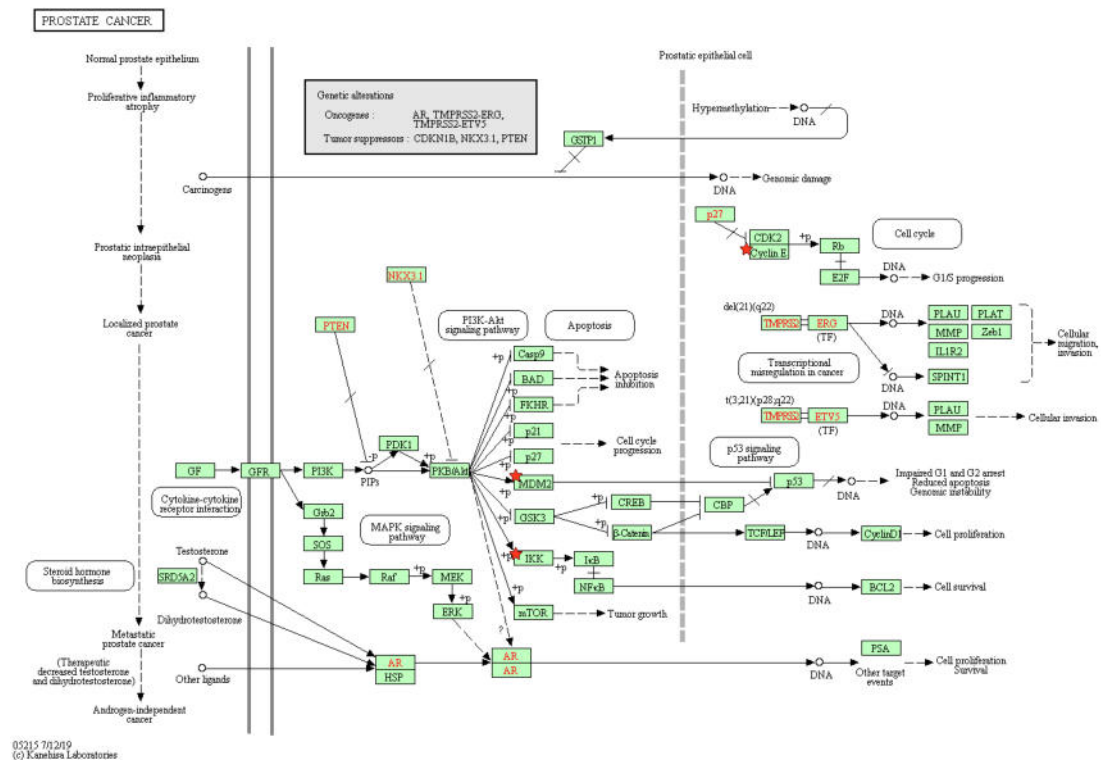
Figure 5.96 Prostate cancer: MDM2) MDM2; CyclinE) CCNE2; IKK) IKBKG. The up-regulated components of the pathway are marked with a red star.

In this route the activity of MDM2 is also correlated to the inactivation of the tumor suppressor p53, which causes the impaired G1 and G2 arrest, reduced apoptosis and genomic instability. Meanwhile IKBKG, through the regulation of NF-κB and indirectly of Bcl-2 regulates genetic expression and cell survival. Cyclin E2 is involved in the cell cycle inducing G1/S phase progression.

5.4.2.2 Down-regulated genes

The principal down-regulated genes are G-coupled receptors, kinases, transferases, protooncogenes and signal transducers. They regulate cell-cell adhesion, protein activation by phosphorylation, protein folding, cell survival, cell growth, proliferation, angiogenesis, migration and invasion, apoptosis and are either peripheral or transmembrane proteins. Some genes are also responsible for the olfactory and sensory transduction and were also found multiple Zn-fingers and transcription factors. The cluster more important for cancer is reported in figure 5.97. Among the down-regulated genes the most interesting are the caspase-9 (CASP9), G2/mitotic-specific cyclin-B2 (CCNB2), Ser/Thr-protein kinase Chk1 (CHEK1), fibroblast growth factor receptor 2 (FGFR2), RAC-β Ser/Thr-protein kinase (AKT2), protein MDM4 (MDM4), NT-3 growth factor receptor (NTRK3), 6-phosphofructo-2-kinase/fructose-2,6-bisphosphatase 2 (PFKFB2), ATP-dependent 6-phospho-fructokinase, platelet type (PFKP), Solute carrier family 2, facilitated glucose transporter member 4 (SLC2A4) and Ser/Thr-protein kinase 11 (STK11).
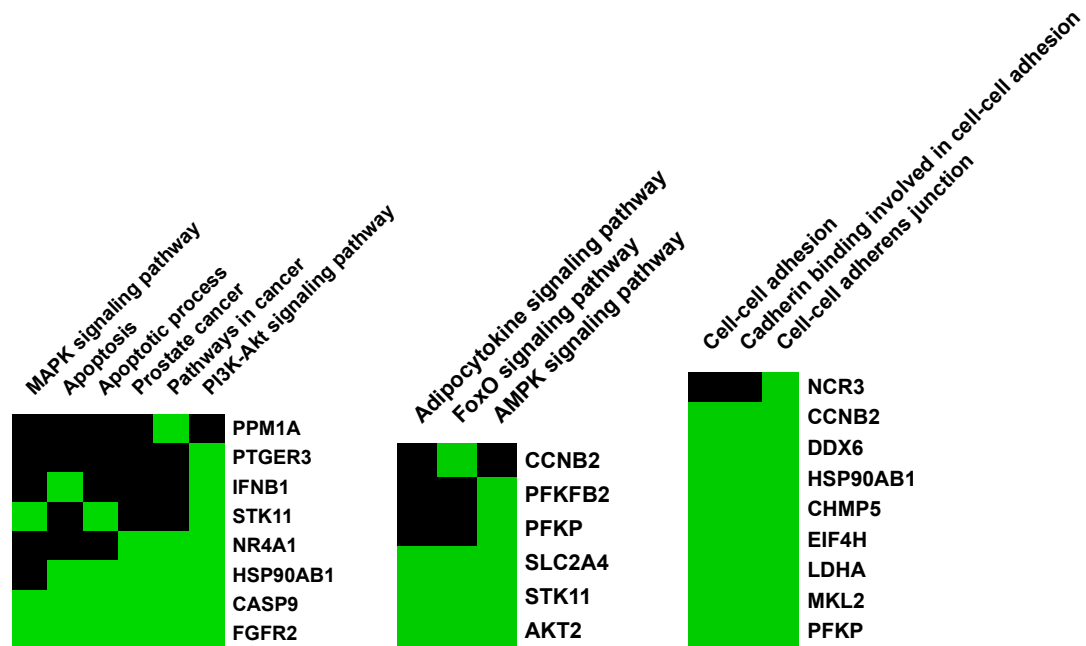
Figure 5.97 Most interesting down-regulated genes clusters (Enrichment Score > 1)

Caspase-9 is a protein involved in the activation of the caspases cascade that leads to the activation of apoptosis promoted by DNA damage (*279*). It has a Cys-type endopeptidase activity which regulates the apoptotic process and signaling. Caspase-9 is also involved in the response to drug and harsh environmental conditions (*280*). Cyclin B2 is an essential regulator for the G2/M transition (mitosis), which activates cyclin-dependent Ser/Thr-protein kinases (*267*). By extension this protein regulates also cell division and growth.

CHEK1 is a Ser/Thr-protein kinase required for cell cycle arrest and DNA repair caused by persistent DNA damage or lack of replication. It is involved in the apoptotic process, transcription maintenance, protein phosphorylation, and regulation of signal transduction by p53 class mediator (*281*, *282*). FGFR2 is a cell surface receptor with Tyr-protein kinase activity essential in the regulation of cell proliferation, differentiation, migration and

apoptosis (*283*). This protein also mediates the activation of Ras, MAP kinase and AKT signaling pathways and is down regulated by ubiquitination. The fibroblast growth factor receptor malfunction is also associated with cancer pathologies (*284*). AKT2 is one of three closely related isoforms (AKT1, AKT2 and AKT3) of Ser/Thr-protein kinases called AKT kinases. These proteins regulate many cellular processes such as metabolism, cell proliferation, survival, growth, angiogenesis and programmed death. They phosphorylate a wide range of downstream substrates, of these more than a 100 have been identified (*285*). MDM4 inhibits p53 and p73-mediated cell cycle arrest and apoptosis and it can reverse MDM2 degradation of apoptosis (*286*). This protein is activated in response to DNA damage, hypoxia and cell population growth, having a negative effect on apoptosis, cell cycle arrest and proliferation (*287*). NTRK3 is a single transmembrane α-helix receptor Tyr kinase, which activates many pathways of signalization including: AKT and MAPK pathways that control cell survival and differentiation (*288*). The protein also regulates cell migration and multiple nervous system-related functions (*289*). PFKFB2 is an enzyme that regulates fructose 2,6-bisphosphate degradation. It responds to the presence of sugar and is part of the glycolysis process (*267*). This protein is also reported to be activated and overexpressed in the AKT signaling pathway in prostate cancer among others (*290, 291*). PFKP is a protein which activity is the phosphorylation of D-fructose 6-phosphate to fructose 1,6-bisphosphate using ATP as phosphate donor. This process consists in the first step of glycolysis and it was found that silencing the genes that activate the transcription of the PFKP gene promotes prostate cancer aggressiveness (*292*). In tumor hypoxia PFKP and PFKFB2 are often

upregulated, which seems contrary to *in vitro* conditions and after the *p*CA treatment. These proteins have crucial roles in the development of malignant tumors since they are rate-limiting enzymes in glycolysis. In addition to tumor growth they also participate in cancer metastasis regulating the transcription of oncogenes (*293*). SLC2A4 is insulin regulated facultative glucose transporter which eliminates glucose from circulation. It also responds to the tumor necrosis factor (TNF) and it is reported to be central in the protein-protein interaction (PPI) network necessary for prostate cancer genesis (*294*). Last but not least STK11 is a tumor suppressor Ser/Thr-protein kinase which is involved in the regulation of the AMP-activated protein kinase (AMPK) members (*295*). Because of its function this protein plays a role in cell metabolism, cell polarity, apoptosis and DNA damage response. STK11 also mediates the p53-dependent apoptosis through the interaction with p53, as a result of this interaction it translocates into the mitochondrion during apoptosis to regulate the apoptotic process (*296*). It was reported that STK11 expression loss or reduction is a crucial step in prostate cancer development and prediction of therapeutic response (*297*).

5.4.2.2.1 Affected pathways

Some pathways were found to be affected by the *p*CA treatment and some of them were also found in the genes' clusters (Table 5.31). All the pathways described herein are related to cancer, some of them were not found in the KEGG database and therefore were not included.

250

The first important pathway is the PI3K/AKT signaling pathway, comprising seven down-regulated genes: AKT2, CASP9, FGFR2, HSP90AB1, IFNB1, NR4A1 and STK11 (Figure 5.98).

Table 5.31 Pathways affected by the selected down-regulated genes

Term	Count	%	Genes
Apoptosis	4	2.00	STK11, CASP9, FGFR2, AKT2
Apoptotic process	4	2.00	NR4A1, CASP9, FGFR2, AKT2
MAPK signaling pathway	4	2.00	AKT2, FGFR2, NR4A1, PPM1A
PI3K-AKT signaling pathway	7	3.50	AKT2, CASP9, FGFR2, HSP90AB1, IFNB1, NR4A1, STK11
Pathways in cancer	5	2.50	AKT2, CASP9, FGFR2, HSP90AB1, PTGER3
Central carbon metabolism in cancer	4	2.00	AKT2, FGFR2, NTRK3, PFKP
Prostate cancer	4	2.00	AKT2, CASP9, FGFR2, HSP90AB1
Adipocytokine signaling pathway	3	1.50	SLC2A4, STK11, AKT2
FoxO signaling pathway	4	2.00	CCNB2, SLC2A4, STK11, AKT2
AMPK signaling pathway	5	2.50	PFKB2, AKT2, PFKP, STK11, SLC2A4
Cell-cell adhesion	8	4.00	CCNB2, DDX6, HSP90AB1, CHMP5, LDHA, EIF4H, MKL2, PFKP
Cadherin binding involved in cell adhesion	8	4.00	CCNB2, DDX6, HSP90AB1, CHMP5, LDHA, EIF4H, MKL2, PFKP
Cell-cell adhesion junction	9	4.50	NCR3, CCNB2, DDX6, HSP90AB1, CHMP5, LDHA, EIF4H, MKL2, PFKP
p53 signaling pathway	4	2.00	MDM4, CASP9, CHEK1, CCNB2

The described pathways were identified by DAVID bioinformatics in the KEGG database.

The most upstream down-regulated gene of this pathway is IFNB1, this gene which encodes for the interferon β which as anticancer activities (*298*). This protein interacts with cytokine receptor and may activate PI3K and consequently AKT. This could allow the cascade to regulate multiple processes, from metabolic like protein synthesis, glucose uptake and glycolysis, to actin reorganization. Also, the downregulation of this gene could affect the cellular cycle progression and apoptosis and finally it could regulate other pathways such as NFκB and p53 signaling pathways. Similar effects should be observed from the downregulation of FGFR2, which affects,

throughout interaction with Ras: cell proliferation, angiogenesis and DNA repair. Other down-regulated genes from this PI3K/AKT pathway are HSP90AB1 and STK11.
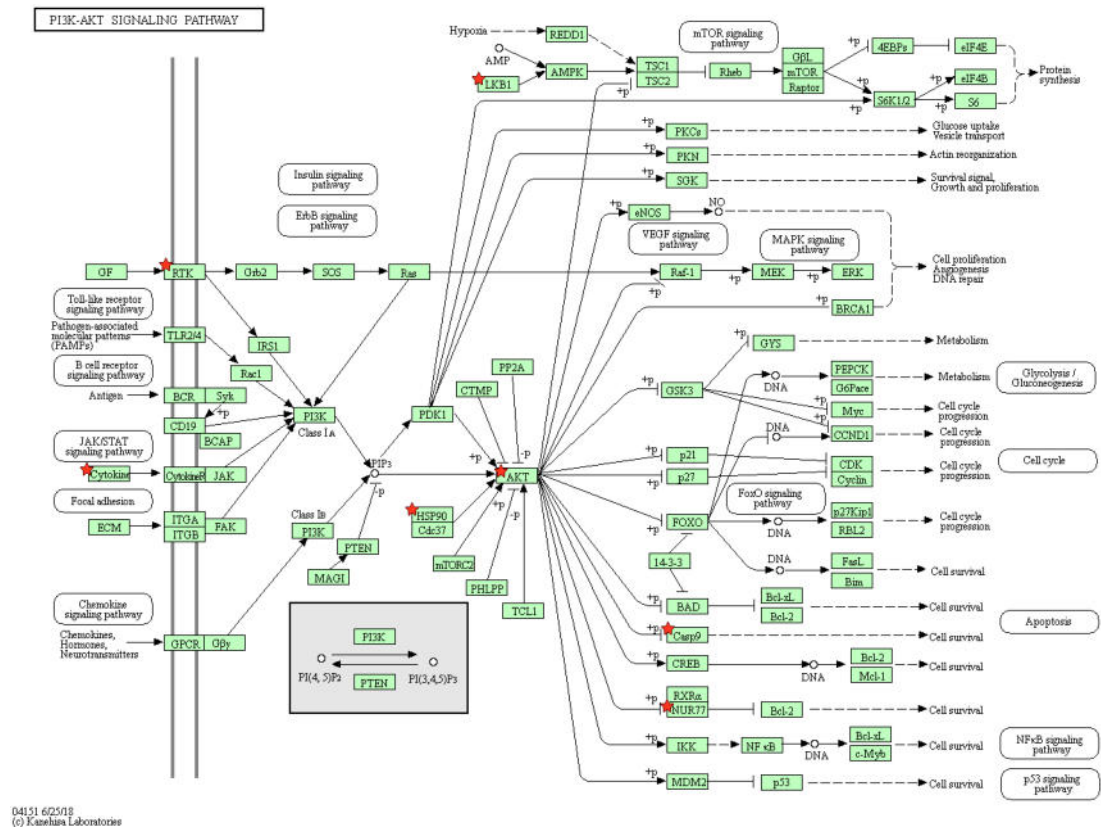
Figure 5.98 PI3K/Akt signalling pathway: Cytokins) IFNB1; RTK) FGFR2; HSP90) HSP90AB1; AKT) AKT2; LKB1) STK11; CASP9) CASP9; NUR77) NR4A1. The down-regulated components of the pathway are marked with a red star.

The first one encodes for a heat-shock protein, which acts as a molecular chaperone that promotes maturation, structural maintenance and proper regulation of specific proteins and activates AKT (*299*). Instead STK11 is a tumor suppressor part of the mTOR signaling pathway which regulates protein synthesis among other processes. Finally, CASP9 and NR4A1 were also down regulated since they are involved in cell survival and apoptosis signaling.

Another important affected pathway is the MAPK signalization pathway, where four genes are reported to be down regulated: AKT2, FGFR2, NR4A1 and PPM1A (Figure 5.99).
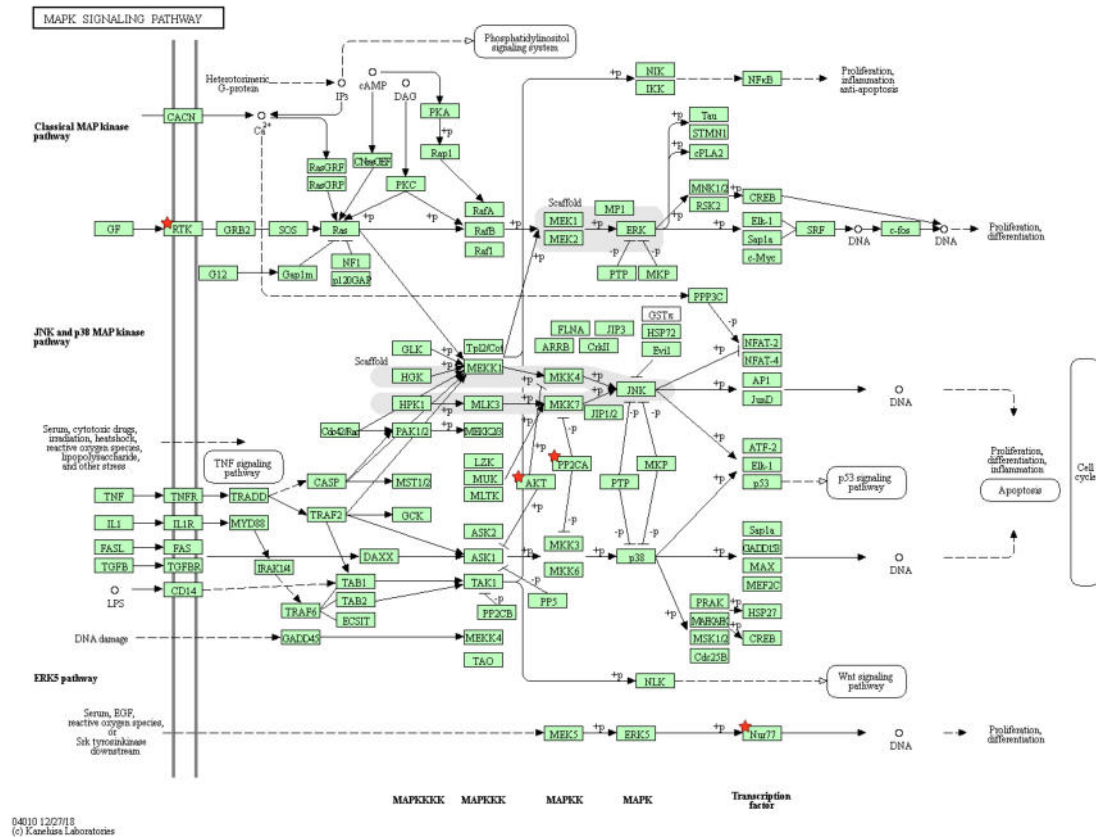
Figure 5.99 MAPK signalling pathway: RTK) FGFR2; AKT) AKT2; PP2CA) PPM1A; Nur77) NR4A1. The down-regulated components of the pathway are marked with a red star.

In this pathway the most upstream of down-regulated genes is FGFR2, which encodes for the fibroblast growth factor receptor 2. This protein kinase has the ability to regulate other downstream processes such as the activation of the Ras cascade, which in turn regulates the proliferation and differentiation of the cell. This cascade can also activate some protein kinases (MEKKKK) like MAP3K1 which can produce the activation of other protein kinases (MAPK). The latter can regulate gene expression throughout the

activation/inactivation of transcription factors that are involved with the activation of tumor suppressors, like p53. Also, this process can regulate the cell cycle and the apoptotic process, and therefore affecting cell proliferation, differentiation and inflammation. Other down-regulated genes that are involved in the regulation of the genetic expression are AKT2 and PPM1A. Their proteins are central to the MAPK pathway, especially AKT2 which can also regulate the Wnt signaling pathway. The last gene that was down-regulate is NR4A1 which is a transcription factor that regulates proliferation and differentiation.

The AMPK signaling pathway was also affected, with five downregulated genes: PFKB2, AKT2, PFKP, STK11 and SLC2A4 (Figure 5.100). The most upstream affected gene is the STK11, this protein takes part in the direct activation of AMPK upon treatment with antidiabetic drugs or antioxidants like quercetin. AMPK in turn can produce the migration of SLC2A4 to the cell membrane and subsequent intake glucose from the blood stream. This protein which can also be activated by transcription factors, is deeply implicated in cellular growth. PFKP and PFKB2 are also implicated in the cellular metabolisms, specifically in the glycolysis regulation. In fact, their activation may increase this process and a speed-up metabolism is one of the principal cancer hallmarks. The last down-regulated gene of the AMPK signaling pathway is AKT2, and as already mentioned the encoded protein is also a fundamental regulator of cellular metabolism (mTOR signaling pathway). In this case the protein may inhibit cell growth and protein synthesis and also it can increase autophagy.
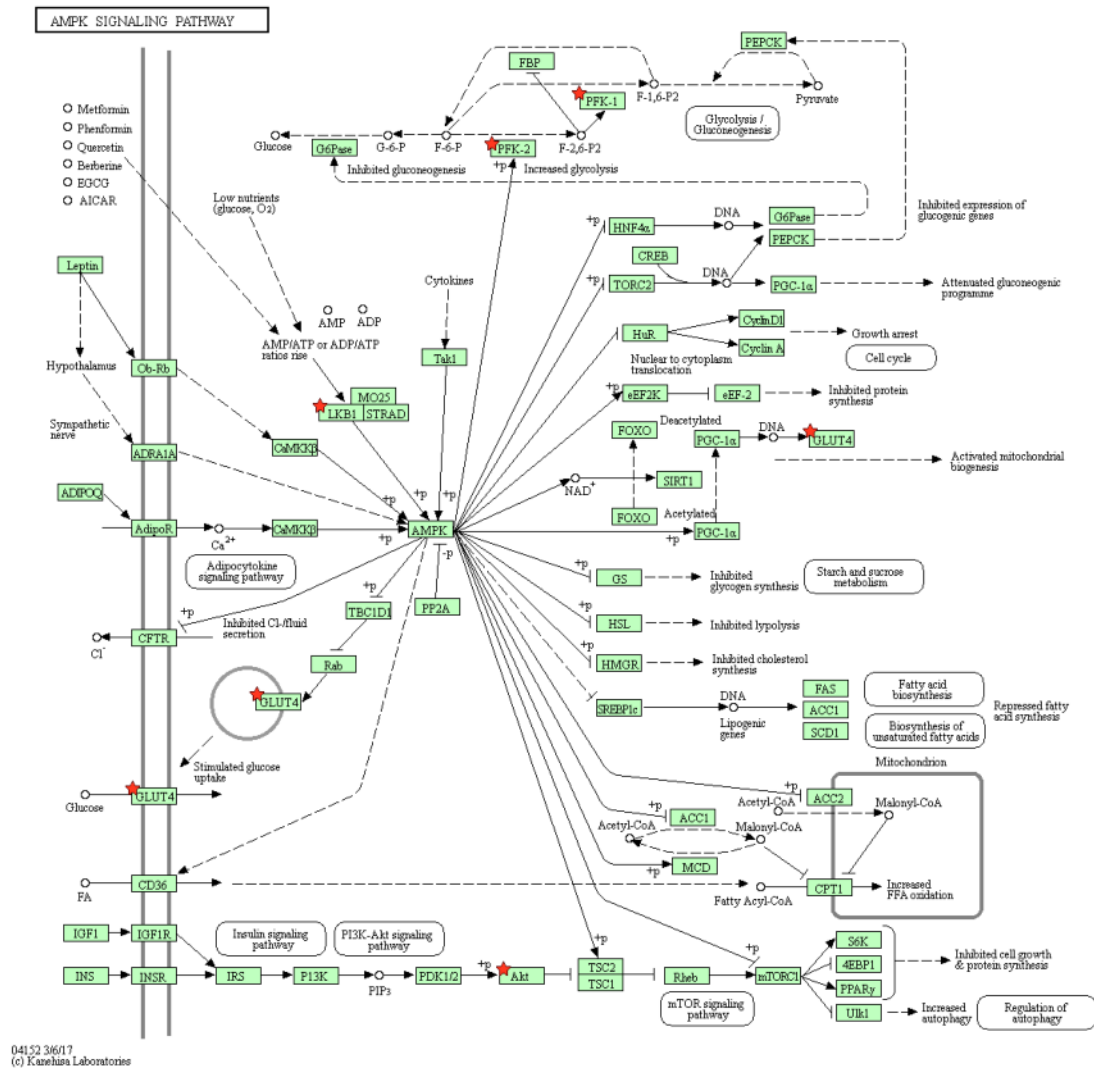
Figure 7.100 AMPK signalling pathway: GLUT4) SLC2A4; LKB1) STK11; Akt) AKT2; PFK-2) PFKB2; PFK-1) PFKP. The down-regulated components of the pathway are marked with a red star.

Several pathways in cancer were also found to contain down-regulated genes, which are five: AKT2, CASP9, FGFR2, HSP90AB1 and PTGER3 (Figure 5.101). The most up-stream genes are FGFR2 and PTGER3, the first one was already described, while the second one is the prostaglandin E2 receptor EP3 subtype. This last receptor modulate response to inflammation and cell death (*267*, *300*), and indirectly regulated different pathways such as PI3K/AKT, Jak/STAT MAPK, Ca and VEGF signaling pathways. These cascades ultimately control various cellular processes: sustained

255

angiogenesis, apoptosis evasion and proliferation. The same effects may be obtained by the downregulation of FGFR2 as shown in figure 5.101. To these genes follow CASP9 and HSP90AB1, these genes are responsible mainly for the evasion of apoptosis and cell proliferation.
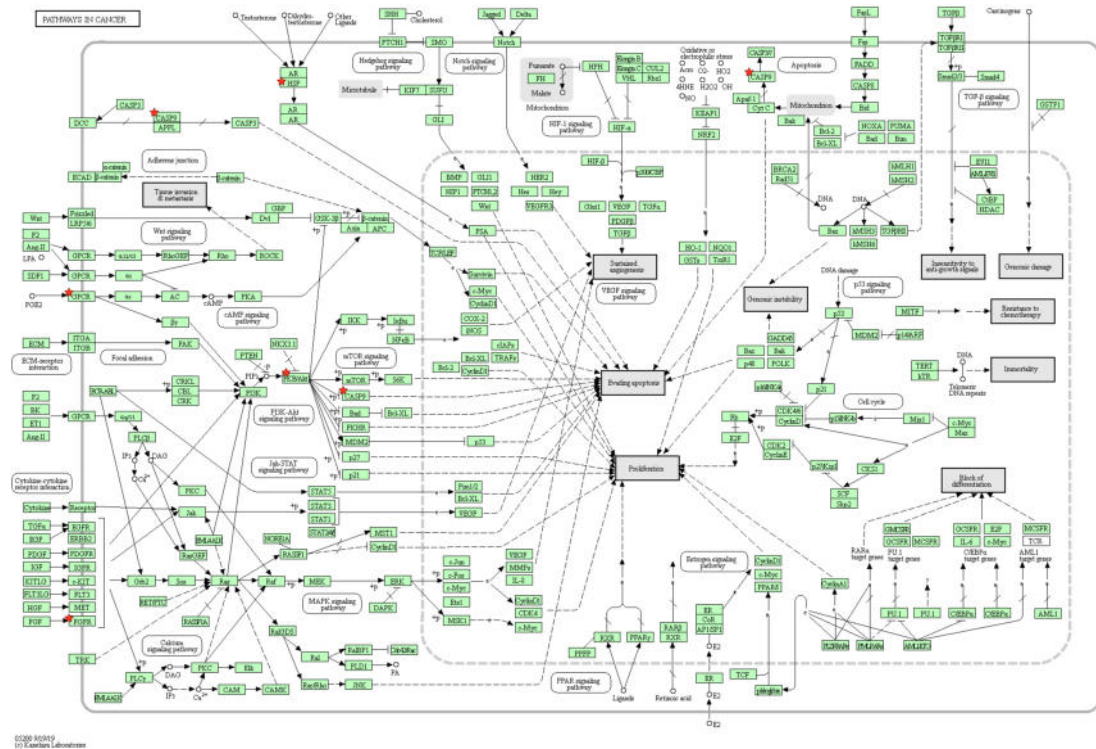
Figure 5.101 Pathways in cancer: GPCR) PTGER3; FGFR) FGFR2; CASP9) CASP9; HSP) HSP90AB1; PKB/Akt) AKT2. The down-regulated components of the pathway are marked with a red star.

In particular the heat-shock protein is activated by the androgen receptor (AR) which is sensible to a variety of antioxidant natural products (*301*). The last affected gene for this pathway is AKT2, which in this case can participate in the activation of various cancer-related proteins and pathways, like the PKB/AKT signaling pathway. Some proteins that interact directly with AKT2 are mTOR (as already mentioned), caspase-9, E3 ubiquitin-protein ligase MDM2 and IKK (see up-regulated genes section), Bad, FKHR, p27 and

p21. All these molecules are related with angiogenesis, apoptosis evasion and proliferation. Other cancer-related pathways were the central carbon metabolism in cancer and prostate cancer signaling pathways (view figure 5.94). The genes down regulated of these signalization cascades were AKT2, FGFR2, CASP9, HSP90AB1, NTRK3 and PFKP. The functions and affected pathways for all these genes were already mentioned in the previous pathways and in cancer they regulate multiple aspects of metabolism (glycolysis, protein synthesis, TCA cycle, FA biosynthesis, AA metabolism and oxidative phosphorylation). Also, they mediate cell survival, migration, invasion, proliferation, apoptosis, cell cycle progression and tumor growth, and are particularly involved in the transition from localized to metastatic prostate cancer.

p53 signaling pathway is also affected by the *p*CA treatment, giving four down-regulated genes: MDM4, CASP9, CHEK1 and CCNB2 (Figure 5.102). The most upstream down-regulated gene is CHEK1, which directly regulates the activation p53 and therefore may activate any response of cell cycle (senescence), apoptosis, angiogenesis, DNA repair and protein synthesis. The same antitumor factor may be regulated indirectly by MDM4 which through the modulation of MDM2 can switch on or off the whole p53 pathway. CCNB2 is instead cell cycle specific and may cause its G2 arrest, while CASP9 takes part in the mitochondrion-mediated apoptosis (*302*).
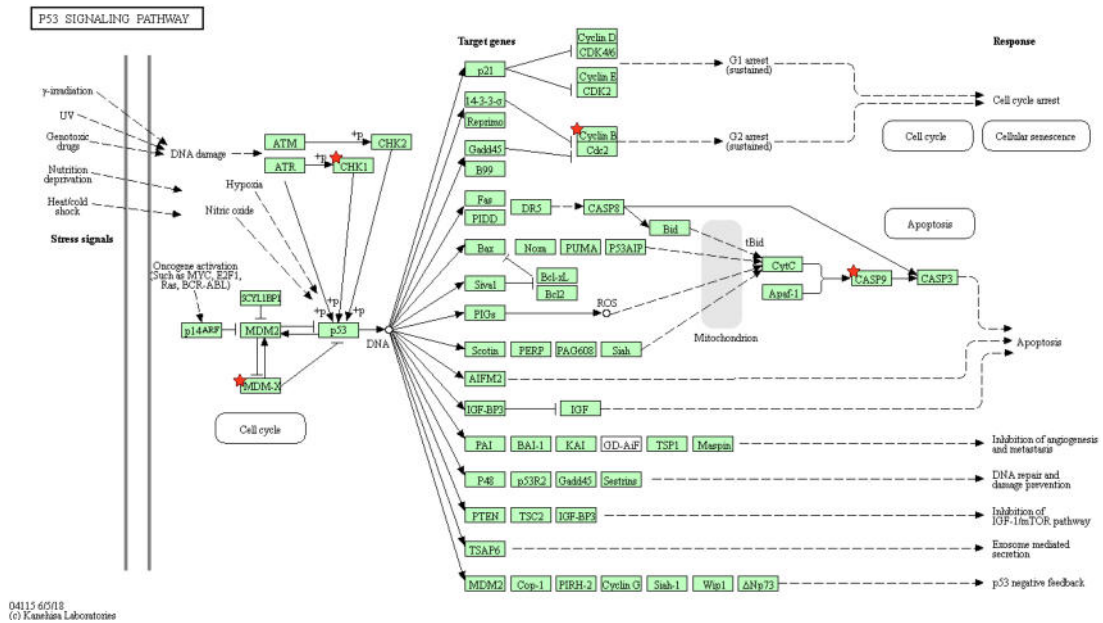
Figure 5.102 p53 signaling pathway: CHK1) CHEK1; MDM-X) MDM4; CASP9) CASP9; Cyclin B) CCNB2. The down-regulated components of the pathway are marked with a red star.

5.5 *In silico* study

The proteins encoded in the selected up- and down-regulated genes were submitted to molecular docking. The type of docking used in these experiments is the flexible ligand docking, where the ligand is allowed to change conformation (poses), while the protein is maintained rigid and doesn't change tis conformation in respond to the ligand binding. The targets were selected in base on their importance in the identified pathways and on their 3D structure availability. The experiments showed the possible binding site and ligand conformation which could cause the observed aberrant gene expression. This was possible through the calculation of a docking score which enlightened the ligand conformation, among the nine generated, with the lower energy of interaction with all the possible binding sites of each protein. This way was possible to select the best conformation of the ligand and the best

258

site of interaction based on the score (lower energy), the ligand-protein interaction (number of AAs interacting with the ligand, type of interactions and site of interaction) and the number of ligand poses found within or close to the same binding site (Clustering). Also, some proteins were modelled to add eventual missing chains and parts to their crystal structure and were submitted to molecular dynamic simulations, with the ligand placed in its best site of interaction and in its best conformation. This way was possible to approximate the strength of the binding interaction in a dynamic environment. These molecules were also selected in base of their functions and role in the analyzed pathways of signalization.

5.5.1 Molecular docking

From the overexpressed proteins 15 were submitted to molecular docking with the pCA as ligand: FGF21, EFNA5, CCNE2, IKBKG, MAPK8, PPP2R3C, MKNK2, MEF2C, STK3, MDM2, ANGPT2, ANGPT4, RASA4, MAP3K1, and CACNA1G (209 to 2,377 residues). Among the proteins which suited the docking requirements, the majority of them were Ser/Thr-protein kinases, such as MAP3K1, MAPK8, MEF2C, MKNK2, PPP2R3C and STK3. Even though these proteins do not have the same sequence, they share a common 3D structure motif which contains the catalytic main site (Figure 5.103A).

Also, some inhibitors bind to this region, like pyrazolanthrone (JNK inhibitor II) which is a MAPK8 inhibitor and Xmu-MP-1, a benzodiazepine with cytotoxic activity which binds to STK3. In these cases *p*CA binds the same active site as the inhibitors, suggesting a similar activity (Figure 5.103 B and

C). These findings could be used in the research for other structurally similar disease-related targets (target fishing), having a high probability of match.
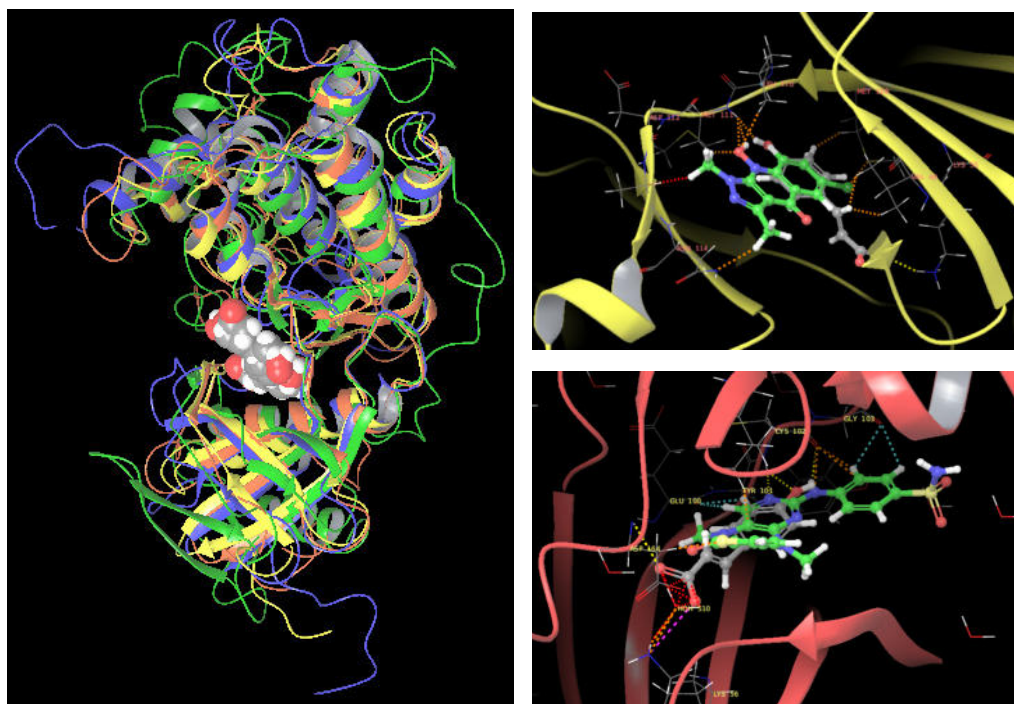
Figure 5.103 A) Conserved proteins structural motif aligned: MAP3K1 (green), MAPK8 (red), MKNK2 (blue), and STK3 (yellow); B) JNK inhibitor II (green) and *p*CA bound to MAPK8; C) Xmu-MP-1 (green) and *p*CA bound to STK3.

From the rest of the proteins CACNA1G was the only transmembrane channel, composed by six large subunits. Its most interesting binding sites of *p*CA are localized on a pocket between the fourth/fifth/sixth transmembrane subunits (833-856 Helical S4; 1411-1434 Helical S5; 1512-1537 Helical S6) and in a separated site on the sixth cytosolic subunit of the protein (1855-2377 Cytoplasmic S6). The first one is responsible for the activation/inactivation of the channel, while the cytosolic terminal part is responsible for its interaction with scaffold proteins (*303*). CCNE2 is instead a small protein (404 residues), which interacts with other two protein kinases (CDK2 and CDK3) to form Ser/Thr kinase holoenzyme complex. The binding site is on a major groove of

the protein and could be interfering with its protein kinase binding (*304*). Ephrin-5 is an activator of EFH receptors and its site of interaction with *p*CA corresponds with the protein-protein interaction with the EFHA2 receptor (29-162 Ephrin RBD; 28-206 Eph LBD) (*305*). This could make the interaction weaker and therefore produce the up regulation of the EFNA5 gene. E3 ubiquitin-protein ligase MDM2 interacts with various proteins forming a ternary complex with p53/TP53, WWOX and a trimeric complex with MDM2, MDM4 and USP2, also it specifically binds to RNA. The ligand (*p*CA) binding site for this protein corresponds to the protein-protein interacting groove (150-230 and 276-491 USP2, PYHIN1, RFFL and FRNF34 binding). These interactions are fundamental for the protein's regulation of the MDM2-p53 signaling pathway (*306*). The interaction of *p*CA and the Ras activator RASA4 is centered on the Zn-finger region of the protein (675-711 Btk-type). This could mean that the ligand is prying with this region's activity which is DNA, RNA or protein binding (*307*). Since the structure of MDM2 and RASA4 were modeled using I-TASSER, cofactors like the Zn^{2+} ions of the Zn-fingers part these molecules were not added. Therefore, for a more precise modeling the cited ions should be considered as part of the molecules. For some of the studied proteins the site of interaction with the ligand was on the surface of the molecule, like for ANGPT2/4, FGF21 and IKBKG with a poor interaction which made them not suitable for subsequent analysis. Also, this lack of a strong ligand-protein binding might suggest that *p*CA is interacting in a different manner. For example, the ligand could be blocking the protein-protein interaction of these molecules with their receptors, or it could be activating these receptors without the need of the signaling protein. Another important molecule that was

discarded was GNG11, because this signaling peptide is too small (73 residues) to be suitable for this type of study and also it is unclear how the *p*CA could interact with this molecule. Therefore, the reason for its up regulation must to be investigated with a different approach which was not part of this study. From the under-expressed proteins 10 were submitted to the explorative docking: SLC2A4, CCNB2, CASP9, STK11, CHEK1, MDM4, PFKFB2, PFKP, FGFR2, and NTRK3 (387 to 839 residues). In this case, the down-regulated genes corresponded to the receptors of the up-regulated proteins, like FGFR2, or to some intimate partners like MDM4/MDMX or to tumor suppressors like STK11/LKB1. We found again the same motif for the Ser/Thr-protein kinases CHEK1, STK11 and NTRK3 in particular these three are tumor suppressors found under-expressed in various cancers and are commonly activated during carcinogenesis by epigenetic mechanisms (*308*). CHEK1 activates by phosphorylation from other protein kinases and *p*CA binds in a site specific for CLSPN mediated activation (1-265 Interaction with CLSPN). STK11 recruits two accesory proteins: STRADA/B and CAB39/MO25, which cause the protein to assume its active conformation. Meanwhile, NTRK3 is found in equilibrium between monomeric (low affinity and dimeric (high affinity) structures and its activation is a ligand-mediated auto-phosphorylation. For both STK11 and NTRK3 the ligand (pCA) is bound close to the protein kinase active site. In all three proteins *p*CA had various binding sites (allosteric and close to the ATP-binding site) on their surface, and it could be enhancing their ability to activate pathways responsible for tumor suppression, like p53 and NF-κB (*309*). Or they could interfere with the deactivation of the targets preventing protein-protein binding. PFKP and

PFKFB2 are both mediators of cancer cell metabolism, and for PFKP the interaction with *p*CA is at an allosteric activation site and catalytic site (538-542 and 583-585 Allosteric activator; 1-399 N-terminal catalytic PFK domain). This protein forms a homotetramer of considerable weight, and this particular binding site is found in a pocket at the interphase of two subunits. This could allow the HCA to control the activity of the enzyme. PFKFB2 is instead a homodimer and the ligand binds close the fructose-2,6-bisphosphate pocket and catalytic site (249-505 Fructos-PP-ase; 2-248 PFK domain). FGFR2 is a receptor found in monomeric form before ligand (heparin) binding and homodimeric after. Its affinity for fibroblast GFs can be modulated (enhanced) by the interaction with other proteins like KLB (*283*, *310*). The binding site of the *p*CA on this receptor is close the protein-protein and the heparin binding sites (154-247 Ig-like C2 type 2; 161-178 Heparin-binding), which could mean that the HCA could be activating the receptor even in absence of its activators and could even be triggering the homodimerization of the receptor. MDM4 is a Zn-finger found in a trimeric complex with MDM2 and USP2, and it is found to be down regulated by anticancer drugs like cisplatin (*311*). *p*CA binds to the region necessary for the interaction of the protein with USP2 (393-490 interaction with USP2) and to its Zn-finger region (437-478 RING-type), which could cause the activation of the protein and deregulation of transcription. SLC2A4 transmembrane channel is a monomeric protein, which is translocated to the cell membrane when needed (*312*). The binding site of the *p*CA in this molecule is situated into the channel lumen, in correspondence to the glucose binding pocket (298-304; 333; 404 Monosaccharide binding). It could compete with the substrate and dysregulate the protein function and

sugar uptake. CCNB2 interacts with cyclin-dependent kinase 1 (CDK1) to form a Ser/Thr kinase holoenzyme known as maturation promoting factor (MPF) and the cyclin imparts specificity to the complex (*267*). The binding site of the *p*CA on this protein is superficial, denoting a probable interference of the acid with the protein-protein interaction of the cyclin. Finally, CASP9 is found as a heterotetramer, which consists in two antiparallel heterodimers. *p*CA binds to the p53 interacting domain and on the active site of the complex (?-315 CASP subunit p35; 287 active site). From the docking results of both up- and down-regulated proteins it is clear that *p*CA effectively binds with most of them or with their receptors, therefore some of them were selected to perform a molecular dynamic simulation experiment in order to determine the ligand-protein interaction in a dynamic way.

5.5.2 MD simulations

The selected *p*CA-protein adducts were allowed to dynamically relax and change conformation in physiological-like environment for 10 ns. Throughout these experiments it was possible to obtain their interaction with each other at any given moment of the simulation, and therefore to approximate their binding strength. The approximated binding energy (ΔE_{bound}) was calculated. Finally, some proteins were also studied for their interaction with the ligand when complexed with their activator/accessory proteins. This allowed to verify how the protein-ligand binding strength changed and to give a more accurate hypothesis of the binding mechanism of *p*CA. Five *p*CA-protein complexes of the up-regulated set were submitted to the MD simulations: *p*CA-CCNE2, *p*CA-MAPK8, *p*CA-MKNK2, *p*CA-RASA4, and

*p*CA-MDM2. Meanwhile six complexes from the down-regulated set were submitted to the analysis: *p*CA-CCNB2, *p*CA-AKT2, *p*CA-NTRK3, *p*CA-SLC2A4, *p*CA-MDM4 and *p*CA-STK11. Furthermore, the targets studied in complex with their accessory proteins were: *p*CA-STK11-STRAD-CAB39 and *p*CA-CCNE2-CDK2.

The calculated ΔE_{bound} and the variables used for its calculation for each of the studied systems are reported in table 5.32.

Table 5.32 Calculated ΔE_{bound} (Kcal/mol) for each studied system

Complex (up-reg.)	E_{lp}^{el}	E_{ls}^{el}	E_{lp}^{vdW}	E_{ls}^{vdW}	ΔE_{bound}
*p*CA-CCNE2	-37.8221	-69.5421	-3.5492	-6.4070	6.5041
*p*CA-MAPK8	-49.7515	-49.1873	-12.0723	-1.7895	-1.9273
*p*CA-MKNK2	-40.9289	-51.7441	-5.6498	-5.9280	5.4521
*p*CA-RASA4	-53.7024	-34.8041	-16.3229	3.1418	-12.5729
*p*CA-MDM2	-55.2929	-43.3222	-15.9776	3.4939	-9.1008
Complex (down-reg.)					
*p*CA-CCNB2	-80.4369	-0.2426	-9.1979	-0.22888	-41.5322
*p*CA-AKT2*	-	-	-	-	-
*p*CA-NTRK3	-65.4647	-9.2353	-18.7596	-1.4521	-30.8839
*p*CA-SLC2A4	-65.0329	-0.2100	-17.6101	-0.3765	-35.1688
*p*CA-MDM4	-53.4211	-19.5824	-18.9772	3.1844	-20.4652
*p*CA-STK11*	-	-	-	-	-
Prot. complex					
*p*CA-STK11-STRAD-CAB39	-50.1094	-49.1381	-19.9641	4.5729	-4.4116
*p*CA-CCNE2-CDK2	-35.4547	-35.4094	-18.1084	0.4557	-2.9929

*The results of these simulations were corrupted and must be repeated.

5.5.2.1 Dynamic interaction of *p*CA with the up-regulated proteins

From the simulation the dynamic ligand interaction diagram was obtained, highlighting a weak interaction between the *p*CA and the cyclin. The diagram shows that only few residues interact with the ligand longer than 10

% of the simulation: a glutamate (Glu161), a serine (Ser245), an asparagine (Asn248) and a tyrosine (Tyr267). Glu161 is the most consistent bonding residue forming H-bond which lasts for 27 % of the MD simulation. Also, few molecules of water interact for a maximum of 2 ns (20%) and create a link with the Leu263 residue. This result is not unexpected since the binding region is on the protein surface, because the latter does not have grooves or pockets useful for a strong ligand interaction (Figure 5.104).

Figure 5.104 *p*CA-CCNE2 dynamic ligand-protein interaction diagram: a schematic of detailed ligand atom interactions with the protein residues. Interactions that occur more than 10.0% of the simulation time in the selected trajectory (0.00 through 10.00 ns), are shown.

These labile interactions mean that the *p*CA interaction with its target could be of a different nature of the observed one. It is also important to notice that the ΔE_{bound} found for the ligand-protein complex accounts for 6.5041 Kcal/mol, which is not a very high value. In fact, it may be that the HCA is disrupting an interaction between cyclin E2 and one of its targets, like cyclin-dependent kinases (CDKs). This interaction could be observed repeating the dynamic simulation in presence of one of these proteins. In this case the

interactions between the *p*CA and its target are stronger, and the diagram shows five aminoacidic residues involved in the ligand's binding for more than 30 % of the simulation: a tryptophan (Trp7), a glutamate (Glu128), a methionine (Met130), an aspartate (Asp131) and an asparagine (Asn133). Glu128 resulted to form the most stable H-bond kept for 92 % of the simulation, followed by Asn133 which forms H-bond that lasts for 7.6 ns (76 %). Meanwhile the rest of the residues interact with *p*CA only through the binding of a water molecule and these saline and H-bonds are kept in place between 43 and 48 % of the simulation time. The dynamic ligand interaction diagram and the selected pose of the ligand in its binding site are reported in figure 5.105.

Figure 5.105 *p*CA-MAPK8 dynamic ligand-protein interaction diagram: a schematic of detailed ligand atom interactions with the protein residues. Interactions that occur more than 30.0% of the simulation time in the selected trajectory (0.00 through 10.00 ns), are shown.

The strong interactions between the ligand and this protein are indicative of a strong interaction, between them. Also, the part of the water molecules found in the binding site is ambiguous since they keep their position for half the simulation time. The calculated ΔE_{bound} (-1.9273 Kcal/mol) is also

a negative value which means that the *p*CA is spontaneously drawn to the binding site. The dynamic interaction between *p*CA and MKNK2 were found to be weaker than the previous kinase. Showing only three aminoacidic residues interacting poorly (>10 %) with the ligand: a methionine (Met162), a lysine (Lys173) and a glutamate (Glu209), plus two molecules of water acting as bridges from the phenolic moiety of the HCA and the methionine and glutamate of the protein. Instead the lysine directly forms two saline-bridges with the carboxylate group. All the interactions are very labile, being observed for less than 20 % of the simulation time (Figure 5.106).

Figure 5.106 *p*CA-MKNK2 dynamic ligand-protein interaction diagram: a schematic of detailed ligand atom interactions with the protein residues. Interactions that occur more than 10.0% of the simulation time in the selected trajectory (0.00 through 10.00 ns), are shown.

Weak binding of *p*CA shows that a different mode of interaction must be the cause of the up regulation of this protein. The small positive ΔE_{bound} of 5.4521 Kcal/mol suggests that the conjunction of the ligand and target are not spontaneous and could involve a different mechanism. It is also worth noting that the simulation time is also very short and therefore gives only a partial and approximated view of the system's evolution. From the AA found in the binding

site of RASA4 seven of them were found interacting with *p*CA functional groups: a glutamate (Glu480), three arginine residues (Arg709, Arg711 and Arg732), a serine (Ser710), an aspartate (Asp719) and a histidine (His723) (Figure 5.107).

Figure 5.107 *p*CA-RASA4 dynamic ligand-protein interaction diagram: a schematic of detailed ligand atom interactions with the protein residues. Interactions that occur more than 20.0% of the simulation time in the selected trajectory (0.00 through 10.00 ns), are shown.

Four of these interactions are mediated by water molecules. The strongest interactions are H-bonds, especially the one between Arg711 and the carboxylate group of *p*CA. Other strong but lesser H-bond is found among Arg732, Glu489 and the carboxylate group. The latter are mediated by H_2O molecules, which could be important in ligand binding. Also, Arg709 forms a saline bridge with the acidic moiety of *p*CA which lasts 72 % of the simulation. The binding energy (ΔE_{bound} = -12.5729 Kcal/mol) of *p*CA with RASA4 is a highly negative value. This implies that the ligand-protein interaction in the physiological-like environment of the simulation is a spontaneous event. Six AA side chains of the protein MDM2, bind *p*CA for more than 20 % of the time:

two tyrosine residues (Tyr100, Tyr104), one arginine (Arg155), two serine residues (Ser157, Ser159) and one phenylamine 490 (Phe490), as well as three water molecules (Figure 5.108).
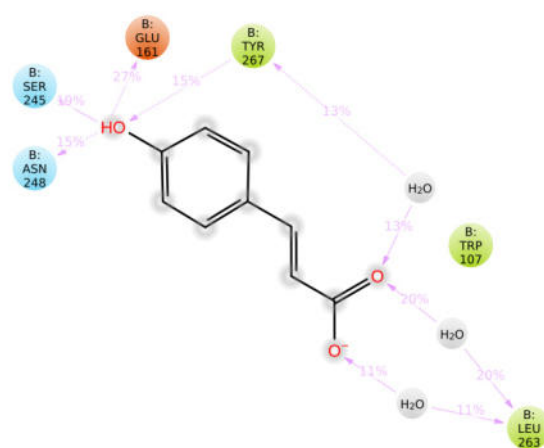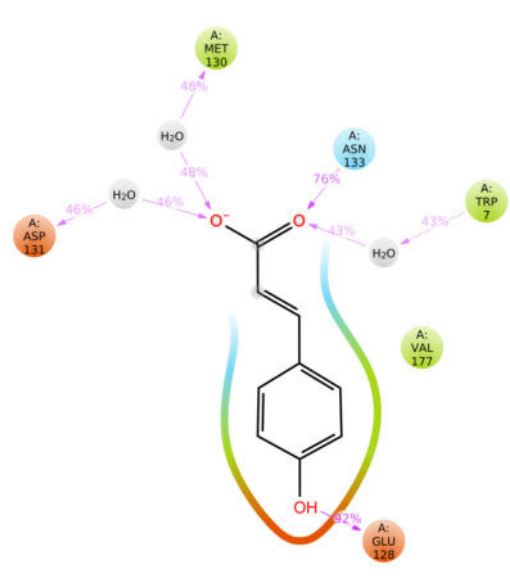

Figure 5.108 *p*CA-MDM2 dynamic ligand-protein interaction diagram: a schematic of detailed ligand atom interactions with the protein residues. Interactions that occur more than 20.0% of the simulation time in the selected trajectory (0.00 through 10.00 ns), are shown.

The strongest interactions are two saline-bridges formed by the arginine residue which last 59 and 80 % of the simulation. The other interactions are much weaker and labile (<50 %), especially the water-bridges which suggests that the water molecules are probably not essential in the ligand-protein binding. Binding energy ΔE_{bound} (-9.1008 Kcal/mol) of *p*CA with MDM2 is a negative value, which confirms that interaction between the two molecules is spontaneously driven, and that this could be its actual binding site. For these two last systems (*p*CA-RASA4 and *p*CA-MDM2) is important to mention that the molecules' crystallographic files used in the simulations lacked Zn^{2+} ions. Adding the ions to the protein structures and adjust them to

their presence would have extended considerably the simulation time (up to 1μs) and doubled the computational cost and simulation time. Therefore, the optimization of these systems exceeded the explorative goal of the present study and was not performed. Still, the Zn^{2+} ions constitute an important part of the proteins since they are both Zn-fingers and should be taken into account to perform a more accurate study on these systems.

5.5.2.2 Dynamic interaction of *p*CA with the down-regulated proteins

Dynamic interaction between *p*CA and CCNB2 is very strong. Five aminoacidic residues are involved in the ligand's binding for more than 30 % of the simulation time: a glycine (Gln149), a serine (Ser150), a tyrosine (Tyr188), an arginine (Arg196) and a threonine (Thr294). The saline (ionic) bridges and H-bonds formed by these side chains with *p*CA are very strong and all last for more than 90 % of the simulation. The only exception is the bond formed by the tyrosine through the water molecule (water-bridge) which is 20 % more labile. Still the interaction lasts long enough to hypnotize the stable presence of the H_2O molecule inside the binding site, or at least the necessity of its presence for the formation of that particular saline bridge. One saline bridge between the ligand and arginine 196 is reported to last more than 100 % of simulations, this means that the AA has more than one interaction with the same atom of the carboxylic group. The dynamic binding of *p*CA to the cyclin B2 is shown in figure 5.109.
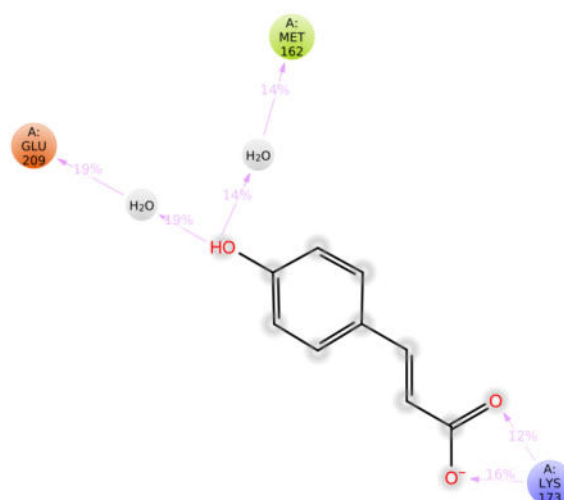
Figure 5.109 *p*CA-CCNB2 dynamic ligand-protein interaction diagram: a schematic of detailed ligand atom interactions with the protein residues. Interactions that occur more than 30.0% of the simulation time in the selected trajectory (0.00 through 10.00 ns), are shown.

Strong interactions of *p*CA with the selected binding site and the extremely negative ΔE_{bound} of -41.5322 Kcal/mol reported for the dynamic simulation, match the experimental results of the treatment. Even if the binding site of the cyclin is not characterized, it is acceptable to speculate that it has an important role in this protein's function. Interactions of the ligand with NTRK3 were also found to be strong, nine AAs bind pCA for more than 30 % of the simulation: two glutamate residues (Glu546, Glu618), an alanine (Ala548), a lysine (Lys572), two methionine residues (Met620, Met700), an aspartate (Asp697), a phenylalanine (Phe698), and a glycine (Gly699) as well as four H_2O molecules. Almost all interactions last more than 5 ns, the strongest interaction is a H-bond between the phenol group and the glutamate 618. Only one interaction of π-π stacking is present among the aromatic ring of the ligand and the one of the phenylalanine 698 side chain, and this interaction lasted for 43 % of the simulation. Three of the interactions mediated by the water molecules were present more than 50 % of the time which could

272

mean that these molecules are needed for the *p*CA-NTRK3 binding interaction (Figure 5.110).
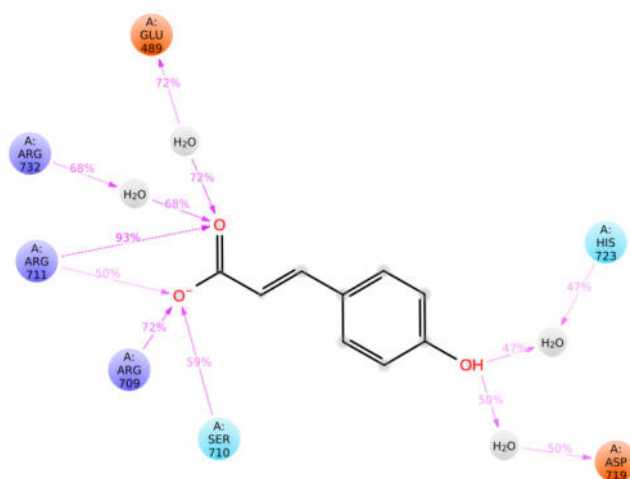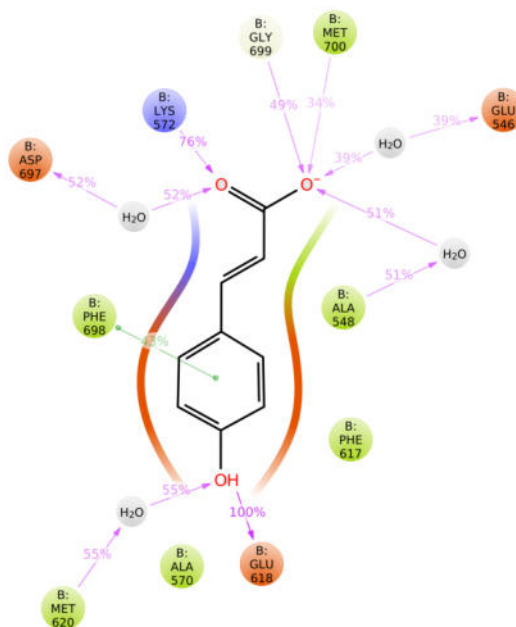

Figure 5.110 *p*CA-NTRK3 dynamic ligand-protein interaction diagram: a schematic of detailed ligand atom interactions with the protein residues. Interactions that occur more than 30.0% of the simulation time in the selected trajectory (0.00 through 10.00 ns), are shown.

The dynamic interaction resulted to be strong with ΔE_{bound} of -30.8839 Kcal/mol confirming the goodness of the binding. The latter happens in a site different from the catalytic one but close to it and therefore *p*CA could be activating the protein without the need of its substrate. The *p*CA-SLC2A4 interaction was also very strong consisting only in saline-bridges and H-bonds, and therefore involving just the carboxylate moiety of the ligand. The interactions lasting above 30 % of the time are given by six AA residues: a valine (Val85), a serine (Ser89), an arginine (Arg142), two aspartate residues (Asn304, Asn431) and a tyrosine (Tyr308) and, three of which mediated by water molecules. Two of the latter lasted for more than 60 % of the simulation,

273

meaning that they could be important for the *p*CA binding to the channel protein. The strongest of all the interactions was a saline bridge between arginine 142 and the deprotonated carboxyl group (Figure 5.111).
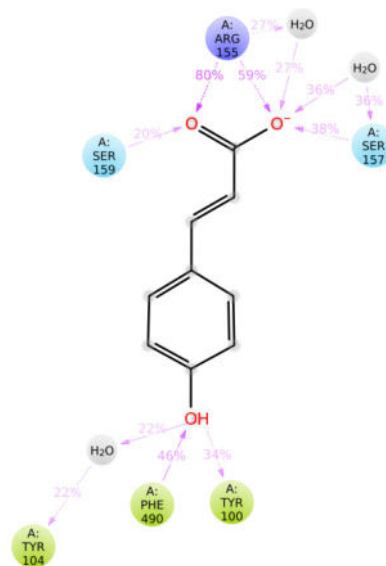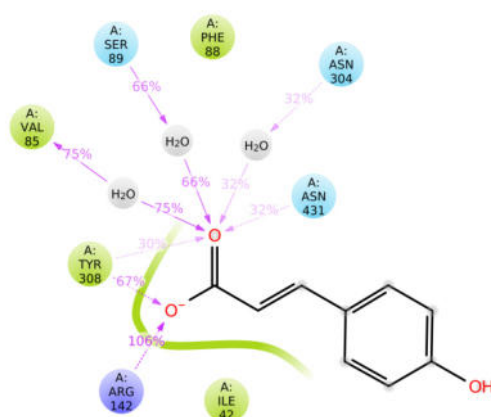

Figure 5.111 *p*CA-SLC2A4 dynamic ligand-protein interaction diagram: a schematic of detailed ligand atom interactions with the protein residues. Interactions that occur more than 30.0% of the simulation time in the selected trajectory (0.00 through 10.00 ns), are shown.

Strong binding of *p*CA in the glucose binding site of the channel protein could block the passage of the monosaccharide into the cytoplasm and consequently cause a cascade of signalizations affecting negatively cell metabolism and proliferation. This hypothesis is reinforced by the calculated ΔE_{bound} for the dynamic simulation of -35.1688 Kcal/mol. This negative value of energy strongly supports the idea of a spontaneous bind of *p*CA in this site of the interaction and hence the inhibition of the protein functions. The *p*CA-MDM4 binding was found to be of medium strength, having four AAs interacting for more than 2 ns (20 %): a tyrosine (Tyr75), a serine (Ser409), histidine (His46) and lysine (Lys469) (Figure 5.112).
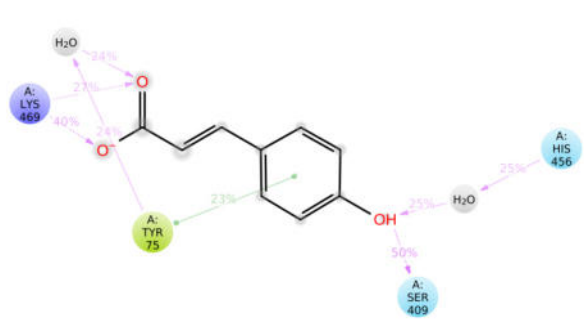
Figure 5.112 *p*CA-MDM4 dynamic ligand-protein interaction diagram: a schematic of detailed ligand atom interactions with the protein residues. Interactions that occur more than 20.0% of the simulation time in the selected trajectory (0.00 through 10.00 ns), are shown.

The majority of the interactions were H-bonds and saline interactions, two of them mediated by water. Meanwhile only one π-π stacking interaction was found, caused by the contact between the ligand aromatic ring and the one on the sidechain if the AA Tyr75. The latter was also the AA with the most intense interaction creating also a water-bridge with the carboxylate moiety of the ligand. Other long-lasting interactions were made by Lys469 which binds both the oxygens of the acidic portion of *p*CA forming an ionic bond for 40 % of the simulation. Also, Ser409 forms H-bond with the phenol moiety of the ligand for half the duration of the simulation. The various interactions found for *p*CA in the MDM4 binding site are sufficient to speculate over the importance of this system. In fact, the calculated ΔE_{bound} remarks these findings consisting of -20.4652 Kcal/mol, this negative value suggest that the binding of the ligand to the protein happens spontaneously. As for RASA4 and MDM2, for this model were also ignored important Zn^{2+} ions, which should be considered if a more accurate study of this system is attempted. In the *p*CA-STK11-STRAD-CAB39 system, the protein STK11 with the ligand in the selected binding pocket was aligned with its complex with its accessory/activating proteins and the system was submitted to a MD simulation (Figure 5.113).
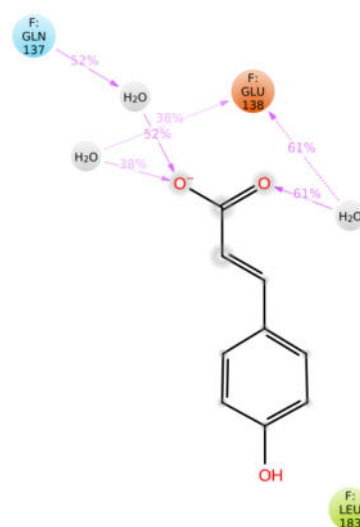
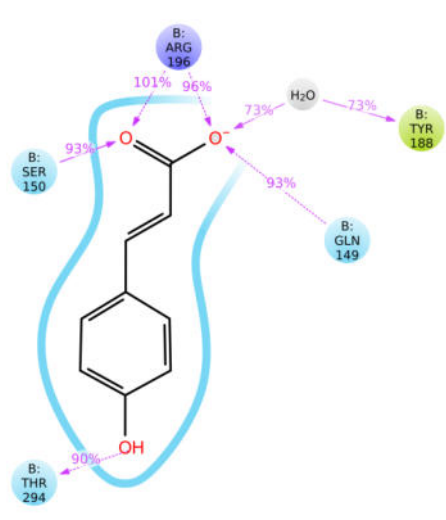**Figure 5.113** *p*CA-STK11-STRAD-CAB39 dynamic ligand-protein interaction diagram: a schematic of detailed ligand atom interactions with the protein residues. Interactions that occur more than 30.0% of the simulation time in the selected trajectory (0.00 through 10.00 ns), are shown.

The dynamic interactions (above 30%) observed were of good strength, all were mediated by H_2O molecules, and the AAs responsible for them were only two: a glycine (Gln137) and a glutamate (Glu138). Gln137 forms a water-bridge with an ionic interaction with the deprotonated carboxylate group of the ligand that lasts for half the simulation. Meanwhile Glu138 has the strongest contacts forming two water-bridges with the oxygens of the carboxylate, the H-bond lasting 61 % of the time while the saline-bridge was present for 38 % of the simulation. The binding of *p*CA to the protein complex STK11-STRAD-CAB39 was eficient, since the value reported for its binding energy (ΔE_{bound}) is -4.4116 Kcal/mol. This negative value, like for the other down-regulated proteins, is an index of its spontaneous interaction with the selected binding site and hence its importance in the mechanism of action of *p*CA. The last studied system was the *p*CA-CCNE2-CDK2, where the interaction between

the two proteins was investigated with the *p*CA placed in its binding site (Figure 5.114).
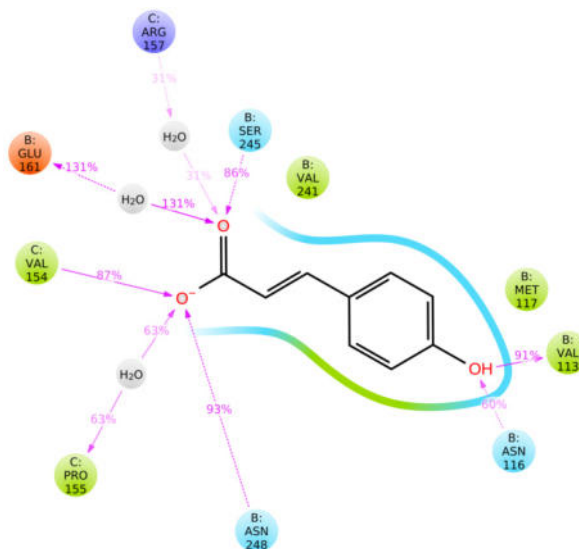
Figure 7.114 *p*CA-CCNE2-CDK2 dynamic ligand-protein interaction diagram: a schematic of detailed ligand atom interactions with the protein residues. Interactions that occur more than 30.0% of the simulation time in the selected trajectory (0.00 through 10.00 ns), are shown.

Five AA residues from CCNE2 (Chain B), three AA residues from CDK2 (Chain C) and three water molecules were found to interact with the HCA functional groups: two valine residues (Val113B and Val154C), two asparagine lateral chains (Asn116B and Asn248B), a proline (Pro155C), an arginine (Arg157C), a glutamate (Glu161B) and lastly a serine (Ser245B). The strongest interaction detected is found between Glu161 and the carboxyl moiety of *p*CA. This H-bond account for 131% of the simulation time, which means that more than one interaction is present between the AA and the functional group at the same time. The latter are also mediated by a H_2O molecule which could be necessary to keep the binding strong. Other interactions that last over 8 ns are the saline bonds between Val113 and the

phenol group, Val154, Asn248 and the carboxylate group and among Ser245

and the carbonyl. In general, almost all the interactions lasted over 50% of

simulation time which means that they are probably important of *p*CA binding

on the protein. The calculated value of the LIE between the HCA and the

protein complex CCNE2-CDK2 is a negative number (-2.9929 Kcal/mol).

Confronting this value with the one found for the sole *p*CA-CCNE2 complex

(6.5041 Kcal/mol) shows that the interaction requires less energy when the

CCNE2 is complexed with its protein target CDK2. Therefore, *p*CA would be

more easily drown to interact with the complexed proteins than when they are

in the monomeric state.

These results need to be confirmed with experimental evidence, but still

they represent a good approximation of the possible interaction of *p*CA with its

targets and give an idea of its possible mechanism or mechanisms of action.

CHAPTER 6

6. CONCLUSIONS

This study was the first pharmacological and chemical study conducted on *H. glomerata*.

The metabolomic study performed on the plant's leaf extracts give a deeper understanding of its chemical composition and highlighted its major biosynthetic pathways.

The results obtained from the antibacterial assays partially confirmed this plant as a source of antibacterial phytochemicals and backed up its use in the Mexican traditional medicine.

The cytotoxic assays showed that the plant also produce cytotoxic compounds, which is in agreement with is taxonomic relation with plants used in the ethnomedical treatment of cancer.

It was possible to confine the biological activity and therefore the bioactive phytochemicals of this plant to its aerial parts, since the root extracts had null activity.

The various non-toxic but bioactive compounds isolated from the organic leaf extracts of *H. glomerata* are partially responsible for the observed biological activities.

Compounds accountable for both antibacterial and cytotoxic activity were identified through bio-directed assays of the fractionated active extracts.

This contributed to the identification of more metabolites produced by this plant.

In this study were also observed the changes in genetic expression of PC3 cancer cells treated with an isolated compound (*p*-coumaric acid), by microarray.

This is the first report of a microarray assay on *p*-coumaric acid. The latter showed the up- and down-regulation of many genes involved in cancer, some of them specific for prostate cancer.

The microarray results and *in silico* study, led to the conclusion that *p*-coumaric acid's cytotoxicity is the results of the dysregulation of various cellular processes involved in cell survival, growth, migration, and metabolism.

The tendency of *p*-coumaric acid to bind with targets possessing a similar secondary structure, does this molecule be considered as a good candidate for target fishing and the development of new anticancer drugs.

6.1 PERSPECTIVES

Synergistic studies on the phenylpropionic acid will be conducted *in vitro*.

It will be considered the isolation/synthesis of some new interesting CAPE-like metabolites, such as 3-(4-hydroxyphenyl) propyl coumarate and 3-(4-hydroxyphenyl-3-methoxy) propyl coumarate.

It will be validated the observed genetic expression of some selected genes by RT-qPCR.

Results of *in silico* experiments will be confirmed performing *in vitro* binding experiments with the available targets of *p*-coumaric acid. The latter will be also derivatized based on its binding sites and its cytotoxic activity assessed.

BIBLIOGRAPHY

1. J. F. Prescott, in *Antimicrobial Therapy in Veterinary Medicine* (John Wiley & Sons, Inc, 2013; http://dx.doi.org/10.1002/9781118675014.ch9), pp. 153–173.

2. M. A. Kohanski, D. J. Dwyer, B. Hayete, C. A. Lawrence, J. J. Collins, A Common Mechanism of Cellular Death Induced by Bactericidal Antibiotics. *Cell*. **130**, 797–810 (2007).

3. T. Gaillard, J. Dormoi, M. Madamet, B. Pradines, Macrolides and associated antibiotics based on similar mechanism of action like lincosamides in malaria. *Malar. J.* **15**, 85 (2016).

4. G. S. Basarab, G. H. Kern, J. McNulty, J. P. Mueller, K. Lawrence, K. Vishwanathan, R. A. Alm, K. Barvian, A. Kimzey, M. Morningstar, A. Kutschke, S. D. Lahiri, M. Perros, R. Singh, V. J. A. Schuck, R. Tommasi, G. Walkup, J. V Newman, Responding to the challenge of untreatable gonorrhea: ETX0914, a first-in-class agent with a distinct mechanism-of-action against bacterial Type II topoisomerases. *Sci. Rep.* **5**, 11827 (2015).

5. M. R. Mulvey, A. E. Simor, Antimicrobial resistance in hospitals: How concerned should we be? *Can. Med. Assoc. J.* **180**, 408–415 (2009).

6. E. J. Soulsby, Resistance to antimicrobials in humans and animals, *BMJ*, 2005, 331:1219.

7. A. P. Magiorakos, A. Srinivasan, R. B. Carey, Y. Carmeli, M. E. Falagas, C. G. Giske, S. Harbarth, J. F. Hindler, G. Kahlmeter, B.

Olsson-Liljequist, D. L. Paterson, L. B. Rice, J. Stelling, M. J. Struelens, A. Vatopoulos, J. T. Weber, D. L. Monnet, Multidrug-resistant, extensively drug-resistant and pandrug-resistant bacteria: An international expert proposal for interim standard definitions for acquired resistance. *Clin. Microbiol. Infect.* **18**, 268–281 (2012).

8.   E. Tacconelli et al., Discovery, research, and development of new antibiotics: the WHO priority list of antibiotic-resistant bacteria and tuberculosis. *Lancet Infect. Dis.* **18**, 318–327 (2018).

9.   A. H. Holmes, L. S. P. Moore, A. Sundsfjord, M. Steinbakk, S. Regmi, A. Karkey, P. J. Guerin, L. J. V Piddock, Understanding the mechanisms and drivers of antimicrobial resistance. *Lancet*. **387**, 176–187 (2016).

10.   T. Frieden, Antibiotic resistance threats in the United States. *Centers Dis. Control Prev.*, 114 (2013).

11.   K. Bush, P. A. Bradford, β-lactams and β-lactamase inhibitors: An overview. *Cold Spring Harb. Perspect. Med.* **6** (2016), doi:10.1101/cshperspect.a025247.

12.   C. L. Ventola, The antibiotic resistance crisis: part 1: causes and threats. *P T A peer-reviewed J. Formul. Manag.* **40**, 277–83 (2015).

13.   R. L. Siegel, K. D. Miller, A. Jemal, Cancer statistics, 2016. *CA. Cancer J. Clin.* **66**, 7–30 (2016).

14.   F. Bray, J. Ferlay, I. Soerjomataram, R. L. Siegel, L. A. Torre, A. Jemal, Global cancer statistics 2018: GLOBOCAN estimates of incidence and mortality worldwide for 36 cancers in 185 countries. *CA.*

Cancer J. Clin. **68**, 394–424 (2018).

15. J. Ferlay, I. Soerjomataram, R. Dikshit, S. Eser, C. Mathers, M. Rebelo, D. M. Parkin, D. Forman, F. Bray, Cancer incidence and mortality worldwide: Sources, methods and major patterns in GLOBOCAN 2012. *Int. J. Cancer.* **136**, E359–E386 (2015).

16. N. F. and S. R. Md. Uzzal Haque, Anti-cancer agents derived from plant and dietary sources: a review. *IJP.* **3**, 55–66 (2016).

17. S. Cetean, T. Ciuleanu, D.-C. Leucuta, C. Cainap, A.-M. Constantin, I. Cazacu, S. Cainap, A. Gherman, L. Oprean, A. Hangan, R. Oprean, Hypersensitivity reactions to platinum derivatives: findings of new predictive markers. *J. BUON.* **20**, 1617–23 (2015).

18. A. E. Prota, K. Bargsten, D. Zurwerra, J. J. Field, J. F. Díaz, K.-H. Altmann, M. O. Steinmetz, Molecular mechanism of action of microtubule-stabilizing anticancer agents, *Science*, 2013, **339** (6119), 587-590.

19. D. Gibson, The mechanism of action of platinum anticancer agents—what do we really know about it? *Dalt. Trans.*, 10681 (2009).

20. L. Amable, Cisplatin resistance and opportunities for precision medicine. *Pharmacol. Res.* **106**, 27–36 (2016).

21. X. Yang, Y. Cheng, N. Luo, C. Gong, Nanomedicine to Overcome Cancer Multidrug Resistance Nanomedicine to Overcome Cancer Multidrug Resistance. *Curr. Drug Metab.* **15**, 632–649 (2014).

22. M. J. Balunas, A. D. Kinghorn, Drug discovery from medicinal plants. *Life Sci.* **78**, 431–441 (2005).

23. D. J. Newman, G. M. Cragg, Natural Products as Sources of New Drugs from 1981 to 2014. *J. Nat. Prod.* **79** (2016), pp. 629–661.

24. Z. S. Moghadamtousi, H. B. Goh, K. C. Chan, T. Shabab, A. H. Kadir, Biological Activities and Phytochemicals of *Swietenia macrophylla* King. *Mol.* . **18** (2013), , doi:10.3390/molecules180910465.

25. J. Sharifi-Rad, M. S. Hoseini-Alfatemi, M. Sharifi-Rad, M. Sharifi-Rad, M. Iriti, M. Sharifi-Rad, R. Sharifi-Rad, S. Raeisi, Phytochemical Compositions and Biological Activities of Essential Oil from *Xanthium strumarium* L. *Mol.* . **20** (2015), , doi:10.3390/molecules20047034.

26. M. Daglia, Polyphenols as antimicrobial agents. *Curr. Opin. Biotechnol.* **23** (2012), pp. 174–181.

27. A. Al-Mariri, M. Safi, In vitro antibacterial activity of several plant extracts and oils against some gram-negative bacteria. *Iran. J. Med. Sci.* **39**, 36–43 (2014).

28. T. P. T. Cushnie, B. Cushnie, A. J. Lamb, Alkaloids: An overview of their antibacterial, antibiotic-enhancing and antivirulence activities. *Int. J. Antimicrob. Agents*. **44**, 377–386 (2014).

29. M. I. Petrova, N. C. E. Imholz, T. L. A. Verhoeven, J. Balzarini, E. J. M. Van Damme, D. Schols, J. Vanderleyden, S. Lebeer, Lectin-Like Molecules of *Lactobacillus rhamnosus* GG Inhibit Pathogenic *Escherichia coli* and Salmonella Biofilm Formation. *PLoS One*. **11**, e0161337 (2016).

30. T. J. Givnish et al., Phylogeny, adaptive radiation, and historical biogeography in Bromeliaceae: Insights from an eight-locus plastid

phylogeny. *Am. J. Bot.* **98**, 872–895 (2011).

31. J. L. Villaseñor, Checklist of the native vascular plants of Mexico. *Rev. Mex. Biodivers.* **87**, 559–902 (2016).

32. Clara R. R. Santana et al., Phytochemical Screening, Antioxidant and Antibacterial Activity of *Encholirium spectabile* (Bromeliaceae). *Int. J. Sci.*, 1–19 (2012).

33. S. R. G. de Lima-Saraiva, J. C. Silva, C. R. C. Branco, A. Branco, E. L. Cavalcanti Amorim, J. R. G. da Silva Almeida, Antinociceptive effect of *Encholirium spectabile*: A Bromeliaceae from the Brazilian caatinga biome. *Pharmacogn. Mag.* **10**, S655–S660 (2014).

34. R. G. de Oliveira-Júnior, C. A. A. Ferraz, G. R. Souza, A. L. Guimarães, A. P. de Oliveira, S. R. G. de Lima-Saraiva, L. A. Rolim, P. J. Rolim-Neto, J. R. G. da Silva Almeida, Phytochemical analysis and evaluation of antioxidant and photoprotective activities of extracts from flowers of *Bromelia laciniosa* (Bromeliaceae). *Biotechnol. Biotechnol. Equip.*, 1–6 (2017).

35. R. Gonçalves de Oliveira-Junior, G. Rocha Souza, A. Leite Guimarães, A. P. de Oliveira, C. de S. Araújo, J. Cabral Silva, A. Gomes Marques Pacheco, S. R. Gomes de Lima-Saraiva, L. Araújo Rolim, J. Pedro, R. N. Castro, J. R. Guedes da Silva Almeida, Photoprotective, antibacterial activity and determination of phenolic compounds of *Neoglaziovia variegata* (Bromeliaceae) by high performance liquid chromatography-diode array detector (HPLC-DAD) analysis. *African J. Pharm. Pharmacol.* **9**, 576–584 (2015).

36. O. et al. Pío-León, J.F., López-Angulo, G., Paredes-López, Physicochemical, Nutritional and Antibacterial Characteristics of the Fruit of *Bromelia pinguin* L. *Plant Foods Hum Nutr*. **64**, 181 (2009).

37. B. Romano, I. Fasolino, E. Pagano, R. Capasso, S. Pace, G. De Rosa, N. Milic, P. Orlando, A. A. Izzo, F. Borrelli, The chemopreventive action of bromelain, from pineapple stem (*Ananas comosus* L.), on colon carcinogenesis is related to antiproliferative and proapoptotic effects. *Mol. Nutr. Food Res.* **58**, 457–465 (2014).

38. J. O. Juvik, B. Holmelid, W. G. Francis, H. Lie Andersen, P. A. De Oliveira, R. Gonçalves de Oliveira Júnior, R. J. Guedes da Silva Almeida, T. Fossen, Non-Polar Natural Products from *Bromelia laciniosa*, *Neoglaziovia variegata* and *Encholirium spectabile* (Bromeliaceae). *Mol.* . **22** (2017), , doi:10.3390/molecules22091478.

39. C. B. Steingass, M. P. Glock, R. M. Schweiggert, R. Carle, Studies into the phenolic patterns of different tissues of pineapple (*Ananas comosus* [L.] Merr.) infructescence by HPLC-DAD-ESI-MSn and GC-MS analysis. *Anal. Bioanal. Chem.* **407**, 6463–6479 (2015).

40. C. T. Hornung-Leoni, Avances sobre Usos Etnobotánicos de las Bromeliaceae en Latinoamérica. *Bol. Latinoam. y del Caribe Plantas Med. y Aromat.* **10** (2011), pp. 297–314.

41. L. M. Manetti, R. H. Deiaporte, A. Laverde, Metabólitos secundários da família Bromeliaceae. *Quim. Nova*. **32**, 1885–1897 (2009).

42. K. J. and C. L. G. K. Pulliainen, H. Nevalainen, H. Vaˑkevaˑinen, An analytical method for the determination of betaine (trimethylglycine)

from hair. *Int. J. Cosmet. Sci.* **32**, 135–138 (2010).

43.   C. B. Steingass, M. P. Glock, R. M. Schweiggert, R. Carle, Studies into

the phenolic patterns of different tissues of pineapple (*Ananas*

comosus [L.] Merr.) infructescence by HPLC-DAD-ESI-MSnand GC-

MS analysis. *Anal. Bioanal. Chem.* **407**, 6463–6479 (2015).

44.   B. Xue, P. Schlapfer, S. Yon Rhee, Z. Peifen, Summary of Ananas

comosus, version 2.0. *Plant Metab. Netw.* (2018), (available at

https://pmn.plantcyc.org/organism-summary?object=PINEAPPLE).

45.   R. Pavan, S. Jain, Shraddha, A. Kumar, Properties and therapeutic

application of bromelain: a review. *Biotechnol. Res. Int.*, 976203

(2012).

46.   S. S. Chavan, M. G. Damale, P. B. Shamkuwar, D. P. Pawar,

Traditional medicinal plants for anticancer activity. *Int J Curr Pharm*

Res. **5**, 50–54 (2013).

47.   S. Dutta, D. Bhattacharyya, Enzymatic, antimicrobial and toxicity

studies of the aqueous extract of *Ananas comosus* (pineapple) crown

leaf. *J. Ethnopharmacol.* **150**, 451–457 (2013).

48.   M. M. Rashad, A. E. Mahmoud, M. M. Ali, M. U. Nooman, A. S. Al-

Kashef, Antioxidant and anticancer agents produced from pineapple

waste by solid state fermentation. *Int. J. Toxicol. Pharmacol. Res.* **7**,

287–296 (2015).

49.   D. D. K. and P. S. Anand, Antiproliferative effect of bromelain like

cysteine protease (psa/bp-07) from *Billbergia pyramidalis* (sims) lindl.

on human malignant cell lines - a preliminary study. *Int. J. Pharma Bio*

Sci. **4**, 821–830 (2013).

50.   H. I. C. Lowe, N. J. Toyang, C. Watson, S. Badal, P. Bahado-Singh, J. Bryant, In Vitro Anticancer Activity of the Crude Extract and two Dicinnamate Isolates from the Jamaican Ball Moss (*Tillandsia Recurvata* L.). *Am. Int. J. Contemp. Res.* **3**, 93–96 (2013).

51.   V. F. Da Silva, I. Franco, T. E. F. Damasceno, J. R. G. Da Silva Almeida, M. M. Da Costa, Potencial antimicrobiano de extratos etanólicos de plantas frente a bacilos gram negativos isolados da mucosa cérvico-vaginal de ovelhas criadas na região de Petrolina-PE. *Semin. Agrar.* **35**, 883–890 (2014).

52.   R. Gomes Coelho, N. Kika Honda, M. do C. Vieira, R. Louzada Brum, F. Rogerio Pavan, C. Q. Fujimura Leite, C. A. Lima Cardoso, Chemical Composition and Antioxidant and Antimycobacterial Activities of *Bromelia balansae* (Bromeliaceae). *J Med Food*. **13**, 1277–1280 (2010).

53.   R. Pavan, S. Jain, Shraddha, A. Kumar, Properties and therapeutic application of bromelain: a review. *Biotechnol. Res. Int.* **2012**, 976203 (2012).

54.   E. J. Hoffman, *Cancer and the Search for Selective Biochemical Inhibitors, Second Edition* (ed. 2nd, 2007).

55.   L. M. Manetti, A. F. Turra, O. S. Takemura, T. I. E. Svidzinski, A. Laverde Junior, Avaliação das atividades antimicrobiana, citotóxica, moluscicida e antioxidante de *Bromelia antiacantha* Bertol. (Bromeliaceae). *Rev. Bras. Plantas Med.* **12** (2010), pp. 406–413.

56. J. Abreu Payrol, M. Miranda Martínez, Estudio farmacognóstico de *Bromelia pinguin* l. (Piña de Ratón). . *Rev. Cuba. Farm. .* **34** (2000), pp. 181–186.

57. J. A. Vite-Posadas, A. E. Brechú-Franco, et *al.*, Morphoanatomical Characterization and Antimicrobial Activity of *Tillandsia Imperialis* (Bromeliaceae). *Polibótanica*, **31**, 21–29 (2011).

58. E. A. Paz, M. P. Cerdeiras, J. Fernandez, F. Ferreira, P. Moyna, M. Soubes, A. Vázquez, S. Vero, L. Zunino, Screening of Uruguayan medicinal plants for antimicrobial activity. *J. Ethnopharmacol.* **45**, 67–70 (1995).

59. K. Burt-Utley, J. F. Utley, A. García-Mendoza, Contributions toward a revision of *Hechtia* (Bromeliaceae, Pitcairnioideae). I. New and noteworthy species of Hechtia from Mexico. *Phytoneuron.* **59**, 1–17 (2011).

60. L. E. Eguiarte, Cactáceas y otras plantas nativas de la Cañada, Cuicatlán, Oaxaca. *Cactáceas y Suculentas México.* **XLIX** (2004).

61. F. Altamirano, Memorial terapéutico de plantas Mexicanas. *Gac. Med. Mex.* **XXXIII**, 310–326 (1896).

62. H. I. C. Lowe, N. J. Toyang, C. T. Watson, K. N. N. Ayeah, J. Bryant, Antileukemic activity of *Tillandsia recurvata* and some of its cycloartanes. *Anticancer Res.* **34**, 3505–3509 (2014).

63. H. Lowe, Unearthing the Medicinal Properties of *Tillandsia recurvata* (Ball Moss): A Mini Review. *European J. Med. Plants.* **4**, 1138–1149 (2014).

64. Henry Lowe, N. J. Toyang, J. Bryant, *Cancer Res.*, in press, doi:10.1158/1538-7445.AM2012-4237.

65. A. Matiz, P. T. Mioto, Ed. (IntechOpen, Rijeka, 2013; https://doi.org/10.5772/56219), p. Ch. 4.

66. A. Andrade-Cetto, M. Heinrich, Mexican plants with hypoglycaemic effect used in the treatment of diabetes. *J. Ethnopharmacol.* **99**, 325–348 (2005).

67. M. del C. Juárez-Vázquez, C. Carranza-Álvarez, A. J. Alonso-Castro, V. F. González-Alcaraz, E. Bravo-Acevedo, F. J. Chamarro-Tinajero, E. Solano, Ethnobotany of medicinal plants used in Xalpatlahuac, Guerrero, México. *J. Ethnopharmacol.* **148**, 521–527 (2013).

68. E. Estrada Castillón, M. Garza López, J. Á. Villarreal Quintanilla, M. M. Salinas Rodríguez, B. E. Soto Mata, H. González Rodríguez, D. U. González Uribe, I. Cantú Silva, A. Carrillo Parra, C. Cantú Ayala, Ethnobotany in Rayones, Nuevo León, México. *J. Ethnobiol. Ethnomed.* **10**, 1–13 (2014).

69. M. A. Fernández-Herrera, H. López-Muñoz, J. M. V Hernández-Vázquez, L. Sánchez-Sánchez, M. L. Escobar-Sánchez, B. M. Pinto, J. Sandoval-Ramírez, Synthesis and selective anticancer activity of steroidal glycoconjugates. *Eur. J. Med. Chem.* **54**, 721–727 (2012).

70. J. L. Rodríguez-Chávez, E. Coballase-Urrutia, G. Sicilia-Argumedo, T. Ramirez-Apan, G. Delgado, Toxicological evaluation of the natural products and some semisynthetic derivatives of *Heterotheca inuloides* Cass (Asteraceae). *J. Ethnopharmacol.* **175**, 256–265 (2015).

71. L. St, S. Wold, Analysis of variance (ANOVA). *Chemom. Intell. Lab. Syst.* **6**, 259–272 (1989).

72. H.-Y. Kim, Analysis of variance (ANOVA) comparing means of more than two groups. *Restor. Dent. Endod.* **39**, 74–77 (2014).

73. J. Chong, O. Soufan, C. Li, I. Caraus, S. Li, G. Bourque, D. S. Wishart, J. Xia, MetaboAnalyst 4.0: towards more transparent and integrative metabolomics analysis. *Nucleic Acids Res.* **46**, W486–W494 (2018).

74. J. M. J. Favela-Hernández, A. García, E. Garza-González, V. M. Rivas-Galindo, M. R. Camacho-Corona, Antibacterial and antimycobacterial lignans and flavonoids from *Larrea tridentata*. *Phyther. Res.* **26**, 1957–1960 (2012).

75. CLSI, M07-A10: Methods for Dilution Antimicrobial Susceptibility Tests for Bacteria That Grow Aerobically; Approved Standard—Tenth Edition. *CLSI (Clinical Lab. Stand. Institute)*. **35** (2015), doi:10.1007/s00259-009-1334-3.

76. V. Bocanegra-García, M. Del Rayo Camacho-Corona, M. Ramírez-Cabrera, G. Rivera, E. Garza-González, The bioactivity of plant extracts against representative bacterial pathogens of the lower respiratory tract. *BMC Res. Notes*. **2**, 95 (2009).

77. J. M. Nguta, R. Appiah-Opong, A. K. Nyarko, D. Yeboah-Manu, P. G. A. Addo, I. Otchere, A. Kissi-Twum, Antimycobacterial and cytotoxic activity of selected medicinal plant extracts. *J. Ethnopharmacol.* **182**, 10–15 (2016).

78. M. R. Grever, S. A. Schepartz, B. A. Chabner, in *Seminars in oncology*

(1992), vol. 19, pp. 622–638.

79. J. Favela-Hernández, A. Clemente-Soto, I. Balderas-Rentería, E. Garza-González, M. Camacho-Corona, Potential Mechanism of Action of 3′-Demethoxy-6-O-demethyl-isoguaiacin on Methicillin Resistant *Staphylococcus aureus. Molecules.* **20**, 12450–12458 (2015).

80. ThermoFisher Scientific, TRIzolTM Reagent (2016), pp. 1–5.

81. D. C. Rio, M. A. Jr, G. J. Hannon, T. W. Nilsen, Ethanol Precipitation of RNA and the Use of Carriers. **2010**, 1–5 (1016).

82. ThermoFisher Scientific, Agarose Gel Electrophoresis of RNA (2018), (available at https://www.thermofisher.com/mx/es/home/references/protocols/nuclei c-acid-purification-and-analysis/rna-protocol/agarose-gel-electrophoresis-of-rna.html#prot3).

83. E. U. Arredondo-espinoza, S. T. López-cortina, M. A. Ramírez-cabrera, I. Balderas-rentería, Synthesis and photodynamic activity of unsymmetrical A 3 B tetraarylporphyrins functionalized with L - glutamate and their Zn (II) and Cu (II) metal complex derivatives. *Biomed. Pharmacother.* **82**, 327–336 (2016).

84. A. F. Clemente-Soto, I. Balderas-Rentería, G. Rivera, A. Segura-Cabrera, E. Garza-González, M. Del Rayo Camacho-Corona, Potential Mechanism of Action of meso-Dihydroguaiaretic Acid on *Mycobacterium tuberculosis* H37Rv. *Molecules.* **19**, 20170–82 (2014).

85. H. M. Berman, J. Westbrook, Z. Feng, G. Gilliland, T. N. Bhat, H. Weissig, I. N. Shindyalov, P. E. Bourne, The Protein Data Bank.

Nucleic Acids Res. **28**, 235–242 (2000).

86.   W.-H. Shin, G. R. Lee, L. Heo, H. Lee, C. Seok, Prediction of protein structure and interaction by GALAXY protein modeling programs. *Bio Des.* **2**, 1–11 (2014).

87.   J. Yang, R. Yan, A. Roy, D. Xu, J. Poisson, Y. Zhang, The I-TASSER suite: Protein structure and function prediction. *Nat. Methods.* **12**, 7–8 (2014).

88.   A. Waterhouse, M. Bertoni, S. Bienert, G. Studer, G. Tauriello, R. Gumienny, F. T. Heer, T. A. P. de Beer, C. Rempfer, L. Bordoli, R. Lepore, T. Schwede, SWISS-MODEL: homology modelling of protein structures and complexes. *Nucleic Acids Res.* **46**, W296–W303 (2018).

89.   Schödinger, Schrödinger Release-3 (2019).

90.   M. D. Hanwell, D. E. Curtis, D. C. Lonie, T. Vandermeersch, E. Zurek, G. R. Hutchison, Avogadro: an advanced semantic chemical editor, visualization, and analysis platform. *J. Cheminform.* **4**, 17 (2012).

91.   E. F. Pettersen, T. D. Goddard, C. C. Huang, G. S. Couch, D. M. Greenblatt, E. C. Meng, T. E. Ferrin, UCSF Chimera—A visualization system for exploratory research and analysis. *J. Comput. Chem.* **25**, 1605–1612 (2004).

92.   M. V Shapovalov, R. L. Dunbrack Jr, A smoothed backbone-dependent rotamer library for proteins derived from adaptive kernel density estimates and regressions. *Structure.* **19**, 844–858 (2011).

93.   Y. Andoh, N. Yoshii, A. Yamada, S. Okazaki, Evaluation of atomic pressure in the multiple time-step integration algorithm. *J. Comput.*

Chem. **38**, 704–713 (2017).

94. J. Aqvist, J. Marelius, The Linear Interaction Energy Method for Predicting Ligand Binding Free Energies. *Comb. Chem. High Throughput Screen.* **4**, 613–626 (2012).

95. F. Jofre, M. E. Anderon, J. L. Markley, Biological Magnetic Resonance Data Bank. *Sept. 15* (2016), p. http://www.bmrb.wisc.edu, , doi:10.13018/BMSE000926.

96. H. Kojima, N. Sato, A. Hatan, H. Ogura, Sterol glucosides from *Prunella vulgaris. Phytochemistry.* **29**, 2351–2355 (1990).

97. A. M. Yang, H. Li, J. L. Liu, W. J. Guo, R. Wu, Chemical Constituents of *Euphorbia altotibetica. Adv. Mater. Res.* **634–638**, 905–908 (2013).

98. C. H. Jeong, H. R. Jeong, G. N. Choi, D. O. Kim, U. Lee, H. J. Heo, Neuroprotective and anti-oxidant effects of caffeic acid isolated from *Erigeron annuus* leaf. *Chin. Med.* **6**, 25 (2011).

99. Y. Ma, E. A. Galinski, W. D. Grant, A. Oren, A. Ventosa, Halophiles 2010: life in saline environments. *Appl. Environ. Microbiol.* **76**, 6971–6981 (2010).

100. U. Lüttge, Ecophysiology of Crassulacean Acid Metabolism (CAM). *Ann. Bot.* **93**, 629–652 (2004).

101. P. S. Nobel, W. L. Berry, Element Responses of Agaves. *Am. J. Bot.* **72**, 686–694 (1985).

102. D. H. Benzing, *Bromeliaceae: profile of an adaptive radiation* (Cambridge University Press, 2000).

103. L. Kunst, L. Samuels, Plant cuticles shine: advances in wax biosynthesis and export. *Curr. Opin. Plant Biol.* **12**, 721–727 (2009).

104. V. Fernández, P. Guzmán-Delgado, J. Graça, S. Santos, L. Gil, Cuticle Structure in Relation to Chemical Composition: Re-assessing the Prevailing Model. *Front. Plant Sci.* **7**, 427 (2016).

105. V. Piironen, D. G. Lindsay, T. A. Miettinen, J. Toivo, A. M. Lampi, Plant sterols: Biosynthesis, biological function and their importance to human nutrition. *J. Sci. Food Agric.* **80**, 939–966 (2000).

106. J. N. Valitova, A. G. Sulkarnayeva, F. V. Minibayeva, Plant sterols: Diversity, biosynthesis, and physiological functions. *Biochem.* **81**, 819–834 (2016).

107. J. Wildt, K. Kobel, G. Schuh-Thomas, A. C. Heiden, Emissions of Oxygenated Volatile Organic Compounds from Plants Part II: Emissions of Saturated Aldehydes. *J. Atmos. Chem.* **45**, 173–196 (2003).

108. X.-L. Qi, Y.-Y. Zhang, P. Zhao, L. Zhou, X.-B. Wang, X.-X. Huang, B. Lin, S.-J. Song, ent-Kaurane Diterpenoids with Neuroprotective Properties from Corn Silk (*Zea mays*). *J. Nat. Prod.* **81**, 1225–1234 (2018).

109. B. Pejin, A. Savic, M. Sokovic, J. Glamoclija, A. Ciric, In vitro evaluation of antiradical and antimicrobial activities of phytol. *Nat. Prod. Res.* **28**, 372–376 (2014).

110. B. Pejin, V. Kojic, G. Bogdanovic, An insight into the cytotoxic activity of phytol at in vitro conditions. *Nat. Prod. Res.* **28**, 2053–2056 (2014).

111. R. C. S. Veneziani, S. R. Ambrósio, C. H. G. Martins, D. C. Lemes, L. C. Oliveira, in *Studies in Natural Products Chemistry*, B. T.-S. in N. P. C. Atta-ur-Rahman, Ed. (Elsevier, 2017; http://www.sciencedirect.com/science/article/pii/B97804446392950000 48), vol. 54, pp. 109–139.

112. V. Kuete, L. K. Omosa, J. O. Midiwo, O. Karaosmanoğlu, H. Sivas, Cytotoxicity of 11 naturally occurring phenolics and terpenoids from Kenyan flora towards human carcinoma cells. *J. Ayurveda Integr. Med.* (2018), doi:https://doi.org/10.1016/j.jaim.2018.04.001.

113. R. K. Sharma, Phytosterols: Wide-spectrum antibacterial agents. *Bioorg. Chem.* **21** (1993), pp. 49–60.

114. E. J. Cho, J. Y. Choi, K. H. Lee, S. Lee, Isolation of Antibacterial Compounds from *Parasenecio pseudotaimingasa*. *Hort. Environ. Biotechnol.* **53**, 561–564 (2012).

115. M. Ayaz, A. Sadiq, A. Wadood, M. Junaid, F. Ullah, N. Zaman Khan, Cytotoxicity and molecular docking studies on phytosterols isolated from *Polygonum hydropiper* L. *Steroids*. **141**, 30–35 (2019).

116. H. Luo, Y. Cai, Z. Peng, T. Liu, S. Yang, Chemical composition and in vitro evaluation of the cytotoxic and antioxidant activities of supercritical carbon dioxide extracts of pitaya (dragon fruit) peel. *Chem. Cent. J.* **8**, 1–7 (2014).

117. S. N. A. Malek, S. K. Shin, N. A. Wahab, H. Yaacob, Cytotoxic components of *Pereskia bleo* (Kunth) DC. (Cactaceae) leaves. *Molecules*. **14**, 1713–1724 (2009).

118. B. Rubis, A. Polrolniczak, H. Knula, O. Potapinska, M. Kaczmarek, M. Rybczynska, Phytosterols in physiological concentrations target multidrug resistant cancer cells. *Med. Chem. (Los. Angeles).* **6**, 184–190 (2010).

119. S. M. Osman, S. M. Abd El-Khalik, A. M. Saadeldeen, M. A. Koheil, M. Wink, Activity guided phytochemical study of Egyptian *Lotus polyphyllos* E.D. Clarke (Fabaceae). *Int. J. Appl. Res. Nat. Prod.* **8**, 18–26 (2015).

120. C.-T. Yen, C.-L. Lee, F.-R. Chang, T.-L. Hwang, H.-F. Yen, C.-J. Chen, S.-L. Chen, Y.-C. Wu, Indiosides G–K: Steroidal Glycosides with Cytotoxic and Anti-inflammatory Activities from Solanum violaceum. *J. Nat. Prod.* **75**, 636–643 (2012).

121. J. Zeng, X. Liu, X. Li, Y. Zheng, B. Liu, Y. Xiao, Daucosterol inhibits the proliferation, migration, and invasion of hepatocellular carcinoma cells via Wnt/β-catenin signaling. *Molecules.* **22** (2017), doi:10.3390/molecules22060862.

122. V. K. Sali, D. P. Mansingh, H. R. Vasanthi, Relative apoptotic potential and specific G1 arrest of stigmasterol and cinnamic acid isolated from the brown algae Padina gymnospora in HeLa and A549 cells. *Medchemcomm.* **7**, 1429–1435 (2016).

123. Z. Lou, H. Wang, S. Rao, J. Sun, C. Ma, J. Li, p-Coumaric acid kills bacteria through dual damage mechanisms. *Food Control.* **25**, 550–554 (2012).

124. K. Pei, J. Ou, J. Huang, S. Ou, p-Coumaric acid and its conjugates:

Dietary sources, pharmacokinetic properties and biological activities. *J. Sci. Food Agric.* **96**, 2952–2962 (2016).

125. L. M. da Silva, Y. Frión-Herrera, A. R. Bartolomeu, C. M. Gorgulho, J. M. Sforcin, Mechanisms involved in the cytotoxic action of Brazilian propolis and caffeic acid against HEp-2 cells and modulation of P-glycoprotein activity. *J. Pharm. Pharmacol.* **69**, 1625–1633 (2017).

126. N. Nasr Bouzaiene, S. Kilani Jaziri, H. Kovacic, L. Chekir-Ghedira, K. Ghedira, J. Luis, The effects of caffeic, coumaric and ferulic acids on proliferation, superoxide production, adhesion and migration of human tumor cells in vitro. *Eur. J. Pharmacol.* **766**, 99–105 (2015).

127. L. Reddivari, J. Vanamala, S. H. Safe, J. C. Miller Jr, The bioactive compounds α-chaconine and gallic acid in potato extracts decrease survival and induce apoptosis in LNCaP and PC3 prostate cancer cells. *Nutr. Cancer.* **62**, 601–610 (2010).

128. H. Ali, S. Dixit, D. Ali, S. M. Alqahtani, S. Alkahtani, S. Alarifi, Isolation and evaluation of anticancer efficacy of stigmasterol in a mouse model of DMBA-induced skin carcinoma. *Drug Des. Devel. Ther.* **9**, 2793–2800 (2015).

129. B. Shanthakumar, M. Sathish, A. Jerad Suresh, In vitro anti oxidant activity of extracts and stigmasterol from leaves of *Clerodendrum inerme* linn. *Res. J. Pharm. Biol. Chem. Sci.* **4**, 1411–1418 (2013).

130. O. Gabay, C. Sanchez, C. Salvat, F. Chevy, M. Breton, G. Nourissat, C. Wolf, C. Jacques, F. Berenbaum, Stigmasterol: a phytosterol with potential anti-osteoarthritic properties. *Osteoarthr. Cartil.* **18**, 106–116

(2010).

131. J.-C. Lim, J. H. Park, M. Budesinsky, A. Kasal, Y.-H. Han, B.-S. Koo, S.-I. Lee, D.-U. Lee, Antimutagenic constituents from the thorns of *Gleditsia sinensis*. *Chem. Pharm. Bull. (Tokyo).* **53**, 561–564 (2005).

132. L. F. C. Dos Reis, C. D. Cerdeira, B. F. DE Paula, J. J. da Silva, L. F. L. Coelho, M. A. Silva, V. B. B. Marques, J. K. Chavasco, G. Alves-Da-Silva, Chemical characterization and evaluation of antibacterial, antifungal, antimycobacterial, and cytotoxic activities of *Talinum paniculatum*. *Rev. Inst. Med. Trop. Sao Paulo.* **57**, 397–405 (2015).

133. A. Ridhay, A. Noor, N. H. Soekamto, T. Harlim, I. van Altena, A stigmasterol glycoside from the root wood of *Melochia umbellata* (Houtt) Stapf Var. degrabrata K. *Indones. J. Chem.* **12**, 100–103 (2012).

134. P. Singariya, P. Kumar, K. K. Mourya, Isolation of new steroids of Kala Dhaman grass (*Cenchrus setigerus*) and evaluation of their bioactivity. *Brazilian Arch. Biol. Technol.* **57**, 62–69 (2014).

135. T. Rukachaisirikul, A. Saekee, C. Tharibun, S. Watkuolham, A. Suksamrarn, Biological activities of the chemical constituents of *Erythrina stricta* and *Erythrina subumbrans*. *Arch. Pharm. Res.* **30**, 1398–403 (2007).

136. S. Arokiyaraj, A. Vimalarasan, M. Hemachandran, D. Priya, Antibacterial activity of beta-sitosterol of *Vitex agnus* castus (2014).

137. Y. Zhao, S. K. C. Chang, G. Qu, T. Li, H. Cui, β-Sitosterol inhibits cell growth and induces apoptosis in SGC-7901 human stomach cancer

cells. *J. Agric. Food Chem.* **57**, 5211–5218 (2009).

138. N. E. Moreno-Anzúrez, S. Marquina, L. Alvarez, A. Zamilpa, P. Castillo-España, I. Perea-Arango, P. N. Torres, M. Herrera-Ruiz, E. R. Díaz García, J. T. García, J. Arellano-García, A cytotoxic and anti-inflammatory campesterol derivative from genetically transformed hairy roots of *Lopezia racemosa* Cav. (Onagraceae). *Molecules*. **22** (2017), doi:10.3390/molecules22010118.

139. D. Cruz-Vega, M. J. Verde-Star, N. R. Salinas-Gonzalez, B. Rosales-Hernandez, I. Estrada-Garcia, P. Mendez-Aragon, P. Carranza-Rosales, M. Gonzalez-Garza, J. Castro-Garza, Review of pharmacological effects of *Glycyrrhiza radix* and its bioactive compounds. *Zhongguo Zhong Yao Za Zhi*. **22**, 557–559 (2009).

140. S. L, D. Lakshmi, S. Bharadwaj, K. Sajidha Parveen, Anticancer activity of phytol purified from *Gracilaria edulis* against human breast cancer cell line (MCF-7). *Int J Curr Sci*. **19**, 36–46 (2016).

141. W. Lee, E. R. Woo, D. G. Lee, Phytol has antibacterial property by inducing oxidative stress response in *Pseudomonas aeruginosa*. *Free Radic. Res.* **50**, 1309–1318 (2016).

142. S. Qian, Y. Xu, Anti-cancer activities of ω-6 polyunsaturated fatty acids. *Biomed. J.* **0**, 0 (2014).

143. T. Tanaka, M. Hosokawa, Y. Yasui, R. Ishigamori, K. Miyashita, Cancer chemopreventive ability of conjugated linolenic acids. *Int. J. Mol. Sci.* **12**, 7495–7509 (2011).

144. C. W. Chang, H. S. Chang, M. J. Cheng, C. F. Peng, I. S. Chen,

Identification of five new minor constituents from the whole plant of *Amischotolype hispida*. *Helv. Chim. Acta*. **98**, 347–358 (2015).

145. C. J. Zheng, J. S. Yoo, T. G. Lee, H. Y. Cho, Y. H. Kim, W. G. Kim, Fatty acid synthesis is a target for antibacterial activity of unsaturated fatty acids. *FEBS Lett.* **579**, 5157–5162 (2005).

146. P. C. Esquivel-Ferriño, J. M. J. Favela-Hernández, E. Garza-González, N. Waksman, M. Y. Ríos, M. Del Rayo Camacho-Corona, Antimycobacterial activity of constituents from *Foeniculum vulgare* var. Dulce Grown in Mexico. *Molecules*. **17**, 8471–8482 (2012).

147. C. J. Van Boxtel, Antimicrobial Agents. **2**, 23–28 (1972).

148. H. Y. Kwan, X. Fu, B. Liu, X. Chao, C. L. Chan, H. Cao, T. Su, A. K. W. Tse, W. F. Fong, Z. L. Yu, Subcutaneous adipocytes promote melanoma cell growth by activating the Akt signaling pathway: Role of palmitic acid. *J. Biol. Chem.* **289**, 30525–30537 (2014).

149. L. J. McGaw, A. K. Jäger, J. Van Staden, Antibacterial effects of fatty acids and related compounds from plants. *South African J. Bot.* **68**, 417–423 (2002).

150. Y. Chikaraishi, R. Tanaka, A. Tanaka, N. Ohkouchi, Fractionation of hydrogen isotopes during phytol biosynthesis. *Org. Geochem.* **40**, 569–573 (2009).

151. E. Collakova, The Role of Homogentisate Phytyltransferase and Other Tocopherol Pathway Enzymes in the Regulation of Tocopherol Synthesis during Abiotic Stress. *Plant Physiol.* **133**, 930–940 (2003).

152. G. H. H. Borner, D. J. Sherrier, T. Weimar, L. V Michaelson, N. D.

Hawkins, A. Macaskill, J. A. Napier, M. H. Beale, K. S. Lilley, P. Dupree, Analysis of Detergent-Resistant Membranes in *Arabidopsis.* Evidence for Plasma Membrane Lipid Rafts. *Plant Physiol.* **137**, 104–116 (2005).

153. S. Mongrand, J. Morel, J. Laroche, S. Claverol, J. P. Carde, M. A. Hartmann, M. Bonneu, F. Simon-Plas, R. Lessire, J. J. Bessoule, Lipid rafts in higher plant cells: Purification and characterization of triton X-100-insoluble microdomains from tobacco plasma membrane. *J. Biol. Chem.* **279**, 36277–36286 (2004).

154. Z. Cantillo-Ciau, W. Brito-Loeza, L. Quijano, Triterpenoids from *Tillandsia fasciculata. J. Nat. Prod.* **64**, 953–955 (2001).

155. W. C. M. C. Kokke, C. S. Pak, W. Fenical, C. Djerassi, Minor and Trace Sterols in Marine Invertebrates. XII. Occurrence of 24 (R + S)-isopropenylcholesterol, 24 (R + S)-methylcholesta-5, 25-dien-3β-ol, and 24 (R + S)-methylcholesta-7, 25-dien-3β-ol in the caribbean sponge, *Verongia cauliformis. Helv. Chim. Acta*. **62**, 1310–1318 (2018).

156. S. KADOTA, T. SHIMA, T. KIKUCHI, Studies on the Constituents of Orchidaceous Plants. VII. The C-24 Stereochemistry of Cyclohomonervilol and 24-Isopropenylcholesterol, Non-conventional Side Chain Triterpene and Sterol, from *Nervilia purpurea* SCHLECHTER. *Chem. Pharm. Bull.* **35**, 200–210 (1987).

157. S.-W. Lee, Z.-T. Chen, C.-M. Chen, The 4α-Methylsterol Violasterol A from Viola *Formosana Hayata. J. Chinese Chem. Soc.* **40**, 305–307

(2018).

158. T. Furuya, K. Kino, Regioselective synthesis of piceatannol from resveratrol: Catalysis by two-component flavin-dependent monooxygenase HpaBC in whole cells. *Tetrahedron Lett.* **55**, 2853–2855 (2014).

159. K. Billet, B. Houillé, S. Besseau, C. Mélin, A. Oudin, N. Papon, V. Courdavault, M. Clastre, N. Giglioli-Guivarc'h, A. Lanoue, Mechanical stress rapidly induces E-resveratrol and E-piceatannol biosynthesis in grape canes stored as a freshly-pruned byproduct. *Food Chem.* **240**, 1022–1027 (2018).

160. A. S. Dubrovina, K. V. Kiselev, Regulation of stilbene biosynthesis in plants. *Planta*. **246**, 597–623 (2017).

161. A. Berim, D. R. Gang, Methoxylated flavones: occurrence, importance, biosynthesis. *Phytochem. Rev.* **15**, 363–390 (2016).

162. C. Schoenbohm, S. Martens, C. Eder, G. Forkmann, B. Weisshaar, Identification of the *Arabidopsis thaliana* Flavonoid 3'-Hydroxylase Gene and Functional Expression of the Encoded P450 Enzyme. *Biol. Chem.* **381** (2000), p. 749.

163. M. Bredebach, U. Matern, S. Martens, Three 2-oxoglutarate-dependent dioxygenase activities of *Equisetum arvense* L. forming flavone and flavonol from (2S)-naringenin. *Phytochemistry*. **72**, 557–563 (2011).

164. A. Samanta, G. Das, S. Das, *Roles of flavonoids in Plants* (2011), vol. 6.

165. S. Grille, A. Zaslawski, S. Thiele, J. Plat, D. Warnecke, The functions

of steryl glycosides come to those who wait: Recent advances in plants, fungi, bacteria and animals. *Prog. Lipid Res.* **49**, 262–288 (2010).

166. M. Landi, M. Tattini, K. S. Gould, Multiple functional roles of anthocyanins in plant-environment interactions. *Environ. Exp. Bot.* **119**, 4–17 (2015).

167. J. Pollier, A. Goossens, Oleanolic acid. *Phytochemistry*. **77**, 10–15 (2012).

168. C. B. Osmond, in *PROGRESS IN BOTANY 68* (2007), p. 405.

169. N. Saito, J. B. Harborne, A cyanidin glycoside giving scarlet coloration in plants of the *Bromeliaceae*. *Phytochemistry*. **22**, 1735–1740 (1983).

170. K. M. Davies, N. W. Albert, Y. Zhou, K. E. Schwinn, Functions of flavonoid and betalain pigments in abiotic stress tolerance in plants. *Annu. Plant Rev.* **1**, 1–41 (2018).

171. R. A. Dixon, N. L. Paiva, Stress-Induced Phenylpropanoid Metabolism. *Plant Cell*. **7**, 1085–1097 (1995).

172. G.-J. Kim, H.-J. Jo, K.-H. Chung, K.-J. Lee, J. H. An, Oleanolic Acid Induces p53 Dependent Apoptosis via the ERK/JNK/AKT Pathway in Cancer Cell Lines. *Preprints* (2017).

173. J. H. Park, H. Y. Kwon, E. J. Sohn, K. A. Kim, B. Kim, S. J. Jeong, J. H. Song, J. S. Koo, S. H. Kim, Inhibition of Wnt/b-catenin signaling mediates ursolic acid-induced apoptosis in PC-3 prostate cancer cells. *Pharmacol. Reports*. **65**, 1366–1374 (2013).

174. M. M. De Los Reyes, G. G. Oyong, V. D. Ebajo, V. A. S. Ng, C. C. Shen, C. Y. Ragasa, Cytotoxic triterpenes and sterols from *Pipturus arborescens* (link) C.B. Rob. *J. Appl. Pharm. Sci.* **5**, 23–30 (2015).

175. A. Y. Ibrahim, S. E. El-gengaihi, H. M. Motawe, Phytochemical and Cytotoxicity Investigations of *Salvadora Persica* Bark Extracts. *Phytochem. Cytotox. Investig. J.* **6**, 127–133 (2011).

176. S. Yan, C. Huang, S. Wu, M. Yin, Oleanolic acid and ursolic acid induce apoptosis in four human liver cancer cell lines. *Toxicol. Vitr.* **24**, 842–848 (2010).

177. H.-X. Sun, Q.-F. Zheng, J. Tu, Induction of apoptosis in HeLa cells by 3β-hydroxy-12-oleanen-27-oic acid from the rhizomes of Astilbe chinensis. *Bioorg. Med. Chem.* **14**, 1189–1198 (2006).

178. J. A. Jesus, J. H. G. Lago, M. D. Laurenti, E. S. Yamamoto, L. F. D. Passero, Antimicrobial Activity of Oleanolic and Ursolic Acids : An Update. *Evidence-Based Complement. Altern. Med.* **2015**, 1–14 (2015).

179. Y. Shukla, R. Singh, Resveratrol and cellular mechanisms of cancer prevention. *Ann. N.Y. Acad. Sci.* **1215**, 1–8 (2011).

180. C. Busch, T. Weiland, S. Venturelli, A. Berger, A. Bo, S. Noor, C. Leischner, S. Schleicher, M. Mayer, T. S. Weiss, S. C. Bischoff, U. M. Lauer, M. Bitzer, Resveratrol as a Pan-HDAC Inhibitor Alters the Acetylation Status of Jistone Proteins in Human-Derived Hepatoblastoma Cells. *PLoS One.* **8**, 1–12 (2013).

181. K. M. Yoo, S. Kim, B. K. Moon, S. S. Kim, K. T. Kim, S. Y. Kim, S. Y.

Choi, Potent Inhibitory Effects of Resveratrol Derivatives on Progression of Prostate Cancer Cells. *Arch. Pharm. (Weinheim).* **339**, 238–241 (2006).

182. Y. Li, J. Liu, X. Liu, K. Xing, Y. Wang, F. Li, L. Yao, Resveratrol-induced cell inhibition of growth and apoptosis in MCF7 human breast cancer cells are associated with modulation of phosphorylated Akt and caspase-9. *Appl. Biochem. Biotechnol.* **135**, 181–192 (2006).

183. J. Wu, K. Tsai, J. Shee, Y. Li, C. Chen, J. Chuang, Y. Liu, 4′-Chloro-3,5-dihydroxystilbene, a resveratrol derivative, induces lung cancer cell death. *Acta Pharmacol. Sin.* **31**, 81 (2010).

184. D. S. L. Ma, L. T. Tan, K. Chan, W. H. Yap, L. Lee, Resveratrol — Potential Antibacterial Agent against Foodborne Pathogens. *Front. Pharmacol.* **9**, 1–16 (2018).

185. L. Paulo, S. Ferreira, E. Gallardo, J. A. Queiroz, F. Domingues, Antimicrobial activity and effects of resveratrol on human pathogenic bacteria. *World J Microbiol Biotechnol.* **26**, 1533–1538 (2010).

186. H. Piotrowska, M. Kucinska, M. Murias, Biological activity of piceatannol: Leaving the shadow of resveratrol. *Mutat. Res. Mutat. Res.* **750**, 60–82 (2012).

187. C. Plumed-Ferrer, K. Väkeväinen, H. Komulainen, M. Rautiainen, A. Smeds, J.-E. Raitanen, P. Eklund, S. Willför, H.-L. Alakomi, M. Saarela, A. von Wright, The antimicrobial effects of wood-associated polyphenols on food pathogens and spoilage organisms. *Int. J. Food Microbiol.* **164**, 99–107 (2013).

188. A. L. Khan, J. Hussain, M. Hamayun, S. A. Gilani, S. Ahmad, G. Rehman, Y.-H. Kim, S.-M. Kang, I.-J. Lee, Secondary Metabolites from *Inula britannica* L. and Their Biological Activities. *Mol.* . **15** (2010), , doi:10.3390/molecules15031562.

189. N. Ji, S. Pan, C. Shao, Y. Chen, Z. Zhang, R. Wang, Y. Qiu, M. Jin, D. Kong, Spinacetin Suppresses the Mast Cell Activation and Passive Cutaneous Anaphylaxis in Mouse Model. *Front. Pharmacol.* **9**, 824 (2018).

190. Z. Kokanova-Nedialkova, P. Nedialkov, M. Kondeva-Burdina, R. Simeonova, V. Tzankova, D. Aluani, *Chenopodium bonus-henricus* L. – A source of hepatoprotective flavonoids. *Fitoterapia*. **118**, 13–20 (2017).

191. Z. Kokanova-Nedialkova, M. Kondeva-Burdina, D. Zheleva-Dimitrova, V. Tzankova, S. Nikolov, J. Heilmann, P. T. Nedialkov, 6-Methoxyflavonol Glycosides with In Vitro Hepatoprotective Activity from *Chenopodium bonus-henricus* Roots. *Nat. Prod. Commun.* **1**, 8–11 (2006).

192. N. Toudert, S. E. Djilani, A. Djilani, Antimicrobial activity of flavonoids of *Ampelodesma mauritanica*. *Am. J. Sustain. Agric.* **3**, 227–228 (2009).

193. B. Csupor-Löffler, Z. Hajdú, I. Zupkó, B. Réthy, G. Falkay, P. Forgo, J. Hohmann, Antiproliferative effect of flavonoids and sesquiterpenoids from *Achillea millefolium* s.l. on cultured human tumour cell lines. *Phyther. Res.* **23**, 672–676 (2008).

194. Y. X. Wu, X. Fang, Apigenin, chrysin, and luteolin selectively inhibit chymotrypsin-like and trypsin-like proteasome catalytic activities in tumor cells. *Planta Med.* **76**, 128–132 (2010).

195. J. Chang, Y. Hsu, P. Kuo, Y. Kuo, L. Chiang, C. Lin, Increase of Bax/Bcl-XL ratio and arrest of cell cycle by luteolin in immortalized human hepatoma cell line. *Life Sci.* **76**, 1883–1893 (2005).

196. K. Han, W. Meng, J.-J. Zhang, Y. Zhou, Y.-L. Wang, Y. Su, S.-C. Lin, Z.-H. Gan, Y.-N. Sun, D.-L. Min, Luteolin inhibited proliferation and induced apoptosis of prostate cancer cells through miR-301. *Onco. Targets. Ther.* **9**, 3085–3094 (2016).

197. G. Seelinger, I. Merfort, U. Wölfle, C. M. Schempp, Anti-carcinogenic Effects of the Flavonoid Luteolin. *Molecules.* **13**, 2628–2651 (2008).

198. Y. Lin, R. Shi, X. Wang, H.-M. Shen, Luteolin, a Flavonoid with Potential for Cancer Prevention and Therapy. *Curr. Cancer Drug Targets.* **8** (2008), pp. 634–646.

199. A. A. El-Gammal, R. M. A. Mansour, Antimicrobial Activities of Some Flavonoid Compounds. *Zentralbl. Mikrobiol.* **141**, 561–565 (1986).

200. W. Xu, J. Liu, C. Li, H.-Z. Wu, Y.-W. Liu, Kaempferol-7-O-β-d-glucoside (KG) isolated from *Smilax china* L. rhizome induces G2/M phase arrest and apoptosis on HeLa cells in a p53-independent manner. *Cancer Lett.* **264**, 229–240 (2008).

201. J. Wang, X. Fang, L. Ge, F. Cao, L. Zhao, Z. Wang, W. Xiao, Antitumor, antioxidant and anti-inflammatory activities of kaempferol and its corresponding glycosides and the enzymatic preparation of

kaempferol. *PLoS One*. **13**, e0197563–e0197563 (2018).

202. R. L. Londonkar, B. S. Awanti, In Vitro Cytotoxicity Effect of Kaempferol in Breast Cancer Cell Lines MCF-7 and Lung Cancer Cell Lines A459. *Int. J. Curr. Microbiol. Appl. Sci.* **5**, 414–421 (2016).

203. M. M. Baruah, N. Sharma, A. P. Khandwekar, Flavonoids and Prostate Cancer. *AIJRFANS*. **15**, 1–7 (2016).

204. A. J. Velanganni, M. Kannan, D. Umapathi, Kaempferol Blocks Angiogenesis Through The Suppression Of VEGF-C and HIF-1_ and Prevent Proliferation Through G1 Cell Cycle Arrest In Hepatocellular Carcinoma (2016).

205. U. F. Ezuruike, J. M. Prieto, The use of plants in the traditional management of diabetes in Nigeria: Pharmacological and toxicological considerations. *J. Ethnopharmacol.* **155**, 857–924 (2014).

206. J. M. Kong, L. S. Chia, N. K. Goh, T. F. Chia, R. Brouillard, Analysis and biological activities of anthocyanins. *Phytochemistry*. **64**, 923–933 (2003).

207. D. Ojeda, E. Jiménez-Ferrer, A. Zamilpa, A. Herrera-Arellano, J. Tortoriello, L. Alvarez, Inhibition of angiotensin convertin enzyme (ACE) activity by the anthocyanins delphinidin-and cyanidin-3-O-sambubiosides from *Hibiscus sabdariffa*. *J. Ethnopharmacol.* **127**, 7–10 (2010).

208. J. Tang, E. Oroudjev, L. Wilson, G. Ayoub, Delphinidin and cyanidin exhibit antiproliferative and apoptotic effects in MCF7 human breast cancer cells. *Integr. Cancer Sci. Ther.* **2**, 82–86 (2015).

209. M. H. Kim, Y. J. Jeong, H. J. Cho, H. S. Hoe, K. K. Park, Y. Y. Park, Y. H. Choi, C. H. Kim, H. W. Chang, Y. J. Park, I. K. Chung, Y. C. Chang, Delphinidin inhibits angiogenesis through the suppression of HIF-1α and VEGF expression in A549 lung cancer cells. *Oncol. Rep.* **37**, 777–784 (2017).

210. B. Bin Hafeez, I. A. Siddiqui, M. Asim, A. Malik, F. Afaq, V. M. Adhami, M. Saleem, M. Din, H. Mukhtar, A dietary anthocyanidin delphinidin induces apoptosis of human prostate cancer PC3 cells in vitro and in vivo: Involvement of nuclear factor-κB signaling. *Cancer Res.* **68**, 8564–8572 (2008).

211. S. Tsuyuki, S. Fukui, A. Watanabe, S. Akune, M. Tanabe, K. Yoshida, Delphinidin Induces Autolysosome as well as Autophagosome Formation and Delphinidin-Induced Autophagy Exerts a Cell Protective Role. *J. Biochem. Mol. Toxicol.* **26**, 445–453 (2012).

212. J. F. Olivas-Aguirre, J. Rodrigo-García, D. N. Martínez-Ruiz, I. A. Cárdenas-Robles, O. S. Mendoza-Díaz, E. Álvarez-Parrilla, A. G. González-Aguilar, A. L. de la Rosa, A. Ramos-Jiménez, A. Wall-Medrano, Cyanidin-3-O-glucoside: Physical-Chemistry, Foodomics and Health Effects. *Mol.* . **21** (2016), , doi:10.3390/molecules21091264.

213. B. P. Gaire, L. Subedi, A Review on the Natural Phytochemicals in Preventing and Treating Cancers. *J. Integr. Med.* **11**, 73–79 (2013).

214. R. Pratiwi, W. A. S. Tunjung, R. Rumiyati, A. R. Amalia, Black Rice Bran Extracts and Fractions Containing Cyanidin 3-glucoside and Peonidin 3-glucoside Induce Apoptosis in Human Cervical Cancer

Cells. *Indones. J. Biotechnol.* **20**, 69–76 (2016).

215. S. Naz, R. Siddiqi, S. Ahmad, S. A. Rasool, S. A. Sayeed, Antibacterial activity directed isolation of compounds from *Punica granatum. J. Food Sci.* **72**, M341–M345 (2007).

216. E. Genskowsky, L. A. Puente, J. A. Pérez-Álvarez, J. Fernández-López, L. A. Muñoz, M. Viuda-Martos, Determination of polyphenolic profile, antioxidant activity and antibacterial properties of maqui [*Aristotelia chilensis* (Molina) Stuntz] a Chilean blackberry. *J. Sci. Food Agric.* **96**, 4235–4242 (2016).

217. M. J. Park, J.-E. Ra, K. H. Seo, K.-C. Jang, S.-I. Han, J.-H. Lee, Y.-H. Kang, M.-H. Nam, W. D. Seo, Identification and evaluation of flavone-glucosides isolated from barley sprouts and their inhibitory activity against bacterial neuraminidase. *Nat. Prod. Commun.* **9**, 1469–1472 (2014).

218. A. M. Yang, H. Li, J. Sun, R. Wu, W. J. Guo, in *Advanced Materials Research* (Trans Tech Publ, 2013), vol. 655, pp. 1945–1948.

219. K. Iwai, N. Kishimoto, Y. Kakino, K. Mochida, T. Fujita, In vitro antioxidative effects and tyrosinase inhibitory activities of seven hydroxycinnamoyl derivatives in green coffee beans. *J. Agric. Food Chem.* **52**, 4893–4898 (2004).

220. P. M. Davidson, A. L. Branden, Antimicrobial activity of non-halogenated phenolic compounds. *J. Food Prot.* **44**, 623–632 (1981).

221. T. Rajavel, R. Mohankumar, G. Archunan, K. Ruckmani, K. P. Devi, Beta sitosterol and Daucosterol (phytosterols identified in *Grewia*

tiliaefolia) perturbs cell cycle and induces apoptotic cell death in A549 cells. *Sci. Rep.* **7**, 3418 (2017).

222. D. Sika, S. Kpoviessi, G. C. Accrombessi, J. D. Gbénou, A. Fernand, Cytotoxic Activities of Sterols and Triterpens Identified by GC-MS in *Justicia anselliana* (NEES) T . Anders Active Fractions and Allelopathic Effects on Cowpea (*Vigna unguiculata* (L .) Walp) plant . It is the most consumed leguminous : its seeds redu. *J. Soc. Ouest-Afr. Chim.* **774**, 59–67 (2008).

223. J. Hao, J. Liu, X. Wen, H. Sun, Synthesis and cytotoxicity evaluation of oleanolic acid derivatives. *Bioorg. Med. Chem. Lett.* **23**, 2074–2077 (2013).

224. W. D. Ong, L.-Y. C. Voo, V. S. Kumar, De novo assembly, characterization and functional annotation of pineapple fruit transcriptome through massively parallel sequencing. *PLoS One.* **7**, e46937 (2012).

225. J. Ma, S. Kanakala, Y. He, J. Zhang, X. Zhong, Transcriptome Sequence Analysis of an Ornamental Plant, *Ananas comosus* var. bracteatus, Revealed the Potential Unigenes Involved in Terpenoid and Phenylpropanoid Biosynthesis. *PLoS One.* **10**, e0119153 (2015).

226. S. Araji, T. A. Grammer, R. Gertzen, S. D. Anderson, M. Mikulic-Petkovsek, R. Veberic, M. L. Phu, A. Solar, C. A. Leslie, A. M. Dandekar, M. A. Escobar, Novel roles for the polyphenol oxidase enzyme in secondary metabolism and the regulation of cell death in walnut. *Plant Physiol.* **164**, 1191–1203 (2014).

227. M. Tattini, C. Galardi, P. Pinelli, R. Massai, D. Remorini, G. Agati, Differential accumulation of flavonoids and hydroxycinnamates in leaves of *Ligustrum vulgare* under excess light and drought stress. *New Phytol.* **163**, 547–561 (2004).

228. A. Rezazadeh, A. Ghasemnezhad, M. Barani, T. Telmadarrehei, Effect of Salinity on Phenolic Composition and Antioxidant Activity of Artichoke (*Cynara scolymus* L.) Leaves. *Res. J. Med. Plant*. **6**, 245–252 (2012).

229. P. A. Lambert, Bacterial resistance to antibiotics: Modified target sites. *Adv. Drug Deliv. Rev.* **57**, 1471–1485 (2005).

230. H. T. Nguyen, D. V. Ho, H. Q. Vo, A. T. Le, H. M. Nguyen, T. Kodama, T. Ito, H. Morita, A. Raal, Antibacterial activities of chemical constituents from the aerial parts of *Hedyotis pilulifera*. *Pharm. Biol.* **55**, 787–791 (2017).

231. A. Sen, P. Dhavan, K. K. Shukla, S. Singh, G. Tejovathi, Analysis of IR, NMR and antimicrobial activity of β-sitosterol isolated from *Momordica charanti*. *Sci. Secur. J. Biotechnol.* **1**, 9–13 (2012).

232. R. Tao, C.-Z. Wang, Z.-W. Kong, Antibacterial/Antifungal Activity and Synergistic Interactions between Polyprenols and Other Lipids Isolated from *Ginkgo Biloba* L. Leaves. *Mol.* . **18** (2013), , doi:10.3390/molecules18022166.

233. G. Huang, M. Lv, J. Hu, K. H. and H. Xu, Glycosylation and Activities of Natural Products. *Mini-Reviews Med. Chem.* **16** (2016), pp. 1013–1016.

234. M. Kartal-Yandim, A. Adan-Gokbulut, Y. Baran, Molecular mechanisms of drug resistance and its reversal in cancer. *Crit. Rev. Biotechnol.* **36**, 716–726 (2016).

235. T. H. Yeats, J. K. C. Rose, The formation and function of plant cuticles. *Plant Physiol.* **163**, 5–20 (2013).

236. C. J. Zheng, J.-S. Yoo, T.-G. Lee, H.-Y. Cho, Y.-H. Kim, W.-G. Kim, Fatty acid synthesis is a target for antibacterial activity of unsaturated fatty acids. *FEBS Lett.* **579**, 5157–5162 (2005).

237. N. Nakajima, S. Fujioka, T. Tanaka, S. Takatsuto, S. Yoshida, Biosynthesis of cholestanol in higher plants. *Phytochemistry*. **60**, 275–279 (2002).

238. E. I. Mercer, Sterol biosynthesis inhibitors: Their current status and modes of action. *Lipids*. **26**, 584–597 (1991).

239. S. S. Gogavekar, S. A. Rokade, R. C. Ranveer, J. S. Ghosh, D. C. Kalyani, A. K. Sahoo, Important nutritional constituents, flavour components, antioxidant and antibacterial properties of Pleurotus sajor-caju. *J. Food Sci. Technol.* **51**, 1483–1491 (2014).

240. T. Kato, B. Frei, M. Heinrich, O. Sticher, Antibacterial hydroperoxysterols from *Xanthosoma robustum*. *Phytochemistry*. **41**, 1191–1195 (1996).

241. P. Kwiatkowski, A. Pruss, H. Masiuk, M. Mnichowska-Polanowska, M. Kaczmarek, S. Giedrys-Kalemba, B. Dołęgowska, H. Zielińska-Bliźniewska, J. Olszewski, M. Sienkiewicz, The effect of fennel essential oil and trans-anethole on antibacterial activity of mupirocin

against *Staphylococcus aureus* isolated from asymptomatic carriers. *Postep. dermatologii i Alergol.* **36**, 308–314 (2019).

242. D. Tholl, in *Biotechnology of isoprenoids* (Springer, 2015), pp. 63–106.

243. H. C. Upadhyay, G. R. Dwivedi, S. Roy, A. Sharma, M. P. Darokar, S. K. Srivastava, Phytol derivatives as drug resistance reversal agents. *ChemMedChem*. **9**, 1860–1868 (2014).

244. J. Kang, W. E. Price, J. Ashton, L. C. Tapsell, S. Johnson, Identification and characterization of phenolic compounds in hydromethanolic extracts of sorghum wholegrains by LC-ESI-MSn. *Food Chem.* **211**, 215–226 (2016).

245. C. Ma, S. yuan Xiao, Z. guo Li, W. Wang, L. jun Du, Characterization of active phenolic components in the ethanolic extract of *Ananas comosus* L. leaves using high-performance liquid chromatography with diode array detection and tandem mass spectrometry. *J. Chromatogr. A*. **1165**, 39–44 (2007).

246. N. Kishimoto, Y. Kakino, K. Iwai, K. Mochida, T. Fujita, In vitro antibacterial, antimutagenic and anti-influenza virus activity of caffeic acid phenethyl esters. *Biocontrol Sci.* **10**, 155–161 (2005).

247. F. A. Ramos, Y. Takaishi, M. Shirotori, Y. Kawaguchi, K. Tsuchiya, H. Shibata, T. Higuti, T. Tadokoro, M. Takeuchi, Antibacterial and Antioxidant Activities of Quercetin Oxidation Products from Yellow Onion (*Allium cepa*) Skin. *J. Agric. Food Chem.* **54**, 3551–3557 (2006).

248. C. Rodríguez-Pérez, R. Quirantes-Piné, J. Uberos, C. Jiménez-Sánchez, A. Peña, A. Segura-Carretero, Antibacterial activity of

isolated phenolic compounds from cranberry (*Vaccinium macrocarpon*) against *Escherichia coli*. *Food Funct.* **7**, 1564–1573 (2016).

249. S. J. N. Tatsimo, J. de D. Tamokou, L. Havyarimana, D. Csupor, P. Forgo, J. Hohmann, J.-R. Kuiate, P. Tane, Antimicrobial and antioxidant activity of kaempferol rhamnoside derivatives from *Bryophyllum pinnatum*. *BMC Res. Notes*. **5**, 158 (2012).

250. W. R. Yao, H. Y. Wang, S. T. Wang, S. L. Sun, J. Zhou, Y. Y. Luan, Assessment of the Antibacterial Activity and the Antidiarrheal Function of Flavonoids from Bayberry Fruit. *J. Agric. Food Chem.* **59**, 5312–5317 (2011).

251. P. Kubica, A. Kot-Wasik, A. Wasik, J. Namieśnik, P. Landowski, Modern approach for determination of lactulose, mannitol and sucrose in human urine using HPLC–MS/MS for the studies of intestinal and upper digestive tract permeability. *J. Chromatogr. B*. **907**, 34–40 (2012).

252. A. F. Hanham, B. P. Dunn, H. F. Stich, Clastogenic activity of caffeic acid and its relationship to hydrogen peroxide generated during autooxidation. *Mutat. Res. Toxicol.* **116**, 333–339 (1983).

253. K. Natarajan, S. Singh, T. R. Burke, D. Grunberger, B. B. Aggarwal, *Proc. Natl. Acad. Sci.*, in press, doi:10.1073/pnas.93.17.9090.

254. H.-P. Lin, S. S. Jiang, C.-P. Chuu, Caffeic acid phenethyl ester causes p21 induction, Akt signaling reduction, and growth inhibition in PC-3 human prostate cancer cells. *PLoS One*. **7**, e31286–e31286 (2012).

255. S. Inoue, K. Ito, K. Yamamoto, S. Kawanishi, Caffeic acid causes

metal-dependent damage to cellular and isolated DNA through H2O2 formation. *Carcinogenesis*. **13**, 1497–1502 (1992).

256. T. T. Huang, S. L. Feinberg, S. Suryanarayanan, S. Miyamoto, The zinc finger domain of NEMO is selectively required for NF-kappa B activation by UV radiation and topoisomerase inhibitors. *Mol. Cell. Biol.* **22**, 5813–5825 (2002).

257. K. Saeki, N. Kobayashi, Y. Inazawa, H. Zhang, H. Nishitoh, H. Ichijo, K. Saeki, M. Isemura, A. Yuo, Oxidation-triggered c-Jun N-terminal kinase (JNK) and p38 mitogen-activated protein (MAP) kinase pathways for apoptosis in human leukaemic cells stimulated by epigallocatechin-3-gallate (EGCG): a distinct pathway from those of chemically induced and recep. *Biochem. J.* **368**, 705–720 (2002).

258. B. Ye, W. Yu, G. M. Thomas, R. L. Huganir, GRASP-1 is a neuronal scaffold protein for the JNK signaling pathway. *FEBS Lett.* **581**, 4403–4410 (2007).

259. Y. Xia, Z. Wu, B. Su, B. Murray, M. Karin, JNKK1 organizes a MAP kinase module through specific and sequential interactions with upstream and downstream components mediated by its amino-terminal extension. *Genes Dev.* **12**, 3369–3381 (1998).

260. L. Girnita, A. Girnita, O. Larsson, Mdm2-dependent ubiquitination and degradation of the insulin-like growth factor 1 receptor. *Proc. Natl. Acad. Sci. U. S. A.* **100**, 8247–8252 (2003).

261. S. Fang, J. P. Jensen, R. L. Ludwig, K. H. Vousden, A. M. Weissman, Mdm2 is a RING finger-dependent ubiquitin protein ligase for itself and

p53. *J. Biol. Chem.* **275**, 8945–8951 (2000).

262. H. T. Yuan, E. V Khankin, S. A. Karumanchi, S. M. Parikh, Angiopoietin 2 is a partial agonist/antagonist of Tie2 signaling in the endothelium. *Mol. Cell. Biol.* **29**, 2011–2022 (2009).

263. H. J. Lee, C.-H. Cho, S.-J. Hwang, H.-H. Choi, K.-T. Kim, S. Y. Ahn, J.-H. Kim, J.-L. Oh, G. M. Lee, G. Y. Koh, Biological characterization of angiopoietin-3 and angiopoietin-4. *FASEB J.* **18**, 1200–1208 (2004).

264. P. J. Lockyer, S. Kupzig, P. J. Cullen, CAPRI regulates Ca(2+)-dependent inactivation of the Ras-MAPK pathway. *Curr. Biol.* **11**, 981–986 (2001).

265. S. Yoon, R. Seger, The extracellular signal-regulated kinase: multiple substrates regulate diverse cellular functions. *Growth Factors*. **24**, 21–44 (2006).

266. B. Zhao, Q. Y. Lei, K. L. Guan, The Hippo-YAP pathway: new connections between regulation of organ size and cancer. *Curr. Opin. Cell Biol.* **20** (2008), pp. 638–646.

267. P. Gaudet, M. S. Livstone, S. E. Lewis, P. D. Thomas, Phylogenetic-based propagation of functional annotations within the Gene Ontology consortium. *Brief. Bioinform.* **12**, 449–462 (2011).

268. M. J. McEachern, A. Krauskopf, E. H. Blackburn, Telomeres and their control. *Annu. Rev. Genet.* **34**, 331–358 (2000).

269. L. L. Cribbs, J. C. Gomora, A. N. Daud, J. H. Lee, E. Perez-Reyes, Molecular cloning and functional expression of Ca(v)3.1c, a T-type calcium channel from human brain. *FEBS Lett.* **466**, 54–58 (2000).

270. M. N. Hossain, R. Sakemura, M. Fujii, D. Ayusawa, G-protein γ subunit GNG11 strongly regulates cellular senescence. *Biochem. Biophys. Res. Commun.* **351**, 645–650 (2006).

271. A. Davy, N. W. Gale, E. W. Murray, R. A. Klinghoffer, P. Soriano, C. Feuerstein, S. M. Robbins, Compartmentalized signaling by GPI-anchored ephrin-A5 requires the Fyn tyrosine kinase to regulate cellular adhesion. *Genes Dev.* **13**, 3125–3135 (1999).

272. X. Chen, B. Gao, M. Ponnusamy, Z. Lin, J. Liu, MEF2 signaling and human diseases. *Oncotarget*. **8**, 112152–112165 (2017).

273. T. Zhan, N. Rindtorff, M. Boutros, Wnt signaling in cancer. *Oncogene*. **36**, 1461–1473 (2017).

274. J. Á. F. Vara, E. Casado, J. de Castro, P. Cejas, C. Belda-Iniesta, M. González-Barón, PI3K/Akt signalling pathway and cancer. *Cancer Treat. Rev.* **30**, 193–204 (2004).

275. E. Lineham, G. J. Tizzard, S. J. Coles, J. Spencer, S. J. Morley, Synergistic effects of inhibiting the MNK-eIF4E and PI3K/AKT/ mTOR pathways on cell migration in MDA-MB-231 cells. *Oncotarget*. **9**, 14148–14159 (2018).

276. L. Furic, L. Rong, O. Larsson, I. H. Koumakpayi, K. Yoshida, A. Brueschke, E. Petroulakis, N. Robichaud, M. Pollak, L. A. Gaboury, P. P. Pandolfi, F. Saad, N. Sonenberg, eIF4E phosphorylation promotes tumorigenesis and is associated with prostate cancer progression. *Proc. Natl. Acad. Sci. U. S. A.* **107**, 14134–14139 (2010).

277. L. Adesso, S. Calabretta, F. Barbagallo, G. Capurso, E. Pilozzi, R.

Geremia, G. Delle Fave, C. Sette, Gemcitabine triggers a pro-survival response in pancreatic cancer cells through activation of the MNK2/eIF4E pathway. *Oncogene*. **32**, 2848–2857 (2013).

278. K. Katayama, M. Yamaguchi, K. Noguchi, Y. Sugimoto, Protein phosphatase complex PP5/PPP2R3C dephosphorylates P-glycoprotein/ABCB1 and down-regulates the expression and function. *Cancer Lett.* **345**, 124–131 (2014).

279. S. Blasche, M. Mörtl, H. Steuber, G. Siszler, S. Nisa, F. Schwarz, I. Lavrik, T. M. A. Gronewold, K. Maskos, M. S. Donnenberg, D. Ullmann, P. Uetz, M. Kögl, The *E. coli* effector protein NleF is a caspase inhibitor. *PLoS One*. **8**, e58937 (2013).

280. D. Raina, P. Pandey, R. Ahmad, A. Bharti, J. Ren, S. Kharbanda, R. Weichselbaum, D. Kufe, c-Abl tyrosine kinase regulates caspase-9 autocleavage in the apoptotic response to DNA damage. *J. Biol. Chem.* **280**, 11147–11151 (2005).

281. H. C. Reinhardt, P. Hasskamp, I. Schmedding, S. Morandell, M. A. T. M. van Vugt, X. Wang, R. Linding, S.-E. Ong, D. Weaver, S. A. Carr, M. B. Yaffe, DNA damage activates a spatially distinct late cytoplasmic cell-cycle checkpoint network controlled by MK2-mediated RNA stabilization. *Mol. Cell*. **40**, 34–49 (2010).

282. R. Fujikane, M. Sanada, M. Sekiguchi, M. Hidaka, The identification of a novel gene, MAPO2, that is involved in the induction of apoptosis triggered by O^6-methylguanine. *PLoS One*. **7**, e44817 (2012).

283. D. M. Ornitz, J. Xu, J. S. Colvin, D. G. McEwen, C. A. MacArthur, F.

Coulier, G. Gao, M. Goldfarb, Receptor specificity of the fibroblast growth factor family. *J. Biol. Chem.* **271**, 15292–15297 (1996).

284. M. Katoh, FGFR2 abnormalities underlie a spectrum of bone, skin, and cancer pathologies. *J. Invest. Dermatol.* **129**, 1861–1867 (2009).

285. X. Zhang, S. Zhang, H. Yamane, R. Wahl, A. Ali, J. A. Lofgren, R. L. Kendall, Kinetic mechanism of AKT/PKB enzyme family. *J. Biol. Chem.* **281**, 13949–13956 (2006).

286. L. Chen, D. M. Gilkes, Y. Pan, W. S. Lane, J. Chen, ATM and Chk2-dependent phosphorylation of MDMX contribute to p53 activation after DNA damage. *EMBO J.* **24**, 3411–3422 (2005).

287. A. Shvarts, M. Bazuine, P. Dekker, Y. F. Ramos, W. T. Steegenga, G. Merckx, R. C. van Ham, W. van der Houven van Oordt, A. J. van der Eb, A. G. Jochemsen, Isolation and identification of the human homolog of a new p53-binding protein, Mdmx. *Genomics*. **43**, 34–42 (1997).

288. P. Werner, P. Paluru, A. M. Simpson, B. Latney, R. Iyer, G. M. Brodeur, E. Goldmuntz, Mutations in NTRK3 suggest a novel signaling pathway in human congenital heart disease. *Hum. Mutat.* **35**, 1459–1468 (2014).

289. S. V Ivanov, A. Panaccione, B. Brown, Y. Guo, C. A. Moskaluk, M. J. Wick, J. L. Brown, A. V Ivanova, N. Issaeva, A. K. El-Naggar, W. G. Yarbrough, TrkC signaling is activated in adenoid cystic carcinoma and requires NT-3 to stimulate invasive behavior. *Oncogene*. **32**, 3698–3710 (2013).

290. J.-S. Moon, W.-J. Jin, J.-H. Kwak, H.-J. Kim, M.-J. Yun, K. I. M. Jae-Woo, S. W. Park, K.-S. Kim, Androgen stimulates glycolysis for de novo lipid synthesis by increasing the activities of hexokinase 2 and 6-phosphofructo-2-kinase/fructose-2, 6-bisphosphatase 2 in prostate cancer cells. *Biochem. J.* **433**, 225–233 (2011).

291. L. Novellasdemunt, I. Tato, A. Navarro-Sabate, M. Ruiz-Meana, A. Méndez-Lucas, J. C. Perales, D. Garcia-Dorado, F. Ventura, R. Bartrons, J. L. Rosa, Akt-dependent activation of the heart 6-phosphofructo-2-kinase/fructose-2, 6-bisphosphatase (PFKFB2) isoenzyme by amino acids. *J. Biol. Chem.* **288**, 10640–10651 (2013).

292. G. Chen, G. Zhou, S. Aras, Z. He, S. Lucas, I. Podgorski, W. Skar, J. G. Granneman, J. Wang, Loss of ABHD5 promotes the aggressiveness of prostate cancer cells. *Sci. Rep.* **7**, 13021 (2017).

293. N. Pinheiro-castro, L. Beatriz, A. Ribeiro, G. M. Novaes, T. P. Ong, *Reviews on Biomarker Studies of Metabolic and Metabolism-Related Disorders* (Springer Nature Switzerland, 2019; http://link.springer.com/10.1007/978-3-030-12668-1), vol. 1134.

294. C. Chen, H. Shen, L.-G. Zhang, J. Liu, X.-G. Cao, A.-L. Yao, S.-S. Kang, W.-X. Gao, H. Han, F.-H. Cao, Construction and analysis of protein-protein interaction networks based on proteomics data of prostate cancer. *Int. J. Mol. Med.* **37**, 1576–1586 (2016).

295. P. Karuman, O. Gozani, R. D. Odze, X. C. Zhou, H. Zhu, R. Shaw, T. P. Brien, C. D. Bozzuto, D. Ooi, L. C. Cantley, J. Yuan, The Peutz-Jegher gene product LKB1 is a mediator of p53-dependent cell death.

Mol. Cell. **7**, 1307–1319 (2001).

296. P.-Y. Zeng, S. L. Berger, LKB1 is recruited to the p21/WAF1 promoter by p53 to mediate transcriptional activation. *Cancer Res.* **66**, 10701–10708 (2006).

297. V. Grossi et al., Loss of STK11 expression is an early event in prostate carcinogenesis and predicts therapeutic response to targeted therapy against MAPK/p38. *Autophagy*. **11**, 2102–2113 (2015).

298. J. Sancéau, J. Hiscott, O. Delattre, J. Wietzerbin, IFN-beta induces serine phosphorylation of Stat-1 in Ewing's sarcoma cells and mediates apoptosis via induction of IRF-1 and activation of caspase-7. *Oncogene*. **19**, 3372–3383 (2000).

299. N. Khurana, S. Bhattacharyya, Hsp90, the concertmaster: tuning transcription. *Front. Oncol.* **5** (2015), p. 100.

300. J. Liu, T. Akahoshi, S. Jiang, R. Namai, H. Kitasato, H. Endo, T. Kameya, H. Kondo, Induction of neutrophil death resembling neither apoptosis nor necrosis by ONO-AE-248, a selective agonist for PGE2 receptor subtype 3. *J. Leukoc. Biol.* **68**, 187–193 (2000).

301. F. Ren, S. Zhang, S. H. Mitchell, R. Butler, C. Y. F. Young, Tea polyphenols down-regulate the expression of the androgen receptor in LNCaP prostate cancer cells. *Oncogene*. **19**, 1924–1932 (2000).

302. S. Xiong, T. Mu, G. Wang, X. Jiang, Mitochondria-mediated apoptosis in mammals. *Protein Cell*. **5**, 737–749 (2014).

303. Y. S. Markandeya, J. M. Fahey, F. Pluteanu, L. L. Cribbs, R. C. Balijepalli, Caveolin-3 regulates protein kinase A modulation of the

Ca(V)3.2 (alpha1H) T-type Ca2+ channels. *J. Biol. Chem.* **286**, 2433–2444 (2011).

304. C. E. Caldon, C. M. Sergio, A. Burgess, A. J. Deans, R. L. Sutherland, E. A. Musgrove, Cyclin E2 induces genomic instability by mechanisms distinct from cyclin E1. *Cell Cycle.* **12**, 606–617 (2013).

305. P. W. Janes, N. Saha, W. A. Barton, M. V Kolev, S. H. Wimmer-Kleikamp, E. Nievergall, C. P. Blobel, J.-P. Himanen, M. Lackmann, D. B. Nikolov, Adam meets Eph: an ADAM substrate recognition module acts as a molecular switch for ephrin cleavage in trans. *Cell.* **123**, 291–304 (2005).

306. D. C. Olson, V. Marechal, J. Momand, J. Chen, C. Romocki, A. J. Levine, Identification and characterization of multiple mdm-2 proteins and mdm-2-p53 protein complexes. *Oncogene.* **8**, 2353–2360 (1993).

307. K. Shimizu, J. K. Hicks, T.-P. Huang, N. P. Keller, Pka, Ras and RGS protein interactions regulate activity of AflR, a Zn(II)2Cys6 transcription factor in *Aspergillus nidulans*. *Genetics.* **165**, 1095–1104 (2003).

308. Y. Luo, A. M. Kaz, S. Kanngurn, P. Welsch, S. M. Morris, J. Wang, J. D. Lutterbaugh, S. D. Markowitz, W. M. Grady, NTRK3 is a potential tumor suppressor gene commonly inactivated by epigenetic mechanisms in colorectal cancer. *PLoS Genet.* **9**, e1003552–e1003552 (2013).

309. H. Tian, A. T. Faje, S. L. Lee, T. J. Jorgensen, Radiation-induced phosphorylation of Chk1 at S345 is associated with p53-dependent cell cycle arrest pathways. *Neoplasia.* **4**, 171–180 (2002).

310. N. E. Hatch, M. Hudson, M. L. Seto, M. L. Cunningham, M. Bothwell, Intracellular retention, degradation, and signaling of glycosylation-deficient FGFR2 and craniosynostosis syndrome-associated FGFR2C278F. *J. Biol. Chem.* **281**, 27292–27305 (2006).

311. N. Allende-Vega, A. Sparks, D. P. Lane, M. K. Saville, MdmX is a substrate for the deubiquitinating enzyme USP2a. *Oncogene*. **29**, 432–441 (2010).

312. D. E. James, M. Strube, M. Mueckler, Molecular cloning and characterization of an insulin-regulatable glucose transporter. *Nature*. **338**, 83–87 (1989).